Penetration of Objects into the Ocean Bottom

(The State of the Art)

by

Werner E. Schmid

FINAL REPORT

CR 69.030

Contract No. N62399-68-C-0044

Project No. Y-F015-21-02-005A

to the

Naval Civil Engineering Laboratory

Port Hueneme, California 93041

March 1969

Penetration of Objects into the Ocean Bottom

(The State of the Art)

by

Werner E. Schmid, P.E.
Princeton, New Jersey

March 1969

Final Report
to the
U.S. Naval Civil Engineering Laboratory
Port Hueneme, California
under Contract No. N62399-68-C-0044
Project No. Y-F015-21-02-005A

Errata

PENETRATION OF OBJECTS INTO THE OCEAN BOTTOM

by

Werner E. Schmid

March 1969

Page	Paragraph	Line	Change
	Figure 3.1		θ reference is incorrect for first angle, correct for second. First angle should be:

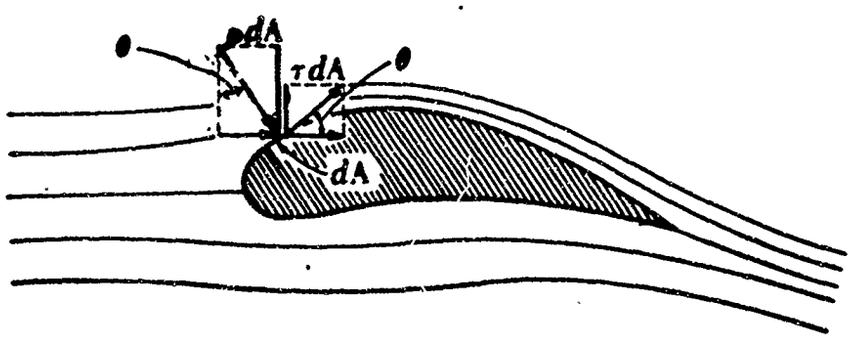

	Figure 3.6		Use a logarithimically spaced grid
34	1 (Equation 4.8)	1	Delete the "2" in the denominator of the first term: $x = \frac{m}{\gamma} \ln \frac{\beta + 2\gamma v_o}{\beta + 2\gamma v} - \frac{\beta}{\gamma} Cm$
34	2 (Equation 4.10)	5	Insert brackets: $x = \frac{m}{\gamma} \left[\ln \cdots \alpha^{\frac{1}{2}} \cdots \right]$
34	2 (Equation 4.11)	7	Insert brackets: $x_{max} = \frac{m}{\gamma} \left[\ln \cdots \right]$

Page	Paragraph	Line	Change
	Figure 4.8		Eqs. at bottom should read: at nose, $\ddot{x} = \ddot{x}_{cg} + a\,\ddot{\theta} \sin \theta$ at tail, $\ddot{x} = \ddot{x}_{cg} - b\,\ddot{\theta} \sin \theta$ Also, at top: "Whip Acceleration, $\ddot{\theta}$" should be legible.
57	2	1	"Thus, assuming γ_{equiv}, k_o, δ, and ---"
	Figure 6.2		Delete "see fig.6," "see fig. 4a," and "see fig. 4b."
	Figures 6.10a & 6.10b		Interchange "a" and "b" in figure numbers to make figures correspond with text.

Table of Contents

Table of Contents (continued)

1.0 Statement of Problem

1.1 Introduction

The ocean floor is one of the last unexplored frontiers on earth. In recent years a tremendous interest has been generated for the discovery and exploration of this unknown portion of the globe and its exploitation, both for military as well as for civilian purposes.

Naval strategists are now openly considering the feasibility of deep, fixed, underwater installations -- manned and unmanned, fixed, underwater monitoring and surveillance stations for naval traffic, marine benchmarks, and navigational aids. In the civilian sector, the last decade has seen an almost unbelievable expansion of ocean floor activities. Offshore drilling, mostly for natural oil and gas, is carried on now in water depths of up to 1000 feet. The feasibility of extracting other raw materials from the bottom of the sea, such as sulfur and nodules of manganese, is seriously being studied. Plans are being made to build manned stations off the east coast of Florida in water depths to 1000 feet by mid-1972 and in 6000-foot water depths by 1973.

One fact is clear: the activities of man on the ocean floor will increase quickly and enormously.

Even for present activities and current problems our knowledge of the ocean floor and its behavior and response to human activity are woefully inadequate. We are referring here, e.g., to such problems as the disappearance of the U.S. submarine Thresher, the extremely difficult and delicate recovery of a thermonuclear bomb off Palomares, Spain, and the failure of several radar platforms off the Atlantic coast.

It is therefore singularly appropriate that the soil mechanics aspects and behavior of ocean bottom sediments be explored and investigated. Thus, a more reliable assessment and prediction of the response of ocean floor sediments to human activities will be possible and a better estimate of the performance of new installations, methods, and processes on the ocean floor will result.

1.2 Statement of Problem and Objective

Many problems of ocean floor technology either are directly concerned with or are reducible to the problem of penetration of an object through the upper layers of the bottom sediments. This, for example, applies to the installation of underwater foundations, the driving of piles for over- and

underwater platforms and for dolphins, the penetration of anchors for ships, buoys, mines, and monitoring stations, the discovery and reclaiming of objects lost and sunk to the ocean floor, the assessment of ocean sediment properties from the dynamic penetration record of ocean floor penetrometers, and even the running aground and refloating of ships and submarines.

Thus, the topic of this study is extremely broad. Our objective is to perform a comprehensive review of the state of the art of assessing and predicting the penetration of objects into the ocean floor, to recommend methods and procedures for immediate use for predicting such penetration, and to recommend future research and development that would significantly advance the state of the art.

The rather broad subject of penetration of an object into the ocean bottom has been subdivided into several categories according to the phases or periods during which driving forces are acting on the penetrating missile. We are distinguishing between these categories as follows.

For a free falling object, the penetration phenomenon is characterized by the fact that some time before as well as during the penetration process no driving forces other than gravitational forces are acting on the object. Therefore, in free fall penetration (ffp) the object follows a free fall trajectory through the water prior to entering the ocean bottom sediments. Typical examples for ffp would be a rock, a bomb, a spent torpedo, or a sunken ship falling to the ocean bottom. The physically significant feature here is the fact that, at some time, say at t_o, travel under power has stopped and in the interval between t_o and the impact time t_i the missile moves along a free fall trajectory which is determined by the velocity v_o at time t_o and the frictional resistance of the medium through which the missile travels.

On the other hand, a missile may still be under power while making impact with the ocean bottom. This type of penetration we have chosen to call powered travel penetration (ptp) and typical examples would be a torpedo driving itself into the ocean bottom, a submarine or ship running aground, or a surface-to-surface or air-to-surface missile impacting on the ocean bottom while still in the powered phase of its flight.

Finally, there are penetration phenomena which are characterized by the fact that the penetration of the objects is assisted by forces or power systems designed to facilitate the piercing of the ocean bottom soils. We have chosen to label this type dynamic penetration (dp). Typical examples for this type of penetration would be the driving of piles, the penetration of anchors and the piercing of soil samplers by explosive charges, and the drilling of holes into the

ocean bottom. Thus, to summarize, the penetration of objects into the ocean bottom can be subdivided into three categories:

a) free fall penetration ffp
b) powered travel penetration ptp
c) dynamic penetration dp

To a large measure, the penetration of an object into the ocean bottom will depend upon the properties of the ocean bottom sediments -- in addition to the mechanical properties of the penetrating object and the dynamical parameters of the penetration process. It is for this reason that in Chapter 2 of this report we first review our state of knowledge on the nature, extent and distribution of ocean bottom sediments, the methods by which knowledge about these factors is obtained, the various methods of sampling and coring of ocean bottom sediments, the methods used for establishing the properties of these sediments and, finally, the actual properties and the range within which they might be expected to fall. It is quite clear that much less is known about submarine soils than about terrestrial soils. Also, submarine soils appear to exhibit as much variety and variability as do terrestrial soils. Thus, it appears that the correct assessment of the properties of the bottom sediment will be one of the important factors -- if not the most critical one -- for the successful prediction of ocean bottom penetration. For these reasons we carefully reviewed the literature regarding ocean bottom sediments. More than 250 reports, papers, and articles were reviewed and of these about 60 were found to merit closer study. The most specific treatment in the literature on ocean bottom penetration is that discussing the penetration of core samplers. However, this is by no means an exhaustive coverage of the topic and the penetration problem has to be studied on a much broader scale, taking into consideration penetration of an object into any kind of plastic material and applying the results to the problems at hand by using the properties of ocean bottom sediments.

The most important dynamic feature in free fall penetration is the impact velocity. In addition, the travel path and the orientation of the object at impact are important. For this reason, Chapter 3 presents the methods that can be used for determining the impact velocity and trajectory of an object falling through sea water.

In Chapter 4 we review the mechanics of penetration of an object striking a target material with an impact velocity u_o. The problem is subdivided into two classes. The first class is penetration with increasing penetration area. This usually will apply most often to large object penetrating only partly into the bottom soil (shallow penetration). The second class is penetration at constant area. While shallow penetration may occur at constant area, deep penetration practically always will be at constant area.

The problem of dynamic, driven penetration is discussed in Chapter 5. For most practical purposes dynamic penetration is the driving of piles or other objects by a series of impact blows into the bottom soils and the mechanics of this process is reviewed.

In Chapter 6 we review the state of our technology for achieving ocean bottom penetration and report on coring tools, anchors and pile driving technology presently existing and available for ocean bottom penetration.

A rather comprehensive and competent offshore construction technology has developed during the past two decades mainly in connection with offshore exploration and production of oil. All fixed platforms are anchored to the ocean bottom by piles driven through template sleeves. The development of this technology has been traced through the literature and the present state of the art was assessed.

The piles anchoring the platforms are usually driven above water and, after they have encountered refusal or the required driving resistance, they are anchored to the platform by welding and/or grouting of the space between the pipe sleeve and the pile.

As of this time, no record exists that piles for an offshore platform have ever been driven under water although at least one offshore contractor has a patent application pending for an underwater pile hammer.

It appears that the most reliably successful method of installing piles under water and at greater water depths (say in excess of 300-400 feet) will be by pile vibrators.

In Chapter 7 we present recommendations for immediate use of methods to assess and predict ocean bottom penetration. Finally, we recommend future research and development to advance the state of the art of achieving ocean bottom penetration as well as predicting it (Chapter 8).

2.0 Ocean Bottom Soils and Their Properties

2.1 Ocean Bottom Topography

The principal topographic features that characterize the ocean bottom are the continental shelf or terrace and the abyssal plain of the deep ocean floor. The abyssal plains cover millions of square miles and are covered with deep sediment. The continental terrace is the gradual extension of a continent into the ocean down to the continental slope. Usually the end of the continental terrace and beginning of the continental slope is taken at a water depth of 600 feet. Beyond that depth the ocean bottom usually drops off steeply to the abyssal deep. The abyssal deep is considered to begin at a depth from 6,000 to 12,000 feet. These main features of the ocean bottom are accompanied by undersea mountain ranges, especially the midocean ridges, isolated, submerged mountains and sea mounts or guyots rising thousands of feet above the bottom and escarpments a mile or more in height cutting across the ocean floor for hundreds of miles. In addition, the ocean floor has been warped by folding and faulting, causing deep submerged trenches up to 20,000 feet deep and resulting in total water depths of nearly 36,000 feet. Cutting into the continental shelves are deep submarine canyons located usually where surface rivers are discharging into the oceans.

Thus, the ocean bottom geology appears to be almost as varied as that of the continents. The general bathymetry of the ocean basins is provided by standard reference texts such as Menard (1964).

2.2 Ocean Bottom Sediments

The soils of the ocean bottom are usually classified into two big groups: the terrigenic soils and the pelagic soils. The terrigenic soils as their name suggests are derived from the continents and are carried into the oceans by rivers and currents. They are the sediments found on the continental shelf and are made up of sands, silts, muds and clays. Submarine sediment transport is controlled by the same physical laws as sediment transport on the continent and, hence, the sediments on the continental shelves have similar particle size, shape and characteristics as soils on land with one important exception: since they have been deposited in deep, salt water, the clay particles are flocculated and, therefore, have a very loose structure and, correspondingly, very low densities and high porosities or void ratios.

Pelagic sediments blanket the abyssal deep. These deep sea sediments are clays and fine silts ground up by the surf and carried from the shore line out into the ocean; they also

contain wind-blown volcanic and cosmic dust and organic or authigenic materials formed in the deep ocean environment. Sediments containing more than 30 per cent of material of organic origin in the form of tests and frustules (or skeletons) of microscopic animals and plants are called oozes. The flora and fauna whose remnants make up the oozes may be either siliceous or calcareous. The oozes are classified as globigerina ooze, radiolarian ooze, pteropod ooze, or diatom ooze, depending upon the predominant type of animal or plant from which the organic portion of the sediment is derived. Red clay is a reddish-to-brown deposit which may be composed partially of terrigenous colloidal matter, the insoluble portion of organism tests and the products of submarine volcanism.

The floor of the Pacific Ocean is covered chiefly by these clastic, red clay deposits. The predominant sediments in the Atlantic and Indian Oceans are calcareous oozes; siliceous oozes are less widely distributed.

The prevalence of these sediments is shown in Table 2.1.

Table 2.1 Percentage of Sea Floor Covered by Sediments

Type of Deposit	Percentage of Sea Floor	Average Depth (in meters)
Shelf sediments (terrigenic)	8.3	100
Muds (hemipelagic)	18	<2300
Pelagic Sediments:		
Globigerina ooze (calcareous)	35.5	3600
Pteropod ooze (calcareous)	0.6	2000
Diatom ooze (siliceous)	8.5	3900
Radiolarian ooze (siliceous)	1.9	5300
Red Clay	28.3	5400

While the descriptive names suggest a clear-cut separation of the various sediments, in reality the sediments on the ocean floor grade into one another and it is somewhat arbitrary whether a specific sample is classified a clay or an ooze and, if the latter, what type of ooze since, again, the population of the organic constituents is usually a mixed one although sometimes with one skeletal species clearly predominating.

The type of pelagic sediment depends very much on the depth, the pressure, and the temperature of the water at the ocean bottom. This is so because the solubility of calcium

carbonate is a function of pressure, temperature, and carbon dioxide content of the water. Thus, calcareous oozes are deposited in more shallow basins where the water temperatures are higher and the pressures lower. In colder waters, diatoms with siliceous skeletons predominate over the calcareous foraminifera. The red clays are found in the coldest and deepest parts of the oceans.

The rates of deposition of recent pelagic sediments have been calculated and vary from 0.01 to 6 centimeters per 1000 years. For red clays, measurements gave a deposition rate of 0.07 to 0.2 centimeters per 1000 years; for globigerina ooze in the equatorial Atlantic Ocean, about 1.6 centimeters per 1000 years were found. These rates of sedimentation depend not only on the geographic location but also on the time of deposition because of the variation of climate over geologic time. According to Hamilton (1959) the observed rates of sedimentation as well as geochemical and other calculations of the total volume of sediment that should be present in deep sea basins, based on materials released in weathering, indicate that the average thickness of sediment solids on the ocean floor should be 1 to 3 kilometers. Seismic surveys in all oceans, on the contrary, report a sediment thickness of 0.1 to 0.5 kilometers, but also reveal that in many areas the surface sediments are underlain by other layers whose elastic wave transmission velocities are intermediate between those of sediment and the "basaltic basement" rock of the oceanic crust. This observation has led Hamilton (1959) to the conclusion that the lower layers are composed of rocks formed by the normal consolidation and lithification of the present types of deep sea sediments.

Rock outcrops occur over only a few per cent of the ocean floor. They are found usually in many isolated areas, particularly on the continental shelves and slopes, around islands, banks, seamounts, submarine ridges and mountain ranges.

2.3 Properties of Ocean Bottom Sediments

In recent years an increasing number of scientists have explored the properties of ocean bottom sediments. At present, direct observation of deep ocean sediments is limited to such samples as may be recovered by dredging or coring operations. These methods permit sampling of the sediment to only shallow depths below the sediment surface. Hopkins (1964) has prepared a comprehensive survey of marine bottom samplers, and Richards and Parker (1967) discuss the problems and methods of coring. Until recently drilling has been carried out only in the shallow waters of the continental shelves.

At present, however, the National Science Foundation is sponsoring a program to drill deep ocean cores at some thirty

locations in the Atlantic and thirty-six locations in the Pacific. This program promises to add significant information about the deeper layers of the deep sea sediments.

The topmost parts of the sedimentary column that could be sampled earlier have been studied and analyzed in detail. Physical properties such as water content, porosity, void ratio, density, particle size and shape, mineral composition, shear strength, consolidation characteristics, elastic wave velocities, attenuation, etc. can and have been determined.

Acoustic measurements play a major role in the study of physical properties of marine sediments. This is so because acoustic-seismic data are very easily obtainable and are plentiful. Nafe and Drake (1963) and Horn et al. (1968) attempt to correlate wave propagation velocities with such elementary properties as porosity, density and shear strength.

The results presented by Nafe and Drake show a fairly good correlation between compression wave velocity and porosity with but a moderate scatter. However, their data, unfortunately, show good discrimination only for sedimentary rocks at fairly low porosities. For unconsolidated ocean sediments measured velocities vary in a very narrow range, largely from 1.5 to 1.8 km/sec. while the porosities range from 35 to 85 per cent. However, the scatter is wide enough to make a correlation questionable. The correlation between wave velocity and density was found to be similar. Nafe and Drake suggest that much more information may become available in the near future from machine computations for dispersion analysis where computed phase and group velocities for assumed sediment structures and properties may be compared to actually observed values.

Horn et al. attempt a correlation between acoustical properties and other physical properties of sediment cores. They plot compressional wave velocities against porosity, moisture content, void ratio, dry density and wet density. The maximum sound velocities were found in a layer of silt from the Norwegian basin with a porosity of 35 per cent (1732 m/sec.) and in a layer of fine grained sand from the Mediterranean with a porosity of 34 per cent (1832 m/sec.). The lowest velocities were observed in clays with porosities varying from 70 to 84 per cent (1455 to 1480 m/sec.). However, again, the scatter of the data is wide. The conclusions of Horn et al., perhaps, deserve to be cited here: "The results of this study reveal that certain bulk and textural properties of unconsolidated marine sediments are indices of their acoustical characteristics. Of the bulk properties, a decrease in porosity, moisture content, and void ratio is matched by an increase in sound velocity. There is no correlation between sound velocity and either dry density or carbonate content.

"When shear strength is plotted against sound velocity, the data fall into distinct groups which, in general, reflect mean grain size and sediment genesis. There is an overall increase in sound velocity as the shear strengths get larger. From the limited amount of data on hand concerning ash layers, these sediments have constant sound velocities regardless of their shear strength.

"The shear strength is not considered to be a reliable index of the acoustical properties of unconsolidated deep sea sediments.

"A definite relationship exists between sound velocity and mean grain size. The coarser a sediment is, the higher is its sound velocity...."

Faas (1968) recently reported a relationship between the reflection coefficients and the porosity of ocean bottom sediments and claims that it can be used for predictive purposes. In addition, he observes that areas of sand could be classified as acoustically "hard," whereas areas of clay, from which reflections were greatly subdued, were classified as acoustically "soft." At any rate, it appears that acoustic measurements are capable of providing much more information than currently is obtained from their records.

Extensive investigations on mass physical properties of ocean bottom sediments were carried out by Richards (1961, 1962), Moore (1961, 1962, 1964), Harrison et al. (1964) and Hamilton (1956, 1964). Table 2.2 shows the data collected by Moore on more than 80 core samples from the North Pacific.

A comprehensive summary of most available data was presented by Keller (1967) who gave the results of tests on some 500 sediment cores (Atlantic, 300; Pacific, 200). He presented in particular the ranges of sediment types, shear strengths, water content, and dry and wet densities that can be expected in both ocean basins. For the problem of penetration the shear strength is the most critical property. Therefore, Figure 2.1 and Figure 2.2 reproduce the data presented by Keller on shear strength in the Atlantic and Pacific respectively. The shear strengths reported were measured on marine sediment cores by either a laboratory vane shear test or an unconfined compression test. The cores used varied in length from 12 inches to 20 feet, with an average of about seven feet.

Average shear strengths found in these cores range from less than 0.5 psi to 2.5 psi for the upper few feet of sea floor sediments. These extremely low values are caused by the extremely low values of dry density and the corresponding high values for porosity and water content of the sediments. An inspection of Figures 2.1 and 2.2 shows that sediments

Table 2.2: Physical Properties of Sediments and Bearing Capacities from the North Pacific (after Moore).

Sample	Water depth m	Water depth Fm.	Sample burial depth below surface cm	Sediment type	Wet density gm/cm³	Void ratio	Direct shear φ deg.	Direct shear c gm/cm²	Vane shear strength gm/cm²	Sensitivity	Bearing capacity psi†	Geomorphic areas
D35a			0 – 10	Sandy silt	1.60	1.82						
D35b			0 – 10	Silty sand	1.65	1.53			11.66	3.10	1.320	San Diego
D35c	13	7	0 – 10	Silty sand	1.67	1.38			12.16	3.50	1.375	Bay, California
D36a	To	To	0 – 10	Sandy silt	1.56	1.97			16.73	7.50	1.893	
D36b	50	27	0 – 10	Sandy silt	1.64	2.29			10.12	3.50	1.450	
D40a			0 – 10	Sandy silt	1.64	1.70			9.84	8.20	1.114	
D51a			0 – 10	Silty sand	1.65	1.50			15.54	7.40	1.757	
P-2	105	57	0 – 20	Silty sand	1.88	0.87			..	..	..	
P-4	137	75	0 – 10	Silty sand	1.93	0.72			9.21	..	1.042	Open continent
P-5	110	60	0 – 10	Sandy silt	1.72	1.62			8.72	3.8	0.986	shelf
P-6	90	49	0 – 10	Silt	1.68	1.53			9.07	6.0	1.025	
P-7	88	48	0 – 10	Silt	1.63	1.82	20	13.76	15.25	4.7	1.725	
P-10	93	51	0 – 10	Silty sand	1.90	0.86			7.03	7.7	0.795	
P-11	90	49	0 – 10	Silt	1.77	1.07			17.72	7.2	1.988	
P-13	121	66	0 – 10	Silty sand	1.88	1.03	..	..	14.84	8.8	1.678	
P-14	126	69	0 – 10	Silty sand	1.89	0.88			10.62	2.7	..	
P-15	102	56	0 – 10	Sandy silt	2.00	2.27	..	..	17.86	6.2	..	
P-16	77	42	0 – 20	Silt	1.73	1.22	36	19.12	5.77	7.5	..	
P-17	93	51	0 – 10	Clayey silt	1.74	1.40	..	..	10.97	6.5	..	
L1-1-57	84	46	0 – 5	Sandy silt	1.84	0.95	..	..	9.21	2.9	1.042	
L2-1-57	66	36	5 – 10	Silt	1.69	1.38	26	19.90	4.01	3.35	0.453	
CB11a	84	46	0 – 15.4	Silt	1.83	1.09	..	..	..	..	..	
CB11b	84	46	15.4 – 30.4	Sandy silt	1.84	1.05			7.59	30.0	0.859	
CB12a	84	46	8.9 – 24.1	Sandy silt	1.82	1.10	..	..	14.13	9.10	..	
									7.59	8.30	..	
2-11-55	650	355	5 – 8		1.39	3.02						
2-11-55	650	355	89 – 94		1.59	1.82	33	23.98	3.16	..	0.358	California
CB1a	1000	547	0 – 12.7		1.39	3.90	..	..	..	..	..	continental
CB1b	1000	547	33.0 – 45.7		1.41	2.91	..	..	14.83	3.40	1.678	borderland
CB2a	890	487	40.6 – 53.3		1.45	2.70	..	..	25.60	7.00	..	basins and
CB2b	890	487	0 – 12.7		1.40	2.97	15.5	15.80	38.67	5.40	..	slopes
CB3a	1142	624	0 – 12.7	Clayey silt	1.30	4.29	..	..	20.67	5.30	2.338	
CB3b	1142	624	22.8 – 35.6		1.34	3.85	..	..	7.17	1.90	0.810	
CB3c	1142	624	40.6 – 53.3		..	..	..	..	14.83	11.10	..	
CB4a	1173	641	0 – 12.7		1.29	5.94	..	..	19.97	3.70	..	
CB4b	1173	641	15.2 – 27.9		1.36	3.90	..	..	7.87	5.90	0.890	
CB5a	1198	655	0 – 12.7		1.29	2.92	..	..	17.72	7.20	..	
CB5b	1198	655	17.8 – 33.0		1.33	3.98	..	..	7.17	6.80	0.810	
CB5c	1198	655	33.0 – 45.7		1.35	3.59	24	13.27	14.62	10.90	..	
CB6b	1218	666	17.8 – 33.0		1.35	3.74	..	..	13.50	4.30	..	
CB6c	1218	666	35.6 – 48.3		1.37	3.50	22	23.43	12.87	8.30	..	
CB7a	132	72	0 – 12	Silt	1.73	1.07	..	..	21.52	12.20	..	
CB8a	183	100	0 – 15.2	Silt	1.58	1.97	..	..	7.17	7.80	0.810	
CB8b	183	100	15.2 – 30.5	Clayey silt	1.59	1.91	..	..	15.26	6.20	1.725	
CB8c	183	100	30.5 – 45.7	Clayey silt	1.59	1.87	54	16.56	21.52	6.00	..	
CB9a	179	98	0 – 15.2	Silt	1.60	1.73	..	..	38.46	4.80	..	
CB9b	179	98	15.2 – 31.8	Clayey silt	1.59	1.93	..	..	8.09	6.10	1.193	
CB9c	179	98	30.5 – 40.6	Clayey silt	1.59	1.86	30	23.43	26.30	6.00	..	
CB10a	127	69	0 – 15	Sandy silt	1.64	1.65	40	15.02	..	..	..	
AHF4740	507	277	2 – 7	Silt	1.80	1.71	30	11.25	26.51	4.90	..	
AHF4740	507	277	143 – 150	Clayey silt	1.71	1.16	30	36.35	16.45	1.62	1.869	
CB13a	99	54	28.6 – 43.8		1.90	0.85	..	..	33.19	1:89	3.775	
CB13b	99	54	13.3 – 28.6		1.90	0.86	..	..	14.41	4.90	..	
CB13c	99	54	0 – 13.3		1.88	0.93	..	..	20.67	6.50	..	
CB14a	99	54	3.2 – 19.7	Sandy silt	1.90	0.95	..	..	14.41	15.80	1.630	
CB15a	137	75	6.4 – 21.6		1.75	1.33	..	..	11.46	8.60	..	
CB16a	137	75	20.9 – 36.2		1.80	1.24	..	..	19.76	7.20	..	
CB16b	137	75	5.7 – 20.9		1.78	1.17	..	..	17.51	10.00	..	
									23.13	13.20	..	
PE-1	2748	1503	145	Silty clay	1.42	2.73	22	28.7				
PE-2	3660	2000	0 – 4	Silty clay	1.32	..	..	..	3.15	5.8	0.358	Continental
									11.57	9.2	1.312	slope
CK-5	5399	2952	0 – 5	Silty clay	1.14	1.22	..	..				
CK-5	5399	2952	85 – 88	Clayey silt	1.30	3.83	47	19.90	7.23	7.20	0.819	Deep-sea
CK-7	5175	2830	0 – 5	Silty clay	1.36	3.15	..	..	..	..	..	terrigeneous
CK-7	5175	2830	65 – 69	Silty clay	1.30	3.12	..	..	11.18	3.80	1.265	
CK-7	5175	2830	162 – 171	Clayey silt	1.36	2.89	52	17.86	53.08	11.00	..	
MUK-7	4722	2582	125	Silty clay	1.42	2.89	0	19.1	..	..	..	
MUK-8	4690	2564	100	Silty clay	1.34	3.29	33	30.6	..	3.1	2.170	
PO6a	3680	2012	0 – 19.1		..	..	..	..	..	..	..	
PO6b	3680	2012	19.1 – 38.1		1.31	..	..	..	11.89	3.70	1.345	
PO6c	3680	2012	38.1 – 57.2		..	4.65	..	..	22.64	2.70	..	
PO6d	3680	2012	57.2 – 76.3	Silty clay	1.32	4.88	..	..	16.59	3.50	..	
PO6e	3680	2012	76.3 – 95.3		..	4.15	..	..	23.70	3.40	..	
PO7	3720	2034	0 – 15		1.49	4.49	..	..	35.50	18.00	..	
PO8	4610	2521	0 – 15	Clayey silt	1.37	2.27	..	..	5.42	3.70	0.605	
CK1a	5660	3095	5 – 10		1.45	3.61	..	..	13.21	..	1.495	
CK-1a	5660	3095	55 – 60		1.44	2.76	14	10.18	15.68	3.06	1.774	
CK-1a	5660	3095	134 – 139	Clay	1.43	2.95	..	..	12.10	3.98	..	
CK-2	5670	3100	200		1.26	2.80	32	14.80	35.86	5.60	..	
CK-3	5692	3112	0 – 5	Silty clay	1.41	5.25	..	..	101.90	2.94	..	
CK-3	5692	3112	113 – 118	Silty clay	1.36	3.33	..	..	8.16	5.15	0.922	
CK-4	5399	2952	0 – 5	Clay	1.35	2.91	..	..	63.42	8.41	..	
CK-4	5399	2952	154 – 163	Silty clay	1.39	3.46	..	..	5.91	3.50	0.678	
						2.56	34	36.90	..	..	..	

with a shear strength from 0.5 to 1.0 psi predominate in the North Atlantic. The highest strengths found in the basin range from 1.0 to 1.5 psi and are associated with calcareous deposits. Values of less than 0.5 psi are often found in coastal areas where local conditions of drainage or current strongly influence the depositional environment. Another area of low shear strength is the red clay deposit. The red clay deposits predominate and cover a large portion of the area in the North Pacific basin. It is for this reason that, in general, the sediments in that basin are weaker than those in the North Atlantic. As far as general deviations from these patterns go, Keller writes:

"In contrast to the North Atlantic, large portions of the North Pacific sea floor are covered with sediments whose average shear strength is less than 0.5 psi. These areas coincide closely with the distribution of 'red clay' and comprise a major portion of the sea floor. Localities of higher shear strength occur within the area of low shear strength as a result of changes in bottom topography influencing the depositional environment. Local currents in and around topographic features can account for changes in the distribution of certain sediment properties. It has been found that on topographic 'highs' shear strengths are slightly higher than in the surrounding areas. This may be attributed to the winnowing effect of currents which tend to keep the 'highs' free of softer sediments.

"Shear strength values are generally higher along the margins of the basin and in the lower latitudes. Coarser sediments and shallower water depths, normally found closer to land, account for the general pattern shown in Figure 2.2. In areas of increased calcium carbonate, such as the low latitudes, shear strength is also found to increase. The highest range of values 2.0 to 2.5 psi observed thus far occur in the calcareous oozes of the Pacific basin (Figure 2.2).

"A comparison of the overall data presented in Figures 2.1 and 2.2 indicates that North Atlantic sediments possess relatively higher shear strengths than do those of the North Pacific. It is also evident from these data, that the North Pacific basin can be divided into two sedimentary provinces, each distinctly different from the other. The northern portion consists of sediment possessing strengths ranging from 0.25 to 0.5 psi; in the lower latitudes, values of 1.0 to 1.5 predominate...."

In addition to the shear strength, the porosity and the water content of the ocean bottom sediments also appear to have some albeit reduced and indirect influence on the penetration problem. The former because of its measure of solid content and hence, its point-to-point contacts and bonds in the sediment, the latter because of the pore water pressures

that result in any straining or deformation process in a fine grained sediment. In general, the water content of ocean bottom samples ranges from 40 per cent to 200 per cent with the majority of samples in the range of 80 to 150 per cent; the porosity ranges from 40 to 85 per cent with the majority of the samples in the range of 60 per cent to 80 per cent.

2.4 Variation of Sediment Strength with Depth

Most seismic and acoustic data on wave propagation indicates that wave velocities increase with depth in the sediment. Also, since the overburden pressure in the sediment increases linearly with depth, one would assume that gradual consolidation takes place in the sediment leading to a gradual decrease in porosity, water content and void ratio and a corresponding increase in shear strength with depth. Actual measurements of the variation of these properties with depth show rather interesting and unexpected results (Hamilton, 1964; Moore, 1964).

Contrary to what one would expect, the porosities and void ratios do not consistently decrease with depth. Except for some decrease close to the sediment surface, the porosity was found to remain constant to depths of up to 140 meters (460 feet). Since the overburden pressure clearly increases with depth, this constancy of the porosity and, hence, of the soil skeleton is only explicable by the fact that, simultaneously with the pressure, the strength also increases. This indeed was found to be true. Various attempts to correlate sediment strength with other mass properties were rather negative except for an apparent correlation of increased shear strength with relative percentage of montmorillonite and rather good agreement between carbonate content and strength. Moore suggests the good agreement between carbonate content and strength to be due to incipient cementation by crystalization of carbonate solutions. Many investigators have observed that slow deposition and great age can contribute to sediment strength. This strength may be attributable both to chemical cementation or to rigid hydrogen bonds of adsorbed water molecules. Both have been suggested to result from age and extended exposure to chemical solutions.

Figure 2.3 shows the variation of sediment strength with depth as a function of the rate of deposition. It is quite evident that the rate of deposition and, hence, the age of the sediment has a most significant influence on the variation of strength with depth. The data show a linear increase of strength with depth. Similarly, Hironaka (1966) reported strength variations close to the surface by performing vane shear tests at 5-inch intervals in 2 to 3-foot long cores taken from the sediment surface near San Miguel Island. By a stepwise, linear regression analysis, he derived the following equation to fit his data:

$$VSS = k_1(D) + k_2(LL) + k_3(MD) + k_4 \qquad (2.1)$$

where

VSS = vane shear strength, psi
D = depth in sediment, inch
MD = mean grain diameter, mm
LL = liquid limit, per cent
k_n = constants (n = 1, 2, 3, 4)

The first term of equation (2.1) again suggests a linear increase of strength with depth. Although Hironaka's analyses were based on laboratory measurements, he believes that these relationships are also valid for in situ strength values. Data reported by Bayles (1965) from cores taken at the site of the Thresher disaster also reveal a linear increase of the shear strength with depth from a value of 0.3 psi at the sediment surface to 1.7 psi at a depth of 200 feet.

2.5 Environmental Effects on Properties of Ocean Sediments

Most of the data available on ocean bottom sediment strength are from laboratory tests by vane-shear, direct-shear box or triaxial compression tests.

This means that the test specimens were removed from their in situ environment and were tested for strength and other properties in the laboratory. It is evident that sampling and removing from the ocean bottom environment exposes the test samples to an entirely different regime than that experienced by the ocean bottom soil in situ.

The question is if and how much such a change in the environment will affect the properties, particularly the shear strength. Crisp (1968) presents an analysis according to which the strength should decrease by 10 to 15 per cent due to the change in particle spacing from the expansion of the pore water when a sample is brought from a water depth of 12,000 feet to the surface. However, in his calculations he does not consider the effect of the shear distortion that is caused in a sample. Since the radial expansion in the core sample is effectively prevented by the sampler, all expansion necessarily must take place in the axial direction.

Crisp also analyzes the effect of dissolved gases (oxygen and carbondioxide) and concludes that it is negligible. Vey and Nelson (1967) performed direct shear tests and vane shear tests in a seawater environment with a hydrostatic environmental pressure chamber capable of providing up to 10,000 psi pressure in a temperature environment of 1 to 3°C. The

results are somewhat inconclusive due to a wide scatter of the data, but their tests indicate that the direct shear tests showed a decrease in shear strength with increasing environmental pressures, while the vane shear test showed an increase in shear strength with environmental pressures (as is suggested by Crisp's analysis) for the more plastic soil but a decrease for the less plastic soil tested. Whatever the effect, in this writer's opinion, the data reported by Vey and Nelson have such a wide scatter that it is difficult to make any conclusions based on these experiments. Certainly, variations in strength of 10 to 15 per cent would not be revealed by the amount and range of data reported by them. This should not be considered as a criticism of their work. The problem of making shear strength measurements at the high void ratios and the low strength properties of ocean bottom sediments is an enormously difficult one.

Another factor that enters the discussion here is the problem of sample disturbance. In addition to the stress release, the sampling procedure may also cause considerable disturbance or remolding. The problems and requirements for proper coring and minimum disturbance were discussed by Richards and Parker (1967).

One might conclude that the extremely low, measured values of the shear strength of ocean bottom sediments must be caused by a combination of stress release, pore water expansion, and sample disturbance, and that in situ strength is considerably higher. However, the limited data available on in situ observations (Hironaka and Smith, 1967) as well as the fairly high porosities of the sediments which, really, are not in doubt preclude a gross divergence from the measurements made on cores. Undoubtedly, all the factors cited above introduce errors into the measurement of shear strength and in situ strength should be higher than the one obtained from cores. However, a drastic increase such as one order of magnitude cannot be expected, but rather an increase of perhaps 30 to 50 or, at most, 100 per cent.

The best solution for overcoming this difficulty would be a relatively simple device capable of measuring the in situ strength of a sediment quickly, reliably, and cheaply. The most promising approach for developing such an instrument is believed to be a penetrometer-type instrument mounted with an accelerometer as developed by Scott (1967) or Schmid (1966). Data from such instruments could be collected easily and quickly. It would have the additional advantage that the results are immediately available and the strength test is performed in the natural environment of the ocean bottom soil. Impact deceleration data could be transformed into shear strength data by relations such as given by equations (4.21), (4.22), (4.23), (4.28) or (4.36) of Chapter 4.

2.6 Summary

While we do know, in a general way, the nature and characteristics of ocean bottom sediments, our knowledge in detail and at specific locations is extremely scant or nil. For example, the information presented by Keller (1967) is based on the results of some 300 sediment cores in the North Atlantic. This amounts to an average coverage of one sample per 30,000 square miles. In the Pacific the situation is even worse. It is quite evident, therefore, that the extrapolation of these data has been carried extremely far. While the variation of soil properties of the ocean bottom in a horizontal direction is not likely to be as great as it is on land, nevertheless such variations do exist and our present knowledge of ocean bottom sediments, their properties, and their topography will present a challenge to the best minds and skills for some time to come.

3.0 Free Fall Velocity and Trajectory

As stated before, the most important parameter determining the penetration characteristics is the velocity at impact. In addition, the direction of the impact as well as the orientation of the object at first contact are controlling factors. Thus, it becomes necessary to evaluate in detail the velocity, attitude, and trajectory of an object falling to the ocean bottom.

3.1 Hydrodynamic Drag

When an object falls through a fluid at rest the gravitational pull tends to accelerate the object in the direction of the gravitational field. At the same time, the fluid exerts a force on the object in a direction opposite to that of the motion. This force is called the profile drag F_D, or "resistance."

Fundamentally, the total force on each element of the object's surface can be resolved into a formal and a tangential component as shown in Figure 3.1.

The normal components are pressure forces and their resultant against the direction of motion is the pressure drag $(F_D)_p$.

This pressure drag is given by:

$$(F_D)_p = \int_A p \sin\theta \, dA \tag{3.1}$$

The tangential components are viscous or frictional resistances and their resultant against the direction of the motion is called the friction drag $(F_D)_f$.

The friction drag is given by:

$$(F_D)_f = \int_A \tau \cos\theta \, dA \tag{3.2}$$

The total drag, then, is the sum of both components:

$$F_D = (F_D)_p + (F_D)_f = \int_A p \sin\theta \, dA + \int_A \tau \cos\theta \, dA \tag{3.3}$$

The relative magnitude of the two drag components depends very much on the shape and orientation of the falling object. For a streamlined body with its axis parallel to the motion, the stream lines conform very well to the surface configuration on the body. Here, the pressure drag is very small and is of the same order of magnitude as the friction drag.

For a plate placed perpendicular to the motion (see Figure 3.2), the total drag is almost entirely due to pressure differences between the upstream and downstream sides, while the friction drag is practically negligible. On the other hand, if the plate is placed parallel to the motion, the pressure drag is practically zero and the total drag is, therefore, essentially equal to the friction drag.

In general, the total resistance or drag is measured experimentally and is then given in terms of the density of the fluid, the velocity of motion, the projected area of the object in the direction of motion, and a drag coefficient C_D:

$$F_D = \frac{1}{2} C_D A \rho_f u^2 \qquad (3.4)$$

where F_D = drag force (pounds)

ρ_f = density of fluid = $\frac{\gamma_f}{g} \left(\frac{\text{lb sec}^2}{\text{ft}^4} \right)$

γ_f = unit weight of the fluid (lb/ft^3)

u = velocity of object (ft/sec)

A = projected area normal to the direction of flow or motion (ft^2)

C_D = drag coefficient

3.2 Drag Coefficients

The drag force against an object depends on its shape, its orientation, the Reynolds number, and also, on the nature of the incident flow. Because of the infinite variety of shapes it is possible to consider only a few typical forms.

A) Smooth Flat Plate of Length 1 at Zero Angle of Attack in Zero Pressure Gradient. The drag is due to the shear stresses on the plate and is said to be frictional. If the boundary layer is laminar from the leading edge to a distance x along the plate and the total drag is given by:

$$F_D = \frac{1}{2} C_f A \rho_f u^2 \qquad (3.4a)$$

the drag coefficient is given by Blasius as:

$$C_f = \frac{1.328}{\sqrt{R_x}} \qquad (3.4b)$$

where $R_x = ux/\nu$ is the Reynolds number and ν is the kinematic viscosity of the fluid (ft^2/sec).

B) Streamline Forms. Streamline forms are defined as those along which there is no separation of flow. Since a form on which separation occurs at low Reynolds number, or in a low-turbulence stream, may become separation-free at higher Reynolds numbers, or in a stream of higher turbulence, whether or not a form is streamlined depends upon these conditions.

The drag of a streamline form is principally frictional, i.e., due to its shear stresses. The boundary layer is laminar up to some transition point x_T (which fluctuates even under steady conditions and can be defined only in a statistical sense), beyond which it becomes turbulent. At Reynolds numbers $R = uc/\nu < 10^5$, in which c is the chord of the profile, laminar separation occurs unless the thickness-chord ratio d/c is less than 0.1 (see Figure 3.4). The experimental results of tests of various streamlined shapes, including elliptical sections, can be summarized in the empirical formula:

$$C_D = 2C_f \left(1 + \frac{d}{c}\right) + \left(\frac{d}{c}\right)^2 \qquad R < 10^5,\ \frac{d}{c} < 0.5 \qquad (3.5)$$

in which C_f is the drag coefficient for a flat plate with a laminar boundary layer (equation 3.4b), and C_D is the drag coefficient for the profile

$$C_D = \frac{F_D}{\frac{1}{2}\rho_f u^2 c}$$

At higher Reynolds numbers turbulent separation occurs except on certain forms having a thickness ratio $d/c < 0.4$. An approximate expression for the drag coefficient (except for "laminar-flow" forms) is then

$$C_D = 2C_f \left[1 + k\frac{d}{c} + 60\left(\frac{d}{c}\right)^4\right] \qquad R > 10^7,\ \frac{d}{c} < 0.4 \qquad (3.6)$$

in which the value of k depends primarily upon the position of the point of maximum thickness x_M, varying approximately from $k = 2.0$ when $x_M/c = 0.3$ to about $k = 1.2$ when $x_M/c = 0.5$, and C_f is now the drag coefficient for a flat plate with a turbulent boundary layer.

In the intermediate range of Reynolds numbers, $10^5 < R < 10^7$, the drag coefficient is sensitive to the pressure distribution along a particular profile and to disturbances in the boundary layer. The turbulent shear stresses downstream from x_T tend to increase the drag coefficient; on the other hand, if laminar separation had been occurring at lower Reynolds numbers, it would now be replaced by turbulent separation or

no separation, which would tend to decrease the drag coefficient. For most forms of thickness ratio $d/c > 0.10$, the drag coefficient in this range is less than that given by equation (3.5). A typical curve showing a composite of the measured drag coefficients vs. Reynolds number of various forms of thickness ratio $d/c = 0.25$ is shown in Figure 3.3.

C) Laminar Flow Profiles. A class of forms, the laminar profiles, designed to maintain a laminar boundary layer over a large part of the surface up to high Reynolds numbers ($R \approx 10^7$), has drag coefficients differing from equations (3.5) and (3.6). These forms have their maximum thickness occurring between 40 and 65 per cent of the chord from the leading edge, a small nose radius of curvature, and negative curvature near the sharp trailing edge (Figure 3.4). Such a shape results in a negative pressure gradient up to about the point of maximum thickness, which consequently stabilizes the laminar boundary layer to much higher Reynolds numbers than for more normal shapes. At Reynolds numbers $R < 10^5$, the drag coefficient would be somewhat larger than that given by equation (3.5) because of more violent laminar separation, but at higher Reynolds numbers, exceeding $R = 10^7$, turbulent separation would occur, but with the boundary layer still laminar ahead of the point of maximum thickness. In their range of effectiveness these forms have about half of the drag of conventional profiles of the same thickness ratio.

D) Blunt Forms. The drag of a blunt form is principally due to its pressure distribution, which differs radically from that for inviscid flow because much of the after end of such a body is immersed in a zone of separation. Separation on a body occurs either at slope discontinuities in the body profile (sharp edges) or at positions in the boundary layer where a positive pressure gradient is beginning to cause reverse flow of the slowly moving fluid near the wall. In the latter case separation occurs farther downstream in a turbulent boundary layer than in a laminar one because fresh momentum is transported to the wall by the process of the random turbulent motions.

A phenomenon observed in the flow about blunt, two-dimensional forms is the periodic, alternate shedding of vortices from the opposite sides at the rear of the body, forming in the wake two staggered rows of uniformly spaced vortices, called a vortex street. It was shown theoretically by von Kármán, by analyzing the stability of such an array, that the ratio of distance between the rows to the distance between successive vortices in a row, h/b, satisfies the equation

$$\cosh \frac{\pi h}{b} = 2 \qquad (3.7)$$

which gives the approximate solution h/b = 0.2806, a value in very good agreement with experiment. The theory also yields an expression for the resistance coefficient of the body,

$$C'_D = \frac{F_D}{\frac{1}{2}\rho_f u^2 d} = \frac{2b}{d}\left[0.7936\,\frac{u_v}{u} - 0.3141\left(\frac{u_v}{u}\right)^2\right] \qquad (3.8)$$

in which d is the maximum width of the profile, and u_v is the velocity of the vortices, a result of the correct order of magnitude. It cannot be used to predict drag, however, since the values of b/d and u_v/u cannot yet be obtained by theory. The frequency n with which the vortices are shed is of great practical interest since the body experiences an oscillating lift as the circulation about it varies from positive to negative. Both theory and experiment show a relationship between the drag coefficient of a body and its dimensionless frequency, S = nd/u, called a Strouhal number. A composite, empirical fit to the data from a wide range of blunt bodies is given by the formula

$$S = \frac{0.21}{C_D^{3/4}} \qquad (3.9)$$

In the range of Reynolds numbers $10^3 < R < 10^8$, blunt bodies with sharp edges show little variation in drag coefficient. The coefficients for some typical cases are given in Figure 3.5.

Blunt but rounded forms show a remarkable reduction in drag coefficient over a small range of Reynolds numbers in which transition from laminar to turbulent separation occurs. The designations "subcritical" or "supercritical" are used to indicate the Reynolds-number ranges in which laminar or turbulent separation occurs. Curves showing the variation of C'_D with R for a circle and a 2:1 ellipse are shown in Figure 3.6. The variation of the drag coefficient with thickness ratio of ellipses is given for both the subcritical and supercritical ranges of Reynolds numbers in Table 3.1.

Table 3.1 Drag Coefficients for Elliptical Sections

c/d	C'_D	
	Subcritical	Supercritical
1	1.17	0.40
2	0.88	0.20
3	0.42	0.12
4	0.37	0.10
6	0.30	0.10
8	0.28	0.12

If the vortices shed by a blunt cylinder of width d cause it to oscillate, the width of the resulting vortex street is increased approximately by the double amplitude of the oscillation, 2a, and the resulting drag is also increased approximately by the factor 1 + 2a/d. Such vibrations commonly occur in cables situated at an angle to a current.

The basic principles recited in this Section 3.2 follow closely the presentation by L. Landweber in the Handbook of Fluid Dynamics, Section 13 (Streeter, 1961).

3.3 Terminal Velocity

If an object begins its fall through sea water with zero velocity it starts accelerating and develops speed in the direction of the gravitational force. Simultaneously with the build-up of speed, it experiences the drag force which, as equation (3.4) shows, grows with the square of the velocity. Thus, very soon a point will be reached where the drag force has grown as large as the gravitational pull and, therefore, no further increase in the velocity is possible. The velocity at which this occurs is called the terminal velocity because this is the highest velocity the object will attain and maintain throughout its fall. Stokes calculated a terminal velocity for a spherical object falling in a viscous fluid when the viscous forces predominate over the inertia forces. The result is given by the well-known Stokes' law which equates the drag force F_D encountered by a sphere of radius r with the net downward force exerted by the gravitational field:

$$F_D = 6\pi\mu r u = \frac{4}{3}\pi r^3(\rho_s - \rho_f)g \qquad (3.10)$$

where μ is the dynamic viscosity of the fluid (lb.sec/ft^2)
ρ_f is the density of the fluid (lb.sec^2/ft^4)
ρ_s is the density of the sphere (lb.sec^2/ft^4)
u is the terminal velocity (ft/sec)

Rearranging terms, we find the terminal velocity u given by:

$$u = \frac{2}{9} r^2 g \frac{\rho_s - \rho_f}{\mu} \qquad (3.10a)$$

Equation (3.10) was obtained by neglecting the inertia forces in the Navier-Stokes equation and, therefore, is only valid for very small Reynolds numbers (R < 0.5). Since R is given by ur/ν, where ν is again the kinematic viscosity (ft^2/sec), Stokes' law is applicable only for very small velocities or very small particles falling in relatively viscous fluids.

In general, the Reynolds numbers for the phenomena we are investigating here will be much higher (our range of interest will extend from R = 1000 to R = 500,000). Thus, Stokes' law is not applicable to the problem at hand.

However, the basic approach of Stokes for calculating the terminal velocity is still valid, provided we introduce the proper driving and resisting forces. The drag or resisting force for any object is given by equation (3.4). The driving force for any free-falling object through a fluid is given by its weight W minus its buoyant force B. Thus, the general equation of equilibrium at the terminal velocity u is:

$$\frac{1}{2} C_D A \rho_f u^2 = W - B = V(\gamma_o - \gamma_f) \qquad (3.11)$$

where V is the volume of the object, γ_o its unit weight, and all other terms have been defined before.

Since the drag coefficient depends on the shape of the falling body, it will be convenient, for the sake of illustration, to select a shape for the purpose of discussion. Also, it is necessary to select the attitude or orientation of the object during fall, and the Reynolds number.

The procedure, then, is one of successive approximations: we first guess the terminal velocity u and calculate the resulting Reynolds number: $R = uc/\nu$. For this Reynolds number we can find the drag coefficient from a diagram such as Figure 3.6, provided we know the shape, attitude, and trajectory of the falling object. Knowing also the unit weight and volume of the object, we have all the terms necessary to calculate the velocity u from equation (3.11). If this calculated velocity is different from the initially assumed one, successive approximations are made and the cycle is repeated until assumed and calculated velocities are essentially in agreement.

The shape of the object of most interest for our considerations here may be a cylindrical body with hemispherical ends as shown in Figure 3.7. If the length of the cylinder is given by L and its diameter by D, the overall length of the body will be L + D and the slenderness ratio L/D will describe the geometric configuration of the object.

Values of the drag coefficients C_D for several slenderness ratios L/D and through a range of Reynolds numbers from R = 1,000 to R = 500,000 now have to be calculated.

3.4 Cylinder Falling with Axis Horizontal

If a cylinder such as shown in Figure 3.7, but without tail fins, and properly balanced, falls through a fluid, it will maintain its axis in a horizontal position. The drag coefficients for a cylinder falling vertically, while its axis remains horizontal, are taken from data given by Prandtl and Tietjens (1957) for an infinitely long cylinder. For a finite length cylinder, the drag coefficient will be smaller because of side leakage. This is so because flow around the ends into the reduced pressure zone above the cylinder occurs. This causes a different pressure distribution which results in a reduced pressure drag. The smaller the L/D ratio, the smaller will be the pressure drag and, hence, the drag coefficient. For L/D = 0 the pressure coefficient must be that of a sphere.

Prandtl and Tietjens also evaluated the reduction of the drag coefficient due to the finite length of a cylinder for various L/D ratios at a Reynolds number of 100,000. Assuming the reduction of the drag coefficient at other Reynolds numbers to be the same, we calculated values of the drag coefficients C_D for various slenderness ratios and Reynolds numbers. This assumption is substantiated by other data given by Schlichting (1968). The values thus obtained are given in Table 3.2.

Experimental verification of the values in Table 3.2 has been carried out by several investigators and they have been generally confirmed. Table 3.2 summarizes the most important results. Thus, using equation (3.4) and the coefficients of

Table 3.2

Drag Coefficients C_D for Cylinders Falling with Axis Horizontal

Reynolds Number	Slenderness Ratio L/D								
	L/D=∞	L/D=50	L/D=20	L/D=10	L/D=5	L/D=3	L/D=2	L/D=1.0	L/D=0
1	10.0	8.15	7.60	6.7	6.0	5.9	5.6	5.2	
10	2.7	2.20	2.05	1.81	1.62	1.59	1.51	1.40	
100	1.45	1.18	1.10	.97	.87	.85	.81	.76	1.1
1,000	1.00	.82	.76	.67	.60	.59	.56	.52	.48
10,000	1.10	.90	.84	.74	.66	.65	.62	.57	.40
50,000	1.20	.98	.91	.80	.72	.71	.67	.62	.48
100,000	1.20	.98	.91	.80	.72	.71	.67	.62	.44
200,000	1.15	.94	.87	.77	.69	.68	.65	.60	.41
300,000	0.80	.65	.61	.54	.48	.47	.45	.42	.095
500,000	0.30	.24	.23	.20	.18	.18	.17	.16	.090
1,000,000	0.35	.29	.27	.24	.21	.21	.20	.18	.15

Table 3.2, the total drag force on a cylinder as depicted in Figure 3.7, but without fins, sinking horizontally is given by:

$$F_D = \frac{1}{2} C_D D(L + \frac{1}{4} \pi D) \rho_f u^2 \qquad (3.12)$$

3.5 Cylinder Falling with Axis Vertical

If tail fins are added to the cylinder as shown in Figure 3.7, or, if the center of gravity and the center of buoyancy in the cylinder do not coincide, the cylinder will eventually fall with its cylindrical axis vertical.

We assume the front and back ends of the cylinder to be hemispherical. The total drag for the cylinder then will be equal to the drag on a sphere of diameter D plus the skin friction drag on the cylindrical surface and on the tail fins. This skin friction drag may be taken to be equal to that for a flat plate having an area and length equal to that of the cylinder body. It is taken from the classical Blasius solution for viscous drag on a flat plate at zero incidence. The total drag, hence, of the cylinder with its axis parallel to the velocity vector is given by:

$$F_{total} = F_{sphere} + F_{cylinder} + F_{fins} \qquad (3.13)$$

The drag components for the sphere are given by:

$$F_{sphere} = \frac{1}{8} C_{sphere} \pi D^2 \rho_f u^2 \qquad (3.14)$$

Again, the dimensionless drag coefficient C_{sphere} is a function of the Reynolds number R. Some values for C_{sphere} for a range of Reynolds numbers $1 < R < 10^6$ are given in Table 3.3.

Table 3.3

Drag Coefficients C_D for Spheres as a Function of Reynolds Numbers

R	C_{sphere}
1	28
10	4.2
100	1.1
1,000	.48
10,000	.40
50,000	.48
100,000	.44
200,000	.41
300,000	.095
500,000	.09
1,000,000	.15

Experimental results given by Schlichting (1968) are shown in Figure 3.8. The sudden drop in the drag coefficient from $R = 2 \times 10^5$ to $R = 5 \times 10^5$ is caused by the change in the regime of flow in the boundary layer going from laminar to turbulent.

The viscous skin friction drag on the cylinder surface is given by:

$$F_{cylinder} = \frac{1}{2} C_{cyl} \pi D L \rho_f u^2 \qquad (3.15)$$

The drag coefficient C_{cyl} is the same as that for a flat plate at zero incidence and is given by:

$$C_{cyl} = 1.328 R_L^{-\frac{1}{2}} \qquad (3.16)$$

It should be noted that the Reynolds number R_L for this case is given by:

$$R_L = \frac{uL}{\nu}$$

where ν is again the kinematic viscosity.

Since the drag contribution of the fins also may be considered to come from the skin friction on a flat plate, the effect of the friction drag on both the cylinder surface and the fins is given by:

$$F_{cyl} = .664 R_L^{-\frac{1}{2}} \pi D L \rho_f u^2 \qquad (3.17)$$

and

$$F_{fins} = .664 R_F^{-\frac{1}{2}} A_F \rho_f u^2 \qquad (3.18)$$

It should be noted that $R_F = u\ell/\nu$ where ℓ is the length of the fins and A_F is the total, wetted area of all fins.

Thus, the total drag for the cylindrical object falling with its axis vertical is:

$$F_{total} = [\pi D(\frac{D}{8} C_{sphere} + .664L(R_L)^{-\frac{1}{2}}) + .664(R_F)^{-\frac{1}{2}} A_F] \rho_f u^2 \qquad (3.19)$$

Another approximate solution for calculating the drag of a cylindrical body in three-dimensional flow parallel to the cylinder axis has been given by Glauert and Lighthill (1955). They present their results in terms of a table of logarithmic values of Reynolds number vs. drag coefficient. These are given in Table 3.4.

Table 3.4

Viscous Drag Coefficient vs. Reynolds Number for Finite Cylinder (after Glauert and Lighthill)

$\log_{10}(\frac{\nu L}{ua^2})$	$\log_{10}(F_d/\rho_f u^2 \pi a^2)$	
-3.0	2.64	
-2.5	2.89	
-2.0	1.16	
-1.5	1.44	
-1.0	1.73	
- .5	0.04	
0	0.37	
0.5	0.73	
1.0	1.11	
1.5	1.50	
2.0	1.91	where
2.5	2.33	
3.0	2.76	a = D/2

3.6 Protuberances and Rough Surfaces

If the falling object has a surface that is hydraulically "rough" or has protuberances, the drag coefficient may or may not be affected. In general, bodies with sharp edges such as, e.g., a flat plate at ninety-degree incidence, are quite insensitive to surface roughness or protuberances. Bluff bodies on the other hand, such as circular cylinders or a flat plate at zero incidence, are very sensitive to surface roughness. Fage and Warsap (1930) reported the effect of varying surface roughness k/d for infinite cylinders with their axis normal to the direction of flow. Their results are reproduced in Figure 3.9, giving the drag coefficient C_D as a function of the Reynolds number and the roughness k/d where k is the height of the protuberances and d is the diameter of the cylinder.

3.7 Correction of Drag Coefficient for Yaw

If, for example, a finite cylinder should fall vertically while its axis has a constant inclination to the horizontal (yaw angle) of magnitude ϕ, the total drag may be roughly approximated in the same manner as is done for swept-back wings in aircraft. If u is the fall velocity and c the chord length measured in the direction of the velocity, the drag coefficient C_D corrected for yaw is given by:

$$C_D(R,\phi) = C_D(R\cos^2\phi,0)\cos\phi \qquad (3.20)$$

where $R = uc/\nu$.

3.8 Other Shapes

If the falling object has a shape different from that of a sphere, a cylinder, or a flat plate, the corresponding drag will have to be established. For complex shapes the drag coefficients will have to be found either by a series of model experiments running through the entire range of Reynolds numbers of interest, or it will have to be approximated by breaking up the complex shape into several simple shapes for which drag coefficients are known and given in Section 3.2 or are computed analogous to the method demonstrated for the cylinder in Section 3.4. A few more drag coefficients for simple shapes are given below.

Detailed procedures for determining the profile drag are given by Schlichting in Chapter 25 of Boundary Layer Theory. The drag coefficients for flat plates at 90° incidence are constant through a wide range of Reynolds numbers.

For a circular disk, according to Wieselsberger:

$$C_D = 1.10, \quad \text{for} \quad 10^3 < R < 10^6$$

For an infinite plate strip:

$$C_D = 1.85, \quad \text{for} \quad 10^3 < R < 10^6$$

For a Joukowsky aerofoil, with a thickness to chord ratio = .05:

$$C_D = 3.6\, R^{-\frac{1}{2}}$$

For an airship hull with flow parallel to its axis, the drag coefficient varies very little with the Reynolds number, as is shown in Table 3.5. This Table also shows the drag coefficients for a streamlined strut with flow normal to its axis.

Table 3.5

Drag Coefficient for an Air Ship Hull and a Streamlined Strut

R	C_D (airship hull)	C_D (strut)
10,000	.12	.18
40,000	.09	.08
100,000	.07	.06
1,000,000	.06	.05

3.9 Terminal Velocity and Fall Trajectory

Assuming the drag coefficient for the object to be known, the terminal velocity can be found by rearranging equation (3.11):

$$u_o = 1.41 \frac{Vg(\rho_o - \rho_f)}{C_D A \rho_f} \tag{3.21}$$

where ρ_o is the average density of the object: $\rho_o = \gamma_o/g$.

Since in most cases C_D is a function of the Reynolds number, that is to say, a function of u, a first estimate of u has to be made for picking the appropriate drag coefficient.

By successive approximations, the correct drag coefficient will eventually be found corresponding to the Reynolds number determined by the terminal velocity. Fortunately, C_D is almost constant for a wide range of R.

If the initial velocity is zero or has a vertical component only, and if ocean currents are absent, the trajectory is a straight, vertical line to the ocean bottom. If, on the other hand, the initial velocity has a horizontal component, or if horizontal ocean currents are present, the trajectory will drift horizontally. In general, for free fall, the effect of an initial velocity will be relatively small because the drag forces are quite high and they rapidly reduce any horizontal velocity component to a negligible value. Ocean currents, however, may cause a considerable drift of any long, free fall trajectory. In both cases the amount of lateral drift can be calculated.

3.9.1 Drift Due to Horizontal Velocity Component

Assuming an object of mass m is at time t = 0 at the point y = 0 and has a velocity component in the (horizontal) y-direction of V_o. The profile drag, also in the y-direction, is assumed to be F_{Dy}. Then, using Newton's law, the equation of motion of the object is given by:

$$\frac{d^2y}{dt^2} = \frac{F_{Dy}}{m} = -\frac{1}{2} C_{Dy} \frac{A_y}{m} \rho_f \left(\frac{dy}{dt}\right)^2 \tag{3.22}$$

where A_y is the projected area of the object onto the plane normal to the y-axis. Assuming, as a first approximation, the drag coefficient C_{Dy} to be independent of the Reynolds number, that is to say, independent of dy/dt, equation (3.22) becomes a second order differential equation:

$$\ddot{y} + K(\dot{y})^2 = 0 \tag{3.23}$$

where

$$K = \frac{1}{2} C_{Dy} \frac{A_y}{m} \rho_f$$

The initial conditions of the problem are given by:

$$t = 0; \qquad y = 0$$

$$\dot{y} = V_o \tag{3.24}$$

The solution of equation (3.23) for the initial conditions of (3.24) is:

$$y = \frac{1}{K} \ell n(1 + KV_o t) \tag{3.25}$$

giving

$$\dot{y} = \frac{V_o}{1 + KV_o t}$$

$$\text{or} \quad t = \frac{1}{K}\left(\frac{1}{\dot{y}} - \frac{1}{V_o}\right) \tag{3.26}$$

If the object has an average unit weight γ_o and $\rho_o = \gamma_o/g$, the coefficient K can be expressed as the ratio of area A_y to the total volume V:

$$K = \frac{1}{2} C_{Dy} \frac{A_y}{V} \frac{\rho_f}{\rho_o} \quad (ft^{-1}) \tag{3.27}$$

For a typical missile, torpedo or instrument package, K might vary from .005 to .02 (ft^{-1}).

Having the solution (3.25), it is interesting to find the distance and the time after which the velocity decreases to a negligible value.

Assuming K = .01 (ft^{-1}) the excursion values y and the times (in terms of V_o) for a decrease of the velocity by increasing orders of magnitude have been calculated and are given in Table 3.6. We note that the drag coefficient was assumed to be constant which is the case, roughly, for Reynolds numbers R = 1000 to R = 200,000. But at the lower velocities, the drag coefficient drastically increases. Hence, the excursions calculated by equation (3.25) are higher than those that actually would occur. The values of Table 3.6 may, therefore, be considered to be an upper bound. Note that the second column gives the distance (in feet) that the object would have traveled if the drag resistance would have been zero. It is quite evident that horizontal excursions due to initial, lateral velocity components will be quite small.

Table 3.6

Typical Excursion y and Residual Velocities $\dot{y}$ of Object Falling through Sea Water with an Initial Horizontal Velocity Component V_o

Residual Velocity $\dot{y}$	$V_o t$	y(ft)
$V_o \cdot 10^{-1}$	900	230
$V_o \cdot 10^{-2}$	9,900	460
$V_o \cdot 10^{-3}$	99,900	690
$V_o \cdot 10^{-4}$	999,900	920
$V_o \cdot 10^{-5}$	9,999,900	1,150

3.9.2 Drift Due to Ocean Currents

If the object falls through water having a horizontal current component V, it will drift off a straight trajectory due to the profile drag produced by the current.

Assuming again an object of mass m falling through water having a horizontal current component = V, the equation of motion is given by:

$$\frac{d^2y}{dt^2} = -\frac{1}{2} C_{Dy} \frac{A_y}{V} \frac{\rho_f}{\rho} \left(V - \frac{dy}{dt}\right)^2 \qquad (3.28)$$

or

$$\ddot{y} + K(\dot{y})^2 - 2KV\dot{y} = -KV^2$$

If the current velocity is constant $V = V_o$, equation (3.28) can be integrated.

From the nature of the problem, it is evident that after some time the falling object assumes the constant horizontal velocity component V_o. Since the vertical velocity is also constant and equal to the terminal velocity u_o, the trajectory will be a straight, inclined line. Typical trajectories for an object falling through water with a constant horizontal current are shown in Figure 3.10.

From Figure 3.10 it is evident that the continuously acting effect of a horizontal drag component can cause large excursions y for long trajectories, i.e. for the object falling through deep water.

3.10 Calculation of Terminal Velocities for a Typical Object

Assuming a typical slenderness ratio for the cylinder of Figure 3.7 of L/D = 10, the drag coefficients for fall with axis horizontal and vertical are given in Table 3.7 and shown in Figure 3.11, Curve B. Curve A shows the drag coefficients for an infinitely long cylinder. The drag coefficients of Table 3.7 were obtained by evaluating equations (3.12) of Section 3.4 and (3.19) of Section 3.5 respectively.

Table 3.7

Drag Coefficients for Cylinder with L/D = 10

Reynolds No.	C_D (axis horizontal)	C_D(axis vert.)
Drag Force	$F_D = \frac{1}{2} C_D D(L + \frac{\pi}{4} D)\rho_f u^2$	$\frac{1}{2} C_D \frac{\pi D^2}{4} \rho_f u^2$
10	1.81	20.8
100	.97	6.4
1,000	.67	2.1
10,000	.74	.93
100,000	.80	.57
200,000	.77	.52
300,000	.54	.22
500,000	.20	.17
1,000,000	.24	.20

We can now calculate the terminal velocities of a cylinder as shown in Figure 3.7 having a slenderness ratio L/D = 10 both for fall with axis horizontal and vertical.

The terminal velocity according to equation (3.21) is:

$$u_o = 1.41 \left[\frac{1}{C_D} \frac{V}{A} g \frac{\rho_o - \rho_f}{\rho_f} \right]^{\frac{1}{2}}$$

Hence, the terminal fall velocity is also a function of the volume to area ratio V/A, and the ratio of the relative object density:

$$\frac{\rho_o - \rho_f}{\rho_f}$$

The terminal velocities for a cylinder with a slenderness ratio of L/D = 10 have been calculated and are shown in Figures 3.12 and 3.13 for the cylinder falling with its longitudinal axis horizontal or vertical respectively.

4.0 Free Fall and Powered Trav[illegible] Penetration

If the velocity of the arrival at the ocean bottom is known or has been calculated by the method discussed in Chapter 3, the penetration into the ocean bottom can be determined.

The problem of an object penetrating into a target material is the classical problem of terminal ballistics. An immense amount of literature both theoretical as well as experimental exists on this very subject. However, most of these investigations are concerned with projectiles striking a relatively hard target at considerably higher ballistic velocities.

The earliest known penetration equation is due to Robins and Euler who assumed that the resistance of a medium to penetration is a constant. This results in a constant deceleration of the projectile and an increase of the depth of penetration with the square of the impact velocity. In the most general formulation one may assume that the resistance of a target material to penetration is the combined result of three components, $f_1(v^o)$, $f_2(v^1)$, $f_3(v^2)$, which are functions of the instantaneous velocity v. Thus, according to Newton's second law:

$$- m \frac{dv}{dt} = f_1(v^o) + f_2(v) + f_3(v^2) \qquad (4.1)$$

Equation (4.1) essentially postulates that during the first phase of penetration, at high velocity, the motion is governed by the resistive forces proportional to the square of the velocity. These forces would be analogous to the drag resistance in fluid flow. Subsequently, at "moderate" velocities, the resistance will be proportional to the first power of the velocity and, hence, during this phase the resistance is analogous to the viscous resistance in fluid flow. In the last phase resistance is primarily caused by static forces.

If the functions in equation (4.1) are assumed to be constant coefficients, the statement is simplified to:

$$- m \frac{dv}{dt} = \alpha + \beta v + \gamma v^2 \qquad (4.2)$$

Equation (4.2) is a general formulation for various well-known penetration formulae. If, for example, one takes $\beta = \gamma = 0$, one obtains the Robins-Euler formula. For the case of $\beta = 0$, we obtain Poncelet's equation:

$$- m \frac{dv}{dt} = \alpha + \gamma v^2 \qquad (4.3)$$

For the case of $\alpha = 0$, we obtain the equation credited to Resal:

$$- m \frac{dv}{dt} = \beta v + \gamma v^2 \qquad (4.4)$$

The problem with all these equations is that the material constants α, β and γ have to be established experimentally. If equation (4.2) or any of its special cases is integrated twice with the initial conditions, $t = 0$; $x = 0$, $v = v_o$, the final, maximum penetration can be calculated by setting the velocity $v = 0$.

The resulting ultimate penetrations for the Robins-Euler, Poncelet and Resal equations respectively are:

$$x_{max} = \frac{m v_o^2}{2\alpha} \qquad \text{Robins-Euler} \qquad (4.5)$$

$$x_{max} = \frac{m}{2\gamma} \ell n \left(1 + \frac{\gamma v_o^2}{\alpha}\right) \qquad \text{Poncelet} \qquad (4.6)$$

$$x_{max} = \frac{m}{2\gamma} \ell n \left(1 + \frac{\gamma v_o}{\beta}\right)^2 \qquad \text{Resal} \qquad (4.7)$$

The solution for the general equation (4.2) is somewhat more involved and depends on the relative magnitude of the coefficients α, β and γ.

For the case where $\beta^2 < 4\alpha\gamma$, integration of (4.2) leads to:

$$x = \frac{m}{2\gamma} \ell n \frac{\gamma v_o^2 + \beta v_o + \alpha}{\gamma v^2 + \beta v + \alpha} - \frac{m\beta}{\gamma} A (4\alpha\gamma - \beta^2)^{-\frac{1}{2}} \qquad (4.8a)$$

$$t = 2 A m (4\alpha\gamma - \beta^2)^{-\frac{1}{2}} \qquad (4.8b)$$

where x is the instantaneous penetration at time t and velocity v and

$$A = \tan^{-1}(2\gamma v_o + \beta)(4\alpha\gamma - \beta^2)^{-\frac{1}{2}} - \tan^{-1}(2\gamma v + \beta)(4\alpha\gamma - \beta^2)^{-\frac{1}{2}}$$

The maximum penetration can be obtained by setting $v = 0$.

If $\beta^2 > 4\alpha\gamma$, integration yields:

$$x = \frac{m}{2\gamma} \ell n \frac{\gamma v_o^2 + \beta v_o + \alpha}{\gamma v^2 + \beta v + \alpha} - \frac{m\beta}{\gamma} B(\beta^2 - 4\alpha\gamma)^{-\frac{1}{2}} \qquad (4.8c)$$

$$t = 2 B m (\beta^2 - 4\alpha\gamma)^{-\frac{1}{2}} \qquad (4.8d)$$

where

$$B = \frac{1}{2} \ell n \frac{[2\gamma v + \beta + (\beta^2 - 4\alpha\gamma)^{\frac{1}{2}}][2\gamma v_o + \beta - (\beta^2 - 4\alpha\gamma)^{\frac{1}{2}}]}{[2\gamma v + \beta - (\beta^2 - 4\alpha\gamma)^{\frac{1}{2}}][2\gamma v_o + \beta + (\beta^2 - 4\alpha\gamma)^{\frac{1}{2}}]}$$

For the special case where $\beta^2 = 4\alpha\gamma$, the integration yields:

$$x = \frac{m}{2\gamma} \ln \frac{\beta+2\gamma v_o}{\beta+2\gamma v} - \frac{\beta}{\gamma} C\, m \qquad (4.8e)$$

$$t = 2\, C\, m \qquad (4.8f)$$

where $C = (2\gamma v+\beta)^{-1} - (2\gamma v_o+\beta)^{-1}$

For this same case β can also be expressed as $\beta = 2\, \alpha^{\frac{1}{2}}\, \gamma^{\frac{1}{2}}$, and equation (4.2) can be written as:

$$-\, m \frac{d^2x}{dt^2} = (\alpha^{\frac{1}{2}} + \gamma^{\frac{1}{2}} v)^2 \qquad (4.9)$$

Then, the integration with the given initial condition leads to:

$$x = \frac{m}{\gamma} \ln \frac{\alpha^{\frac{1}{2}}+\gamma^{\frac{1}{2}} v_o}{\alpha^{\frac{1}{2}}+\gamma^{\frac{1}{2}} v} - \alpha^{\frac{1}{2}}\gamma^{\frac{1}{2}} \frac{v_o - v}{(\alpha^{\frac{1}{2}}+\gamma^{\frac{1}{2}} v_o)(\alpha^{\frac{1}{2}}+\gamma^{\frac{1}{2}} v)} \qquad (4.10)$$

and the maximum penetration is given by:

$$x_{max} = \frac{m}{\gamma} \ln\left(1 + \frac{\gamma^{\frac{1}{2}}}{\alpha^{\frac{1}{2}}} v_o\right) - \frac{\gamma^{\frac{1}{2}} v_o}{(\alpha^{\frac{1}{2}} + \gamma^{\frac{1}{2}} v_o)} \qquad (4.11)$$

Also:

$$t = m \frac{v_o - v}{(\alpha^{\frac{1}{2}} + \gamma^{\frac{1}{2}} v_o)(\alpha^{\frac{1}{2}} + \gamma^{\frac{1}{2}} v)} \qquad (4.12)$$

As stated before, the material constants α, β, γ have to be determined for each material and impacting object. While these formulae have been used in expressing a wide variety of test results, their validity has been tested only within limited ranges of impact velocities and often, by the very nature of the experiments, the data show a considerable scatter. Also, the coefficients α, β, γ do not appear to have any clear relationships to the basic, mechanical properties of the target material. At any rate, such a relationship has not yet been sufficiently explored.

For this reason we consider it risky to apply these formulae directly to the ocean bottom penetration problem. Normally, it is highly improbable that in situ tests for α, β, γ can be performed at reasonable cost. Before this is attempted, an analysis should be made how the coefficients α, β, γ are related to the basic material properties of the ocean bottom soils.

Apart from terminal ballistics investigations, a group of impact penetration studies in the literature are concerned with meteorite impacts. These are definitely beyond the practical range of ocean bottom penetrations. Meteorite impact usually occurs at hypervelocities resulting in liquefaction and vaporization of the target material, as well as scattering and splattering of the impacting object. These phenomena are beyond the scope of this study.

Other investigations reported in the literature were concerned with the soft-landing problem of a space vehicle on an unexplored soil surface.

While the theoretical aspects of an object striking a target material do not appear to be drastically different, certainly the experimental investigations are greatly dependent upon projectile and target material and also, on the impact velocity and energy.

All impact phenomena are controlled by the ratio of specific impact energy of the projectile to the potential strain energy of the target material. Therefore, even purely analytical studies have to concentrate on those phenomena that predominate the particular problem at that ratio. Below we are presenting those methods that appear most promising and applicable within the present state of the art for analyzing ocean bottom penetration within the range of probable parameters. First, however, we must point out two fundamentally different phases of the penetration process. The first one is the penetration phase with increasing penetration area. (The penetration area is defined as the orthogonal projection of the contact surface on a plane normal to the penetration trajectory.) This phase occurs, for example, during the initial penetration when a sphere, a conical- or an ogive-nosed projectile penetrates into a target material. During this initial penetration, the projected, cross-sectional contact area continuously increases. At a penetration of $p = D/2$ for a sphere, or equal to the length of the nose cone for a projectile, the maximum projected contact area has been reached and any penetration thereafter occurs at a constant area. Also, a flat, cylindrical punch (such as a flat-ended pile) will always have a constant penetration area. Since the mechanics of the two problems is somewhat different, we have to make a distinction between increasing area- and constant area-penetration.

4.1 Penetration with Increasing Area

Increasing area penetration usually occurs as the initial phase of deep penetration or for shallow penetrations with the penetrating object having a geometry such that any increase in penetration Δx causes an increase in the penetration area ΔA. This condition can be expressed by:

$$\frac{\Delta A}{\Delta x} > 0$$

Studies investigating increasing area penetration were carried out by the Aeronutronic Division of Philco for developing a lunar penetrometer (Anon. 1966) and by Schmid (1966) and Tsai and Schmid (1969) for determining soil properties in situ by an impact penetrometer.

These investigations analyze the penetration of a spherical penetrometer into a soil material. The Aeronutronic study integrated the resulting equation of motion, a nonlinear differential equation utilizing a Taylor series expansion. The solution was given in the following form:

$$v^2 = \exp\left[\frac{\pi\rho}{10\,D^2m}\left(4x^5 - 10\,Dx^4 + 10\,D^2x^3 - 5\,D^3x^2\right)\right] \cdot \left\{v_o^2 + \frac{2\sigma\pi}{m}\left[\frac{x^3}{3} + \frac{\pi\rho}{10\,D^2m}\left(-\frac{1}{2}x^8 + 2\,Dx^7 - \frac{10\,D^2}{3}x^6 + 3\,D^3x^5 - \frac{5D^4}{4}x^4\right) + \frac{1}{2}\left(\frac{\pi\rho}{10\,D^2m}\right)^2 \frac{16}{13}\left(x^{13} - 8\,Dx^{12} + \frac{260\,D^2}{11}x^{11} - 42\,D^3x^{10} + \frac{440\,D^4}{9}x^9 - \frac{300\,D^5}{8}x^8 + \frac{125\,D^6}{7}x^7 - \frac{25\,D^7}{6}x^6\right) - \frac{D}{2}x^2\right]\right\} \qquad (4.13)$$

where v is the instantaneous velocity, ρ and σ are the density and compressive strength of the target material respectively. The term v_o represents the initial or impact velocity of the penetrometer, while D is the penetrometer diameter and m is its mass.

Equation (4.13) is valid for the entrance phase of the penetration process. That is for $x < D/2$.

A considerably simpler solution was obtained for motion within the second phase, i.e., after the nose of the penetrometer is completely embedded and the surface area of contact is no longer varying with depth of penetration. This solution is:

$$v^2 = v_1^2 + \frac{4\sigma}{\rho}\exp - \left[\frac{\pi D^2\rho}{8m}\left(x - \frac{D}{2}\right)\right] - \frac{4\sigma}{\rho} \qquad (4.14)$$

where v_1 is the velocity at the end of the entrance phase obtained from equation (4.13) for $x = D/2$. Thus, equations

(4.13) and (4.14) define the instantaneous velocity of the penetrometer at any depth of penetration x. This theoretical prediction of penetration behavior has been verified experimentally for some range of projectile geometries, impact velocities, and types of target materials.

Very good agreement is claimed for the velocity range from 500 to 6,000 ft/sec and for target materials ranging from soft polyethylene to glass fiber reinforced epoxy resins. However, for the impact velocity range of interest in ocean bottom penetration, no experimental confirmation of the validity of equations (4.13) and (4.14) exists and, therefore, they must be used with caution.

Even though equation (4.13) is rather lengthy, its evaluation does not present any problem with the help of a computer. Previous work by Schmid (1966) also dealt with the penetration of a sphere into soils.

For the penetration of a rigid sphere into a soft, plastic target material, one can make the assumption that the resistance to penetration offered by the target material is equal to a constant yield stress or flow pressure p_o times the projected area of contact. Hence, using the terms defined in Figure 4.1:

$$P = \pi p_o a^2 = \pi p_o (2Rx - x^2) \tag{4.15}$$

Thus, if m is the mass of the penetrating object, applying Newton's law furnishes:

$$\ddot{x} + \frac{\pi p_o}{m} (2Rx - x^2) = 0 \tag{4.16}$$

If the penetration is small, say $x < R/4$, the second term in the parentheses becomes relatively small and can be neglected compared to the first term. Then the solution of equation (4.16) is given by:

$$x = v_o \beta \sin \frac{t}{\beta} \tag{4.17}$$

where

$$\beta = \left(\frac{m}{2\pi R p_o} \right)^{+\frac{1}{2}}$$

The maximum depth of penetration occurs at the end of the impact period, when

$$\dot{x} = v_o \cos \frac{t}{\beta} = 0$$

which is satisfied if

$$\frac{t}{\beta} = \frac{\pi}{2}$$

Thus, the impact period T is:

$$T = 1.57\ \beta$$

and the maximum penetration

$$x_{max} = v_o\beta \qquad (x < R/4)$$

If the penetration is larger than R/4, then the x^2 term in equation (4.16) cannot be neglected and the solution of the equation

$$\ddot{x} + Ax - Bx^2 = 0 \qquad (4.18)$$

leads to an integral that can be evaluated only numerically:

$$t = \int \frac{dx}{(v_o^2 - Ax^2 + \frac{2}{3}Bx^3)^{\frac{1}{2}}} + C$$

where $A = 2RB$

and $B = \frac{\pi p_o}{m}$

If, on the other hand, the penetration is larger than R, we have the case of constant area penetration and equations (4.15) through (4.17) respectively are modified to:

$$P = \pi p_o R^2 \qquad (4.15a)$$

$$\ddot{x} + \frac{\pi p_o}{m} R^2 = 0 \qquad (4.16a)$$

$$x = -\frac{1}{2}\pi p_o R^2 \tau^2 + v_o t \qquad (4.17a)$$

and penetration period T and maximum penetration respectively are given by:

$$T = \frac{m}{\pi p_o R^2} v_o$$

and

$$x_{max} = \frac{1}{2}\frac{m}{\pi p_o R^2} v_o^2$$

We note that these results now correspond to the solution of Robins-Euler (equation 4.5) with $\alpha = \pi p_o R^2$.

Rather than assuming a constant flow pressure type of resistance (i.e., an ideally plastic target material), one can also assume the target to have the rheological properties of a four-parameter model as shown in Figure 4.2.

This approach also was explored by Schmid (1966) who calculated a penetration quantity b(t) by using the principle of elastic-viscoelastic analogy using Laplace transforms. The results are given in terms of a deformation parameter b(t). This parameter had to be chosen because the elastic-viscoelastic analogy requires a linear relationship between the load and the deformation parameter. Since for the problem of penetration of a sphere into a target neither the penetration "x" nor the contact radius "a" (see Figure 4.1) is directly proportional to the load, the quantity $b = x \cdot a$ was chosen which is a linear function of the load as long as $x < R$, i.e. as long as the penetration is an "increasing area" penetration.

The resulting differential equation for the four-parameter model is:

$$D^2\tau + \left(\frac{G_1}{\eta_1} + \frac{G_1}{\eta_2} + \frac{G_2}{\eta_2}\right)D\tau + \frac{G_1 G_2}{\eta_1 \eta_2}\tau = G_1 D^2\gamma + G_1 \frac{G_2}{\eta_2} D\gamma \quad (4.19)$$

Here the moduli G_1, G_2, η_1 and η_2 are the spring and dashpot constants respectively of the four-parameter model target material (see Figure 4.2), τ and γ represent the stress and strain tensors respectively, and the operator D represents differentiation with respect to time: $D = d/dt$.

Equation (4.19) was solved for an impact pulse having a sinusoidal variation with time:

$$P = P_m \sin \omega t \quad (4.20)$$

Experimental accelerometer measurements performed by a penetrometer showed that for most soils (e.g. for clays, silts and even loose sands) the impact force pulse could indeed be approximated by a sinusoidal curve. Figure 4.3 shows such a typical accelerometer curve.

The solution, obtained by a Laplace transform, is given by:

$$b(t) = \frac{3P_m}{16} \int_0^t \phi(t-\tau) \sin \omega\tau \, d\tau$$

$$= \frac{3P_m}{8G_1} \left\{ \left[\frac{1+4\Gamma}{1+\Gamma} + \frac{k\omega_2^2}{\omega^2+\omega_2^2} + \frac{\beta_1\omega_3}{\omega^2+\omega_3^2} + \frac{\beta_2\omega_4}{\omega^2+\omega_4^2} \right] \sin \omega t \right.$$

$$- \left[\frac{\omega_1}{\omega} + \frac{k\omega\omega_2}{\omega^2+\omega_2^2} + \frac{\beta_1\omega}{\omega^2+\omega_3^2} + \frac{\beta_2\omega}{\omega^2+\omega_4^2} \right] \cos \omega t$$

$$\left. + \frac{\omega_1}{\omega} + \frac{k\omega\omega_2}{\omega^2+\omega_2^2} e^{-\omega_2 t} + \frac{\beta_1\omega}{\omega^2+\omega_3^2} e^{-\omega_3 t} + \frac{\beta_2\omega}{\omega^2+\omega_4^2} e^{-\omega_4 t} \right\} \quad (4.21)$$

where

$$\Gamma = \frac{G_1}{6K}\ , \quad k = \frac{G_1}{G_2}\ , \quad \omega_1 = \frac{G_1}{\eta_1}\ , \quad \omega_2 = \frac{G_2}{\eta_2}\ ,$$

$$\omega_{\substack{3\\4}} = \frac{1}{2}\left\{\omega_2+\frac{1}{1+\Gamma}(\omega_1+k\omega_2)\right\} \pm \frac{1}{2}\left\{[\omega_2+\frac{1}{1+\Gamma}(\omega_1+k\omega_2)]^2 - \frac{4}{1+\Gamma}\,\omega_1\omega_2\right\}^{\frac{1}{2}}$$

and K is the bulk modulus of the target material.

Also:

$$\beta_1 = \frac{1}{1+\Gamma}\,\alpha_1\left\{\frac{1+2\Gamma+4\Gamma^2}{1+\Gamma} + \frac{k\omega_2}{\omega_2-\omega_3} - \frac{\omega_1}{\omega_3}\right\}$$

$$\beta_2 = \frac{1}{1+\Gamma}\,\alpha_2\left\{\frac{1+2\Gamma+4\Gamma^2}{1+\Gamma} + \frac{k\omega_2}{\omega_2-\omega_4} - \frac{\omega_1}{\omega_4}\right\}$$

$$\alpha_1 = \frac{\omega_1\omega_2-\omega_1\omega_3-k\omega_2\omega_3}{\omega_4-\omega_3}$$

$$\alpha_2 = \frac{\omega_1\omega_2-\omega_1\omega_4-k\omega_2\omega_4}{\omega_3-\omega_4}$$

The resulting equation (4.21) is rather complicated and cumbersome to evaluate.

Later Tsai and Schmid (1969) considerably simplified this solution by separating volumetric and deviatoric components of the deformation.

Under high energy impact, soils behave essentially like a liquid material and consolidation is relatively small. It appears reasonable then to assume that the deviatoric deformations predominate. This means that the volumetric change is negligible, or K = ∞, during impact. This assumption yields Γ = 0 also, and the solution of equation (4.21) is then simplified to:

$$b(t) = \frac{3P_m}{8}\left[C_1\sin\frac{\pi t}{T} - (C_2+C_3)\cos\frac{\pi t}{T} + C_2 + C_3\, e^{-\frac{G_2 t}{\eta_2}}\right] \tag{4.22}$$

where

$$C_1 = \frac{1}{G_1} + \frac{\frac{G_2}{\eta_2^2}}{(\frac{\pi}{T})^2 + (\frac{G_2}{\eta_2})^2}$$

$$C_2 = \frac{T}{\eta_1 \pi}$$

$$C_3 = \frac{\frac{\pi}{T}}{\eta_2 [(\frac{\pi}{T})^2 + (\frac{G_2}{\eta_2})^2]}$$

To evaluate soil parameters from an impact penetrometer test, the theoretical equation (4.22) and the experimental curves were matched. By using the principle of the least square method, soil parameters were obtained for the theoretical curve giving the best fit. Since these soil parameters can have physical significance only for non-negative values, the occurrence of negative values were excluded in the process of curve fitting.

The results thus obtained showed that the four-parameter model (Figure 4.2) could be simplified to a Maxwell model, since G_2 was nearly equal to zero and η_2 could be combined with η_1 to represent a single dashpot.

For the simplified soil model, equation (4.22) simplifies further to:

$$b(t) = \frac{3P_m}{8} [\frac{1}{G_1} \sin \frac{\pi t}{T} + \frac{T}{\pi \eta_1} (1 - \cos \frac{\pi t}{T})] \qquad (4.23)$$

where T is the penetration period (sec.). This simplified theoretical curve (equation 4.23) was then matched with the experimental curve by using the same approach that was discussed previously. The calculated soil parameters are shown in Table 4.1.

The problem when using any one of these rheological solutions invariably is the determination of the model constants G and η. The rheological parameters G and η, in essence, may be regarded here as material properties corresponding, in conventional soil mechanics terminology, to a modulus of elasticity and a shear strength at a constant strain rate.

4.2 Constant Area Penetration

If an object has penetrated into a target material up to the maximum cross-sectional area, any further penetration thereafter will take place at a constant area. Formulating the resistance to penetration then, according to equation (4.2), and assuming the coefficients α, β, and γ to be constants, we see that the total resistance is made up of a static component α, a viscous component βv and a drag component γv^2. Such a

Table 4.1 Calculated Soil Parameters for Soil as a Maxwell Model (after Tsai and Schmid, 1969)

Target Material	Remarks	G_1 (psi)	η_1 (psi-sec)	Unconfined compressive strength (psi)
Sandy Princeton clay	Natural soil after two days soaked in heavy rain, W = 27.42%	262.5 264.3 251.4 266.2	0.5885 0.5721 0.5357 0.5436	
Princeton red clay	Dry, relatively loose material, W = 2.65%	156.6 201.7 182.8	0.4402 0.4987 0.4587	18.4
Silty sand at soil surface	Natural soil	665.3 882.0	0.8938 1.0219	31.2
Silty sand, 20" below surface	Natural soil	669.3 626.9 610.0	0.9133 0.8810 0.8287	42.5
Sandy silt and clay	Natural soil, dry	1178 1192 1331	1.222 1.234 1.271	62.2
Sandy clay	Field recently plowed and disked	150.1 225.9 201.5	0.4093 0.5021 0.4726	39.7
Crushed rock ½-1"	Compacted	1709	1.5010	CBR[1] = 18.5
Fine Sand	Natural soil	373.6 373.6	0.6466 0.6466	CBR[1] = 5.8
Wax: Cambar M-348 at 31°C	Material used for comparison purposes	155.6 151.1 164.1 161.7	0.4249 0.4111 0.4288 0.4227	

[1]CBR = California Bearing Ratio

formulation means implicitly that, during the first phase of penetration (the object having high velocity), the motion is governed mainly by resistive forces proportional to the square of the velocity. Subsequently, at "moderate" velocities, the resistive forces will be proportional mainly to the first power of the velocity. Finally, towards the end of the impact period, at very low velocities, the resistance is caused mainly by static forces.

As evident from Chapter 3, the free fall terminal velocities are so low that the drag component of the total resistance to

penetration will be extremely small and can be neglected. This component is of importance for the penetration of targets at very high, ballistic velocities which occur rarely, if ever, in ocean bottom penetration. Thus, we will confine ourselves here to the evaluation of the resistance equation.

$$P = \alpha + \beta v \tag{4.24}$$

4.2.1 Constant Area Penetration with Static Penetration Resistance

Assuming the target material to be made up of an ideally plastic material, the resistance to penetration is given by:

$$P = A \cdot p_o \tag{4.25}$$

where A is the constant area of the penetrating object and p_o is the bearing capacity of the target material. If the impact is ideally plastic (no rebound) the maximum penetration x_{max} can be calculated from the energy relationship:

$$P \cdot x_{max} = \frac{1}{2} m v_o^2 \tag{4.26}$$

where m is the mass of the impacting object. Thus,

$$x_{max} = \frac{m}{2Ap_o} v_o^2 \tag{4.27}$$

The impact period can be calculated from the equation of motion:

$$-m\ddot{x} = Ap_o \tag{4.28}$$

The solution of this simple differential equation is given by:

$$x = -\frac{A}{2m} p_o t^2 + v_o t \tag{4.29}$$

which for $\dot{x} = 0$, yields:

$$T = \frac{v_o m}{Ap_o} \tag{4.30a}$$

and

$$x_{max} = \frac{v_o^2 m}{2Ap_o} \tag{4.30b}$$

The results (4.26) through (4.29) are exactly as those given by (4.15a) through (4.17a) except that here the penetration area does not have to be circular. Thus, the maximum penetration for constant area penetration into perfectly plastic soil is directly proportional to the mass, the square of the impact velocity, and is inversely proportional to the penetration area and the bearing capacity of the ocean bottom.

The determination of the ultimate bearing capacity requires information about the shear strength characteristics of the ocean bottom (see Chapter 2).

According to Terzaghi (1943), the bearing capacity of shallow foundations is given by:

$$p_o = 1.3\ cN_c + 0.4\ \gamma BN_\gamma + \gamma D_f N_q \qquad (4.31a)$$

for a square footing, and

$$p_o = 1.3\ cN_c + 0.6\ \gamma RN_\gamma + \gamma D_f N_q \qquad (4.31b)$$

for a circular footing, where c is the cohesion and γ the unit weight of the soil. The values N_c, N_γ and N_q are influence values depending on the angle of friction. B, R and D_f are the dimension of the footing or the depth of foundation respectively.

In most instances the friction angle of ocean bottom soils will be zero. Hence the bearing capacity can be expressed as given by Tschebotarioff (1951):

$$p_o = 5.52\ c\left(1 + 0.38\ \frac{D_f}{B} + 0.44\ \frac{B}{L}\right) \qquad (4.32a)$$

or by Skempton:

$$p_o = 5.0\ c\left(1 + 0.2\ \frac{B}{L}\right)\left(1 + 0.2\ \frac{D_f}{B}\right) \qquad (4.32b)$$

Moore (1962) has calculated bearing capacity values from shearing strength data of ocean bottom cores. These are given in Table 2.2.

4.2.2 Constant Area Penetration with Viscous Penetration Resistance

Assuming the target material to be an ideally viscous substance, the resistance to penetration for a, say, circular penetration area is given by:

$$P = 2\pi a\mu v \tag{4.33}$$

where a is the radius of the penetrating area, μ (poise) is the viscosity of the target material, and v is the penetration velocity. The equation of motion then furnishes:

$$-m\ddot{x} = 2\pi a\mu\dot{x} \tag{4.34}$$

or $$\ddot{x} + \alpha\dot{x} = 0$$

where $$\alpha = \frac{1}{m} 2\pi a\mu \tag{4.35}$$

The solution of (4.35) is given by:

$$x = \frac{v_o}{\alpha}(1 - e^{-\alpha t}) \tag{4.36}$$

By inspection of equation (4.36) one recognizes that the maximum penetration is given by:

$$x_{max} = \frac{v_o}{\alpha} = \frac{v_o m}{2\pi a\mu} \tag{4.37}$$

which occurs for a value of $t = \infty$. Similar to the case of the four-parameter rheological model, the problem will be how to assess or determine the viscosity μ (g sec/cm^2) of the ocean bottom soil. We note that in this formulation of the problem the penetration period T at which maximum penetration is achieved is infinite which means that the deformation really never stops, but asymtotically creeps up to the ultimate value v_o/α.

This comes from the very formulation of the problem as a purely viscous phenomenon. Often for such problems the retardation time τ is a more concrete measure of the time scale of a process. Assume, for example, we were interested in the time at which $t = \tau = 1/\alpha$. At that instant

$$x = \frac{v_o}{\alpha}(1 - e^{-1}) = 0.63\,\frac{v_o}{\alpha}$$

and, from (4.35)

$$\tau = \frac{m}{2\pi a\mu}$$

The retardation time is, hence, that time after which the major portion (namely 63 per cent) of the deformation in a purely viscous process has taken place.

4.2.3 Empirical Penetration Formulae

Quite a large number of empirical penetration formulae can be found in the literature. These are, however, mostly concerned with high impact velocities. For example, Goldsmith (1960) reports, in addition to equation (4.27), also the following:

$$x_{max} = \frac{1}{2} \frac{m}{B_1} \ln \left(\frac{B_1}{B_3} v_o^2 + 1\right) \tag{4.38}$$

and

$$x_{max} = DB\left(\frac{v_o}{c_o}\right)^n \quad \text{for} \quad 0.1 < \frac{v_o}{c_o} < 1.0 \tag{4.39}$$

where D is the diameter of a projectile and c_o is the wave velocity in the target material. The values B_1, B_3, and B are values determined from test data. The value B is given as approximately 2.5 and n = 1.4.

Kornhauser (1964) reports several penetration formulae found in the literature. For penetration into rock, Maurer and Rinehart (1960) find:

$$x_{max} = K_1 \frac{W}{D^2} (v_o - K_2) \tag{4.40}$$

where x_{max} is the total penetration in inches, W is the weight of the impacting object in pounds, D is the diameter of the object in inches, and v_o is the impact velocity in ft/sec. The coefficients K_1 and K_2 are material parameters.

Tolch and Bushkovitch (1947) recommend for small projectiles striking soft rock:

$$x_{max} = 4.6 \frac{W}{D^{1.83}} 0.001\ v_o \tag{4.41}$$

and for large projectiles:

$$x_{max} = 1.4 \frac{W}{D^{1.53}} (0.001\ v_o)^{1.8} \tag{4.42}$$

Lang (1956) on the other hand reports:

$$x_{max} = \frac{KW}{D^2} v_o^{1.96/s^{0.065}} \tag{4.43}$$

where s is the unconfined compressive strength of the target rock or soil.

Rinehart (1960) and Palmore (1961) suggest for softer materials such as soil, the following type of equation:

$$x_{max} = \frac{K_1 W}{D^2} \ln (1 + K_2 v_o^2) \qquad (4.44)$$

which is very similar to equation (4.38) given by Goldsmith.

Kornhauser reduced the data reported by several investigators to the common basis of impact by steel spheres. His comparison is shown in Figure 4.4.

As can be seen, these data are all for impact velocities of more than 100 feet per second. For this reason, they appear to have limited applicability to ocean bottom penetration.

Comparing equations (4.38) and (4.44), we note them to be identical, except for the use of a different nomenclature. Also, recalling the classical equations of ballistics of Section 4.1, we find that these two equations are nothing but the Poncelet equation.

Comparing the penetration formula derived in Section 4.2.1 assuming an ideally plastic target material (equation 4.30b) with any one of the empirical formulae, we find that equation (4.42) is basically the same, differing only slightly in the exponent of the impact velocity. This exponent is 2.0 in equation (4.30b) vs. 1.8 in (4.42). Most surprisingly, the equation derived by assuming an ideally viscous target material (equation 4.37) is in its structure identical to the empirical formula (4.41) and also, except for a constant, agrees with the empirical formula (4.40).

While these empirical formulae (4.40 and 4.41) were obtained by evaluating data from projectiles striking rocks at relatively high impact velocities, the results indicate that a formulation as used in the derivation of equation (4.37) has, perhaps, the greatest promise of describing properly the ocean bottom penetration problem. Particularly also, because the lower velocities and the much softer target materials of the ocean bottom penetration problem must be a much closer approximation to the theoretical assumptions made in the derivation of equation (4.37) than the conditions that prevailed in those tests.

4.2.4 Empirical Penetration Results of Sandia Penetrator

The penetration into soils and soft rocks by a specially designed penetrator dropped by an airplane from a large height has been investigated by a research and development program of several years by Sandia Corporation. The device is described in detail in Section 6.4, and a cross-section is shown in Figure 6.30. The experience gained in this development program has been evaluated on an empirical basis in the form of a nomogram (Figure 4.5). Young (1969) shows how the empirical parameters for developing this nomogram have been determined. The nomogram is used as follows: For the given diameter of the penetrator (for example, 8 inches), one passes horizontally to the left until the horizontal intersects the curve corresponding to the given weight of the projectile (1000 lbs.). From there a vertical line follows upward to the intersection with the curve that corresponds to the impact velocity (1400 fps.). From there a horizontal to the right intersects with the line corresponding to the soil constant of the target material. This soil constant must be known either from a prior test or it must be estimated from experience with impacts on similar materials (S = 4.6). From this intersection a vertical line downward follows to the intersection with the line N corresponding to the nose performance coefficient N (N = 1.11). Finally, from this intersection a horizontal line to the left indicates the penetration (104 ft.) of the projectile.

Young states that the accuracy of the nomogram depends most strongly on the accuracy with which the soil constant S is determined.

For a series of tests reported by him, the predicted penetration depths exceeded actual, observed depths by 20% on 9% of the tests and by 25% on less than 1.5% of the tests.

4.2.5 Computer Programs to Calculate Penetration

Noh (1964) and Wilkins (1964) have treated the problem of an object or projectile impacting upon and penetrating into a target material analytically and numerically by substituting the differential equations of motion by finite difference equations and using a coupled Euler-Lagrange (CEL) mesh. The central feature of the CEL calculation is the solution of a time-dependent, two-space dimensional, Eulerian hydrodynamics problem for a region with an arbitrary, polygonal, approximating mesh having a general moving (i.e. time-dependent) boundary.

The resulting CEL-code is a time-dependent, two-space dimensional computer program (for a compressible, non-heat-conducting material) which makes it possible to couple an Eulerian approximation of some regions of a material with a

Lagrange approximation for each of the adjacent regions of the material. The major problem in such a method is developing a suitable, Eulerian formulation. In the CEL method the Eulerian boundary is defined by one or more Lagrange lines and, hence, is defined by a polygonal traverse. A moving traverse intersecting the fixed, Eulerian mesh creates irregular, time-dependent boundary zones which, in general, can be defined as the union of closed polygons. The problem then, for the Eulerian calculation, is one of approximating the differential equations for a time-dependent, polygonal region at the boundary in a way that is consistent with the equations in the interior. An additional requirement demands overall consistency of the difference approximations for both the Lagrange and Eulerian regions.

The CEL method was pioneered at the Lawrence Radiation Laboratory, Livermore, California under sponsorship of the U.S. Atomic Energy and has since been applied to a series of problems from nuclear cratering to armor penetration. See, for example, Wilkins, Honodel and Sawle (1967) and Wilkins (1968). The resulting program was called the HEMP Code, which solves the following equations of continuum mechanics by finite difference methods.

The basic equations in the HEMP Code for the calculation of elastic-plastic flow are:

a) Equations of motion in cylindrical coordinates with radial symmetry about the z-axis:

$$\frac{\partial \sigma_z}{\partial z} + \frac{\partial \tau_{rz}}{\partial r} + \frac{\tau_{rz}}{r} = \rho \ddot{z}$$

$$\frac{\partial \tau_{rz}}{\partial z} + \frac{\partial \sigma_r}{\partial r} + \frac{\sigma_r - \sigma_\theta}{r} = \rho \ddot{r}$$

$$\sigma_z = s_z - (p + q)$$

$$\sigma_r = s_r - (p + q)$$

$$\sigma_\theta = s_\theta - (p + q)$$

b) Equation of continuity:

$$\frac{\dot{V}}{V} = \frac{\partial \dot{z}}{\partial z} + \frac{\partial \dot{r}}{\partial r} + \frac{\dot{r}}{r}$$

c) Energy equation:

$$\dot{W} = -(p+q)\dot{V} + V(s_z \dot{\varepsilon}_z + s_r \dot{\varepsilon}_r + s_\theta \dot{\varepsilon}_\theta + \tau_{rz} \dot{\gamma}_{rz})$$

d) Equations of State:

1) Stress components:

$$\dot{s}_z = 2\mu(\dot{\varepsilon}_z - \frac{1}{3}\frac{\dot{V}}{V}) + \delta_z$$

$$\dot{s}_r = 2\mu(\dot{\varepsilon}_r - \frac{1}{3}\frac{\dot{V}}{V}) + \delta_r$$

$$\dot{s}_\theta = 2\mu(\dot{\varepsilon}_\theta - \frac{1}{3}\frac{\dot{V}}{V})$$

$$\tau_{rz} = \mu\,\dot{\gamma}_{rz} + \delta_{rz}$$

2) Strain rate components:

$$\dot{\varepsilon}_z = \frac{\partial \dot{z}}{\partial z}$$

$$\dot{\varepsilon}_r = \frac{\partial \dot{r}}{\partial r}$$

$$\dot{\varepsilon}_\theta = \frac{\dot{r}}{r}$$

$$\dot{\gamma}_{rz} = \frac{\partial \dot{r}}{\partial z} + \frac{\partial \dot{z}}{\partial r}$$

3) Hydrostatic pressure:

$$p = a(\eta-1) + b(\eta-1)^2 + c(\eta-1)^3 + d\eta W,$$

$$\eta = \frac{1}{V} = \frac{\rho}{\rho_o}$$

4) Von Mises yield criterion:

$$s_1^2 + s_2^2 + s_3^2 - \frac{2}{3}\sigma_o^2 < 0$$

where the symbols used define the following:

r, z - space coordinates,
$\dot{r}$, $\dot{z}$ - velocity in r and z directions,
$\sigma_r, \sigma_z, \sigma_\theta$ - total stresses,
τ_{rz} - shear stress,

s_r, s_z, s_θ - stress deviators,
s_1, s_2, s_3 - principal stress deviators,
μ - shear modulus,
σ_o - yield strength of the target material,
$\varepsilon_r, \varepsilon_z, \varepsilon_\theta$ - strains,
δ - corrections for rotation,
p - hydrostatic pressure = $\frac{1}{3}(\sigma_r + \sigma_z + \sigma_\theta)$,
V - relative volume,
W - internal energy per original unit of volume,
ρ - density,
q - artificial viscosity: $q = C_o^2 \rho_o (\frac{\dot{V}}{V})^2 \frac{A}{V}$,
C_o - constant,
A - zone area,
ρ_o - reference density.

The dot over any parameter signifies a time derivative along the particle path.

Noh (1964) describes the basic steps for using this procedure as follows (pp. 125-126):

"... The basic idea in the CEL code is that the boundary ∂R (of the region $R = U_i R_i$ we wish to approximate) and the curves D_i (which separate the subregions R_i) are to be approximated by Lagrange lines. Thus, the moving boundaries (∂R and the D_i) are made to correspond to some Lagrange lines in the Lagrange approximating grids.

"A subregion R_i which is approximated by the Eulerian mesh will consequently have its boundary ∂R_i prescribed by the Lagrange calculations. Thus, the Eulerian calculation reduces to a calculation on a fixed mesh having a prescribed, moving boundary and, therefore, constitutes one of the central calculations in the CEL code.

"The CEL code consists of a large[1] rectangular Eulerian mesh which we denote by E, and, depending on the problem we wish to solve, from one to six separate Lagrange grids which we denote by $L_i(t)$, $i = 1, 2, \ldots, 6$ [i.e., E and the $L_i(t)$ are the sets of lattice points which define the Eulerian and the Lagrange grids, respectively; also, the Lagrange grids are denoted as functions of time since their grid points move with the fluids they approximate].

[1]Up to 7000 mesh points are provided for in the IBM 7094 version of CEL and up to 20,000 mesh points can be used in the IBM 7030 (Stretch) version of the CEL code.

"The calculations that are made at each time step in the code are divided into three main parts: Lagrange calculations, Eulerian calculations, and a calculation which couples the Eulerian and Lagrange regions by defining that part of the Eulerian mesh E which is active and by determining the pressures from the Eulerian region which acts on the Lagrange boundaries.

"We suppose that we are at the nth time step ($t^n = \Sigma_j^n \Delta t_j$) of the CEL calculation and that we wish to advance all quantities by one time step to the time t^{n+1}. We assume that the state of the fluids (density, energy, etc.) is known at t^n and also that we know the positions of the Lagrange grids [i.e., we have determined $L_i^n = L_i(t^n)$]. In addition, we suppose that we have determined that subset of the Eulerian mesh E, which is interior to, or on the boundary of, those subregions R_i having an Eulerian approximation. We denote this subset of E at $t = t^n$ by $E^n = E(t^n)$. The calculations for the next time step proceed in the following way.

"The first calculation uses the known ($t = t^n$) state of the Lagrange fluids and the pressures acting on the Lagrange boundaries to solve the Lagrange difference equations for each of the grids L_i^n. The solution to the differences equations gives us the $t = t^{n+1}$ state of the Lagrange fluids and new grid positions L_i^{n+1}.

"Next it is necessary to determine the set E^{n+1}, and this is done by one phase of the coupling calculation which uses the new grid positions L_i^{n+1}. We are then in a position to solve the Eulerian difference approximation equations for the t^{n+1} state of the fluid in the region E^{n+1}. This is done in the Eulerian phase of the CEL calculation.

"Having determined the t^{n+1} state of the Eulerian region, the second phase of the coupling calculation determines the t^{n+1} pressures which act on the boundaries of the Lagrange grids L_i^{n+1}. We have thus advanced all of the fluid quantities and grid positions to their $t = t^{n+1}$ values and this then completes one basic calculational cycle (or one basic time step of the calculation).

"The description of the CEL calculation will be complated by giving the 'start up' or initial ($t = 0$) state of the fluids and the initial positions of the mesh points for the grids L_i^0, $i = 1, 2, \ldots, E$ and the subset E^0...."

The basic HEMP-CEL Code has been modified by Physics International Company to cover projectile impact at relatively high velocities onto target materials of essentially zero strength such as water. This modification was called the PIPE Code and is applicable when the projectile and

target deform rather than break up and splatter. Figure 4.6 shows the penetration calculations of the basic HEMP Code at four different instances for a steel cylinder penetrating into an aluminum plate. In Figure 4.7 the mesh grid of the PIPE Code for a conical projectile before and after entering water at a velocity of 2.44 km/sec 25 μsec after contact is shown.

The basic principle of the HEMP computational procedure could also be applied to penetration calculations for the ocean bottom. However, the existing codes will have to be modified to account for the extremely low impact velocities of the ocean bottom sediments and their special properties, such as the development of pore pressures, the increase of strength with depth, and possible thixotropic or rheological stress-strain behavior. Such a computer program indeed should be developed.

4.2.6 Powered Travel Penetration

As stated in Chapter 1, one can make a distinction of the various kinds or types of penetration according to the forces acting during the penetration process. A missile, ship, or submarine may still be under power while striking the ocean bottom. However, in most cases the preponderant part of the energy exchanged during impact is most likely to come from the kinetic energy of the missile rather than from the propulsion system during the short period of impact. Therefore, the penetration phenomena for free fall and powered travel penetration will be essentially the same. The only possible difference may be that, in powered travel penetration, when power is supplied continuously and constitutes an important source of energy during impact, the energy furnished during the impact period must be added to the kinetic energy to account for the total energy being supplied. This can best be done by adding a kinetic energy correction in terms of an equivalent, additional velocity to the impact velocity. If, for example, during the impact period T power is supplied to the impacting object at a constant rate w, the total energy added to the object during penetration is:

$$E = wT = \frac{1}{2} m(\Delta V)^2 \tag{4.45}$$

where m is the mass of the object and ΔV is the equivalent velocity:

$$\Delta V = \frac{2wT}{m}^{\frac{1}{2}} \tag{4.46}$$

IF ΔV is now added to the original impact velocity V_o, the problem can be treated as before using

$$V_o' = V_o + \Delta V \tag{4.47}$$

Also, the object may have a greater horizontal velocity component than in free fall penetration.

This horizontal velocity component or the lack of alignment of initial impact point and center of gravity on the same impact trajectory causes a phenomenon called whip. For a cylindrical object with hemispherical nose, as shown in Figure 4.8, the impact decelerations in terms of the decelerations of the center of gravity c.g. are given as follows:

At the nose:

$$\ddot{x}_{nose} = \ddot{x}_{c.g.} + a \cdot \ddot{\theta} \sin \theta$$

At the tail:

$$\ddot{x}_{tail} = \ddot{x}_{c.g.} - b \cdot \ddot{\theta} \sin \theta$$

where $\ddot{\theta}$ is the whip acceleration.

The resulting impact will be a complex phenomenon of point- and broadside impact whose relative severity will depend on the obliquity of the impact θ and/or the horizontal velocity component.

It is because of the whip acceleration and the impact alignment problem that Schmid (1966) suggested a spherical shape if a remote sensing impact penetrometer is to be developed. This would eliminate one course of spurious data and results. While the problem in water is not as critical as it is in air, it nevertheless still exists and a spherical or hemispherical penetrometer shape rather than a cone is strongly recommended if this shape can be adopted without excessive penalties.

5.0 Dynamic Penetration - Penetration Resistance - Bearing Capacity

Dynamic penetration, where specific forces are applied to facilitate the penetration process, is most likely to occur when an object is forced deeply into the sea floor sediment, that is to say, when a pile, or a caisson, is driven into the ocean bottom. Thus, it is necessary to review that process of penetration in which a long, slender member is forced into a soil stratum. This is the problem of driving resistance and bearing capacity of piles. When an object such as a pile penetrates into a foundation material, the force required to achieve penetration is called the ultimate load Q or the bearing capacity. This ultimate load Q is made up of two components: the load transmitted through normal stresses at the point of the pile Q_p and the load Q_s transmitted through shear stresses along the circumferential surface area of the shaft of the pile (see Figure 5.1). If the area of the pile tip and pile shaft are defined as A_p and A_s respectively, the total ultimate load can be expressed by:

$$Q = Q_p + Q_s = A_p\, p_o + \int_{A_s} \tau_o dA \qquad (5.1)$$

where p_o (psi or tsf) is the bearing capacity of the soil at the tip of the pile and τ_o is the shear strength of the soil-pile interface. Both p_o as well as τ_o are material properties depending on the shearing strength of the soil.

5.1 Point Resistance

The first solution for calculating p_o was given by Prandtl (1920), (see Figure 5.2), applying the classical theory of plasticity to the problem of a rigid punch penetrating into a rigid-plastic solid. Reissner (1924), Caquot (1934), Buisman (1935), Terzaghi (1943), Meyerhoff (1951), De Beer (1948), and Berezantsez (1952) used the same approach and applied it with variations to the bearing capacity of soils. A recent review of their solutions was presented by Vesic (1967). The general formulation of the bearing capacity was given by Terzaghi as:

$$p_o = cN_c\zeta_c + qN_q\zeta_q + \frac{1}{2}\gamma BN_\gamma\zeta_\gamma \qquad (5.2)$$

where c and γ are the cohesion (shear strength) and the unit weight of the soil respectively, q is the overburden pressure at the tip of the foundation, and B the foundation width. N_c, N_q, N_γ are dimensionless bearing capacity factors for an

infinitely long strip and ζ_c, ζ_q, ζ_γ are shape factors. The coefficients N and ζ are functions of the friction angle ϕ.

For a cohesionless soil such as sand or gravel, equation (5.1) reduces to:

$$p_o = qN_q\zeta_q + \frac{1}{2}\gamma BN_\gamma\zeta_\gamma \qquad (5.3)$$

For a frictionless soil ($\phi = 0$) the coefficients $N_q = 1$, $N_\gamma = 0$, and $\zeta_q = 1$ and equation (5.1) reduces to:

$$p_o = cN_c\zeta_c + q \qquad (5.4)$$

The coefficients N were evaluated by Prandtl-Reissner, Terzaghi, Meyerhoff, Jaky and de Beer sometimes assuming different yield lines or shear patterns.

Figure 5.3 shows the failure pattern assumed by Reissner and by Caquot and Buisman. Figures 5.4 show the failure patterns assumed by Meyerhoff, and Figure 5.5 shows the yield line pattern of de Beer and Jaky where the yield lines revert to the shaft of the deep foundation.

The resulting bearing capacity factors N_c, N_q and N_γ as obtained by Meyerhoff are given in Figures 5.6, 5.7, and 5.8.

Inspection of equation (5.2) shows that the bearing capacity increases linearly with depth due to the second term: $qN_q\zeta_q$ since q is the overburden pressure prevailing at the point of the foundation. For uniform soil conditions $q = \gamma d$. Hence, for deep foundations this term should furnish the major part of the total point bearing capacity Q_p. Vesic (1967) compared the bearing capacity factors $\zeta_q N_q$ obtained by various investigators either by theoretical derivation or by empirical deduction with data from experiments both for an infinitely long, deep strip as well as for a deep, circular footing or pile. His results are reproduced in Figures 5.9 and 5.10 respectively.

As can be seen, a considerable spread of almost one order of magnitude exists between the influence coefficients obtained by de Beer-Jaky and those of either Terzaghi or Prandtl-Reissner. Also, a comparison of Figures 5.7 and 5.9 shows that the results of Meyerhoff for N_q are identical to those of de Beer.

5.2 Skin Resistance for Deep Penetration

According to the classical concepts of the sliding resistance offered by a surface in contact with a soil, the total

skin resistance is made up of friction and adhesion. Thus, for a cylindrical shaft

$$Q_s = \int_{A_s} \tau_o dA = A_s a + C \int_{z=0}^{d} \sigma \tan \delta dz \qquad (5.5)$$

where a is the adhesion between soil and the foundation shaft which, for uniform soil conditions, is usually assumed constant throughout a soil layer, C is the shaft circumference, σ is the normal pressure on the shaft surface, and δ is the angle of wall friction between soil and shaft. If we assume the normal stresses essentially to be "at rest" lateral earth pressures, we can calculate σ as:

$$\sigma = q(z)\, k_o = k_o \int \gamma dz = k_o z \gamma_{equiv} \qquad (5.6)$$

where k_o is the coefficient of lateral earth pressure at rest and γ_{equiv} is the equivalent unit weight of the soil from z = 0 to z.

Thus, assuming k_o, δ, and a to be constant with depth, the total skin resistance is given by:

$$Q_s = A_s a + \frac{1}{2} C d^2 \gamma_{equiv} k_o \tan \delta$$

$$= Cd(a + \frac{1}{2} d \gamma_{equiv} k_o \tan \delta) \qquad (5.7)$$

Now, the total resistance to penetration can be formulated and yields:

$$Q = A_{tip}(cN_c\zeta_c + \gamma_{avg} dN_q \zeta_q + \frac{1}{2} \gamma B N_\gamma \zeta_\gamma)$$

$$+ Cd(a + \frac{1}{2}\gamma_{equiv} d k_o \tan \delta) \qquad (5.8)$$

According to equation (5.8) the resistance to penetration should increase with the square of the depth of penetration d for large values of d.

The validity of the formulation as derived above for penetration into sand has been investigated recently by Vesic. He conducted large-scale model tests as well as prototype field tests and compared these results with the theoretical formulations. His findings are summarized below.

5.3 Surface Penetration into Sand

If we apply equation (5.8) to the penetration of a footing at the surface into a cohesionless material, then, because c = 0 and d = 0, the only remaining term is:

$$p_o = \frac{Q}{A} = \frac{1}{2} \gamma B N_\gamma \zeta_\gamma \qquad (5.9)$$

Vesic found that for this case three distinct types of shear failures could develop underneath the penetrating surface depending on the relative density of the sand D_r. For $D_r > 0.7$ shear failure would occur suddenly with a pronounced peak on the load-penetration diagram when the penetration reached about 7% of the foundation width. This type of failure was accompanied by the appearance of clearly defined shear failure zones and bulging of the sheared mass of sand very much in accord with the phenomenon described as general shear failure by Terzaghi.

For intermediate relative densities ($0.35 < D_r < 0.70$) no such sudden failure occurred and the load-penetration diagram gradually, and with irregular jumps, moved up to higher loads.

The wiggles in the diagram are caused by small, localized shear failures that gradually develop starting at a penetration of about 8% of the foundation width. At 15% penetration a shear zone boundary becomes visible at the surface. This phenomenon was described by Terzaghi as local shear failure.

On loose sand ($D_r < 0.35$) penetration occurs without any bulging of the surface. The resistance increases as penetration progresses and sudden, small shears occur as soon as penetration reaches about 6 to 8 per cent, again giving rise to a wiggly load-penetration curve. This phenomenon was called punching shear in an earlier report by De Beer and Vesic. The three types of failure as demonstrated by Vesic are reproduced in Figure 5.11.

The magnitude of the measured resistance to penetration is compared with the theoretically predicted values in Figure 5.12. Theoretical and observed values reported by Vesic for the bearing capacity coefficient N_γ (Caquot-Kerisel, 1953) are shown as a function of the dry unit weight. According to Vesic, the experimental values are generally 1.2 to 4 times higher than the corresponding theoretical values. This is in accord with the experience of other investigators (Hansen and Odgard, 1960; De Beer and Vesic, 1958; and L'Herminier et al., 1961), although a satisfactory explanation for this phenomenon is not yet available.

5.4 Penetration into Sand at Shallow Depths

The same three characteristic types of failure that occur in surface penetration also are observed at shallow depths. As the depth of embedment d increases, the relative density D_r at which the general shear failure changes into local shear and then into punching shear also increases. The approximate limits of D_r where these changes take place are shown in Figure 5.13. This figure shows relative depth d/B versus relative density D_r for the three types of failure.

From Figure 5.13 we can note that there are certain depths below which only a punching type failure occurs. For a circular foundation this is around d/B = 4.4; for a long, rectangular foundation it occurs beyond d/B = 9.4.

The limits delineated in Figure 5.13 also depend on the compressibility of the soil. In general, the more compressible a soil, the smaller will be the relative depth at which, say, general shear failure changes into local shear failure. Therefore, some materials may only exhibit punching shear failure.

5.5 Penetration into Sand at Large Depths

According to equation (5.8), the penetration resistance for a pile in sand should increase continuously at least linearly with depth d and as d^2 for large values of d.

Practical observations show that at shallow depths, penetration resistance indeed does increase linearly with depth up to about a relative depth of d/B = 4. However, thereafter, for larger depths, the bearing capacity or penetration resistance increases at a smaller rate until, at about d/B = 15, any increase in penetration resistance with depth ceases. This certainly is in conflict with any theoretical prediction of bearing capacity. However, the observation is confirmed by several investigators. Kerisel claims this is due to a complex dependence of N_q on the friction angle ϕ, d/B and B. Vesic attempts to explain it by redefining the quantity q as q_f, the effective normal stress at failure acting on a plane, horizontal element next to the foundation base. For depths d/B > 15 this stress q_f remains constant while at d/B < 4, q_f is equal to the overburden q. Whatever the reason, the practical fact and experience remains that penetration resistance and bearing capacity in a homogeneous sand increase first linearly with the depth of embedment up to about d/B = 4.0, then it increases less rapidly until at about d/B = 15 no further increase in the penetration resistance occurs. This latter fact can,

perhaps, also be explained by the facts that (a) for larger values of d/B only a localized punching type of failure occurs (see Figure 5.13), and (b) in the vicinity of the pile point actual tensile stresses are produced. While the soil immediately underneath the point is severely compressed, a certain stress relief due to the tensile stresses in the vicinity is possible. Figure 5.14 shows the strain distribution around a pile point in deep penetration as reported by Robinsky and Morrison (1964).

Vesic derived an expression for the bearing capacity coefficient for punching shear failure, using a shear failure pattern shown in Figure 5.15, and obtained:

$$N_q = \exp(3.8\ \phi\ \tan\ \phi)\tan^2(45 + \frac{\phi}{2}) \qquad (5.10)$$

A comparison between these theoretical values and experimental values observed with circular model foundations is shown in Figure 5.16. The shape factors ζ (equation 5.2) used for evaluating the test results were $\zeta = 3.0$. The results show good agreement with the values of equation (5.10) at low and intermediate relative densities while at high relative densities the test results are in better agreement with the values for N_q obtained by the Prandtl-Reissner theory. The bearing capacity coefficients N_q based on general shear as given by Meyerhof, De Beer, and Jaky are about one order of magnitude too high when compared with experimentally observed values. Another fact that supports this observation is the experience with actual pile driving. If the general shear bearing capacity factors were correct, it would be practically impossible to drive piles into sand at large depths. This, however, is done quite frequently. Since ocean bottom soils usually are very loose, with low relative densities, bearing capacity factors N_q obtained from equation (5.10) appear more appropriate for ocean bottom penetration.

5.6 Surface Penetration into Frictionless Material

Sandy and silty soils are terrigenic ocean bottom soils and will, therefore, be encountered mostly close to shore. The pelagic bottom sediments on the other hand, mostly oozes, and terrigenic clays, may be found farther offshore and in the deep ocean. Pelagic sediments may be considered essentially frictionless, having only a cohesion shear strength component. For these materials the original Prandtl solution may be applied directly (Figure 5.2). Applying equation (5.8) to a frictionless material at the surface ($d = 0$, $\phi = 0$, hence, $N_\gamma = 0$), we find it reduced to:

$$Q = A_{tip}\ cN_c\zeta_c \qquad (5.11)$$

The value of N_c can be taken directly from Prandtl's problem shown in Figure 5.2 and is given by:

$$N_c = (2 + \pi) = 5.14$$

The value of the shape factor for both a square or a circular cylinder is usually taken as $\zeta_c = 1.3$.

Hence, the total penetration resistance for a square or circular object penetrating into the surface of the ocean bottom is

$$Q = A_p \; s \; 5.14 \times 1.3 = 6.7 \; s \; A_p \qquad (5.11a)$$

where s is the shear strength of the ocean bottom soil and A_p is the projected area of penetration. One of the main problems in using this formula will be in the determination of the proper value of s.

5.7 Penetration into Frictionless Material at Depth d > 0

For values of d > 0, we find $N_q = 1.0$, $\zeta_q = 1$, and equation (5.8) becomes:

$$Q = A_{tip} \; (cN_c\zeta_c + q) + Cda \qquad (5.12)$$

We are concerned here with the penetration resistance and not with bearing capacity for a static load. Therefore, any adhesion is most unlikely to develop during the driving process because of remolding. Thus, the second term of equation (5.12) may be neglected.

According to Henky's theorem for the theory of plasticity, the bearing capacity coefficient for a long strip penetrating into plastic materials at d > B is given by:

$$N_c = 2 + 2\pi = 8.28 \qquad (5.13)$$

The values N_c are also given by Figure 5.6 for $\phi = 0$.

Now, the penetration resistance may be written as:

$$Q = A_{tip} \; (c \; 8.28 \times 1.3 + q)$$

$$= A_{tip} \; (10.8 \; c + \gamma_{avg} d) \qquad (5.14)$$

Practical experience indicates that, in general, the bearing capacity factor as given by equation (5.13) is a good, reliable value for the penetration resistance. While

values of N_c as low as 5 and as high as 20 have been reported, the preponderance of experimental and field data supports the value as given by equation (5.13) or by Figure 5.6 at $\phi = 0$. Also, it is not at all clear how much of the extreme deviations from equation (5.13) are attributable to errors in the determination or deviation from the assumed value for c. It appears then that these values can be used with reasonable confidence for the determination of ocean bottom penetration for frictionless soils.

5.8 Penetration Dynamics

If an object is to penetrate into the ocean bottom the penetration resistance as developed in the soil and calculated by the prior articles of this Chapter has to be overcome. This can be accomplished by the application of intermittent, high energy impact blows as is done in conventional pile driving; it may be accomplished by a high, statically applied jacking force which, of course, requires corresponding counterweights or reactions; or it may be achieved by continuously pulsating, vibratory forces (vibratory driving).

For all cases of penetration, the driving force F must be greater than Q and, if so, the motion of the penetrating object could be given by Newton's equation:

$$m\ddot{x} = F + W - Q \tag{5.15}$$

where m is the mass of the object and W its weight. Since both F and Q may be functions of time (5.15) can also be written:

$$\ddot{x} = \frac{F(t) - Q(t)}{m} + g \tag{5.16}$$

In order to solve this equation, the time variations of F(t) and Q(t) will have to be specified. For impact type pile hammers F(t) depends on the energy of the hammer and the cushioning of the blow. These factors will be discussed briefly in Chapter 6 in the sections discussing penetration equipment.

If the penetration is achieved by jacking, F(t) is, of course, the jacking force.

For vibratory driving, if the driving force is generated by counterrotating eccentrics, the dynamic force is given by:

$$F(t) = m_o r_o \omega^2 \sin \omega t \tag{5.17}$$

where m_o is the mass of the eccentrics, r_o the eccentricity, and ω is the angular velocity of rotation. Thus, equation (5.16) becomes:

$$\ddot{x} = \frac{m_o r_o}{m} \omega^2 \sin \omega t - \frac{Q(t)}{m} + g \qquad (5.18)$$

The principles of vibratory pile driving are briefly discussed in Section 5.9.

The resisting force Q(t) may also be a time dependent function. As in Chapter 4, one can attempt a formulation of Q(t) according to Poncelet's law:

$$Q(t) = Q_o + Q_1\dot{x} + Q_2(\dot{x})^2 + \ldots \qquad (5.19)$$

The static components Q_o of the penetration resistance for the various cases was discussed in the preceding articles of this Chapter.

Very little information is available on the viscous component $Q_1\dot{x}$ of equation (5.19). For sands at high vibratory energy input experimental data as well as practical experience suggest that this second term may be negative. The vibrations in sand cause a softening or liquefaction of the soil around the pile such that penetration is enhanced. This phenomenon is the cause for the remarkable success of vibratory pile driving.

Cohesive soils such as pelagic clays and oozes are likely to have the rheological properties of a Bingham body. That is to say, they will have a definite yield or shear strength τ_o and beyond that a small viscous component increasing with the penetration velocity $\dot{x}$. The shear strength τ_o and viscosity of kaolinite and bentonite soil pastes were investigated by Wenz (1963) who found that the shear strength τ_o was very sensitive to the water content, and that the additional, viscous strength increase due to $\dot{x}$ was small for kaolinite clays and absolutely negligible for bentonite clays.

Recently, Goble and Scanlan (1967) and Tomko (1968) have attempted to use Poncelet's law (equation 5.19) to determine experimentally the static bearing capacity Q_o. The basic principle chosen is to substitute equation (5.19) into equation (5.15):

$$m\ddot{x} = F(t) + W - (Q_o + Q_1\dot{x} + Q_2\dot{x}^2 + \ldots) \qquad (5.20)$$

If $\ddot{x}$ is measured by an accelerometer and F(t) by a set of strain gages, say, at the top of the pile, then the driving resistance Q(t) can be evaluated in principle since:

$$Q(t) = (Q_o + Q_1\dot{x} + Q_2\dot{x}^2 + \ldots) = F(t) + W - m\ddot{x} \qquad (5.20a)$$

Since the weight and mass of a pile are generally known, all terms on the right-hand side of equation (5.20a) are known or measured experimentally and Q(t) thus can be evaluated.

The static bearing capacity Q_o is particularly convenient to determine by considering the measured data at an instant t_o where $\dot{x} = 0$. Then equation (5.20a) reduces to:

$$Q_o - W = F(t_o) - m\,\ddot{x}(t_o) \qquad (5.20b)$$

The practical use of this principle for field application requires dynamic instrumentation that at this stage of development is probably still too sensitive and perhaps too complicated for general field application on a normal construction site. Such instrumentation has to be rugged, yet sensitive and reliable, to serve under the varying field conditions of the construction industry. Tomko (1968) reports and evaluates a series of tests using such instrumentation and reports moderate success. His final conclusions are perhaps worth recording here: "The present study has resulted in an intense familiarization with the rapidly passing response profiles occurring over a few tens of milliseconds after the hammer impact. That these profiles are both believable and physically explainable is in the author's opinion, to be considered a step forward in pile dynamic action."

Nevertheless, even though this method of assessing the bearing capacity of a pile cannot yet rely on wide experience and, at this time, is not yet strongly underpinned by empirical verification, it appears extremely interesting since it may make it possible, at last, to measure the static bearing capacity of a pile without resorting to a pile load test. Since load tests require large, often expensive reaction force - particularly in marine applications - the continued development and full proof-testing of this method is clearly warranted. With the ever-increasing pile dimensions and pile loads in offshore platform construction and the absence of established and empirically verified relationships between driving resistance and the ultimate bearing capacity, this approach acquires added significance and ought to be given high priority.

5.9 Pile Driving by Vibrations

Practical experience in the construction industry has shown that pile driving, and especially also extracting, can be done very effectively and efficiently by pile vibrators. Vibratory pile driving was initiated in the Soviet Union in the late 1940s and has found ever wider applications from year to year. A wide variety of pile vibrators has been developed (Schmid and Hill, 1966) and, especially during the last two years, vibrators powered by hydraulic motors have come on the market. The pile vibrators operate on the principle that, due to the high vibrations, the skin friction along the length of the piles is reduced to a negligible amount since the soil particles adjacent to the pile are kept in continuous motion. The remaining resistance to penetration is practically made up entirely of the point resistance which is overcome by a high, dynamic force F(t) given by equation (5.17), and a dead load W consisting of the weight of the pile, pile vibrator and any bias surcharge that may be added. If the penetration resistance of the pile point is known from a relationship as, for example, given by equation (5.14), the required dynamic force of the pile vibrator can be determined from equation (5.16).

There are basically two different methods of vibrating piles: by low frequency-rigid body vibrations and by high frequency-longitudinal resonance vibrations. The former are employed by most commercial pile vibrators both in the U.S. and abroad (Schmid and Hill, 1964). The resonance vibration principle is based on a U.S. patent issued to A. Bodine and the resulting machine was originally called a "Sonic Pile Driver." The principle of longitudinal resonance is without question applicable to driving piles. However, practical experience has shown that the high power necessary for resonance pile driving (the power requirements increase with the cube of the frequency) as well as the exacting tolerances demanded by such a high frequency machine and its maintenance problems make this method impractical and uneconomical. Especially since almost all the advantages of vibrodriving can also be reasonably obtained at lower frequencies and at much lower costs. For these reasons the development of the resonant pile vibrator was plagued by numerous disappointments (Jochums and Denny, 1961) and the commercial rights and development of the machine had a checkered corporate history. The last owner and operator, the Resonant Pile Corporation, is now defunct.

The limitations of vibratory pile driving are determined by the fact that the maximum available, dynamic driving force F(t) is limited:

$$\max F(t) = m_o r_o \omega^2$$

where m_o is the mass of the eccentrics, r_o is their eccentricity and ω is their angular velocity.

Since the operating frequency is usually limited, the maximum driving force of any pile vibrator has an upper limit. An impact hammer, in contrast, has a given impact energy E_o available. In easy driving the set per blow Δs is large and hence, the average driving force $P = E_o/\Delta s$ is relatively small. As the pile "fetches up" and encounters heavier driving resistance, the set Δs becomes smaller and, thus, the available driving force increases. Therefore, an impact hammer has the ability to furnish a higher punching force in hard driving, albeit at a considerably reduced driving rate. A vibratory pile driver, under tough driving conditions, just stops and fails to move the pile at all. This happens when the total weight plus bias, plus max F(t) is smaller than the total resistance to penetration as given by equations (5.8) or (5.12). This situation occurs most frequently in dense clays, hardpan, glacial till or in very compact and cemented sands and gravels.

6.0 Penetration Instruments and Equipment, The State of the Art

There are a series of activities that may be considered penetration into the ocean bottom that have been going on for some time and it is appropriate to review the current state of the art and the available equipment for these activities.

Probably the most immediately thought of penetration activity is the coring and sampling of ocean bottom sediments. A wide variety of new samplers and corers has been developed and put to use recently with great ingenuity. They are reviewed and discussed below in Section 6.1.

The anchoring of ships, buoys, mines and fixed installations often requires the penetration of anchors or anchoring devices into the ocean bottom. Although the penetration of most vehicle anchors is quite shallow, their state of development is reviewed briefly in Section 6.2.

One of the most effective and permanent methods of anchoring a structure is by driving piles into the ocean bottom. This method is extensively employed in fixing offshore platforms for oil drilling and production, offshore light-ships and radar towers, etc. Therefore, a review of the current status of the offshore pile driving technology is also presented in this Chapter in Section 6.3.

Finally, there is an interesting instrument developed recently that, while not yet used extensively for ocean bottom penetration, nevertheless has been used there occasionally or has the clear potential of so being used. We think here of the Sandia Corporation terradynamic penetrator. This instrument is suitable either for penetration into the ocean bottom as an exploratory tool or as an anchoring device.

6.1 Penetration of Sediment Samplers and Corers

A great variety of sediment samplers and corers have been developed in recent years and a thorough review of all of them would be beyond the scope of this study. However, it is obvious that the principles discussed in earlier chapters apply fully to the problem of penetration of sediment samplers and corers. For example, the terminal velocity for a free fall corer clearly can be calculated by the method demonstrated in Section 3.9. The depth of penetration can be assessed by one of the methods discussed in Section 4.2 and/or Chapter 5, bearing in mind, however, that for corer penetration the area of penetration is that of the projected area of the instrument minus the area of the resulting core.

It is also clear that, for submarine samplers, the same principles govern as for ordinary soil samplers (Hvorslev, 1949), namely, that the area ratio of the sampler C_a should be reduced to a minimum. The area ratio is defined as:

$$C_a = \frac{D_w^2 - D_e^2}{D_e^2}$$

where D_w is the outside diameter of the sampler and D_e is the entrance diameter of the core. Hvorslev also made recommendations regarding the inside clearance ratio C_i of the sampler, stating that

$$C_i = \frac{D_s - D_e}{D_e}$$

should not exceed 1.5 per cent, D_s being the inside diameter of the core barrel (see Figure 6.1a). The reason for this rule is that too large a ratio would permit excessive expansion of the soil sample, while too small a ratio would cause increased disturbance.

The problem of sample expansion may be even more severe for a marine sediment sample taken at large water depth because of the expansion of the pore fluid. A detailed analysis of this problem, however, is beyond the scope of this study.

To increase depth of penetration, while keeping sample disturbance at a minimum, we feel that the terminal velocity should be kept at some optimum range of, say, 15 feet per second and any increased penetration be obtained at the cost of increased mass rather than increased velocity. Also, one of the most critical parameters for good sample recovery is the perfect alignment of the corer at impact. For this reason the marine sampler should be designed in such a way that the vertical distance between the submerged center of gravity and the center of buoyancy is a maximum.

Without claiming to present a complete review of all submarine sediment samplers and corers, the more representative ones are reviewed in the following section.

6.1.1 The Gravity Corer

This instrument is a long, cylindrical tube weighted by heavy blocks to provide a large penetration force and a high impact energy. A typical section of an older gravity corer is shown in Figure 6.1 as reported by Emery and Dietz

(1941). This corer was used on the research vessel E. W. Scripps and yielded cores with an average length of 6.3 feet, and a maximum length of over 16 feet. The operation of the corer is described as follows:

"After the instrument is lowered into the water, it is dropped slowly until within about 300 feet of the bottom as indicated by the ship's echo sounding device and is then allowed to run rapidly with only a slight brake pressure to insure a vertical descent. Velocities of 12 to 21 feet per second are attained just before striking bottom, regardless of the length of cable paid out. In depths shallower than 3000 feet a slackening of cable indicates that the instrument has hit bottom. Between depths of 3000 and 6000 feet, a pointer attached to an accumulator spring has been found useful, but at greater depths and in rough weather there is some difficulty in determining the instant of impact. When bottom is reached, the winch is stopped immediately to prevent kinking of the cable."

A more modern gravity corer is the Sphincter 120 mm corer (Kermabon, Blavier, Cortis and Delauze, 1966) which seals the cores within a watertight container during retrieval and also has an electrical release system. Its details are shown in Figure 6.2.

A similar arrangement in which a pilot weight releases the gravity corer to obtain a higher free fall energy than would be possible by paying out the cable is reported by Hvorslev and Stetson (1946) and is shown in Figure 6.3.

Recently, unattached sediment corers have been developed (Moore, 1961; Sachs and Raymond, 1965). The operation of such an unattached instrument involves (i) the launching of an over-ballasted, deep, submersible float to which the instrument is attached, (ii) the release of the ballast at some predetermined depth, and (iii) the recovery of the pay-load at the surface. Particularly in deep water, unattached instruments can often be operated more effectively and with less difficulty than wire-line instruments, and, in some instances, they are usable where wire-line instruments are not.

Recently, Moore (1961) solved the problem of withdrawing, with little force, a short core from the bottom, and this made possible the successful development of a free, unattached sediment sampler.

The resulting sampling instruments are shown in Figures 6.4 and 6.5.

6.1.2 Vibratory Impact Coring

A quite recent development is the coring of ocean bottom sediments by vibrations. While vibratory soil sampling on land has been going on for about twenty years, especially in the Soviet Union, it is only recently that ocean bottom sediments are being sampled with the help of vibrators.

Figure 6.6 shows a vibratory core sampler developed by the Water Resources Division, U.S. Geological Survey, Portland, Oregon for a cooperative study with the U.S. Atomic Energy Commission (Prych and Hubbel, 1966). This sampler has been used successfully in water depths up to 20 meters and in mean flow regimes up to 1.5 m/sec in the Columbia River estuary. Ordinarily, it is used off the aft end of a 12 m commercial fishing vessel and achieves total penetrations of 180 cm (6 ft.) by inducing longitudinal vibrations with a vibrating time of less than one minute.

Another vibratory sampler of ocean bottom sediments that is capable of applying longitudinal as well as torsional vibrations is described by Menard (1965). Details of his device and method are reproduced in Figures 6.7 and 6.8. Menard claims that this equipment is capable of operating in water depths up to 500 fathoms.

A list of recent developments in ocean bottom sampling appeared in the 1968 Handbook on Under Sea Technology and is reproduced below as Table 6.1.

6.2 Penetration of Anchors

There are various types of anchors available for holding a ship or object in a relatively fixed position. These anchors and several new anchor types developed by the Naval Facilities Engineering Command were discussed by Tudor (1967). A short discussion of them is presented below.

6.2.1 Gravity or Dead Weight Anchors

These are the most elemental type of anchors. They are massive and have a low holding power to weight ratio. Because of their mass they are expensive and difficult to handle and transport. They also have a tendency to move laterally at small lateral loads and are not very reliable if the ocean bottom is sloping or unstable. Their penetration characteristics are negligible.

Table 6.1.

TABLE III—RECENT DEVELOPMENTS IN SUBMARINE SAMPLING HARDWARE*

Name	Manufacturer	System	Depth of water	Depth of hole	Dia. of hole	Power req.	Platform	No. of opr.	Type of ground
Am dril	Alluvial Mining & Shaft Sinking Co. (U.K.)	hydropneumatic jetting, continuous	150'	30'	12"	300 HP	bottom	3	gravel 5"
Vibro drill	Compagnie Francaise de Geomecanique Technip (Fr)	hydraulic vibratory sample tube	600'	90'	14"-40"	300 HP	bottom	n.k.	gravel
Ocean bottom Corer	Precision Surveys Inc. (U.S.A.)	pneumatic vibratory sample tube	150'	6'	2"	60	bottom	3	sediment
Ringhammer	Dusterloh Ltd. (U.K.)	air hammer sample tube	100'	6'+	to 8"	n.k.	ship or barge	n.k.	sediment & boulders
Vibrator drill	Consortium of 1. Bruce White, Wolfe Barry & Partners 2. N.V. Billiton Maatschaapji 3. Vibratechniques Ltd. 4. Holman Bros Ltd. (U.K., Neth.)	pneumatic vibratory	45'-60'+	15'+	6"	250 HP	bottom	n.k.	alluvial minerals deposits
Horton Sampler	Ocean Science & Engineering Co. (US)	hydraulic vibratory continuous wire line, or sample tube	200'	100'	6"	100+	ship	4	alluvial minerals deposits
Sonico	Sonico Corp. (U.S.A.)	hydraulic resonant vibrator continuous	100+	100+	5½"	100 HP	ship	4	alluvial mineral deposits
Koken Marine Drill	Koken Boring Machine Co. Ltd. (Japan)	Electric rotary corer	450'	45'	2½"	40 HP	bottom	4	hard rock
Outward bound drill	Offshore Drillers Pty. Ltd. (Aus.)	vibratory continuous jet lift	100'+	100'+	1"	n.k.	ship	n.k.	alluvial mineral deposits

6.2.2 The Standard Drag-Type or Fluke-Type Anchors

These anchors, such as the Navy standard, stockless anchor, the Admiralty anchor, or the Danforth anchors, provide primarily a horizontal holding power. Large, flat flukes penetrate into the ocean bottom by being dragged along the bottom and gain their holding power from the shear strength of the bottom sediment. Details of such a fluke-type anchor are shown in Figure 6.9 which shows the BUDOCKS STATO mooring anchor (Towne, 1959). Superior holding power in mud bottom is claimed for this anchor. The penetration of these anchors is limited to the fluke length. Often, a large, horizontal distance is needed to set this kind of anchor adequately, requiring large amounts of line and gear. Typical ratios ℓ/d of length of anchor cable to depth of water are 2.0 to 3.0.

6.2.3 Explosive Anchors

Explosive anchors stem from a relatively recent and intensive development. They are small, lightweight, rapidly installed, and are adaptable to a variety of ocean bottom conditions. Development has been carried out primarily by the Concept Engineering Company, by Aerojet-General Corporation, and by the U.S. Army Engineering Research and Development Laboratory (ERDL). Explosive anchors are currently being used in shallow depths of 200-300 feet but there is no obstacle that would preclude their use in depths to 1000 feet or more.

Figure 6.10a shows an explosive embedment anchor developed by the U.S. Army Engineers Research and Development Laboratory (ERDL). This anchor, according to Tudor, is being modified by NCEL for use in water depths up to 6000 feet. Figure 6.10b shows a cross-section of another explosive self-embedment anchor developed by the Magnavox Company. It consists of a flotation assembly, electronics package, the anchor, and cable pack. When the system enters water, the assemblies separate and the cable pays out from the back of the anchor package during descent, preventing cable drag. When the anchor package hits bottom, the unit fires, driving the anchor into the ocean floor. At the same time the cable is locked up, preventing further payout. The anchor is tied to its package housing by a cable long enough to ensure against breakage due to premature anchor snubbing. As the cables pull taut, the spring-loaded anchor flukes dig in and spread out. System safety is assured by design. The fuse is armed by hydrostatic pressure, and the arming mechanism is locked until the system enters water and descends to a preset depth. The use of mechanical devices also eliminates unwanted initiation by stray electromagnetic signals.

For all explosive anchors, the explosive charge must be properly designed so that the required penetration is achieved. If the driving energy is too little, the desired penetration and, hence, holding power will not be attained. If it is grossly in excess, the anchor may be damaged. The required explosive energy can be calculated for any given penetration from a penetration formula, say, equation (4.26):

$$E_{req} = P \cdot X_{req} = A\, p_o\, X_{req} \qquad (6.1)$$

where A is the cross-sectional area, p_o the bearing capacity and X_{req} is the required depth of penetration determined by the desired pull-out force.

Tudor reports recorded holding power for the ERDL explosive anchor in sand and clay of 60,000 lbs. for the 50 kip rated anchor and of 200,000 lbs. for the anchor rated at 300 kip. In soft mud these two anchors held 15,000 lbs. and 58,000 lbs. respectively.

6.2.4 Free-Fall Embedment Anchors

Like the free-fall corer or sampler, this anchor achieves its penetration by the energy of its impact when hitting the bottom. Thus, the determination of the striking velocity must follow the principles and methods described in Chapter 3 and the penetration phenomenon is controlled by the relationships discussed in Chapter 4.

One such typical free-fall anchor and its placement is shown and discussed by Smith and Dantz (1963). Tudor (1967) also shows a free-fall embedment anchor with a holding power to weight ratio of 6:1. Terminal velocities obtainable appear to be in the range of 20 to 25 fps.

6.2.5 Umbrella Pile Anchors

These anchors were designed to be driven or vibrated into the sea bottom like a pile and then open up to obtain greater bearing capacity or holding power and/or greater resistance to uplift or break-out. A typical example is shown by Tudor (1967) who also gives bearing or holding capacities that can be achieved with this anchor. Umbrella pile anchors are used where conventional anchors cannot be dragged, c do not provide sufficient embedment, or where the bedrock is too deep for obtaining point support of bearing piles. The Vertohold Embedment Anchor of Edo-Western Co. is an umbrella type anchor that is driven into the bottom soil by an explosive charge fired either upon bottom contact or by remote control.

Holding capacities of 220 kips in bearing and of 300 kips in uplift have been reported for such umbrella type anchors at an embedment of 20 ft. in sand. When embedded in blue mud interspersed with fine sand and shells, a capacity in excess of 100 kips has been recorded. In general, the holding power of such umbrella pile anchors should be proportional to the projected area of the opened umbrella and to the square of the depth of embedment.

6.2.6 U.S. Patents on Sea Bottom Anchors

The problem of anchoring a device in the ocean bottom has attracted the interest and imagination of a wide variety of scientists, engineers and inventors, as a look at the list of U.S. patents given in Table 6.2 will reveal:

Table 6.2

List of Recent U.S. Patents on Sea Bottom Anchors

U.S. Patent #	Subject	Inventor	Date
2,993,461	Embedment Anchor	A. M. Feiler	7/25/61
3,018,752	Projectile Anchors and Anchoring Emplacing Devices	R. T. Sorrell	1/30/62
3,032,000	Embedment Anchor	A. M. Feiler	5/1/62
3,118,417	Method and Apparatus for Anchor Embedment	T. Stanwick	1/21/64
3,164,042	Embedment Anchor	R. A. Thomason et al.	10/27/64
3,170,433	Imbedment Anchor Assembly	J. T. Gardiner	2/23/65
Re. 25,764	Embedment Anchor	R. S. Robinson	4/13/65
3,187,705	Dynamic Anchor	R. B. Costello et al.	6/8/65
3,207,115	Explosive-Operated Anchor Assembly	M. H. Anderson	9/21/65
3,280,782	Marine Anchor	C. H. Holm	10/25/66
3,291,092	Mooring Apparatus	P. V. Halberg et al.	12/13/66
3,311,080	Pressure Actuated	V. C. Anderson et al.	3/28/67
3,315,629	Underwater Anchor Gun Device	J. A. Standridge et al.	4/25/67

Table 6.2 (continued)

U.S. Patent #	Subject	Inventor	Date
3,330,338	Anchor and Method of Installing	J. R. Dozier	7/11/67
3,370,566	Embedment Device	J. A. Dorr et al.	2/27/68
3,371,643	Hydraulically Actuated Driver	W. H. Dunham	3/5/68
3,399,646	Submarine Anchor Assembly	R. P. Vincent	9/3/68
3,411,473	Deep Water Anchor	G. E. Mott et al.	11/19/68
3,417,724	Vibratory Sea Anchor Driver	T. B. Edwards	12/24/68

Nearly all of these patents concern mechanisms and details for explosive anchors describing and claiming specific features for arming, igniting, and achieving penetration and anchorage for these devices.

6.3 Penetration of Piles into the Ocean Bottom

Piles have been driven into the ocean bottom for hundreds of years. These installations usually were for nearshore facilities such as docks, wharfs, quays and piers, and the piles are usually driven from above the water.

Within the last two or three decades, however, an entire new industry has developed concerned with the exploration and production of natural oil and gas far offshore on the continental shelves. Most of this activity takes place on platforms anchored to the ocean bottom by long, penetrating piles and some of the technical developments of this new industry are of interest here.

6.3.1 Offshore Construction and Its Technology

Beginning in rather shallow water offshore Louisiana shortly before and after the Second World War, offshore drilling and oil production progressed at a dizzying pace such that by the end of 1957 approximately 1200 producing oil and gas wells and 500 nonproductive wells had been drilled on the northern shelf of the Gulf of Mexico. Since then "offshore fever" has spread all over the globe and by 1969 offshore oil exploration and production is carried out among other places off the coasts of California, Alaska, West Africa, Australia, Indonesia, Brazil, Nicaragua, Peru, Trinidad, Nova Scotia,

Spain, France, Tunisia, New Zealand, Borneo, Egypt, and in the Arabian Gulf, the Gulf of Suez, the Sea of Japan, the Adriatic, the Java Sea, the Nigerian Gulf, the Caspian Sea, Lake Maracaibo, Lake Erie and in the North Sea. By 1967, after 20 years of operation, well over 2000 platforms had been installed and over 9000 wells had been drilled.

Expenditures in the offshore industry at present are in excess of one billion dollars per year and the world petroleum industry is expected to invest at least 25 billion dollars off the coasts of more than 60 nations during the next decade to explore, develop, and produce offshore oil fields.

At a cost of several million dollars apiece, the current inventory of the industry includes 150 mobile offshore drilling rigs and 120 self-contained drilling platforms. Table 6.3 shows the extent of recent, new construction of mobil rigs supported on piles. In addition, during the same period covered by the Table, twelve drill ships and ten semi-submersibles were under construction. Drillships and submersibles do not utilize piles that penetrate into the ocean bottom.

With all this activity in ocean bottom pile driving, it is proper and necessary in the context of this study to review the state of the art of pile driving and penetration into the ocean bottom as currently practiced by the offshore industry. Before doing this it may be useful to present some general background information on offshore platforms and structures and the associated engineering problems.

The current technology of offshore structures has limited the exploration and exploitation of reserves to the relatively shallow depths of the continental shelf. Even so, the structural design of production platforms has imposed great challenges on the engineer.

6.3.2 Types of Offshore Structures

The basic objective of the offshore structure is to drill and support several oil wells in the ocean floor. To meet this end, several different types of structures are available. The selection of one structure over another would necessitate a performance comparison of at least the following items:

(1) Stability on location

(2) Ease of movement

(3) Minimum dependence on other craft

Table 6.3 Mobil Rig Construction for 13 Months Ending June 1968

Rig Type	Name	Owner	Builder	Completion	Water Depth Capacity
Propulsion-Assisted Jackup	Rig 58	Penrod Drilling Co.	LeTourneau	Late 1968	200
Propulsion-Assisted Jackup	Rig 59	Penrod Drilling Co.	LeTourneau	1969	200
Self-Elevating Drillship	Un-named	The Offshore Co.	Upper Clyde Ship-builders, Ltd.	Winter 1969	250
Jackup	Maersk Explor-er	Zapata Offshore	LeTourneau	May 1967	125
Jackup	Rig 59	Trans-world Drlg Co.	Bethlehem	May 1967	125
Jackup	Gulf-tide	Husky Oil (Alberta)	John Brown & Co. (Clydebank) Ltd.	August 1967	200
Jackup	Chazar	USSR	IHC Holland	August 1967	200
Jackup	Petro-bras I	Petro-bras	Companhia Commercio E.Navagacao	Imminent	100
Jackup	Sed-neth II	Sea Drig Nether-lands	Rotterdam Dockyards	May 1968	200
Jackup	Norsmec I	Norsmec	Norsmec	June 1968	150
Jackup	Un-named	Japan Ocean Drlg.	Seeking Contract		
Workover-Jackup	Dresser Rig I	Dresser Offshore	McDermott Shipyard	May 1967	60
Workover-Jackup	Dresser Rig II	Dresser Offshore	McDermott Shipyard	May 1967	60
Workover-Jackup	Dresser Rig III	Dresser Offshore	McDermott Shipyard	May 1968	70

Table 6.3 (continued)

Rig Type	Name	Owner	Builder	Completion	Water Depth Capacity
Workover-Jackup	Dresser Rig IV	Dresser Offshore	McDermott Shipyard	Imminent	70
Workover-Jackup	Topper II	Crestwave Offshore	LeTourneau	March 1968	125
Workover-Jackup	Cowrie I	Shell (U. K.) Ltd.	IHC Holland	May 1968	30
Workover-Jackup	Ranger I	Walker-Huthnance	Bethlehem	Imminent	70

(4) Towability

(5) Ease of equipment and personnel transfer under adverse sea conditions

(6) Efficiency of drilling operation

(7) Storage capacity

The structures available may be grouped as follows:

(1) Mobile platforms

(2) Fixed platforms

Mobile platforms, possessing the ability to move to different locations, were conceived as an exploratory tool. Fixed platforms would subsequently develop those areas which were found to contain sufficient petroleum reserves to justify permanent installations. In practice, the mobile platforms have been found capable of economical production of complete oil fields. Both types will be described briefly.

6.3.3 Mobile Platforms

Jack-Ups

This structure is the most widely used mobile platform in use today. In concept, the structure, consisting of a hull and three or more legs, is towed out to sea, and the legs are jacked down far enough to raise the hull out of the water a predetermined amount. (See Figures 6.11, 6.12, and 6.13.) The structure must fulfill the following functions:

(1) Position of the platform must not be unduly influenced by the action of the sea and wind.

(2) Platform must be seaworthy.

(3) Raising and lowering of legs must be safe and efficient.

(4) Withdrawal of legs which have penetrated the sea bottom must be possible without endangering the structure.

The jack-up legs may be circular, triangular or square in cross-section and are usually of tubular design. The bottom of the legs are usually fitted with a watertight can in order to increase the bearing area and prevent excessive penetration into the ocean floor. Difference in bottom conditions will determine the shape of this can. Water jets are often used to settle the legs in the ocean floor or free a wedged leg before rig transfer.

Submersible Jack-Ups

This is the further refinement of the jack-up for operation in soft bottom conditions. The jack-up legs are attached to a large, submerged barge and do not penetrate into the ocean bottom. (See Figures 6.14 and 6.15.) The submerged hull can permit a fixed condition to be assumed for the column legs.

Semi-submersibles

Semi-submersibles can work as bottom-supported units or floaters. (See Figures 6.16 and 6.17.) The bottom hull is attached to the working hull by large diameter, tubular columns. Stability is maintained by the fact that the center of gravity is below the surface of the water. Position may be maintained by anchors. The rig is extremely difficult to tow, but is capable of production in 1500-foot water depths.

The area requirements for the bottom can of the jack-up legs or the submerged hull of a submersible jack-up - once the strength of the bottom sediment is known or estimated - can be calculated by the methods of Section 4.2.1 and 4.2.2.

6.3.4 Fixed Platforms

Fixed platforms (see Figures 6.18 and 6.19) consist of three main parts: template (jacket), piles, and hull. The template is fabricated from trussed, tubular steel at a shipyard and towed to sea. At arrival on location, the

jacket is lifted or launched in the water with its hollow legs upright. The structure is then leveled. Piles (consisting of large diameter steel tubes) are driven through the template to the desired depth. The tops of the piles are subsequently welded to the template. Finally, the hull, consisting of trussed or plate girders, is welded to the top of the piles. The disadvantage of this unit is the lack of mobility. Platforms have been designed to work in 340-foot depths and, at present, a design for a platform in 400 feet of water has been completed and is in the process of bidding.

Structural Evolution of the Fixed Platform

Current versions of fixed platforms have been profoundly influenced by structural improvement of the earliest designs. At the beginning of the oil industry's quest for underwater deposits, the structures were simple. Rigs were supported by 200-300 timber piles of a maximum length of about 90 feet. The decks were large enough to accommodate the normal, land-based drilling apparatus. Structural design was limited to a normal design for the weight and configuration of the deck versus the bearing capacity of the piles. The effects of wind and waves were acknowledged by a liberal amount of bracing above the water line, but insufficient knowledge of these forces prevented a rigorous analysis.

In retrospect we must admire the offshore pioneer and his timber pile rig. Admittedly, many losses did occur, but pre-war daring provided a basis for post-war burgeoning. In 1946, steel was substituted for timber and the size of the deck was reduced to a minimum. The drilling operation was supported by a tender which was anchored near the rig. Access was maintained between the rig and the tender by a ramp or "widow maker." During heavy seas, operations had to be suspended while the tender backed away from the drilling platform. This discontinuity in operation led by evolutionary change to the "self-contained platform." (The tender operation has not been discontinued.)

This concept placed all of the operation back on one deck, and forced the structural designer to more sophisticated methods of analysis. Proceeding with a minimum of data, an imperfect knowledge of the theory of wave motion, and a few newspaper accounts of the magnitude of hurricanes, the early structures were designed and built. According to the "eternal amazement" of one authority, some of them are still in use after more than 20 years of service.

The configuration and size of the structure, the choice of structural materials and the varied type of drilling requirements resulted in many different designs. The final

approach, as noted in the description of fixed platforms, was to build a template out of tubular steel, float this template out to sea, sink it to the bottom at the desired location and drive piles through the tubes. The original designs called for many tubes - 30 to 40 - about 12 to 16 inches in diameter and 12 to 15 feet apart. After the piling had been set in place, the structure was placed on top and drilling could begin. The relatively close spacing of these piles formed a wall which storm waves would strike with enormous impact, overturning moment, and uplift. Many structures based on this concept were lost. The idea was further refined by decreasing the number of tubes in the template and increasing their diameter. Consequently, modernized designs called for eight to ten 30-inch piles of about 300-ton capacity apiece at a spacing of 30 feet. The fewer number of piles allowed waves to pass through the structure with far less wave impedance. This, in turn, meant that trussed spans were required to carry the deck loads between the fewer supporting piles.

Of course, bigger piles meant bigger hammers, leads, cranes, fabrication techniques and barges. The requirements of design spawned a new, heavy industry.

6.3.5 Pile Driving in Offshore Construction

The evolution of offshore platform design and construction was reviewed recently by Lee (1968). Figures 6.20 and 6.21 show the development in the design from 1947 to 1967 and the records of water depth for fixed platform construction.

What this development has meant for the problem of driving the piles was discussed and shown by McClelland, Focht and Emrich (1967, Figures 6.22 through 6.25).

Piles presently used in offshore construction are typically 30 to 48-inch diameter. Penetrations to produce the required ultimate capacities are frequently in the range of 250 to 350 feet - although these vary widely. Since the piles generally extend some distance above the water level, total pile lengths of 400 to 600 feet occur frequently.

McClelland et al. show some typical pile dimensions (Figure 6.22) and the range of pile loads (Figure 6.23).

The installation procedure is shown in Figure 6.24. When considering the problem of offshore platform construction one must bear in mind that the installation of a pile, above or below water, not only consists of driving the pile home. Before this can be done the pile has to be properly

positioned and has to be guided throughout the driving process. Also, the pile driver has to rest on or be attached or clamped to the pile. It is for these reasons that we foresee future underwater construction in water depths up to, perhaps, 1000 to 2000 feet to follow very much the technology developed by the offshore platform construction industry and suggested by Figures 6.24A through C:

(1) A template towed (horizontally) to location and positioned by properly sequenced flooding of selective compartments.

(2) The driving of piles through the template sleeves by pile drivers that follow into the sleeves below the water.

(3) Connecting the driven piles and the lower part of the template by grouting the pile into the sleeve.

(4) Cutting off the upper section of the template, refloating it and returning it to port for reuse. The bottom part of the template either would completely contain the fixed structure to be installed on the ocean bottom, or it would have a template device for easily docking the facility onto the pile trestle resulting from this construction.

One of the major problems in offshore pile penetration has been the availability, or rather the lack of the necessary pile hammers. The difference between a normal pile driving job on land and a typical offshore job is enormous (see for example, Figure 6.25 comparing the load range of conventional pile load tests on land to a typical offshore pile load). The biggest pile hammers that were on the market until just a few years ago had a maximum energy of about 60,000 ft.lbs./blow.

The past few years, however, have seen the advent of significantly heavier equipment. Delmag has introduced a new D-44 Diesel pile hammer with a maximum energy of 87,000 ft.lbs./blow (Figure 6.26). The Vulcan Ironworks have developed the 040 single acting steam hammer with a ram weight of 40,000 lb., a drop height of 3 ft., and, hence, a maximum energy of 120,000 lbs. (Figure 6.27). And the MKT Corporation has developed a special offshore single acting steam hammer, the OS-60, with a ram weight of 60,000 lb., a fall of 3 ft., and, thus, a total energy of 180,000 ft.lbs/blow (Figure 6.28).

The most important new development, however, for pile driving and penetration into the ocean bottom, in our

opinion, appears to be the development of a hydraulically-powered pile vibrator recently introduced by the MKT Division of Koehring Company, Dover, New Jersey: the MKT V-10 (Figure 6.29). This vibratory pile driver has a maximum dynamic force of 112,000 lbs., a total weight of 9,500 lbs., and operates at frequencies from 1500 to 1850 cpm at a total power of 110 h.p. It is sealed against submersion in water although operation at large water depth undoubtedly will require special gaskets and packing seals, etc.

The advantage of hydraulic power for an underwater pile driver is that the prime mover (e.g. electric or diesel motor and hydraulic pump) can remain above the water on a barge or ship and the driving tool, powered through a hydraulic hose umbilical cord, is driven by hydraulic motors. This is a closed system requiring no exhaust under water. Such a system does not have the hazard nor the sealing-connection problems associated with high power electric cables. Also, since pressure in the hydraulic hose as well as the ambient pressure in the ocean increases linearly with water depth and, in both cases, almost at the same rate, the pressure difference and, hence, the circumferential stress in the hose remains practically constant throughout the entire depth. The only depth limitations, in principle, appear to be the friction losses in the hydraulic hoses between the driving tool and the prime mover.

As the water depths in which piles have to be driven continue to increase, it is quite clear that sooner or later piles will have to be driven not from a platform or from a template above water but from below the water surface. The method of providing the required power for the prime mover for such an underwater job then becomes critical.

A limited underwater driving capability exists today with existing equipment by the use of an MKT single acting pile driver that can be modified for underwater operations. This type of pile driver is capable of driving in water depths of 150 to 200 feet. The deepest operation of such an underwater pile driver so far was accomplished during the construction of the pier foundations for the Narragansett Bay Bridge in Newport, Rhode Island where 12-inch steel H-piles were driven at water depths of up to 162 feet. The operation of the pile driver at these depths required compressed air at 125 psi and 2400 cfm. In most cases, however, where piles are driven into the ocean bottom, driving still is carried out above water level.

There are a number of possible alternatives for powering an underwater pile driving operation (see, for example, Publication No. 1702, National Academy of Sciences) and the possibilities and limitations should be explored by a detailed feasibility and preliminary design study particularly if the present state of the art is to be advanced

significantly. But we believe that a hydraulically-powered vibrator (or impact hammer) is uniquely suited for underwater application where the prime mover remains above water and power is supplied by hydraulic hoses. A pile driving tool such as the V-10 should be able to operate easily with but minor modifications in water depths up to 1000 feet. The only limitation for extending operational capabilities to even larger depths appears to be the friction losses in the hydraulic fluid hose lines between prime mover and driving tool. Clearly, at some water depth of, say, 2000 feet or more it will become advantageous to dispense with any umbilical cord and develop an integral system of prime mover and driving tool both operating under water. The development costs for such a system, however, will be considerable. It will certainly be many multiples of the costs of adapting a hydraulic vibrator for underwater operation.

As explained in Section 5.9, pile vibrators have, as of this date (1969), definite limitations in driving capacity in stiff, dense clays, hardpan, and very compact or cemented sands and gravel. Vibrators normally outperform impact hammers under medium and light driving conditions by increasing driving speeds by a factor of at least ten. If soil conditions prevail, however, as those cited above, vibrators may not be able to drive piles at all. This is due to the still relatively low power tools that are available. Maximum power ratings of most commercial vibrator lines on the market are in the 100 to 140 h.p. range. However, second generation machines are under development that will significantly increase the available power and, hence, the available driving force.

6.4 The Sandia Penetrator

An interesting new arrival under exploration already for a number of years is the earth-penetrating projectile developed by Sandia Corporation (Colp, 1965, 1967, 1968; Thompson et al., 1965; Thompson, 1966; Young, 1969). A section of a typical penetrator is shown in Figure 6.30. This tool is essentially a solid steel cylinder with a conical or ogive nose that is given very high, up to ballistic, vertical velocities by dropping it at large heights from an airplane or helicopter. Near vertical position at release and aerodynamic fins assure nearly vertical alignment at impact. The afterbody of the penetrator holds a piezo-electric accelerometer giving the deceleration of the instrument through a trailing wire. The device has a potential both as a penetrometer measuring the deceleration experienced as it traverses soil layers of various strengths and depth as well as for the embedment of an anchor. The use of the device as a soil exploration instrument is demonstrated by Figures 6.31 through 6.34 which are taken from

various reports by Colp and Thompson cited above. In particular, Figure 6.32 shows how the instrument might be used for exploring the properties of ocean bottom sediments. It appears that the method, however, is rather expensive, requiring the use of an aircraft or helicopter and entailing the loss of the penetrometer for every point where the properties are measured. Also, it does not lend itself for use at large water depths because the loss of energy may become significant. The long trailing wire required to take out the signal may present problems. Therefore, instrumentation to preclude the use of trailing wire may be necessary.

The penetrator could also be used as a device for the emplacement of soil and rock anchors or instrument stations in the ocean bottom. A penetration nomogram based on the past experience with such devices is shown in Figure 4.5 and is discussed in Section 4.2.3 (Young, 1969).

7.0 Immediate Use Recommendations for Predicting Object Penetration into the Ocean Bottom

Recommendations for calculating and predicting object penetration into the ocean bottom depend very much on the conditions and circumstances of each particular problem. There are a number of important parameters that control the penetration process. It is of great significance how detailed and reliably these parameters are known or can be determined.

The controlling parameters according to our preceding considerations clearly are:

1. The impact velocity;
2. The mass, geometry and structure of the penetrating object;
3. The impact configuration (i.e. impact trajectory and geometry);
4. The properties of the ocean bottom.

The impact velocity can be calculated fairly well by the methods discussed in Chapter 3.

Which one of the various methods should be used to calculate penetration depends now largely on the reliability with which the four impact parameters are known. Clearly, it makes not much sense to spend an excessive amount of effort to, say, determine the impact velocity within a fraction of one per cent if the soil properties can only be ascertained between, say, ±50 per cent and vice versa.

Similarly, it does not make sense to go through complex calculations that try to compute penetration or velocities to a fraction of a per cent such as equations (4.13) or (4.21) if the properties or parameters that have to be used in these equations are not known or have to be guessed.

Then again, some approaches or methods might be more suitable than others for the particular set of parameters known. At any rate, to be most successful with any calculation, one should strive to have a balance in the reliability or the probability with which all the data entering into the computation are known.

In the absence of reliable information one can always work from two extreme assumptions and narrow the solution down to the more or most probable middle range.

Except for equations (4.13) and (4.21), none of the equations of Chapters 4 and 5 are complicated or cumbersome to solve and one would probably do well to make trial calculations with several formulae.

7.1 Recommendations for Free Fall Penetration

For an essential rigid body penetration of a more or less bulky (spherical or eliptical) object, one should try first equations (4.17) and (4.23) if the impact velocity is very low such that one would have to assume the phenomenon to be that of increasing area penetration.

If the impact parameters are such that a constant area penetration is indicated, one should try equations (4.14), (4.27), and (4.37). Also, equations (4.43) and (4.44) would be possible if a reasonable way exists to assess the value of the constants K.

As far as equation (4.43) is concerned, it is entirely empirical and the coefficients will have to be determined from several series of tests. Any extrapolation far beyond the range of the tests will be hazardous. Equation (4.44) is semi-empirical due to the fact that its structure basically follows the Poncelet solution. But again, the actual coefficients must be determined from experimental results. The difference is that here extrapolation may perhaps be carried farther with higher confidence. Since experimentation increases rapidly in cost with the scale of the experiment, the major part of the experimental work could be done on small-scale models and only a few experiments would be necessary at large-scale to check the validity over a wide range.

The parameters for the rheological models, for example G_1 and η_1 of equation (4.23), can be obtained by a curve fitting technique comparing curves obtained experimentally with those calculated theoretically by varying combinations of the parameters G_1 and η_1 (Tsai and Schmid, 1969).

If an impact penetrometer, for example, furnishes a certain signal trace giving the deceleration as a function of time, a corresponding $\ddot{x}$ versus time curve can be calculated assuming estimated values for G_1 and η_1. If the two curves do not match within acceptable limits, a new set of parameters G_1 and η_1 is assumed and the theoretical curve is recomputed. The comparison is repeated until all discrepancies are within acceptable limits. This process can be computerized facilitating the evaluation of a large amount of data and permitting a close match.

7.2 Recommendations for Dynamic (Driven) Penetration

For dynamic, driven penetration into sand or other cohesionless bottom sediment, the penetration resistance and bearing capacity is best calculated by using equation (5.8) with the bearing capacity factor N_q given by equation (5.10). For penetration into clay or cohesive materials, equations (5.12) or (5.14) are indicated.

These formulae are also indicated when the bearing capacity of a driven pile has to be calculated. The only difference is that the skin friction is more pronounced than during driving.

7.3 Recommendations for Powered Travel Penetration

A missile or vehicle may penetrate into the ocean bottom while still under power. For such a case the following procedure for calculating penetration is recommended:

The power furnished by the power plant during the impact period is considered to be constant and equals q (ft.lbs./sec.). The duration of the impact period T can be calculated from equation (4.30). The energy supplied by the power plant during impact then is $q \cdot T$. This energy can be converted into an equivalent velocity u_1 to be added to the impact velocity u_o as a velocity correction. Thereafter, the problem can be treated as a problem of free fall penetration (see Section 7.1) with impact velocity u_2 and:

$$u_2 = u_o + u_1 = u_o + \left(\frac{2qT}{m}\right)^{\frac{1}{2}}$$

where m is the mass of the missile.

7.4 Recommendations for Use of Sandia Nomograph

If information on the soil parameter S for the ocean bottom sediment is available from prior tests or experience, the penetration of a Sandia penetrator may be calculated by use of the nomograph of Figure 4.5 as described in Section 4.2.3. For this purpose, however, the impact velocity u_o must be calculated from the impact velocity u_1 at water surface impact minus the change in velocity Δu due to the drag loss between the water surface and the ocean bottom. The phenomenon is the same as that described by equations (3.22) to (3.25), (assuming a constant drag coefficient), and the impact velocity u_o at the ocean bottom would be given by:

$$u_2 = u_1 e^{-Kh} + u_o$$

where K is given by:

$$K = \frac{1}{2} C_D \frac{A}{m} \rho_f ,$$

h is the water depth, and u_o is the free fall-terminal velocity in sea water for the penetrator. Hence, the bottom impact velocity u_2 decreases exponentially with water depth and approaches asymptotically the terminal velocity of the penetrator u_o.

As a consequence, in deep water, little can be gained by dropping the penetrator from the air that could not be gained by dropping it from a ship. By evaluating the penetrator record and, hence, using the penetrator as a penetrometer, a measure of the strength of the soils traversed can be obtained. However, considerable additional research work appears to be required to get good quantitative data and results for deep penetrations.

7.5 Sample Calculations

To indicate in detail the use of the methods and equations recommended, a few sample calculations may be appropriate.

To calculate free fall penetration we consider the hypothetical case of a submarine, its hull intact, sinking to the ocean bottom. We assume the submarine to be of the class Guppy II with a length of 306 ft., a beam of 27 ft., a submerged displacement of 2,445 tons, and a minimum and maximum surface displacement of 1500 tons and 1840 tons respectively (Muga, 1968). The first parameter to be obtained is the impact velocity.

We may consider two cases:

case a): The hull sinking with longitudinal axis horizontal due to, say, a general flooding of the entire hull.

case b): The hull sinking vertically due to preferential flooding at the bow and a remaining air pocket at the stern of the hull, thus giving a center of buoyancy above the center of gravity of the partially flooded hull. For this case we assume a degree of flooding of 75%.

The terminal velocity is calculated from (3.21) as follows:

Total volume (submerged) of submarine: 2,445 m^3

Total gross weight of submarine: 1,500 tons

Air space in ballast tanks: 945 m^3

Volume of steel: V_s = 1,500/7.9 = 190 m^3

Available space in hull: 1500 - 190 = 1,310 m^3
Consider 20% of hull space filled by light weight equipment.

Weight of water flooding hull (case a):

$$W_f = 0.8 \cdot 1310 \cdot 1.0 = 1{,}050 \text{ tons}$$

Weight of water flooding hull (case b):

$$W_f = 0.8 \cdot 0.75 \cdot 1310 \cdot 1.0 = 785 \text{ tons}$$

Average density of sinking object:

case a): $$\rho_o = \frac{1500 + 945 + 1050}{2{,}445} = 1.425 \text{ t/m}^3$$

case b): $$\rho_o = \frac{1500 + 945 + 785}{2{,}445} = 1.325 \text{ t/m}^3$$

Assuming drag coefficients for both cases from Table 3.7 (since L/D ≈ 10), and respective drag areas:

case a): $C_D^* = 0.7$; $A \approx \frac{2}{3} \cdot 27 \cdot 306 = 5500 \text{ ft}^2 = 512 \text{ m}^2$

case b): $C_D^* = 0.5$; $A \approx \left(\frac{27}{2}\right)^2 \pi = 575 \text{ ft}^2 = 53.4 \text{ m}^2$

The terminal velocities u_o then are given by:

case a): $$u_o = 1.41 \left(\frac{2.445 \cdot 0.395}{0.7 \cdot 512 \cdot 1.030}\right)^{\frac{1}{2}} = 2.28 \text{ m/sec}$$

case b): $$u_o = 1.41 \left(\frac{2.445 \cdot 0.295}{0.5 \cdot 53.4 \cdot 1.030}\right)^{\frac{1}{2}} = 7.20 \text{ m/sec}$$

The formula that is applicable to this problem is equation (4.27) giving the maximum penetration:

$$X_{max} = \frac{m}{2Ap_o} u_o^2 = \frac{W}{g} \frac{u_o^2}{2Ap_o}$$

*C_D-values are extrapolated beyond the available data due to the large Reynolds numbers.

Assuming a bearing capacity for the ocean bottom of 1.5 psi = 0.105 kg/cm^2, and introducing the values found previously (using metric units throughout), we obtain:

case a):

$$X_{max} = \frac{3.495 \cdot 10^6 \cdot (2.28)^2 \cdot 10^4}{981 \cdot 2 \cdot 512 \cdot 10^4 \cdot 0.105} = 182 \text{ cm} = \underline{5.95 \text{ ft}}.$$

Also, the impact period is given by:

$$T = \frac{u_o m}{A p_o} = \frac{228 \cdot 3.495 \cdot 10^6}{981 \cdot 512 \cdot 10^4 \cdot 0.105} = \underline{1.51 \text{ seconds}}$$

Since this penetration is relatively small and to check by a second calculation whether this result is in the right order of magnitude, we may try equation (4.17) which is based on an "increasing area penetration" formulation. However, this equation was derived for the penetration of a sphere and, hence, it can, at best, give us a rough approximation provided we convert the penetration area into an equivalent circular area:

$$R^2\pi = 512 \text{ m}^2, \text{ giving } R = 12.7 \text{ m} = 1270 \text{ cm}$$

Now, using (4.17) we get:

$$X_{max} = u_o \left(\frac{m}{2\pi R p_o}\right)^{\frac{1}{2}} = 228 \left(\frac{3.495 \cdot 10^6}{981 \cdot 6.24 \cdot 1270 \cdot 0.105}\right)^{\frac{1}{2}}$$

$$= 470 \text{ cm} = 14.4 \text{ ft}.$$

and the impact period:

$$T = 1.57 \left(\frac{m}{2\pi R p_o}\right)^{\frac{1}{2}} = 3.2 \text{ seconds}.$$

This second calculation shows that both equations are consistent and essentially in agreement. The second results indicate that if a mass equal to that of the submarine had a spherical shape and would arrive with the same impact velocity, its penetration would be about 240 per cent of the one calculated by equation (4.27).

case b):

Using again equation (4.27) with the impact velocity and penetration area values for this case yields:

$$X_{max} = \frac{3.495 \cdot 10^6 \cdot (7.20)^2 \cdot 10^4}{981 \cdot 2 \cdot 53.4 \cdot 10^4 \cdot 0.105} = \underline{16,400 \text{ cm} = 540 \text{ ft}}.$$

and the impact period for this case yields:

$$T = \frac{720 \cdot 3.495 \cdot 10^6}{981 \cdot 53.4 \cdot 10^4 \cdot 0.105} = \underline{50.2 \text{ seconds}}$$

While these values are probably somewhat excessive due to the fact that no consideration was given to the increase in shear strength and, hence, bearing capacity p_o with depth, we feel, nevertheless, that they are entirely realistic values and must be within the right range.

The actual attitude of a submarine during free fall to the ocean bottom most probably will neither conform to case a) nor to case b). It will have some intermediate attitude which, given the usual ignorance about the details of a mishap, is difficult to assess. Nevertheless, the sample calculations show the limits that may be expected. Together with some calculations at several different yaw angles one could probably construct a diagram for probable penetration vs. yaw angle at impact. The final discovery photographs of the submarine Thresher (Buchanan, 1965) showed that only the tail section and the sail projected above the ocean bottom sediment a distance of about twelve and eight feet respectively. Since the sediment shear strength at the Thresher disaster site was about 0.3 psi, thus giving an ultimate bearing capacity p_o = 1.5 psi, these observations confirm the general correctness of the results obtained.

In general, we wish to emphasize that possibly none of the various equations or methods will turn out to yield the one, only and always correct result.

There will most likely be varying and changing success with several of the proposed approaches, and in the absence of any extensive proof testing, it is difficult to even hazard a guess which one is likely to be most successful.

Also, successful prediction depends very much on the success with which the properties or the parameters that enter into any formula can be measured or otherwise ascertained. Hence, the quality of any penetration prediction really cannot be assessed until some practical experience has been gained.

There is, nevertheless, a tremendous possibility and opportunity for improving our potential prediction capabilities and their reliability by perhaps at least one order of magnitude or more.

The details of this opportunity are outlined in Chapter 8.

8.0 Recommendations for Future Research and Development

To advance our present capabilities of predicting, as well as achieving penetration into the ocean bottom, a number of research and development projects can and should be initiated. To increase the reliability of penetration predictions, those parameters that are the "weak links" in the logic of the prediction process should be attacked first. The two weakest links are clearly the reliability of the strength assessment of the ocean bottom soils and the reliability of the various formulae discussed or derived in Chapters 4 and 5.

There exists very little evidence on the "in situ" strength of ocean bottom soils and the evidence on the relationship between the "in situ" shear strength and the strength obtained from measurements on core samples considering the data of Vey and Nelson (1967) is inconclusive.

It is not that we can claim an abundance of data from cores. Most of the strength information available is that obtained from core samples reported by Richards (1961), Moore (1962), and Keller (1967). Considering the vastness of the ocean floor, the volume of information is nothing to be complacent about. Therefore, there exists an urgent need to develop apparatus and instrumentation to measure the shear strength of ocean bottom soils in situ in a manner that is fast, reliable and cheap such that many measurements can be performed over a small area in one trip. Only then will it become practically a routine for any oceanographic activity to carry out also a bottom strength determination. The work reported by Kretschmer (1967) is considered truly a pioneering effort in this direction.

Preferably, however, rather than work with a static-load type plate bearing test, one might investigate a dynamic impact test such as that used by Scott (1967) or Schmid (1966). It is believed such instrumentation will lead to cheaper, more manageable equipment. Any such development of measurement instrumentation must account for the fact that the water content of the ocean bottom soils usually is far above the liquid limit and, therefore, the conceptual formulation of the stress-strain behavior should be one that is based on the principles of visco-elasticity rather than on those of elasto-plasticity. The treatment of most problems in conventional soil mechanics is based on the elasto-plastic failure concept. This is, perhaps, an admissible simplification for most conventional foundation problems. It becomes an entirely inadequate oversimplification, however, for ocean bottom soils. The data reported by Kretschmer (1967) on average, constant

penetration rates and stress relaxation for in situ, sea floor plate bearing tests clearly support this observation. Thus, it appears that an approach such as suggested by Schmid and Kitago (1965) or Tsai and Schmid (1969) is necessary for the evaluation of in situ shear strength data.

There are two recommendations for future research and development that can be deduced from these observations, namely:

1) Research on the visco-elastic stress-strain characteristics of typical ocean bottom soils should be carried out with soil constituents, porosities, void ratios, water contents and pore pressure environments as prevail on the ocean bottom.

2) Apparatus and instrumentation should be developed that will permit rapid, reliable, and cheap routine determination of the ocean bottom sediment stress-strain and strength characteristics. The author believes that the most promising approach in this direction would be the development of an impact penetrometer for deep underwater application using accelerometers, such as described by Scott, Schmid, or the Sandia device. However, we do not wish to exclude other methods that may have promise such as, e.g., an in situ vane shear test.

The second weak link in the reliability of the penetration prediction capability is the validity of the various formulae reviewed in Chapter 4. Again, two recommendations are suggested to improve existing capabilities, namely:

3) A computer program development should be initiated patterned after the HEMP Code and the coupled Euler-Lagrange (CEL) formulation as explained in Section 4.2.5. Such a program should be developed with the view in mind that any plausible, rheological stress-strain and failure characteristic that might result from work as recommended in 1) can be accommodated.

4) A carefully controlled, model test program (on a laboratory model scale) of idealized objects (preferably spheres) free-falling through water onto ocean bottom model test beds should be carried out to test the validity of the various formulae both for a larger number of small-scale and some larger-scale model tests. The smaller-scale model tests will permit the testing under a variety of conditions; the larger-scale model tests should provide sufficient data for extrapolation to check the scaling laws and similitude considerations. Perhaps later, also, some data for prototype confirmation may become available.

At any rate, the complete absence of data on the reliability of the available formulae for assessing ocean bottom penetration should be corrected. It is believed best to be accomplished by model scale experiments. We wish to note, however, that we believe maximum benefit will result from such an experimental program only after recommendations 1) and 3) have been carried out and the experimenters have the benefit of the results obtained there.

Alternately, if time is pressing, the experimental work might be carried out concurrently with the work recommended under 1) provided it is done by the same group or at least carried out in closest cooperation between both research task forces.

After a clearer picture is obtained on the stress-strain and strength characteristics of ocean sediments from programs initiated to follow up recommendations 1) through 4), it might also be useful to reexamine the wealth of acoustical data that is available for ocean bottom soils and attempt, perhaps, a better correlation between such data and stress-strain or strength parameters of the sediments. Prior work in this direction reported by Nafe and Drake (1963) and Horn et al. (1968), while not completely encouraging, nevertheless gives an indication of some promise that possible relationships might be explored. Horn et al. show that some causal relationship exists between wave velocity on the one hand and porosity, wet density, and moisture content on the other. No such clear-cut indication is given for the shear strength data. Faas (1968) reports an inverse, linear relationship between the reflection of an acoustic impulse from the ocean bottom and the porosity of the bottom sediment. This relationship has been shown to be consistent for sediments taken from different oceans and different environments. For these reasons we believe it worthwhile to take another look at the data to see whether some useful correlation can be established between the wealth of acoustic-seismic data and strength parameters. For example, a relationship should exist between observed dispersion of acoustic waves and the viscosity of the sediment. Thus, we recommend that

5) The relationships between acoustic properties and data of ocean bottom sediments and their stress-strain-strength parameters be investigated particularly in the light of experiences gained under work done according to recommendation 1).

Finally, with respect to efforts for increasing our capabilities of achieving deep ocean bottom penetration, we feel that deep penetrations in deep waters eventually will become an operational necessity and it will be useful to have an understanding, at least, of the problems with

which one will be confronted. Any deep penetration by piles, for example, in the deep ocean will have to be done by underwater pile driving since the present state of the art is pushing close to the limits of technological feasibility as far as driving piles from above the water is concerned. Piles having a length of 400 to 600 feet being driven above the water in water depths of up to 350 feet is the present advanced state of the art. Any significant increase in water depth and, consequently, in pile length will result in piles either so slender that they will buckle under the driving loads or so big and bulky as to make them unwieldy and unmanageable even with the heaviest, waterborne equipment. Hence, the only reasonable solution eventually will be to drive the piles underwater.

There are a number of possible approaches to the problem of driving piles below the water. Whichever method is best clearly will depend upon the water depth at which an underwater pile driver has to operate. The various possibilities may be grouped into three classes:

A) Atmospheric exhaust tools.

B) Closed systems (hydraulic or electric) with power supplied through an umbilical cord from a surface barge or tender.

C) Self-contained systems with power package and fuel supply on board for deep submergence operations.

A) Atmospheric exhaust tools are steam or compressed air hammers with exhaust to the atmosphere through exhaust hoses. This is the current state of the technology. The prototype tool is essentially a conventional, MKT single-acting pile hammer modified with pressure seals to operate under water. As mentioned before, the maximum water depth at which it has been used in the past is 162 feet. This, perhaps, can be pushed to 300+ feet. But the method becomes rapidly inefficient at water depths in excess of 200-250 feet due to the pressure losses and the large diameter hoses that will be required. The long hoses present quite a handling problem during operations. Nevertheless, achieving operational capability within this water depth range (say, up to 300 feet) probably can be accomplished at a relatively low cost.

B) Closed systems are hydraulically-powered pile drivers with a prime mover (hydraulic pump) on a barge driving hydraulic motors or pistons on the driving tool. The prime mover and driving tool are connected by an "umbilical cord" in the form of hydraulic hoses. Since such a system

could be operated at pressures of 1,500, 3,000 or 5,000 psi respectively, the corresponding sizes of the required pumps, motors and/or pistons become progressively smaller. Also, since internal pressure in the hose as well as external, ambient pressure increases linearly and at almost or, if sea water is used as hydraulic fluid, at exactly the same rate with water depth, no serious depth limitation would exist because of the pressure capacity limits of the hose. The limitations, again, would come from the friction losses in the hoses and the handling problems due to the hose length. We believe that these limitations may present serious handicaps if such a system is to operate at water depths beyond 1,500 to 2,000 feet.

An alternate method would be to supply power from the surface by an electric generator set and electric cables. This method, however, will present even more serious problems of sealing the electrical motors and cable connections. It has the additional disadvantage of being quite hazardous in case the cable gets sheared or damaged. Also, the electric motors are much more bulky than hydrauiic motors for the same power output.

As of this instance, there is one driving tool on the commercial market that is suitable for adaptation to underwater environment and the pressure ranges that appear practical for this type of driving system. This is the MKT V-10 hydraulic pile vibrator. Operating specifications for this machine are given in Figure 6.29.

Sufficient experience exists in vibratory pile driving that one can safely say it has been proven out technologically. As discussed in Section 5.9, however, pile vibrators in the power range commercially available at this time (1969) still have definite limitations with respect to the maximum driving force available under tough driving conditions. Fortunately, there are vibrators now under development with a significantly stepped up maximum dynamic force that should put them into the same range as conventional, heavy, single-acting hammers.

Since hydraulically-driven vibrators appear to be ideally suited for underwater application and, moreover, since such vibrators are already developed commercially and, hence, may be adapted to underwater use at relatively low costs of development, we recommend that

6) the adaptation of these tools for underwater operation be investigated.

The limits of suitability should be explored, as well as the design changes that would become necessary to achieve underwater operational capability, and the limits up to which an underwater hydraulic vibrator powered by hydraulic pumps above water is practicable.

Another similar tool in this group, equally suitable for underwater pile driving applications, is a hydroacoustic oscillator developed by the Electronics Division of General Dynamics Corporation as an outgrowth of underwater Sonar development (Anon., 1966). The principle of this tool is, essentially, a hydraulic piston that serves simultaneously as a valve and thus represents a machine with only one moving part (see Figure 8.1). This feature makes it extremely attractive.

The tool could be used as a linear oscillator or, with appropriate anvil coupling, as an impact tool (Figure 8.2). The configuration and dimensions of such a machine depend largely on the frequency of the hydraulic piston-valve and the required power output. Figure 8.3 shows some typical dimensions for such a tool operating at a 1500 psi pressure differential and various frequencies and power outputs.

The disadvantages of the tool lie in its extremely narrow frequency range -- the tool is essentially a single-frequency machine. Also, the machine is not yet developed commercially and, hence, there may be considerable development costs. There is no question, however, that the system has promise for underwater applications.

C) The self-contained system is, essentially, a closed system having prime mover, fuel supply, and driving tool aboard and, hence, such a system requires nothing more than a cable connection for lifting and lowering. Thus, it has the largest depth capability of all possible systems. There are no problems of friction losses nor those of handling long lengths of hoses. The power for the required intensities and duration of operations is most practically obtained by providing chemical steam through burning hydrogen and oxygen or, preferably, hydrogen and hydrogen peroxide. The actual driving too, then, can be an especially sealed, conventional type steam hammer. A fairly detailed concept for such a system has been proposed by the MKT Corporation (Anon., 1967). Again, there will be considerable costs associated with such a development but, eventually, it will have to be undertaken.

For these reasons we recommend that

7) Feasibility studies on tne design and development of underwater pile driving systems possible within the present and future state of the art should be carried out. Such studies might reasonably begin with assessing the underwater capabilities achievable with slight modifications of presently commercially available vibratory equipment and proceed from there with establishing the design envelopes for underwater pile drivers of increasing

capabilities both with respect to water depth and operational capacity. Concurrent with such studies or, perhaps, even preceded by it, there should be a study made on projected U.S. Navy requirements for operational capabilities on the ocean floor. As difficult as this may appear at this time, we believe much can be learned from a record of the growth of past requirements. This would also permit a reasonable phasing of any development work that will be required as a consequence of the study.

We conceive these studies as a two-phase or two-pronged program. One phase would investigate the technical possibilities within a short or intermediate time range by maximum use of existing equipment and technology to advance present capabilities at relatively low cost. We consider this a high priority, high payoff item capable of significantly advancing the state of the art at a relatively low cost. The second phase should be a long range look at technological capabilities and possibilities, particularly assessing overall development and operation costs for the various possible alternates such as, for example, the self-contained systems with great depth capabilities.

Since many future deep sea installations are very likely to be founded on piles penetrating deep into the ocean bottom sediment, which may be driven by vibrations, we recommend that

8) The bearing capacity of vibro-driven piles be established experimentally both in an ocean environment and in a near land or land foundation situation. There is only very limited data available both from prototype and model tests on the bearing capacity of vibro-driven piles. Also, some driving-bearing capacity relationship would be highly desirable not only as a construction quality control device but also, ideally, as a direct relationship similar to the various pile driving formula used for conventional pile foundations. Although the validity of many pile driving formulae is subject to grave doubts and reservations, the possibility of some relationship might be explored.

Here, particularly, the new developments reported by Goble et al. (1967) and discussed in Section 5.8 look most promising.

Another possibility is the use of the one-dimensional wave equation (Lowery et al., 1967).

Also, bearing capacity formulae have been derived for terrestial foundations and applications. Their applicability in the marine environment at the high porosities and high pore pressures prevailing in the marine environment should be reviewed.

Explosive anchors are an effective and relatively cheap method of achieving penetration into the upper stratum of the ocean bottom. Hence, we recommend

9) Continued development and proof-testing of explosively driven anchors, umbrella piles and similar devices.

The Sandia penetrator has applicability as a penetration device in shallow water depths only. As we have shown, its bottom impact velocity decreases exponentially with water depth and asymptotically approaches that of its own terminal velocity in water. We, therefore, see its usefulness as a penetration device severely limited to shallow water depths. However, we believe its potential as a penetrometer should be explored. Its use could be conceived as a free falling penetrometer (although we believe a spherical shape to be preferable for such a purpose) or, more promising, as a deep penetration device that is discharged from a frame lowered to the bottom (by an explosive or by a hydraulically-powered charge) into the deeper layers of the ocean bottom sediment. Therefore, we recommend that

10) The use of a Sandia-type penetrometer for measuring the penetration resistance at large depth in the ocean bottom sediment be explored.

In summary, then, we recommend the following future work to advance the state of the art of predicting as well as achieving ocean bottom penetration:

1) Investigation of the viscoelastic stress-strain and strength characteristics of ocean bottom sediment soils.

2) Development of reliable apparatus for quick and cheap routine determination of the strength of ocean bottom soils.

3) Development of a computer program similar to the HEMP-CEL Code for calculating penetration that is capable of accommodating any visco-elastic stress-strain-strength law.

4) Experimental model studies of actual free-fall penetration phenomena and their comparison with available formulae.

5) Review of the possible relationships of acoustical data to strength and viscosity properties of ocean bottom soils.

6) Feasibility studies for the development of underwater pile drivers at various depth and

operational capability levels, both with a short range and longer range objective. These studies should be coupled with, or preceded by, a study of U.S. Navy operational requirements projections.

7) Establishment of the bearing capacity of vibro-driven piles both in an ocean environment and on land, and development of some relationship between driving parameter(s) and bearing capacity both for vibro-and impact-driving.

8) Continued development and proof-testing of explosive anchoring devices.

9) Study of the application of a Sandia type penetrator lowered in a frame to the ocean bottom and then discharged into the deeper sediment layers as a penetrometer to measure the strength of the deeper layers.

Respectfully submitted,

Werner Schmid

Werner E. Schmid, P.E.

Princeton, New Jersey
March 31, 1969

ACKNOWLEDGMENTS

The author gratefully acknowledges the help of Messrs. Bruce C. Wheeler and John O'Donnell, undergraduates at Princeton University, who helped in the search and retrieval of the literature, and to Major John F. Sobke, U.S. Army, Corps of Engineers, graduate student in the Department of Civil and Geological Engineering at Princeton, who researched and wrote the major part of Sections 6.3.1 to 6.3.4 in Chapter 6 concerned with offshore platforms.

BIBLIOGRAPHY

Adams, D. F. and Tsai, S. W.: A Mechanics Analysis of Armor Penetration, Philco Research Lab. Publication No. U-2600, May 1964.

Allen, W. A.; Mayfield, E. B.; Morrison, H. L.: "Dynamics of a Projectile Penetrating Sand," Journal Applied Physics, Vol. 28, No. 3, 1957.

Anon.: Study of Mechanisms of Armor Penetration Resistance, Philco Research Lab. Publication No. U-2500, Jan. 1964.

Anon.: "Probing the Sea Bed by Transistor," Engineering, 198, Dec. 4, 1964, p. 708.

Anon.: Research, Development, and Preliminary Design for the Lunar Penetrometer System Applicable to the Apollo Program, Aeronutronic Publication No. P-14378(U), Jan. 1965.

Anon.: "NCEL Reports Steady Advance in Polar Research, Deep-Sea Engineering; Soil, Pavement, Power, Shelters Included in Scientific Investigation," The Navy Civil Engineer, 6(2), March-April 1965, pp. 41-45.

Anon.: "Undersea Mining: Progress Report," Engineering & Mining Journal, 166, August 1965, pp. 79-96.

Anon.: "New Drilling Platform" (Sea Quest), Engineering, 201, Jan. 21, 1966, p. 140.

Anon.: "Final Report on Research, Development and Preliminary Design for the Lunar Penetrometer System Applicable to the Apollo Program," Publication No. U-3556, Aeronutronic Division of Philco, 1966.

Anon.: "Drilling in 3000-ft waters seen within the next decade," Oil & Gas Journal, 64, May 23, 1966, pp. 110-111.

Anon.: "Compilation of Project Mohole Scientific and Technical Reports for the Period November 1963 through September 1966," Brown & Root, Inc., Houston, Texas, 1966, 15,128 pp.

Anon.: "Hydroacoustic Energy for Industrial Applications," General Dynamics Corporation, Electronics Division, Rochester, N. Y., Nov. 1966, 13 pp.

Anon.: "Technical Proposal for a Deep Underwater Pile Driving System," MKT Corporation, Dover, N. J., Feb. 1967, 57 pp.

Anon.: "Energy Systems of Extended Endurance in the 1-100 Kilowatt Range for Undersea Applications," Publication 1702, National Academy of Sciences, Washington, D.C., 1968, 132 pp.

Arnor, L. Lane: "A Compilation of Industrial Capabilities Available for the National Oceanographic Program," AMF Co., Ventura Div., 1964, 71 pp.

Arx, William S.: An Introduction to Physical Oceanography, Addison-Wesley, Reading, Mass., 1962.

Barton, Jr. R. and Thompson, L. J.: Earth Resistance to Projectile Impact, University of New Mexico, Engineering Experiment Station Report No. PR-53, March 1964.

Bascom, Willard: A Hole in the Bottom of the Sea, The story of the Mohole Project, Doubleday, 1961.

Bayles, John J.: "Trafficability on the Ocean Floor," Technical Note N-649, U.S. Naval Civil Engineering Laboratory, Port Hueneme, Calif., 1965.

Benuin, R. S. and Clay, C. S.: "Development of an In Situ Sediment Velocimeter," Technical Report, Columbia University, Dobbs Ferry, New York Hudson Laboratory, 52 pp., 9 Jan 1967, Report No. TR-131, Contract Nonr-266(84) AD 649-696.

Berezantsev, V. G.: Osesimetrichnaia zadacha teorii predel'nogo ravnovesia sypuchei sredy, Moskva, 1952 (Gostechizdat).

Berezantsev, V. G.: Raschet prochnosti osnovania sooruzhenii, Moskva, 1960 (Gosstroiizdat), Ch. III.

Bernett, E. C., et al.: "The Bearing Capacity of Simulated Lunar Surfaces in Vacuum," NASA-JPL Technical Report, 32-326, Aug. 1963.

Bilderbeek, F. W. and Manson, D. H.: "Future Trends in Offshore Rig Design," World Petroleum, April 1967.

Biscaye, P. E.: "Mineralogy and Sedimentation of Recent Deep-Sea Clay in the Atlantic Ocean and Adjacent Seas and Oceans," Geological Society of America Bulletin, Vol. 76, 1965, pp. 803-832.

Bishop, R. F.; Hill, R.; and Mott, N. F.: "The Theory of Indentation and Hardness Test," Proceedings of the Physical Society, 57 (1945), pp. 147-159.

Blenkarn, K. A.: "Borehole Competence at Mohole Depth," Journal Petroleum Tech., 15(4), April 1963, pp. 389-390.

Brooks, W. B. and Reis, G. E.: Soil Penetration Theory, Sandia Corp. Report No. SC-4950 (RR), Sept. 1963.

Buchanan, C. L.: "The Development of Deep Ocean Search and Inspection Techniques by the Naval Research Laboratory - An Aftermath of the THRESHER Tragedy," ONR Naval Research Reviews, XVIII, 6, June 1965, pp. 1-8.

Buisman, A. S. K.: "De weerstand van paalpunten in zand," De Ingenieur, 50 (1935), pp. Bt. 25-28, 31-35.

Burkart, W. F.: "Deep Ocean Engineering," The Navy Civil Engineer, 6(5), September-October 1965, pp. 10-15.

Burns, R. E.: "Free-Fall Behavior of Small, Light-Weight Gravity Corers," Marine Geology, Vol. 4, Feb. 1966, pp. 1-9.

Caidin, Martin: Hydrospace, Dutton, New York, 1964, 320 pp.

Caquot, A.: Equilibre des massifs afrottement interne, Paris, 1934 (Gauthier-Villars).

Caquot, A. and Kérisel, J.: "Sur le terme de surface dans le calcul des fondations en milieu pulvérulent," Proceedings, Third International Conference Soil Mechanics and Foundation Engineering, Zurich, 1953, Vol. I, pp. 336-337.

Clark, L. V. and McCarty, J. L.: The Effect of Vacuum on the Penetration Characteristics of Projectiles into Fine Particles, NASA-LRC Technical Note D-1519, Sept. 1962.

Coffee, C. E.: "A New Technique in Sand Coring," UnderSea Technology, 9(3), March 1968, pp. 35-37.

Cok, A. E. and others: "Marine Geology Studies on the Scotian Shelf and Slope," Maritime Sediments, 1(4), Oct. 1965, pp. 2-11.

Colp, J. L.: "An Experimental Investigation of the Continuous Penetration of a Blunt Body into a Simulated, Cohesionless Soil," Report SC-RR-65-220, Sandia Corp., Albuquerque, N.M., 1965.

Colp, J. L.: "An Earth Penetration Post-Test Soil Exploration Technique," Report SC-RR-66-2617, Sandia Corp., Albuquerque, N.M., 1967.

Colp, J. L.: "Terradynamics: A Study of Projectile Penetration of Natural Earth Materials," Report SC-DR-68-215, Sandia Corp., Albuquerque, N.M., 1968.

Corcoran, W. H.; Opfell, J. B. and Sage, B. H.: Momentum Transfer in Fluids, Academic Press, Inc., New York, 1956, 394 pp.

Cox, W. R. and Womack, D. P.: "Measurement of Dynamic Characteristics of Soils with Penetrometers," Texas University (NASA-CR-849, Contract NAS 9-3559, NSG-604), Aug. 1967, 124 pp.

Crisp, Hugh A.: "The Measurement of Pelagic Submarine Soil Strength," Master's Thesis, School of Engineering and Applied Science, George Washington University, Aug. 1968, 117 pp.

Dantz, P. A.: "The Padlock Anchor - A Fixed Point Anchor," Technical Report No. R577, U.S. Naval Civil Engineering Laboratory, Port Hueneme, Calif., May 1968, 37 pp.

De Beer, E. E.: "Etude des foundations sur pilotis et des foundations directes," Annales des Travaux Publics de Belgique, 46 (1945), pp. 1-78.

De Beer, E. E.: "Données concernant la résistance au cisaillement deduites des essais de pénétration en profondeur," Géotechnique, 1 (1948), pp. 22-40.

De Beer, E. E. and Vesić, A. S.: "Etude expérimentale de la capacité portante du sable sous des foundations directes établies en surface," Annales des Travaux Publics de Belgique, 59 (1958), No. 3, pp. 5-58.

De Beer, E. E. and Ladanyi, B.: "Etude expérimentale de la capacité portante du sable sous des foundations circulaires établies en surface," Proceedings, Fifth International Conference Soil Mechanics and Foundation Engineering, Paris, 1961, Vol. I, pp. 577-585.

Defaut, Albert: Physical Oceanography, Pergamon Press, Oxford, 1961, Vols. I and II.

Denington, R. J.: "Terminal Ballistics Studies," Proj. Doan Brook Techn. Memo. No. 20, Case Institute, Feb. 1958, ASTIA AD 146 913.

Dietrich, Guenter: Allgemeine, Meereskunde, Gebr. Borntraeger, Berlin, 1957, 588 pp.

Emery, K. O. and Dietz, R. S.: "Gravity Coring Instrument and Mechanics of Sediment Coring," Geol. Soc. Am. Bull. 52, Oct. 1941, pp. 1685-1714.

Euler, L.: "Neue Grundsätze der Artillerie," Euler's Opera Omnia, B. G. Teubner, Berlin, 1922.

Ewing, M. and Ewing, J.: "Sediments at Proposed LOCO Drilling Sites," Journal Geophysical Research, 68(1), January 1, 1963, pp. 251-256.

Faas, R. W.: "An Empirical Relationship between Reflection Coefficients and Ocean Bottom Sediments," Transactions, National Symposium on Ocean Sciences and Engineering of the Atlantic Shelf, Marine Technology Society, March 1968, pp. 149-167.

Felsher, M.: "A Core Aligner Designed to Recover Oriented Recent Marine Cores," Limnology & Oceanography, 9 (4), Oct. 1964, pp. 603-605.

Fisk, H. N. and McClelland, B.: "Geology of Continental Shelf off Louisiana: Its Influence on Offshore Foundation Design," Geological Society of America Bulletin, Vol. 70, 1959, pp. 1369-1394.

Fuchs, Otto P.: "Impact Phenomena," AIAA Journal, Vol. 1, No. 9, Sept. 1963, pp. 2124-2126.

Gaskell, T. F.: "Drilling Deep Boreholes," Engineering, 190 (4924), Sept. 2, 1960, pp. 327-329.

Geer, R. L.: "Impact Studies on Lunar Dust Models at Various Vacuums," USAF ASD Technical Report 61-595, Jan. 1962.

Glauert, M. B. and Lighthill, M. J.: "The Axisymmetric Boundary Layer on a Long Thin Cylinder," Proc. Roy. Soc. A230, 188-203 (446-51), 1955.

Gleason, Jr., G. R. and Ohlmacher, F. J.: "A Core Sampler for In Situ Freezing of Benthic Sediments," Marine Technology Soc. Trans. Joint Conference & Exhibit, June 14-17, 1965, Washington, D.C., pp. 737-41.

Goble, G. G.; Scanlan, R. H. and Tomko, J. J.: "Dynamic Studies on the Bearing Capacity of Piles," Paper presented to the HRB Annual Meeting, Jan. 18, 1967, Washington, D.C.

Goldsmith, W.: Impact, Edward Arnold Publishers, London, 1960, 379 pp.

Gorsline, D. S.: "Bottom Sediments of the Atlantic Shelf and Slope Off the Southern United States," J. Geol., 71, July 1963, pp. 422-440.

Hakala, W. W.: Resistance of Granular Media to Normal Impact of a Rigid Projectile in a Subsonic Regime, Virginia Polytechnic Institute, Dept. of Civil Engineering, PhD Thesis, June 1965.

Hamilton, E. L.; Shumway, G.; Menard, H. W.; and Chipek, C. J.: "Acoustic and other physical properties of shallow water sediments off San Diego," Journal Acoustical Soc. America, Vol. 28, 1956, pp. 1-15.

Hamilton, E. L.: "Thickness and Consolidation of Deep-Sea Sediments," Geological Society of America Bulletin, Vol. 70, 1959, pp. 1399-1424.

Hamilton, E. L.: "Ocean Basin Ages and Amounts of Original Sediments," Journal of Sedimentary Petrology, Vol. 30, No. 3, p. 370, 1960.

Hamilton, E. L.: "Data on Recent Marine Sediments," Am. Geol. Inst., AGI Data Sheet 39 in GeoTimes, 7(5), January-February 1963, pp. 41-42.

Hamilton, E. L. and Menard, H. W.: "Density and porosity of sea-floor surface sediments off San Diego, California," Amer. Assoc. Petroleum Geologists, Vol. 40, pp. 754-761.

Hamilton, E. L.: "Consolidation characteristics of related properties of sediments for experimental Mohole (Guadalupe site)," Jour. Geoph. Research, Vol. 69, 1964, pp. 4257-4269.

Hansen, Bent and Odgaard, D.: "Bearing Capacity Tests on Circular Plates on Sand," Bulletin No. 8, The Danish Technical Institute, Copenhagen, 1960, 19 pp.

Harrison, W.; Lynch, M. P.; and Altschaeffl, A. G.: "Sediments of Lower Chesapeake Bay, with Emphasis on Mass Properties," Jour. Sed. Petrology, Vol. 34, 1964, pp. 727-755.

Hauber, F. R.: "Drilling and Production Structures for Oil and Gas on the Continental Shelf," Proceedings of OECON, M. J. Richardson, Inc., 1966.

Hay, D. A.: "Flow About Semi-Submerged Cylinders of Finite Length," Final Report to David Taylor Model Basin, Princeton University, School of Engineering, October 1, 1947, 174 pp.

Herrmann, W. and Jones, A. H.: Survey of Hypervelocity Impact Information, Mass. Institute of Technology, A.S.R.L. Report No. 99-1, Sept. 1961.

Hill, M. N.: The Sea, Ideas and Observations on Progress in The Study of the Seas, Interscience Publishers, 1963, 3 volumes.

Hinde, Peter, Fortune in the North Sea, G. T. Foulis and Co., Ltd., London, 1966.

Hironaka, Melvin C.: "Engineering Properties of Marine Sediments Near San Miguel Island, California," U.S. Naval Civil Engineering Laboratory, Technical Report R503, Port Hueneme, California, December 1966, 45 pp. (AD 644 192).

Hironaka, Melvin C. and Smith, R. J.: "Foundation Study for Materials Test Structure," Proceedings, Civil Engineering in the Oceans, ASCE Conference, San Francisco, California, 1967, pp. 489-530.

Hironaka, M. C.: "Computer Reduction of Data from Engineering Tests on Soils and Ocean Sediments," Technical Report R566, U.S. Naval Civil Engineering Laboratory, Port Hueneme, California, 1968.

Holmes, C. W. and Goodell, H. G.: "The Prediction of Strength in the Sediments of St. Andrew Bay, Florida," Journal of Sedimentary Petrology, 34(1), March 1964, pp. 134-143.

Hopkins, Thomas, L.: "A Survey of Marine Bottom Samplers," Proceedings in Oceanography, Vol. II, MacMillon Co., New York, 1964.

Horn, D. R.; Horn, B. M. and Delach, M. N.: "Correlation between Acoustical and Other Physical Properties of Deep Sea Cores," Journal of Geophysical Research, Vol. 73, No. 6, March 15, 1968, pp. 1939-57.

Hortley, H. O.; Gates, C. E.; Berry, W.: "Earth Penetration and Dynamic Soil Mechanics," Statistical Design Report SC-CR-68-3537, Sandia Corp., Albuquerque, N.M., 1968.

Horton, E. E.: "Preliminary Drilling Phase of Mohole Project. I. Summary of Drilling Operations (La Jolla and Guadalupe Sites)," Bulletin, American Association of Petroleum Geologists, 45(11), November 1961, pp. 1789-1792.

Hubert, J. F.: "Textural Evidence for Deposition of Many Western North Atlantic Deep-Sea Sands by Ocean-Bottom Currents Rather than Turbidity Currents," J. Geol., 72, Nov. 1964, pp. 757-785.

Hunt, L. M.: Glossary of Ocean Science and Undersea Technology.

Hvorslev, M. J. and Stetson, H. C.: "Free-Fall Coring Tube: A New Type of Gravity Bottom Sampler," Bull. Geological Soc. of America, Vol. 57, Oct. 1946, pp. 935-949.

Hvorslev, M. J.: "Subsurface Exploration and Sampling of Soils," Report on the Joint Research Project for ASCE, the Engineering Foundation, Harvard University and the U.S. Waterways Experiment Station, New York, 1949, 521 pp.

Igelman, K. R. and Hamilton, E. L.: "Bulk Densities of Mineral Grains from Mohole Samples (Guadalupe Site)," Jour. Sed. Petrology, Vol. 33, 1963, pp. 474-478.

Jáky, J.: "On the Bearing Capacity of Piles," Proceedings Second International Conference Soil Mechanics and Foundation Engineering, Rotterdam, 1948, Vol. 1, pp. 100-103.

Jochums, R. E. and Denny, A. A.: "Study of Pile Driving by Vibration," Technical Note N-386, U.S. Naval Civil Engineering Laboratory, Port Hueneme, California, Feb. 1961, 8 pp.

Kastrop, J. E.: "Sea Floor Drilling - Completion System Proved," Petroleum Engineer, 34, Sept. 1962, pp. 112-139.

Keller, G. H.; Richards, A. F.; and Recknagel, J. H.: "Prevention of water loss through CAB plastic sediment core liners," Deep-Sea Res., Vol. 8, 1961, pp. 148-151.

Keller, G. H.: "Deep-sea nuclear sediment density proble," Deep-Sea Res., Vol. 12, 1965, pp. 373-376.

Keller, George H.: "Shear Strength and Other Physical Properties of Sediments from Some Ocean Basins," Proceedings, Civil Engineering in the Oceans, ASCE Conference, San Francisco, California, 1967, pp. 391-417.

Kérisel, J.: "Foundations profondes en milieu sableux," Proceedings, Fifth International Conference Soil Mechanics and Foundation Engineering, Paris, 1961, Vol. II, pp. 73-83.

Kermabon, A.; Blavier, P.; Cortis, V.; and DeLauze, H.: "The 'Sphincter' Corer: A Wide-Diameter Corer with Watertight Core-Catcher," Marine Geology, Vol. 4, April 1966, pp. 149-162.

Kornhauser, M.: Structural Effects of Impact, Spartan Books, Inc., Baltimore, 1964, 205 pp.

Kornhauser, M.: "Prediction of Cratering Caused by Meteoroid Impacts," J. Astron. Soc., Vol. V, No. 3-4, 1958.

Kretschmer, T. R.: "In Situ, Sea Floor Plate Bearing Device: A Performance Evaluation," Technical Report R537, U.S. Naval Civil Engineering Laboratory, Port Hueneme, California, June 1967, 50 pp.

Kretschmer, T. R.: "Settlement Response of Cohesive and Noncohesive Bottom Sediments," Technical Report, U.S. Naval Civil Engineering Laboratory, Port Hueneme, California, June 1967, 57 pp. Report No. NCEL TR-537 AD-654-714.

Kuenen, P. H.: "Deep-Sea Sands and Ancient Turbidites," Turbidites (Bouma, A. H. and Brouwer, A., editors), Elsevier Pub. Co., 1964, pp. 3-33.

Lang, H. A.: "Lunar Instrument Carrier - Landing Factors," Rand RM-1725, ASTIA Doc. N AD.112403, June 4, 1956.

L'Herminier, R.; Habib, P.; Tcheng, Y.; and Bernede, J.: "Fondations superficielles," Proceedings, Fifth International Conference Soil Mechanics and Foundation Engineering, Paris, 1961, Vol. I, pp. 713-717.

Lee, G. L.: "Offshore Structures, Past, Present, Future and Design Considerations," Offshore, Vol. 28, No. 6, June 5, 1968, pp. 45-55.

Lowery, L. L.; Hirsch, T. J.; and Samson, Jr., C. H.: "Pile Driving Analysis - Simulation of Hammers, Cushion, Piles and Soil," Research Report 33-9, Texas Transportation Institute, Texas A & M College, Aug. 1967, 81 pp.

McCaslin, Jr., L. S.: "Offshore Drilling," Oil & Gas Journal, 48(2), May 19, 1949, pp. 112-113.

McClelland, B.; Focht, Jr., J. A.; and Emrich, Wm. J.: "Problems in Design and Installation of Heavily Loaded Pipe Piles," ASCE Conference Proceedings, Civil Engineering in the Oceans, San Francisco, Sept. 1967, pp. 601-634.

Macy, R. H.: "Mobile Drilling Platforms," Journal of Petroleum Technology, Sept. 1966.

Mandl, P. and Givens, G.: Dynamics of High-Velocity Penetration into Clay, National Research Laboratories, Ottawa, Canada, Report No. MA-248, July 1964.

Maurer, W. C., "Impact Crater Formation in Sandstone and Granite," Master's thesis submitted to Colorado School of Mines, Golden, Colorado, 1959.

Maurer, W. C. and Rinehart, J. S.: "Impact Crater Formation in Rock," Journal of Applied Physics, Vol. 31, No. 7, July 1960, pp. 1247-1252.

Maxwell, D.: Physics International Co., San Leandro, California (private communication).

Menard, L. and Gambin, M.: "Use of Hydraulic Vibrodriving in Submarine Sounding," Sols-Soils, No. 14, Paris, 1965, pp. 24-39.

Menard, H. W.: Marine Geology of the Pacific, McGraw-Hill, 1964, 271 pp.

Meyerhof, G. G.: "The Ultimate Bearing Capacity of Foundations," Géotechnique, 2 (1951), pp. 301-332.

Meyerhof, G. G.: "Recherches sur la force portante des pieux," Annales de l'Institut Technique du Bâtiment et des Travaux Publics, 6 (1953), No. 63-64, pp. 371-374.

Miller, R. E.: Papers in Marine Geology (Shepard Commemorative Volume), The Macmillan Co., New York, 1964, 531 pp.

Moore, G. G. and Shumway, G.: "Sediment Thickness and Physical Properties: Pigeon Point Shelf, California," Journal of Geophysical Research, 64(3), March 1959, pp. 367-374.

Moore, D. G.: "The Free-Corer: Sediment Sampling Without Wire and Winch," Journal Sed. Petrology, 31(4), Dec. 1961, pp. 627-630.

Moore, D. G. and Richards, A. F.: "Conversion of Relative Shear Strength Measurements by Arrhenius on East Pacific Cores to Conventional Units of Shear Strength," Geotechnique, Vol. XII, No. 1, p. 55, 1962.

Moore, D. G.: "Bearing Strength and Other Physical Properties of Some Shallow and Deep-Sea Sediments from the North Pacific," Geol. Soc. America Bull., Vol. 73, 1962, pp. 1163-1166.

Moore, D. G.: "Shear strength and related properties of sediments from experimental Mohole (Guadalupe site)," Jour. Geoph. Research, Vol. 69, 1964, pp. 4271-4291.

Moore, K.: Theory of Laminar Flows, Princeton University Press, Princeton, N. J., 1964, 869 pp.

Moore, W. W. and Smoots, V. A., "Foundation Studies for Offshore Structures," Proceedings of OECON, M. J. Richardson, Inc., 1966.

Muga, B. J.: "Ocean Bottom Breakout Forces," Technical Report R-591, U.S. Naval Civil Engineering Laboratory, Port Hueneme, California, June 1968, 140 pp.

Murphy, G.: Ordinary Differential Equations and Their Solutions, D. Van Nostrand Co., Inc., New York, 1960, p. 26.

Nafe, J. E. and Drake, C. L.: "Physical Properties of Marine Sediments," The Sea, Interscience Publishers, N. Y., 1963, pp. 794-815.

Nielsen, J. P.: "Consolidation Characteristics of Pure Clays and Pelagic Sediments," U.S. Naval Civil Engineering Laboratory, Technical Report R-477, Port Hueneme, California, 1966.

Neumann, G. and Pierson, W. J., Jr.: Principles of Physical Oceanography, Prentice Hall, Inc., Englewood Cliffs, 1966, 545 pp.

Noh, W. F.: "CEL: A Time-Dependent Two-Space-Dimensional Coupled Eulerian-Lagrange Code," Methods in Computational Physics, Vol. 3, Academic Press, New York, 1964, pp. 117-179.

Oser, R. and Fagot, M.: "Design and Use of a Bottom Environmental Sensing System (BESS)," Informal Report, Naval Oceanographic Office, Washington, D. C., 20 pp., Report No. NOO-IR-67-74 AD-660-181.

Palmore, J. I.: "Lunar Impact Probe," ARS Jour., Aug. 1961, pp. 1066-1073.

Perkins, R. L.: "Floating Rig Takes Core Samples in Deep," Engineering News-Record, 159(11), Sept. 12, 1957, pp. 60-62.

Peters, R. I.: "Diamond Coring Technology's Contribution to the Moho Project," Canadian Mining Journal, 84(3), March 1963, pp. 49-53.

Phleger, F. B.: "Origin and Deposition of Deep Sea Sediments," Trans. Amer. Geophys. Union, 30(2), 1949, pp. 180-182.

Pickard, George L.: Descriptive Physical Oceanography, The Macmillan Co., 1964, 199 pp.

Piggot, C. S.: "Apparatus to Secure Core Samples from the Ocean Bottom," Bull. Geol. Soc. America, Vol. 47, 1936, pp. 675-684.

"Piling Pontoon with Hydraulic Legs," Engineering, 200, Oct. 1, 1965, p. 441.

Prandtl, L.: "Uber die Eindringungsfestigkeit plastisher Baustoffe und die Festigkeit von Schneiden,".Zeitschrift fur Angewandte Mathematik und Mechanik 1 (1921), No. 1, pp. 15-20.

Prandtl, L.: "Uber die Härte plastisher Körper," Nachrichten Kön. Gesell. der Wissenschafften, Göttingen, 1920, Math. Phys. Klasse, pp. 74-85.

Prandtl, L. and Tietjens, O. G.: Applied Hydro- and Aeromechanics, Dover Publications, Inc., New York, 1957, 311 pp.

Pratje, O.: "Die Erfahrungen bei der Gewinnung von rezenten marinen Sedimenten," Mitt. Geogr. Ges., Hamburg Vd. 50, 1952.

Prych, E. A. and Hubbell, D. W.: "A Sampler for Coring Sediments in Rivers and Estuaries," Geological Soc. of America Bulletin, Vol. 77, May 1966, pp. 549-555.

Reese, L. C. and O'Neill, M. W.: "The Analysis of Three-Dimensional Pile Foundations Subjected to Inclined and Eccentric Loads," ASCE Proceedings, Civil Engineering in the Oceans, 1967, pp. 245-276.

Reissner, H.: "Zum Erddruckproblem," Proceedings, First International Conference Applied Mechanics, Delft, 1924, pp. 295-311.

Richards, A. F.: "Investigations of Deep-Sea Sediment Cores, I. Shear Strength Bearing Capacity, and Consolidation," U.S. Hydrographic Office Tech. Report 63, 1961, 70 pp.

Richards, A. F. and Keller, G. H.: "Plastic-barrel Sediment Corer," Deep-Sea Res. 8, 1961, pp. 306-312.

Richards, A. F.: "Investigation of Deep-Sea Sediment Cores," Technical Report 106, U.S. Navy Hydrographic Office, Oct. 1962, 146 pp.

Richards, Adrian F. and Parker, Harvey W.: "Surface Coring for Shear Strength Measurements," Proceedings, Civil Engineering in the Oceans, ASCE Conference, San Francisco, California, 1967, pp. 445-487.

Rinehart, J. S., "Stresses Associated with Lunar Landings," Contribution No. 11, Mining Research Laboratory, Colorado School of Mines, Feb. 27, 1960.

Robins, B.: New Principles of Gunnery, London, 1742.

Robinsky, E. I. and Morrison, C. F.: "Sand Displacement and Compaction Around Model Friction Piles," Canadian Geotechnical Journal, Vol. I (1964), No. 2, pp. 81-93.

Rosenhead, L.: Laminar Boundary Layers, At the Clarendon Press, Oxford, 1963, 687 pp.

Rosfelter, A. M.: "Hydrostatic Actuation of Deep Sea Instruments," Journal of Ocean Technology, Vol. I, No. 1, pp. 53-63 (1966).

Rowe, R. D. and Selig, E. T.: "Penetration Studies of Simulated Lunar Dust," Seventh Symposium on Ballistic Missile and Aerospace Technology, Aug. 1962.

Ruffin, J. V.: "Steel Offshore Towers Replace Lightships," Civil Engineering, 35, Nov. 1965, pp. 72-75.

Ryan, W. B. F. and others: "Sediments on the Tyrrhenian Abyssal Plain," Geol. Soc. Bull., 76, Nov. 1965, pp. 1261-1282.

Sachs, P. L.: "A Tension Recorder for Deep-Sea Dredging and Coring," Journal Marine Research, 22(3), Sept. 15, 1964, pp. 279-283.

Sachs, P. L. and Raymond, S. O.: "A New Unattached Sediment Sampler," Journal Marine Research, 23(1), Jan. 15, 1965, pp. 44-53.

Schlichting, H.: Boundary Layer Theory, McGraw-Hill Book Co., New York, 1968, 747 pp.

Schmid, W. E.: "Driving Resistance and Bearing Capacity of Vibro-Driven Model Piles," Performance of Deep Foundations, ASTM Special Technical Publication 444, 1969, pp. 322-340.

Schmid, W. E. and Hill, H. T.: "The Driving of Piles by Longitudinal Vibrations," Princeton Soil Engineering Research Series No. 4, June 1966, 145 pp.

Schmid, W. E. and Kitago, S.: "Shear Strength of Clays and Safety Factors as a Function of Time," Proceedings, Sixth International Conference on Soil Mechanics and Foundation Engineering, University of Toronto Press, 1965, Vol. 1, pp. 345-349.

Schmid, W. E.: "The Determination of Soil Properties in Situ by an Impact Penetrometer," Princeton Soil Engineering Research Series No. 3, Report to Air Force Cambridge Research Laboratory, AFCRL-66=43, 1966, 192 pp.

Scott, Ronald F.: "In-Place Measurement of the Strength of Ocean Floor Soils by Accelerometer," Proceedings, Civil Engineering in the Oceans, ASCE Conference, San Francisco, California, 1967, pp. 419-444.

Shumway, G.: "Sound Speed and Absorption Studies of Marine Sediments by a Resonance Method," Geophysics, 25, April-June 1960, pp. 451-467.

Siever, R. A. and Kastner, M.: "Mineralogy and Petrology of Some Mid-Atlantic Ridge-Sediments," Journal of Marine Research, Vol. 25, No. 3, pp. 263-78 (1967).

Smith, J. E, "Umbrella Pile Anchors," Technical Report R-247, U.S. Naval Civil Engineering Laboratory, Port Hueneme, California, May 1963, 41 pp.

Smith, J. E. and Dantz, P. A.: "A Perspective on Anchorages for Deep Ocean Constructions," Technical Note TN-522, U.S. Naval Civil Engineering Laboratory, Port Hueneme, California, Dec. 1963 (AD426202), 18 pp.

Smith, R. J.: "Deep-Ocean Core Boring and Soil Testing Investigations," U.S. Naval Civil Engineering Laboratory, Port Hueneme, California, Technical Note N-445, 66 pp., 1962.

Smith, R. J. and Hironaka, M. C.: "Strength of Sea Floor Sediments from Laboratory Tests," Proceedings of First U.S. Navy Symposium on Military Oceanography, U.S. Naval Oceanographic Office, Washington, D. C., 1964, pp. 361-378.

Streeter, V. L.: Handbook of Fluid Dynamics, McGraw-Hill Book Co., New York, 1961.

Sutton, G. H.; Berckheimer, H.; and Nafe, J. E.: "Physical Analysis of Deep Sea Sediments," Geophysics, Vol. 22, 1957, pp. 779-812.

Sverdrup, Johnson and Fleming: The Oceans, Their Physics, Chemistry and General Biology, Prentice Hall, Englewood Cliffs, 1961.

Terry, Richard D.: Ocean Engineering, National Security Industrial Association, 1966, 4 volumes.

Terzaghi, K.: Theoretical Soil Mechanics, John Wiley & Sons, New York, 1943.

Thompson, L. J.; Colp, J. L.; and Thigpen, L.: "Some Observations on Earth Penetration by a Projectile," Report SC-RR-65-495, Sandia Corp., Albuquerque, N.M., 1965.

Thompson, L. J.: "Dynamic Penetration of Selected Projectiles into Particulate Media," Report SC-RR-66-376, Sandia Corp., Albuquerque, N. M., 1966.

Tolch, N. A. and Bushkovitch, V. A.: "Penetration and Crater Volume in Various Kinds of Rocks as Dependent on Caliber, Mass, and Striking Velocity of Projectile," BRL Report No. 641, Oct. 1947.

Tomko, J. J.: "Dynamic Studies on Predicting the Static Bearing Capacity of Piles," Research Report No. 68-6, Department of Civil and Geol. Engineering, Princeton University, Sept. 1968, 362 pp.

Towne, R. C.: "Mooring Anchors," Proceedings, Society of Naval Architects and Engineers, New York, 1960, pp. 290-302.

Tsai, K. W. and Schmid, W. E.: "Penetrometer Method for Determining Soil Parameters," Proceedings, 7th International Conference on Soil Mechanics and Foundation Engineering, Mexico, 1969 (in press).

Tschebotarioff, G. P.: Soil Mechanics, Foundations and Earth Structures, McGraw-Hill Book Co., 1951, 655 pp.

Tudor, W. J.: "Moorings and Anchoring of Deep Ocean Platforms," ASCE Conference Proceedings: Civil Engineering in the Oceans, 1967, pp. 351-390.

Velzeboer, P. T.: "Designing a Mobile Drilling Platform for the North Sea," World Petroleum, April 1967.

Vesic, A. S.: "A Study of Bearing Capacity of Deep Foundations," Final Report, Project B-189, Georgia Institute of Technology, 1967, 263 pp.

Vey, E. and Nelson, R. D.: "Environmental Effects on Engineering Properties of Deep Ocean Sediments," U.S. Naval Civil Engineering Laboratory, Report CR 67.020, 1966, Port Hueneme, California.

Vey, E. and Nelson, R. D.: "Environmental Effects of Properties of Ocean Sediments," Proceedings, Civil Engineering in the Oceans, ASCE Conference, San Francisco, California, 1967, pp. 531-567.

Vitter, A. L. and Ben, C. P.: "Offshore Operations," Chapter 5 to Impact of New Technology on the Petroleum Industry 1946-1965, National Petroleum Council, 1967.

Weeks, Lewis G.: "The Ocean's Resources," Offshore, June 1968.

Wenz, K. P.: "Ueber die Grösse des Seitendrucks auf Pfähle in bindigen Erdstoffen," Ver öffentlichungen d. Inst. f. Bodenmechanik u. Grundbau d. Techn. Hochschule Karlsruhe, 1963, 133 pp.

Wilde, P.: "Estimates of Bottom Current Velocities from Frain Size Measurements for Sediments from the Monterey Deep-Sea Fan," Marine Technology Soc., Trans. Joint Conference & Exhibit, June 14-17, 1965, pp. 718-727.

Wilkins, M.; Honodel, C.; Sawle, D.: "An Approach to the Study of Light Armor," UCRL 50284, Lawrence Radiation Laboratory, University of California, Livermore, California, June 1967, 43 pp.

Wilkins, M. L.: "Third Progress Report of Light Armor Program," UCRL-50460, Lawrence Radiation Laboratory, University of California, Livermore, California, July 1968, 53 pp.

Wilkins, Mark, L.: "Calculation of Elastic-Plastic Flow," Methods in Computational Physics, Vol. 3, Academic Press, New York, 1964, pp. 211-263.

Worzel, J. L.: "Ocean Bottom Sampler for Ships Under Way," Geophysics, Vol. 13(3), 1948, pp. 452-456.

Yew, Ch.-H. and Goldsmith, W.: "Stress Distribution in Soft Metals Due to Static and Dynamic Loading by a Steel Sphere," Journal Applied Mechanics, Dec. 1964, pp. 635-646.

Young, C. W.: "Depth Prediction for Earth-Penetration Projectiles," Journal, Soil Mech. Found. Div. ASCE, Vol. 95, No. SM3, May 1969, pp. 803-817.

Zumberge, J. H.: "A New Shipboard Coring Technique," Jour. of Geophysics Res., 67(6), June 1962, pp. 2529-2536.

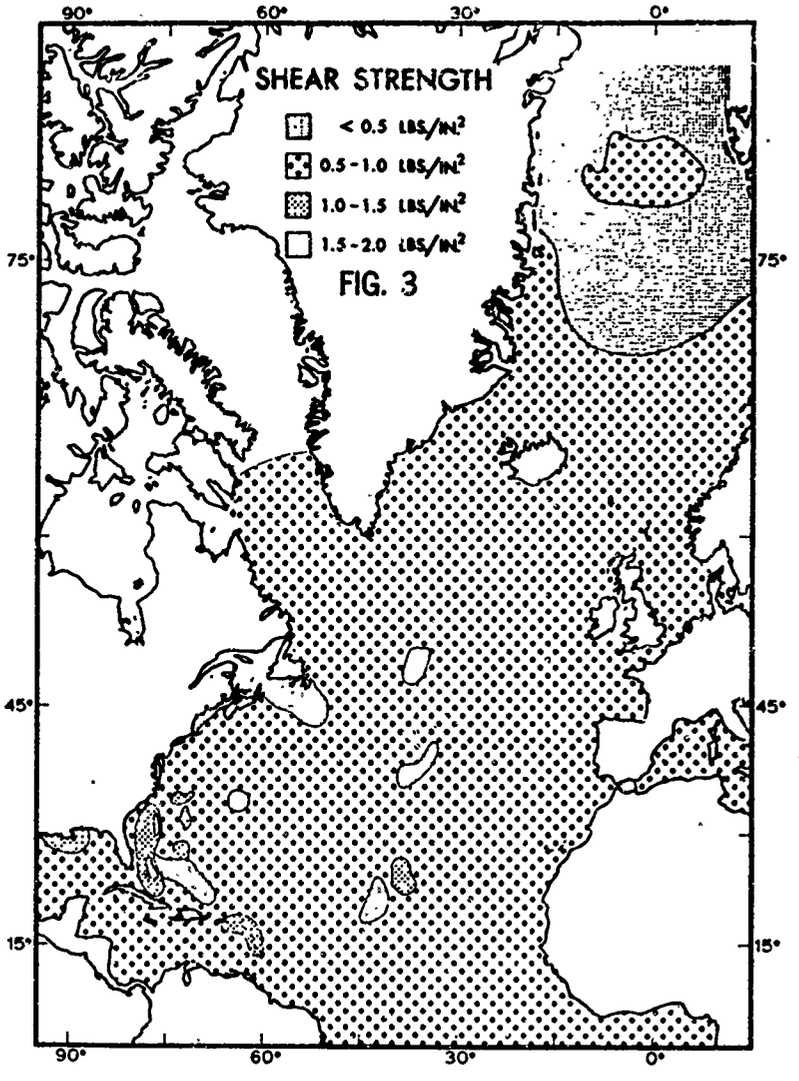

Figure 2.1

Shear Strength Distribution of Bottom Sediments in the North Atlantic (after Keller, 1967)

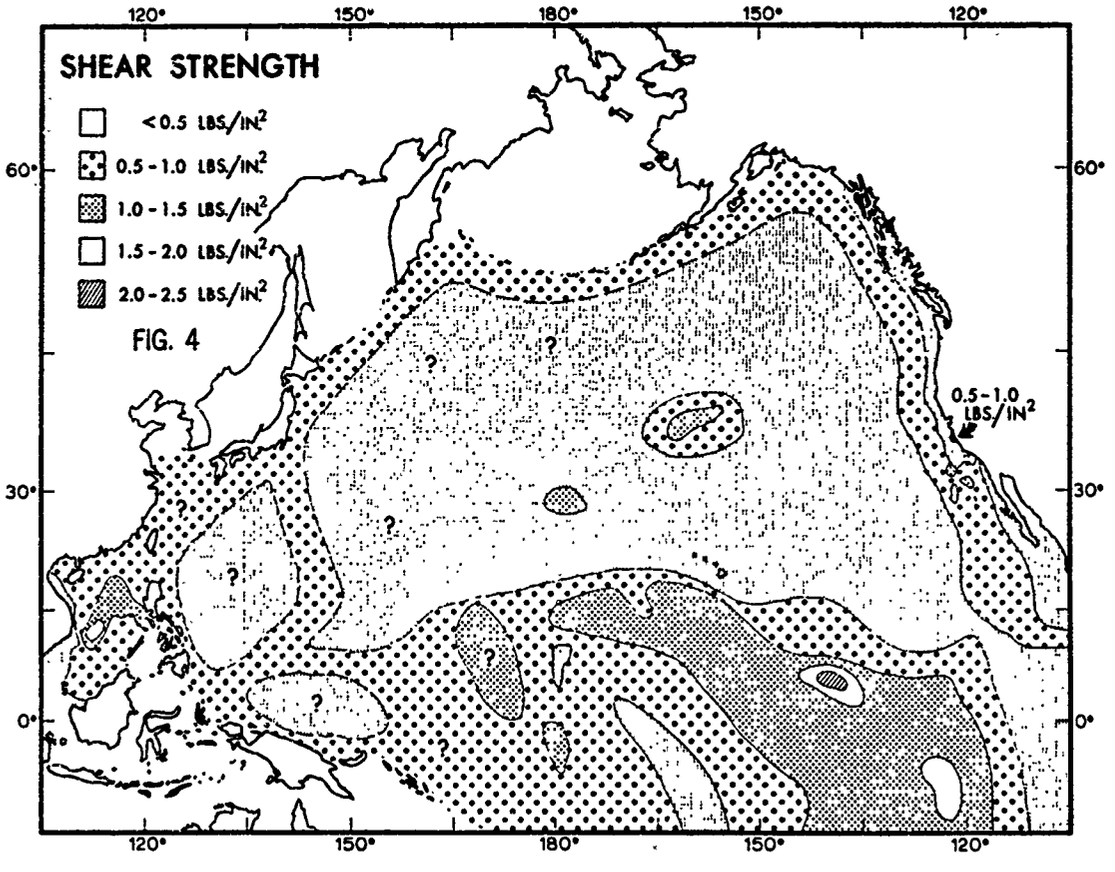

Figure 2.2

Shear Strength Distribution of Bottom Sediments in the North Pacific (after Keller, 1967)

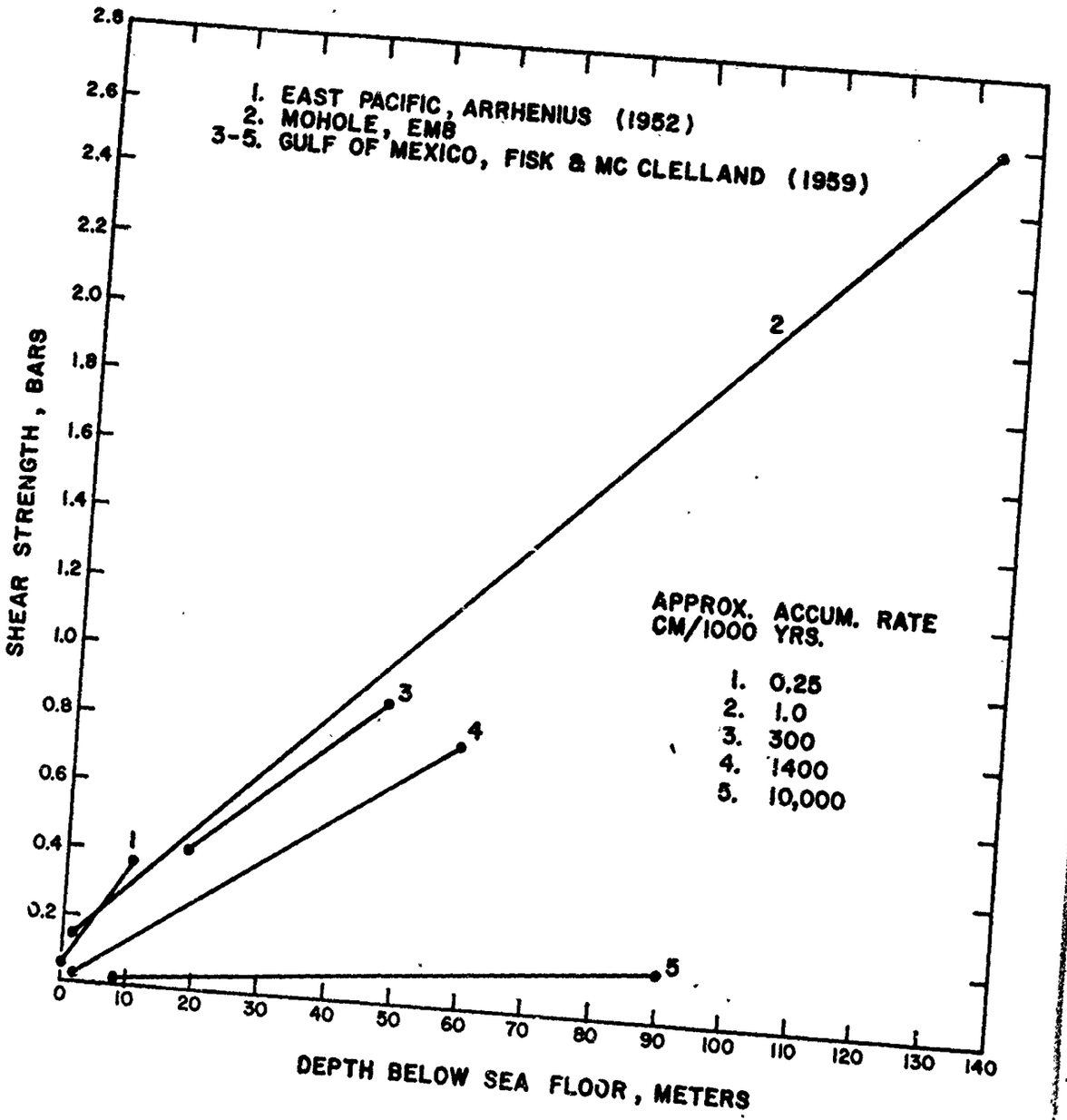

Figure 2.3

Rate of Increase in Shear Strength with Burial Depth from Several Areas of Known Approximate Depositional Rates. Note: Slope of Mohole data line (2) is intermediate between deep-sea clay and very rapidly deposited delta front sediments (5).

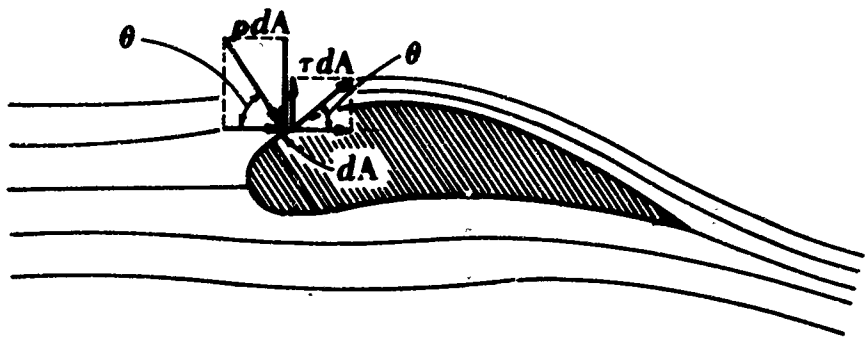

Figure 3.1 Normal and tangential components of pressure and frictional forces on an element of surface of an immersed body.

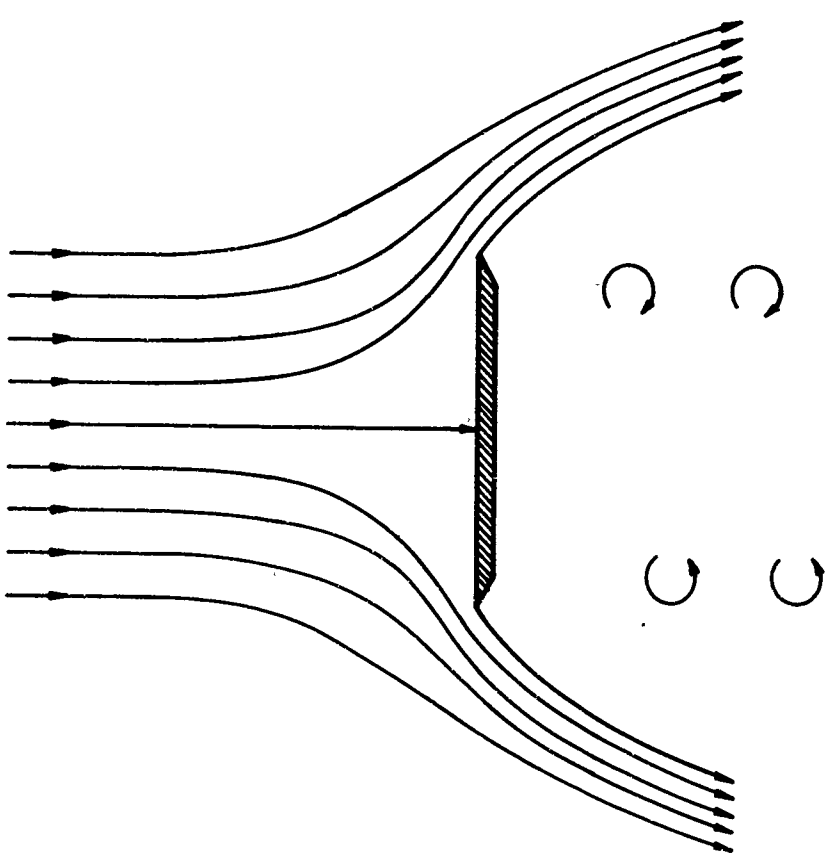

Figure 3.2 Flow separation from the edges of a plate which is placed perpendicularly in a fluid stream.

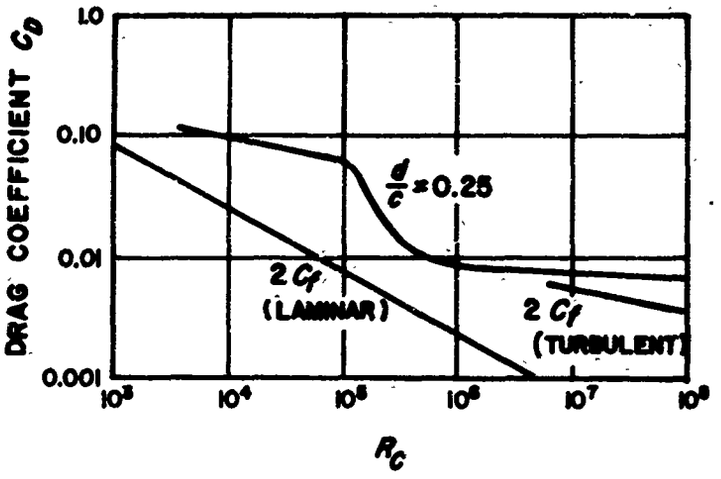

Figure 3.3 Drag coefficients of two-dimensional forms of thickness-chord ratio d/c = 0.25.

Figure 3.4 Typical streamline and laminar flow profiles.

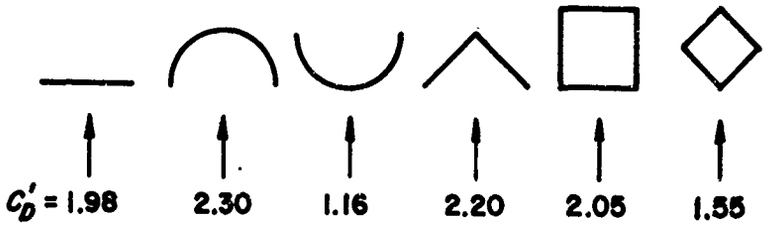

Figure 3.5 Drag coefficients of various blunt forms.

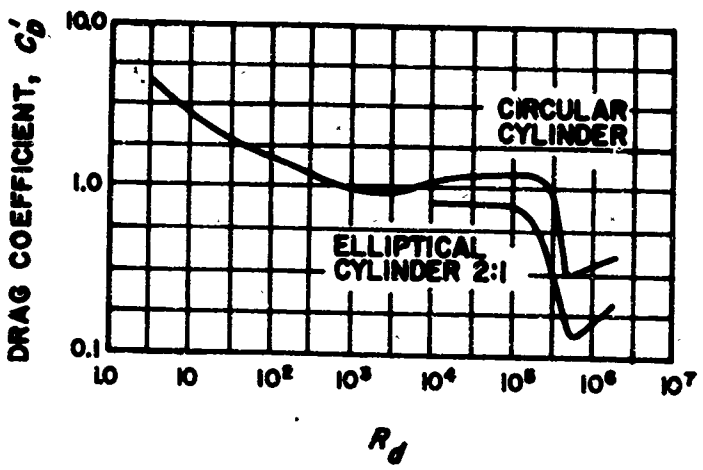

Figure 3.6 Drag coefficient vs. Reynolds number for circular and elliptical cylinders.

Figure 3.7 Cylindrical Body for Drag Force Calculation Example.

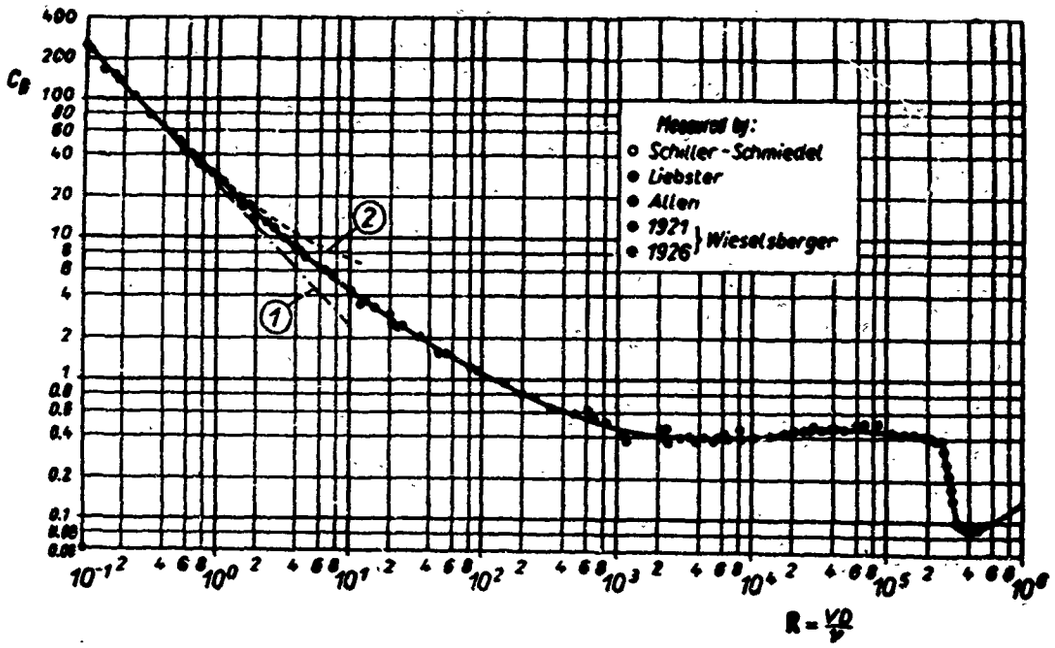

Figure 3.8. Drag coefficient $C_D = 2F_D/A\rho u^2$ of the sphere in terms of the Reynolds numbers. Curve 1: $C_D = 24/R$, theory of very slow motion. (A = cross section area of sphere.)

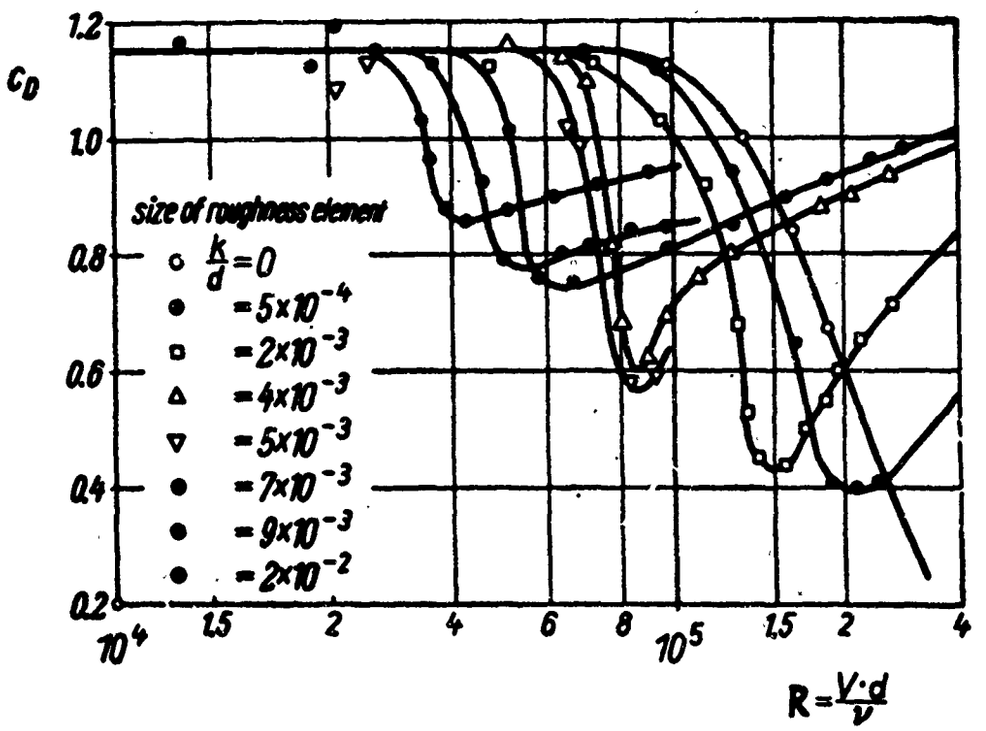

Figure 3.9

Drag Coefficients C_D as a Function of Reynolds

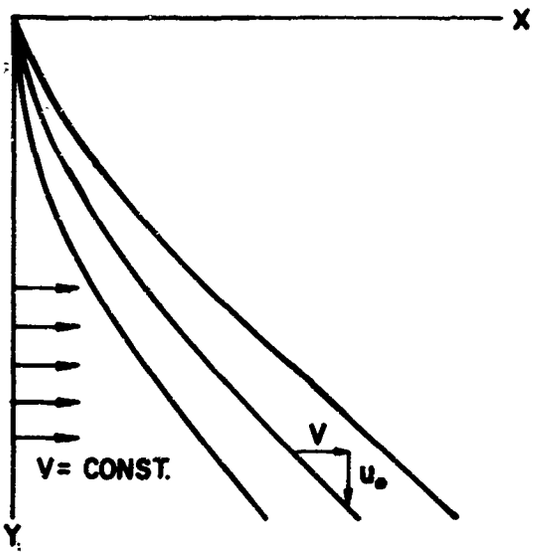

Figure 3.10. Trajectory of Object Falling through Constant Horizontal Current.

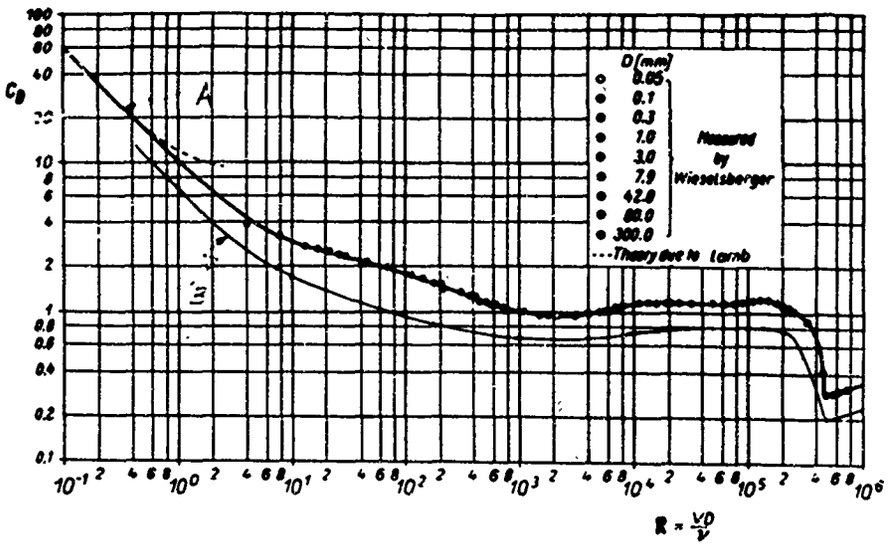

Figure 3.11 Drag Coefficients C_D vs. Reynolds Number

Curve A: infinite cylinder
Curve B: cylinder of Fig. 3.7
L/D = 10 with axis horizontal

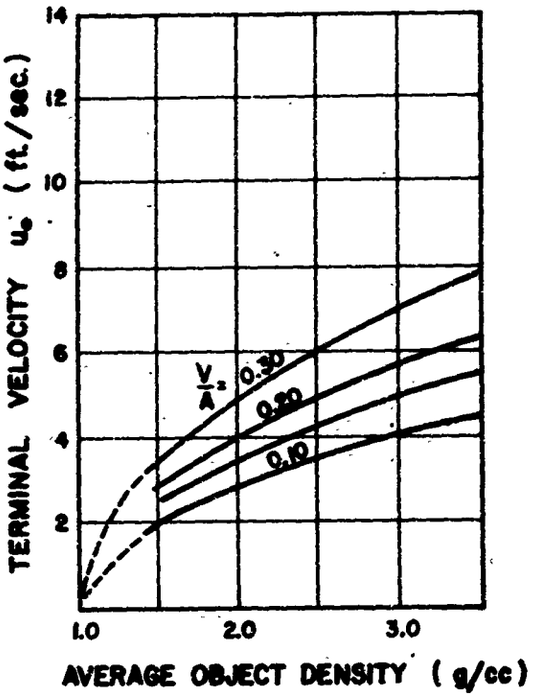

Figure 3.12 Terminal Velocity u_o for Cylinder L/D = 10 falling with Axis Horizontal.

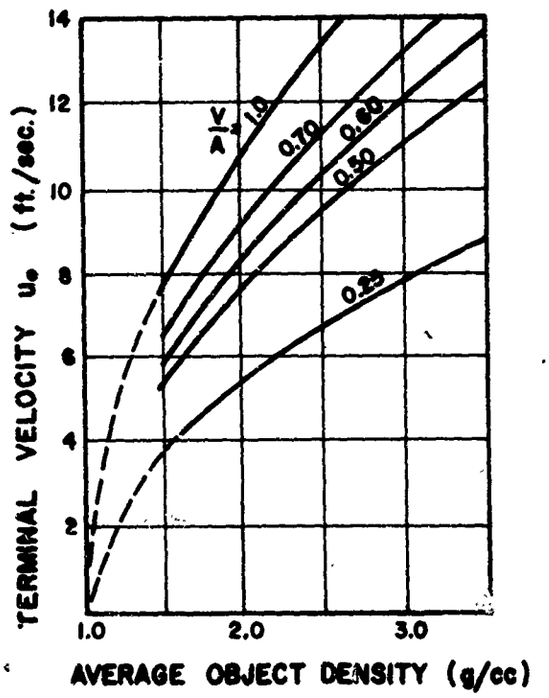

Figure 3.13 Terminal Velocity u_o for Cylinder L/D = 10 falling with Axis Vertical.

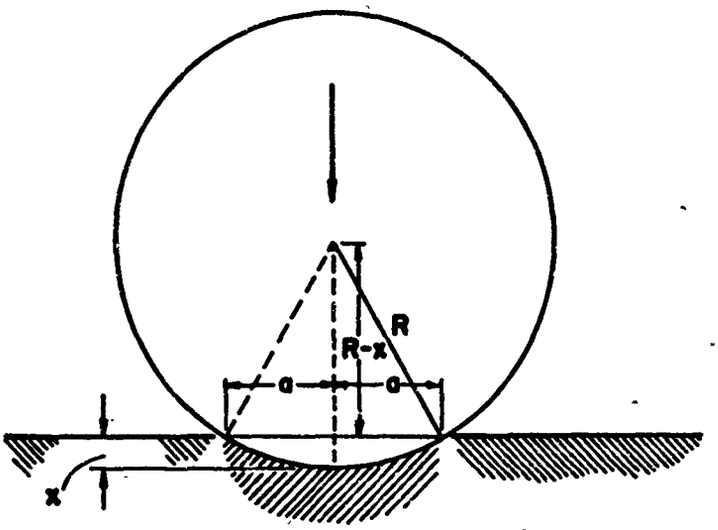

Figure 4.1

Definition of Penetration Parameters

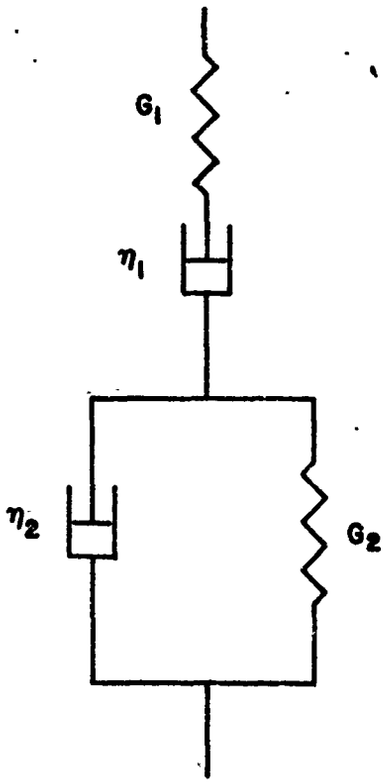

Figure 4.2

Four Parameter Model Representing Mechanical Soil Properties

T e s t S e r i e s No. 38

Target Material: Clayey, Sandy Silt, Undisturbed

Calibration Factors: Penetrometer: K = 8.6 mV/g

r_1: K = 31 mV/g; r_2: K = 34 mV/g

Drop Height: H = 275 cm

Oscilloscope Calibration:

Penetrometer:

M_a = 200 mV/cm

M_t = 2 msek/cm

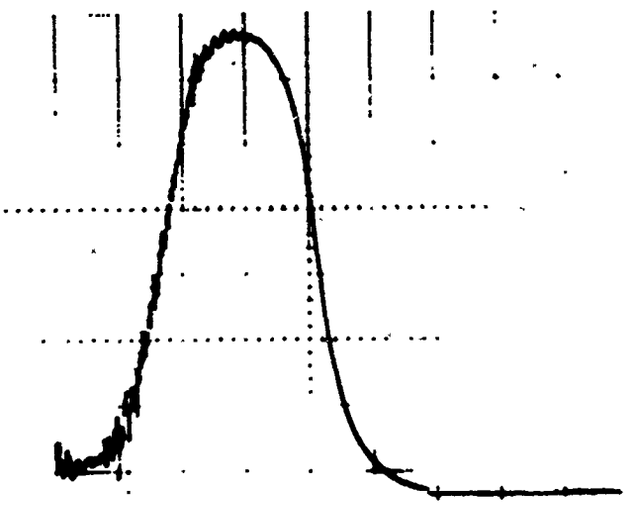

Figure 4.3

Typical Impact Penetrometer Data
(after Schmid, 1966)

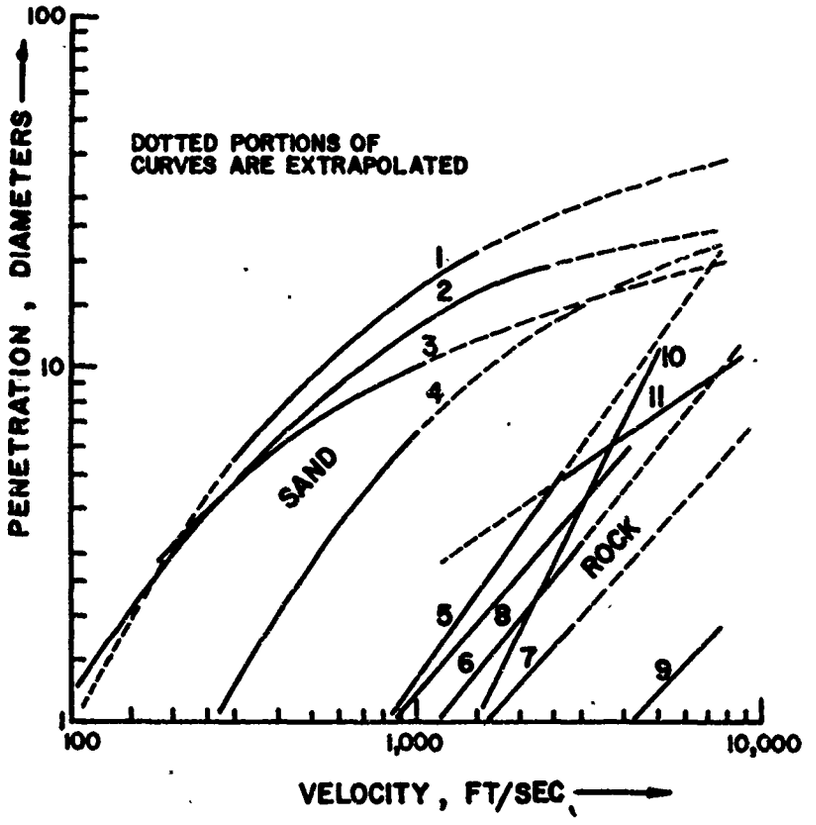

Figure 4.4

Penetration of Steel Spheres into Target Materials
(after Kornhauser)

Curve	Projectiles	Target
1	4.3-in. cannon balls	Sand and gravel
2	Many sizes, high ballistic density	Sand
3	0.356-in. steel balls	Loose sand
4	0.356-in. steel balls	Weakly cemented sand
5	Many	Rock - 250 psi crushing strength
6	Many	Rock - 2,000 psi crushing strength
7	Many	Rock - 10,000 psi crushing strength
8	3/16-in. steel balls	Red sandstone - 2,780 psi
9	9/32-in. and 7/16-in. steel balls	Granite - 16,500 psi
10	Many high ballistic density	Soft rock
11	Many high ballistic density	Rock or sand - hypervelocity cratering

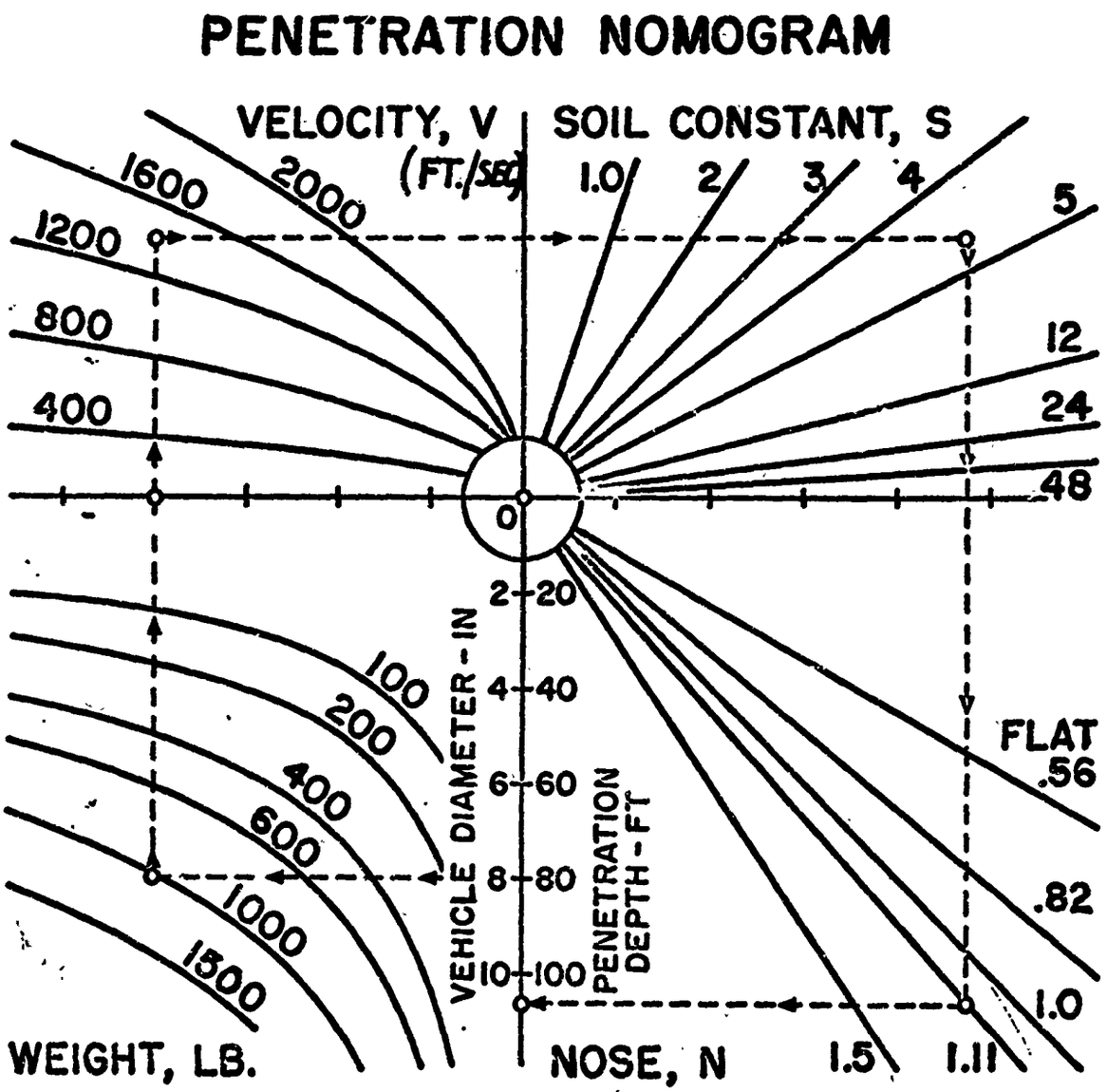

Figure 4.5 Penetration Nomogram for Sandia Penetrator.

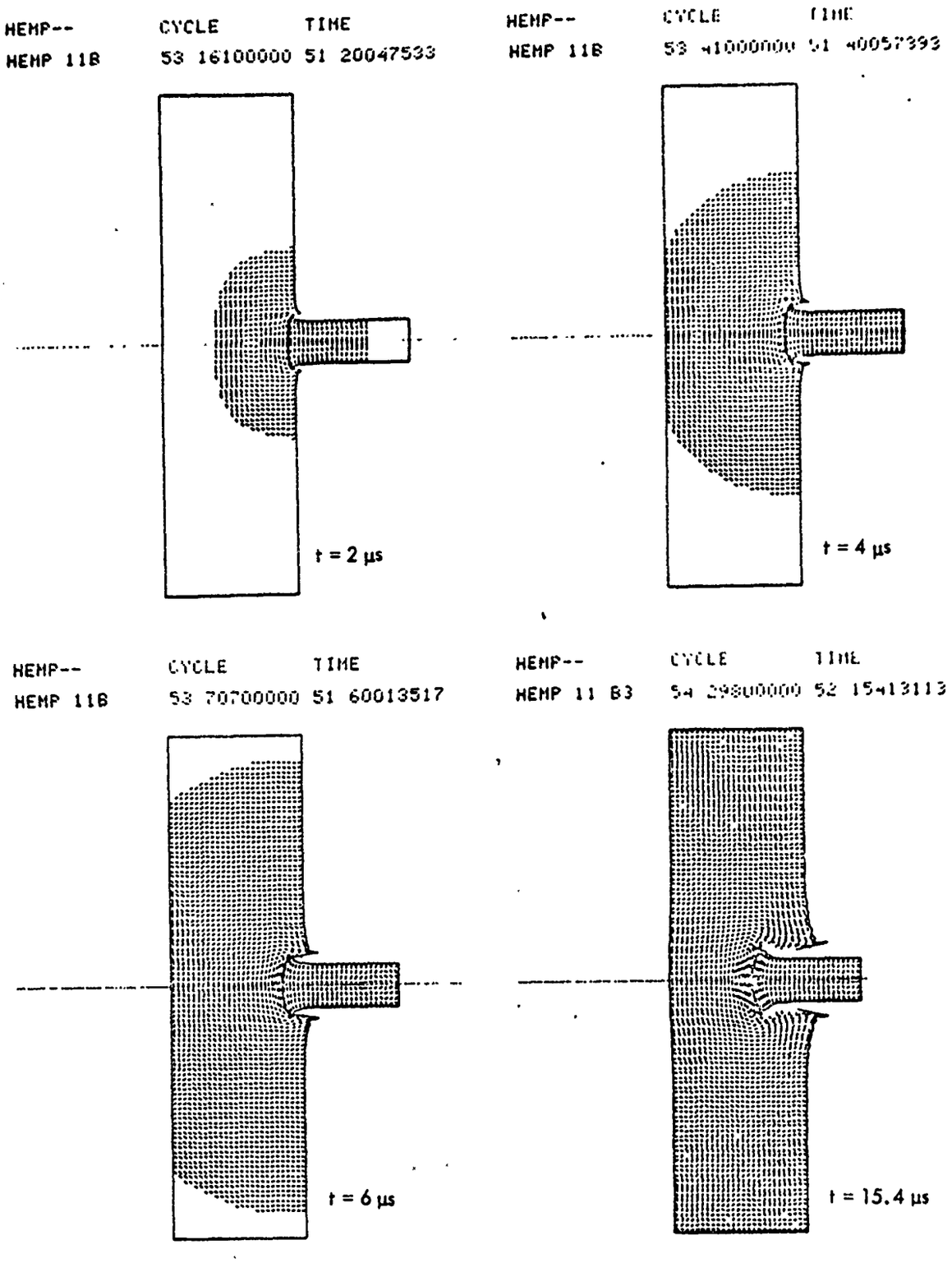

Figure 4.6

HEMP Code Calculation of Steel Cylinder
Impacting Upon Aluminum Plate

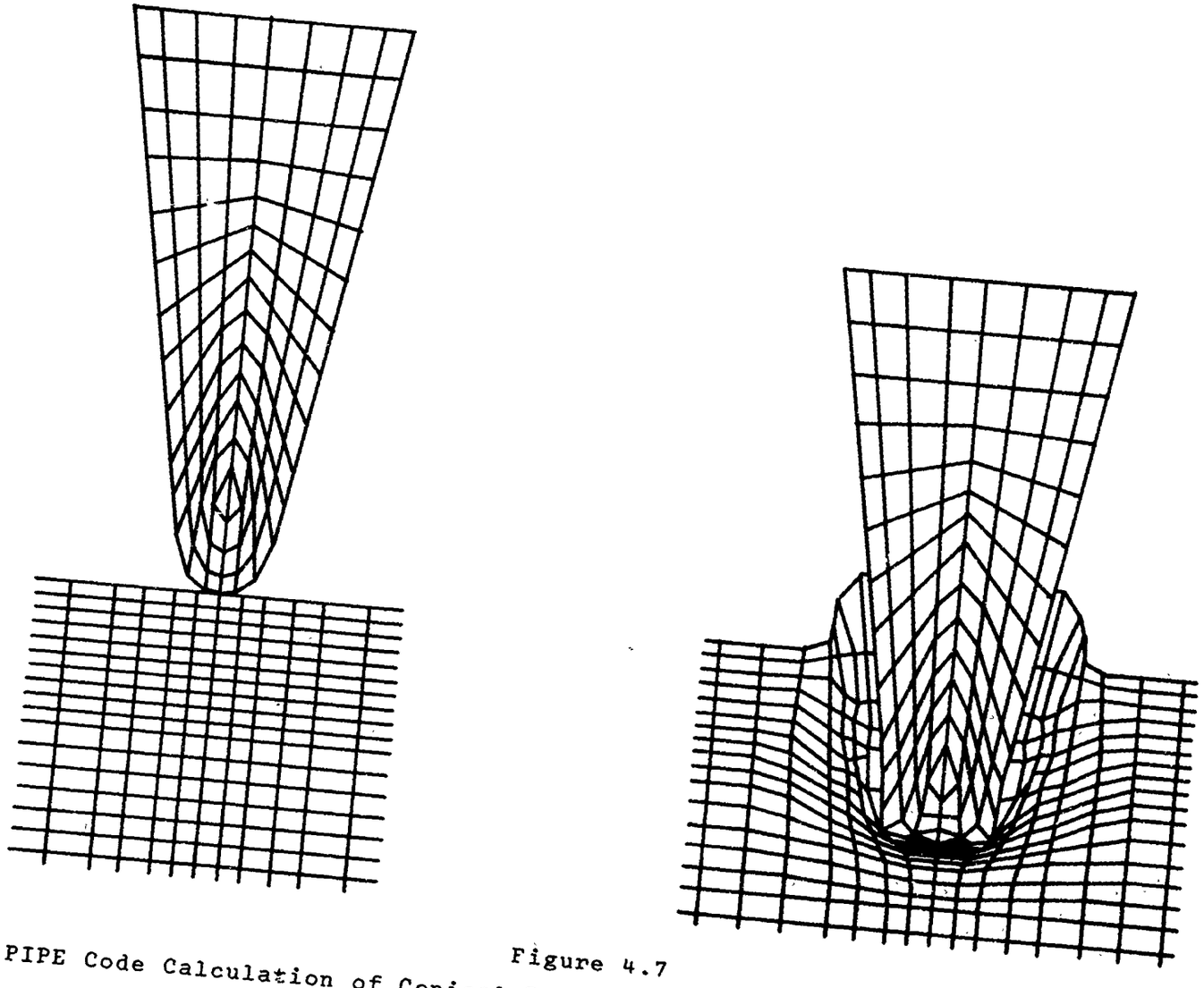

Figure 4.7

PIPE Code Calculation of Conical Projectile Entering Water at 2.4 km/sec.
(a) at instant of contact;
(b) 25 μ sec after initial contact

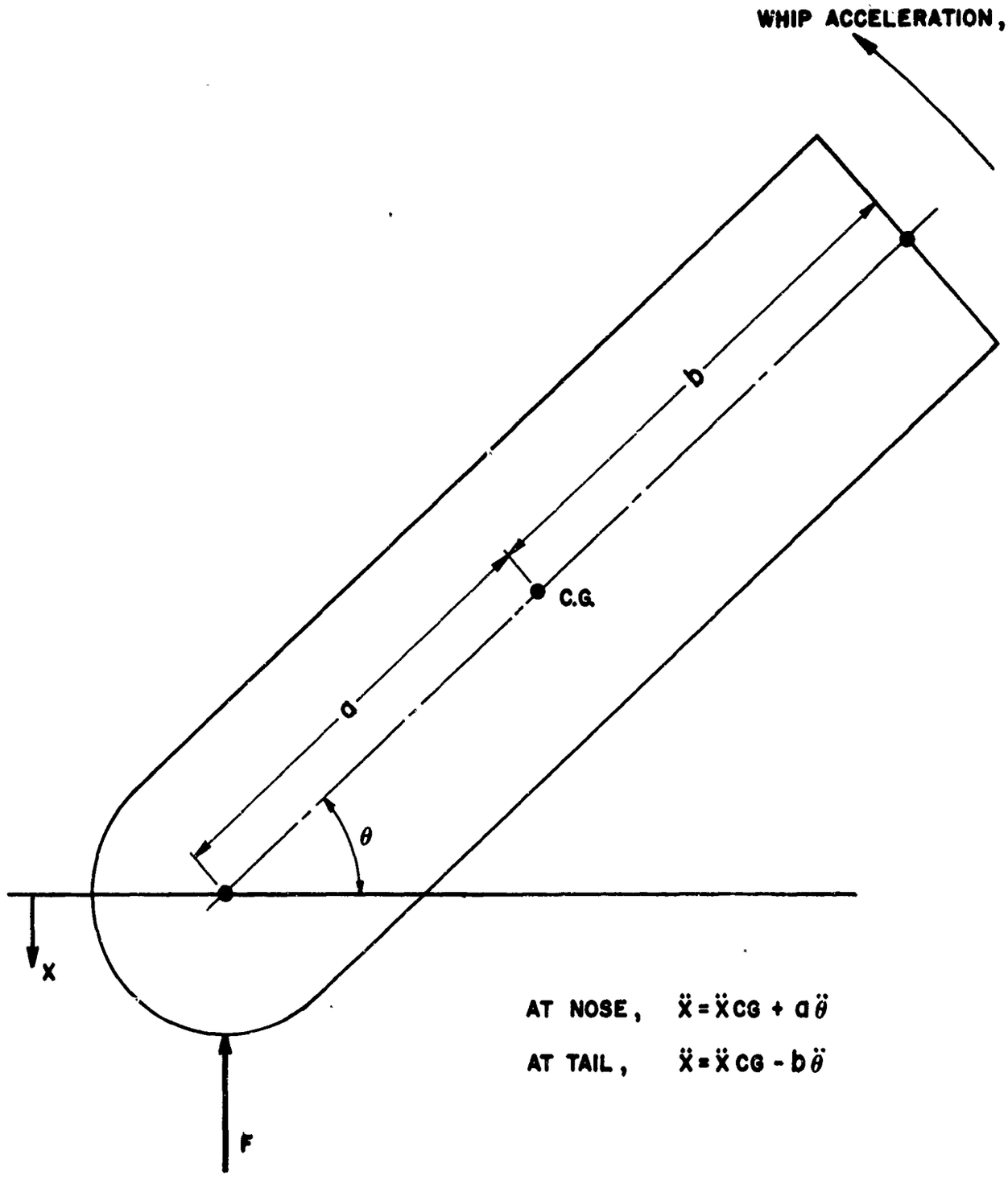

Figure 4.8

Acceleration Components for Oblique Impact

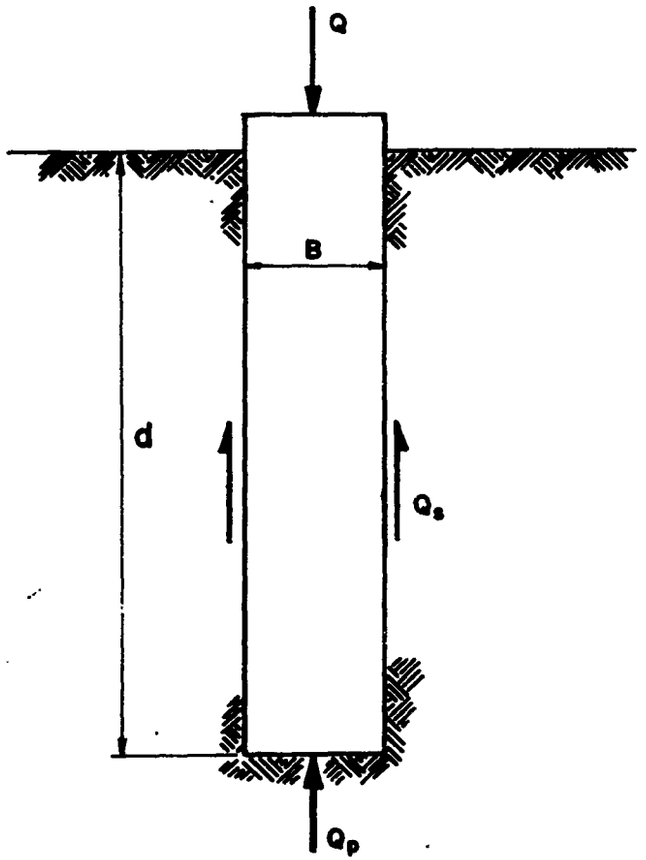

$$Q = Q_p + Q_s = P_0 A_p + t_0 A_s$$

Figure 5.1

Definition of Bearing Capacity Parameters for a Deep Foundation.

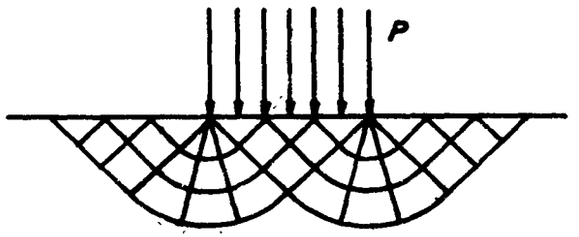

Figure 5.2

Prandtl's Yield Line Pattern for Penetration of a Punch into a Soft, Ductile Material.

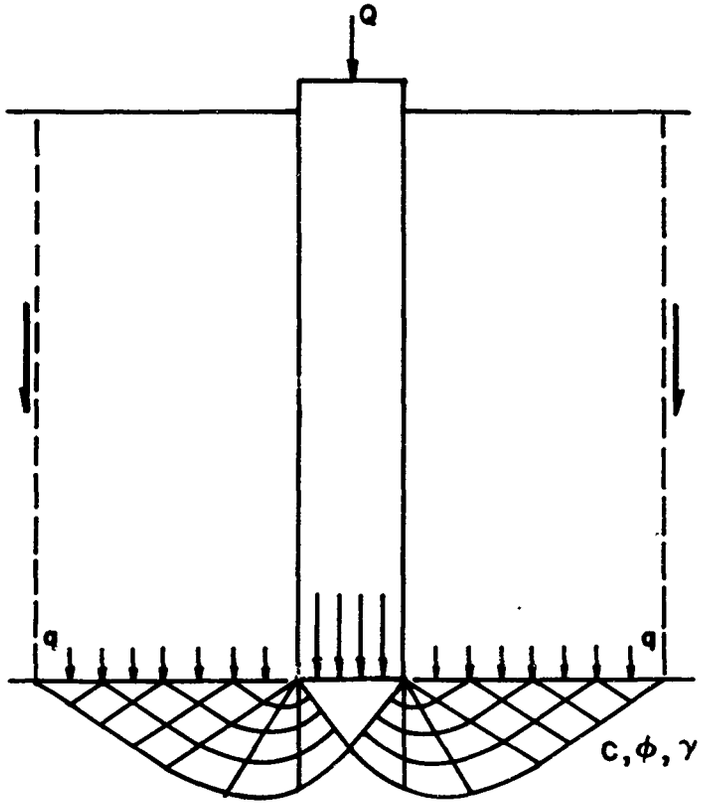

Figure 5.3

Prandtl-Reissner Solution of Assumed Yield Lines as Applied by Caquot and Buisman.

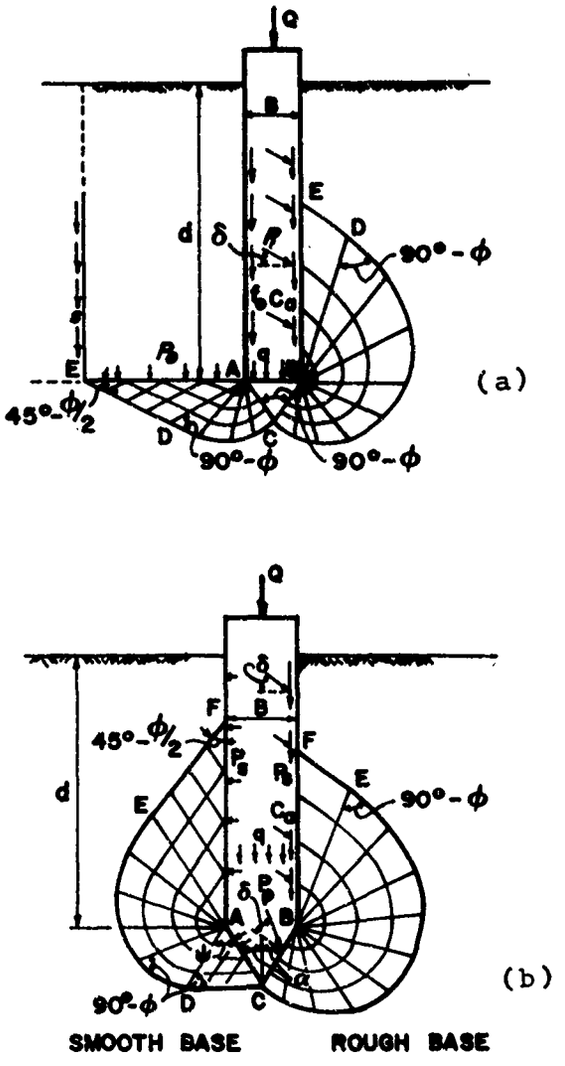

Figure 5.4

Assumed Failure Pattern

(a) For flat tip pile;
(b) For wedge or conical tip pile.

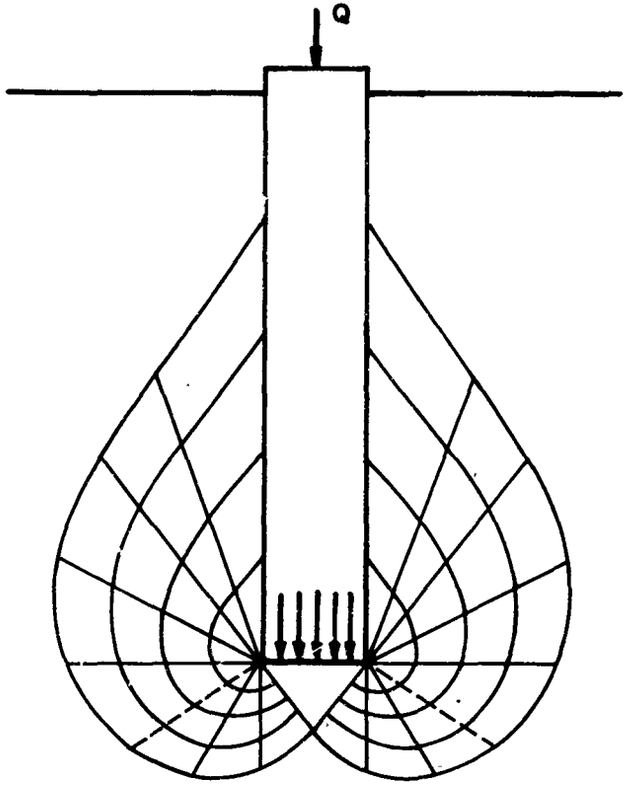

Figure 5.5

Yield Line Pattern with Rupture Lines
Reverting to the Shaft
(assumed by De Beer and Jáky)

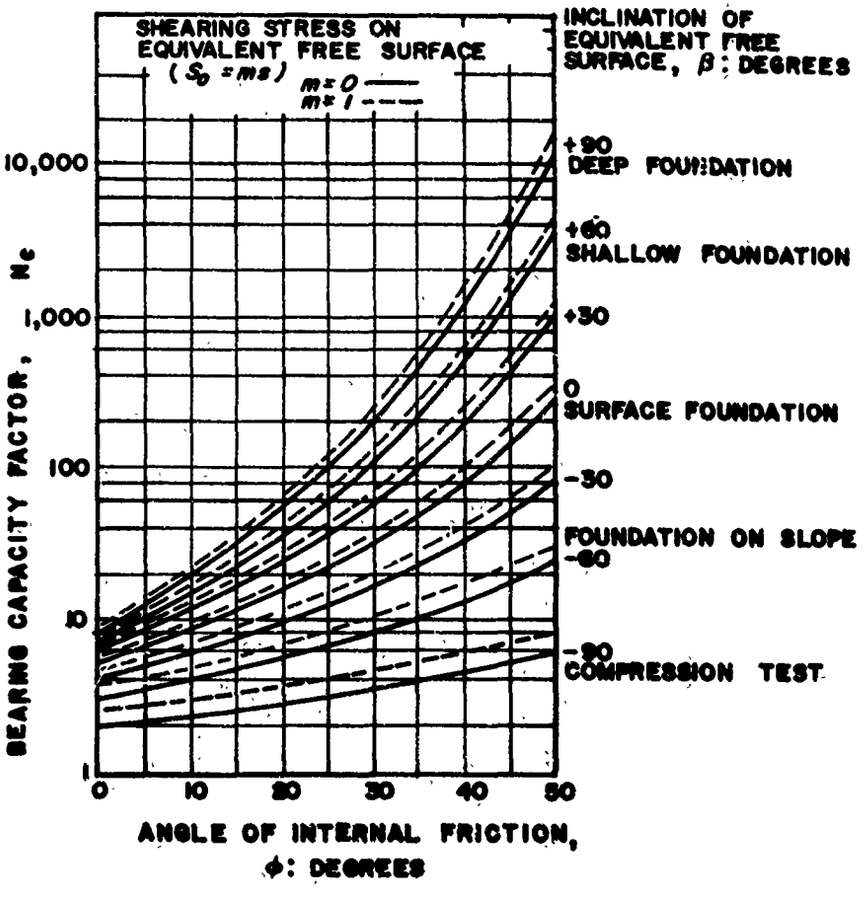

Figure 5.6

Bearing Capacity Factor N_c as Function
of Friction Angle ϕ (after Meyerhof).

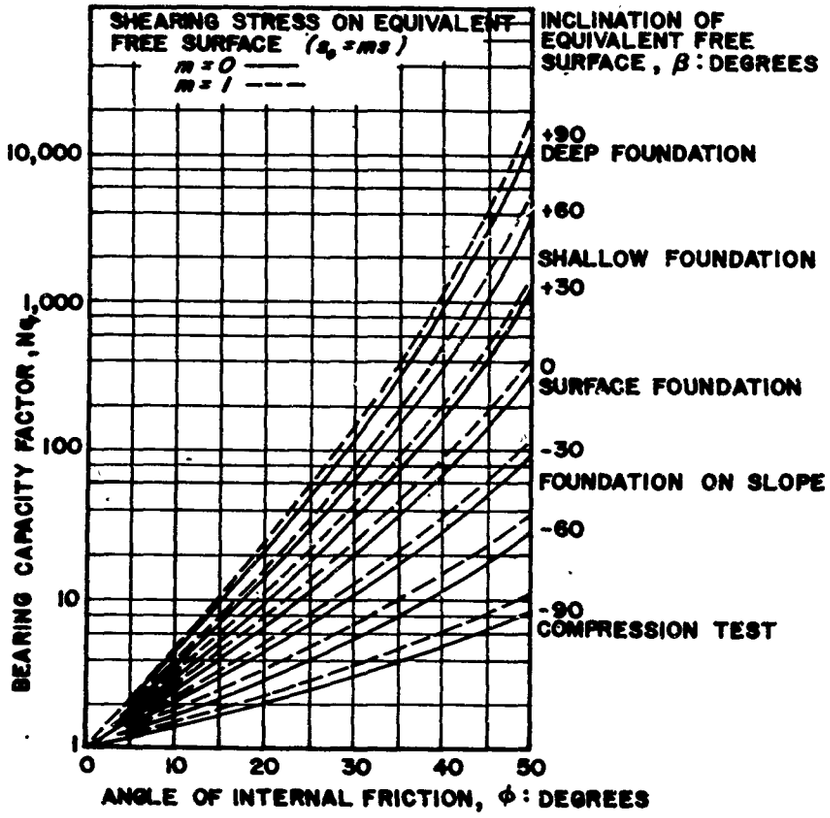

Figure 5.7

Bearing Capacity Factor N_q as a Function of Friction Angle ϕ (after Meyerhof).

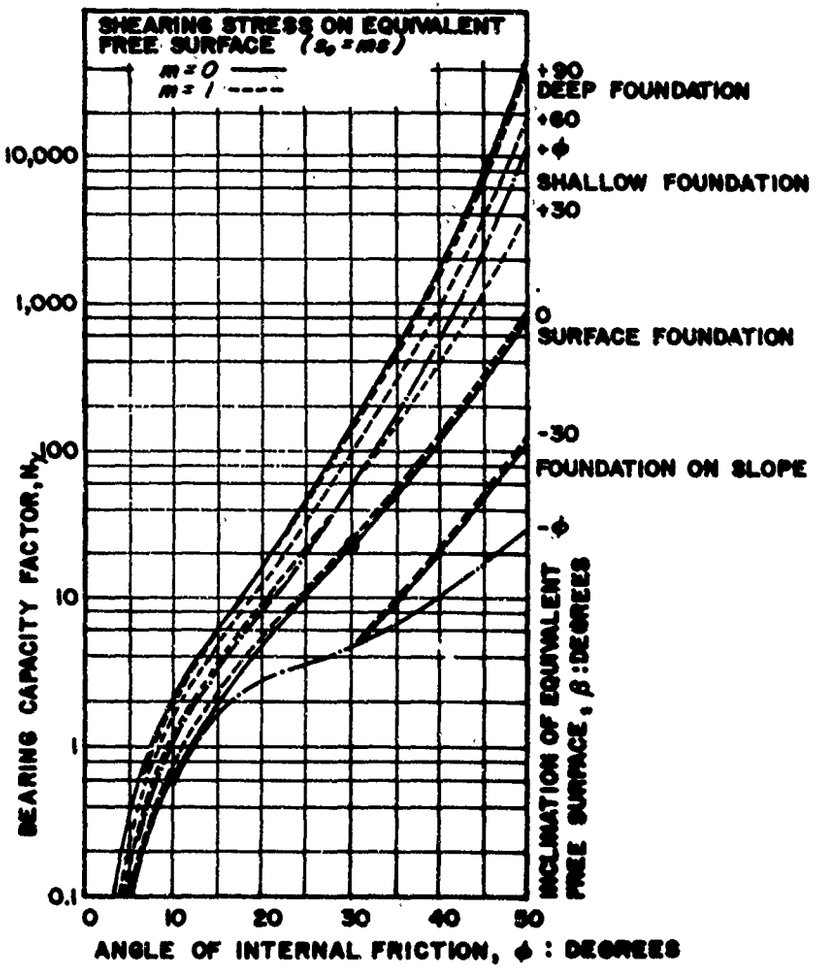

Figure 5.8

Bearing Capacity Factor N_γ as a Function of Friction Angle ϕ (after Meyerhof).

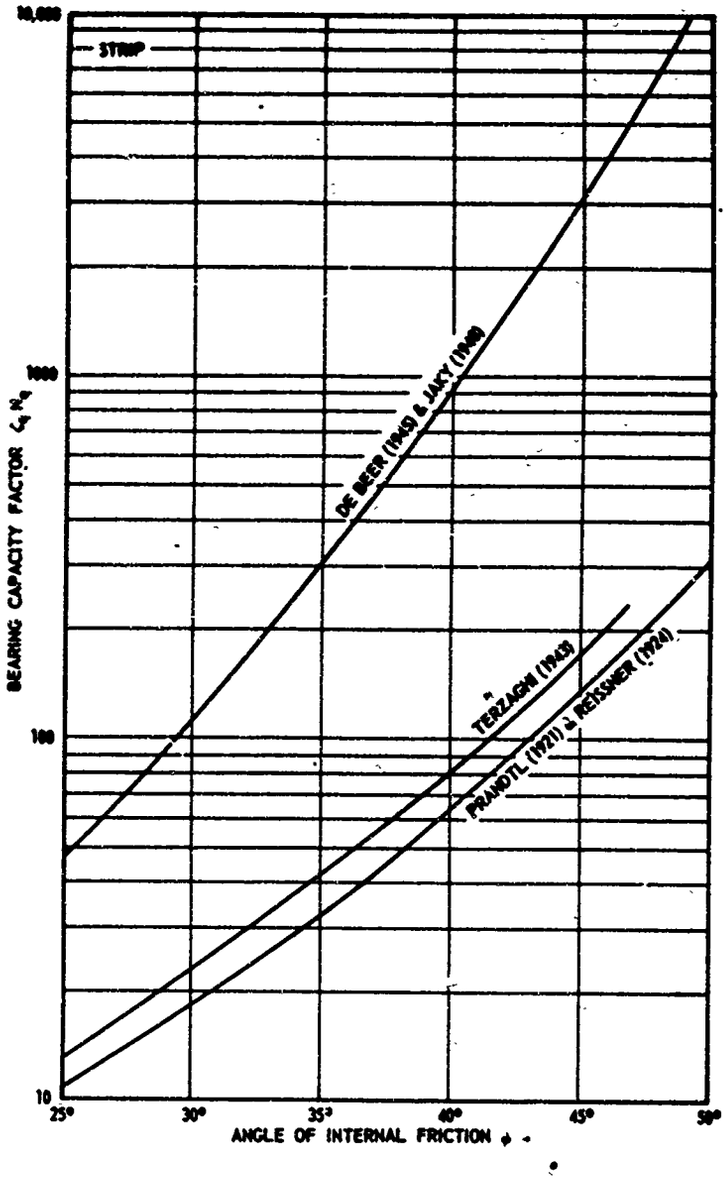

Figure 5.9

Comparison of Theoretical Bearing Capacity Factors N_q for Strip Foundation.

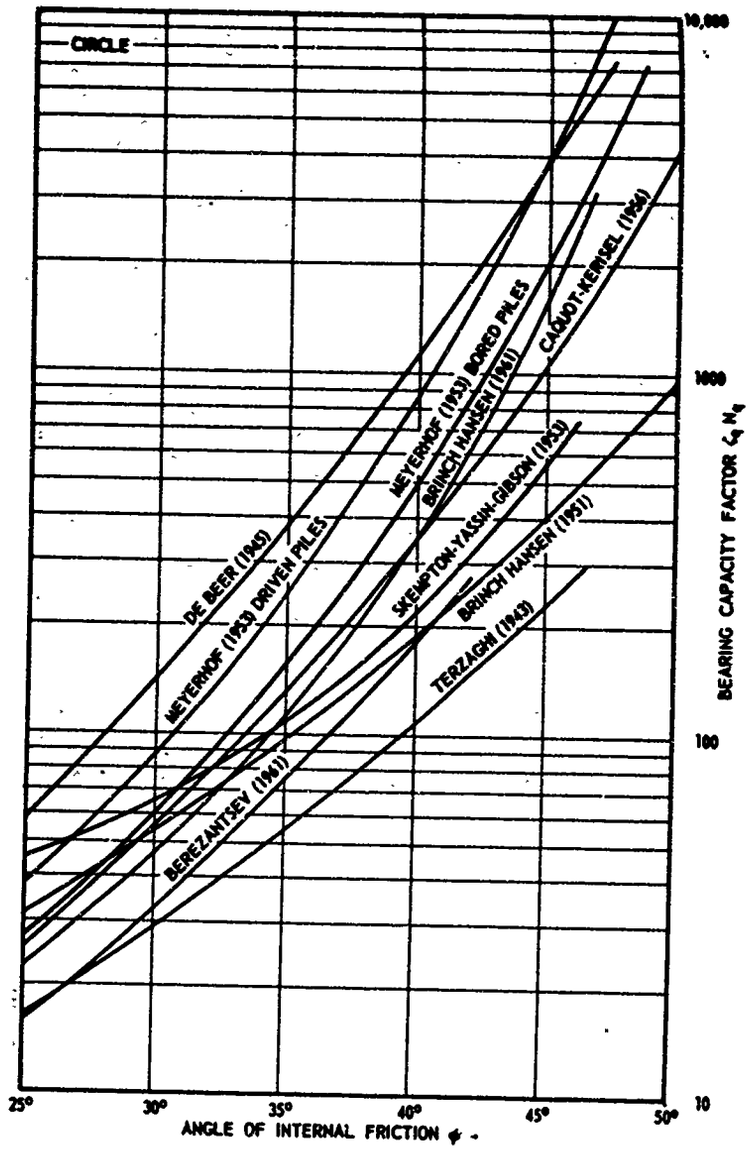

Figure 5.10

Comparison of Theoretical Bearing Capacity Factors N_q for Circular Foundation.

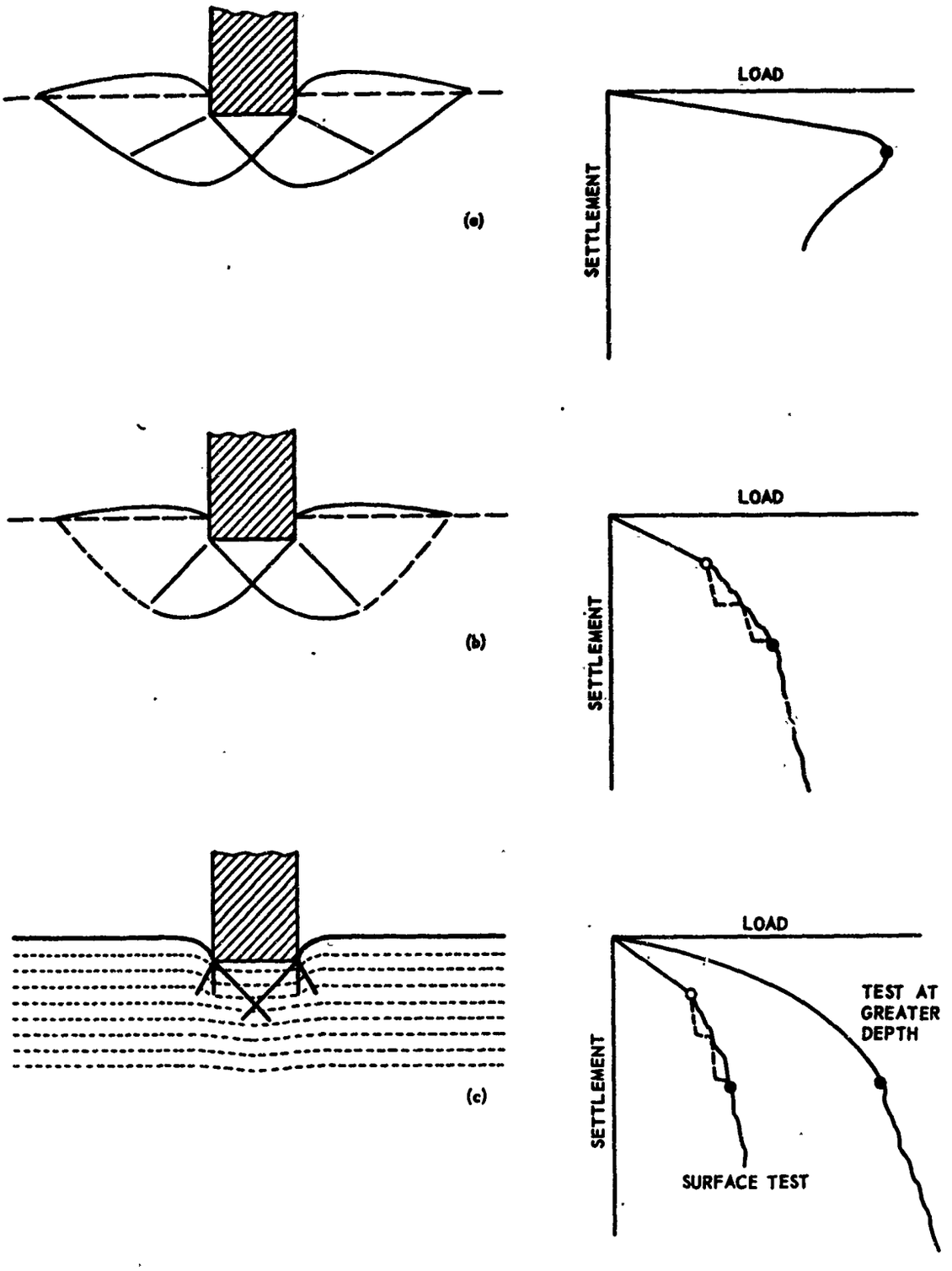

Figure 5.11

Types of Shear Failure (after Vesic)
a) general shear; b) local shear;
c) punching shear.

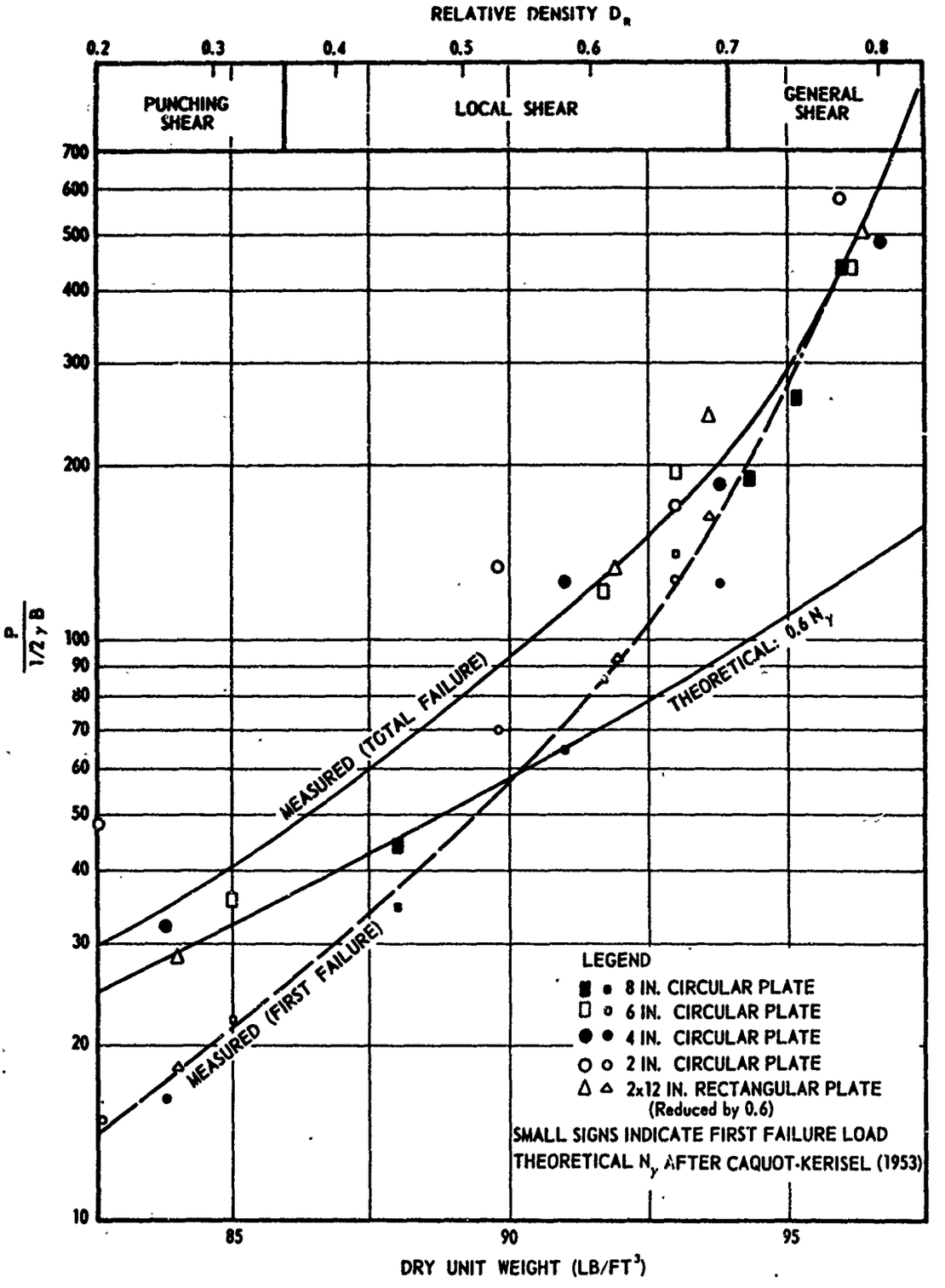

Figure 5.12

Theoretical and Observed Bearing Capacities of Foundations at Surface (after Vesic).

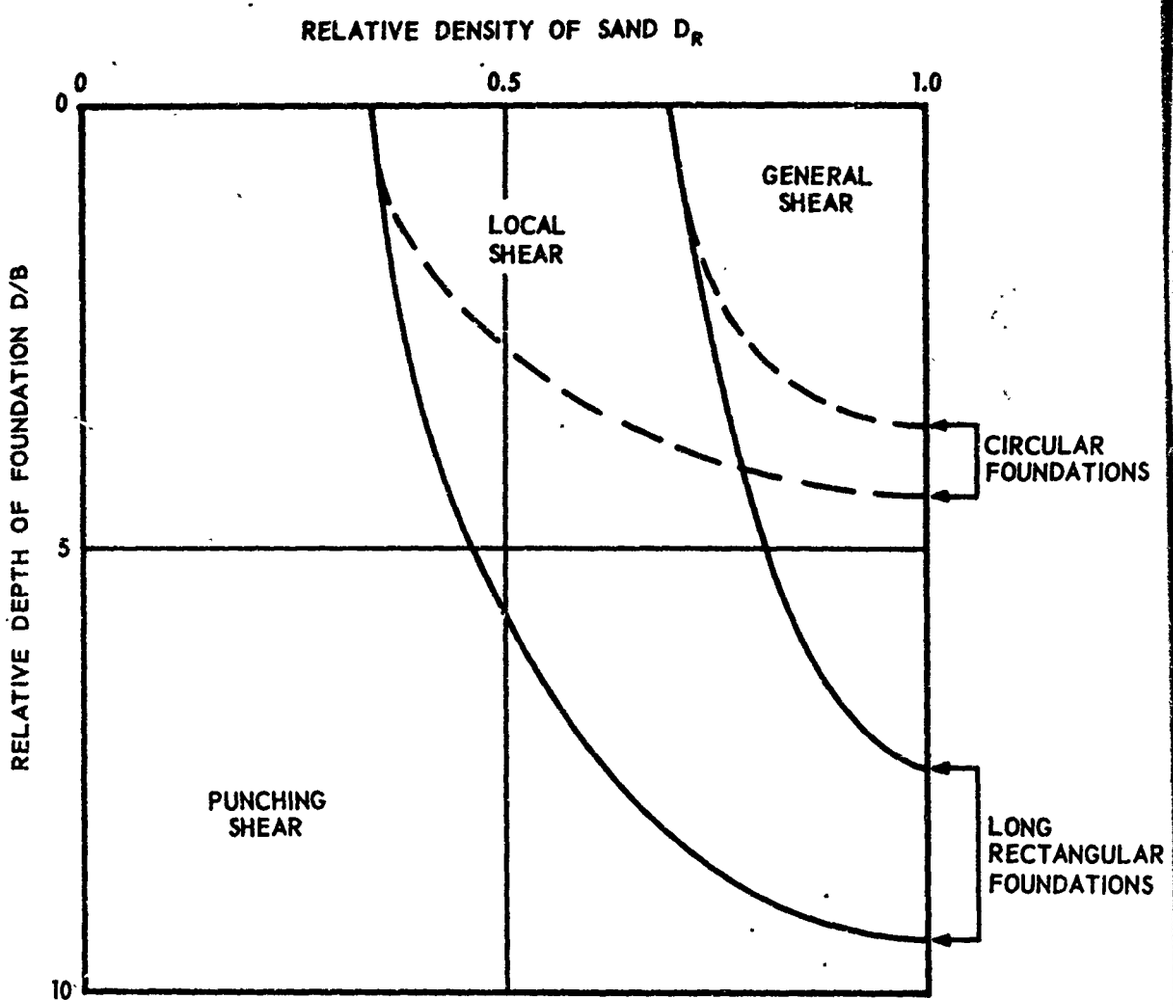

Figure 5.13

Types of Shear Failure
Relative Depth vs. Relative Density
(after Vesic, 1967)

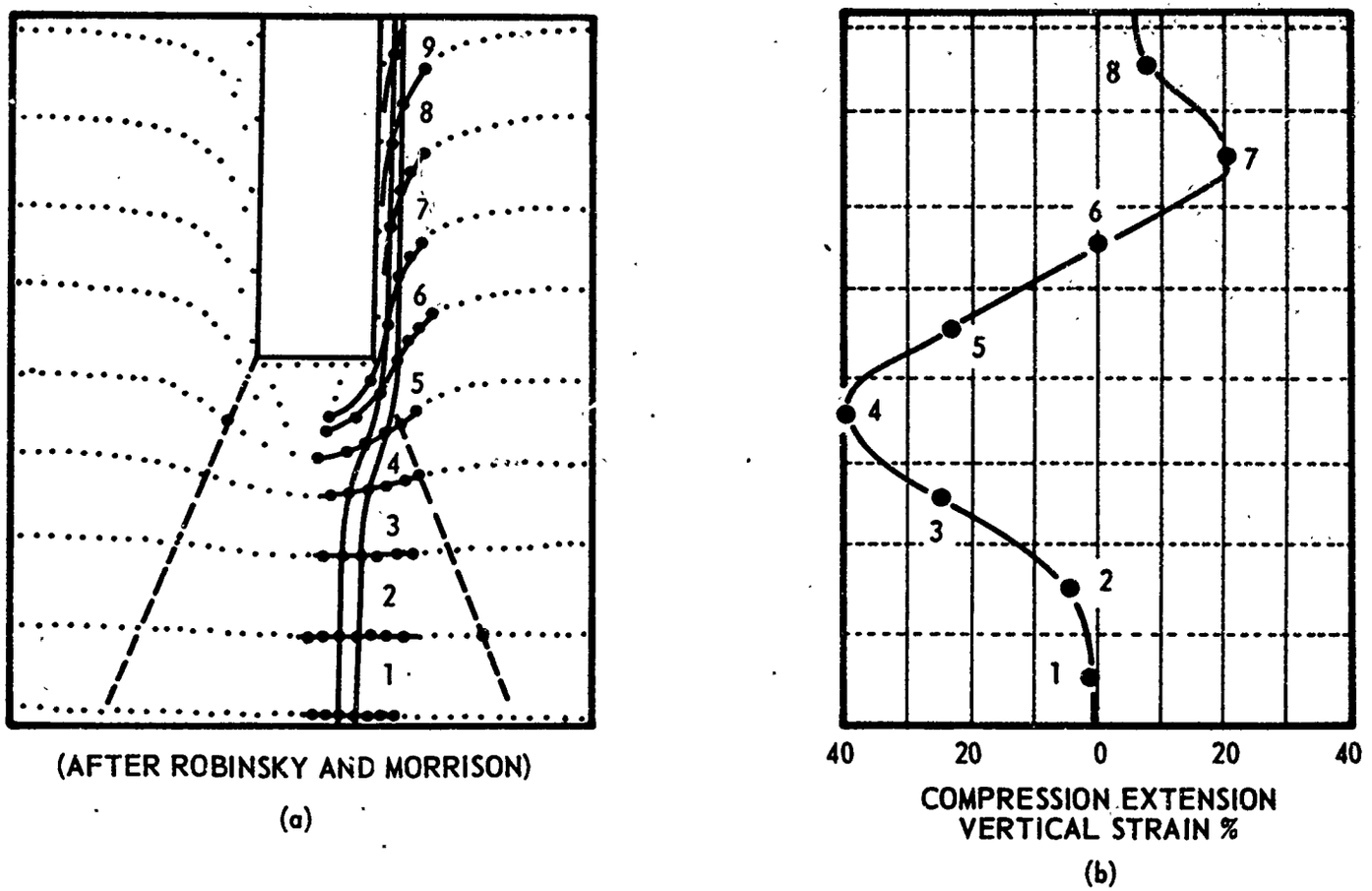

Figure 5.14 Strain Pattern around Point for Deep Penetration

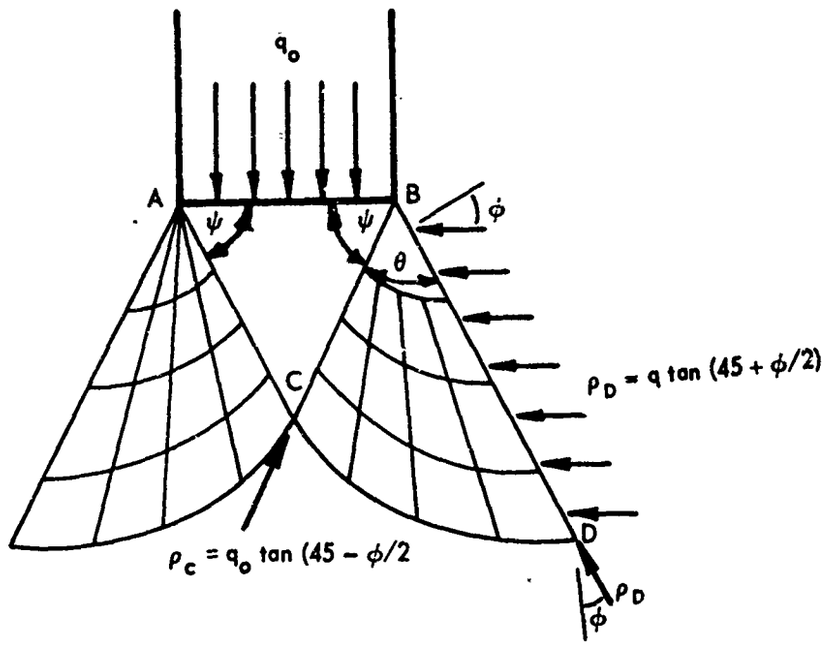

$$\rho_D = \rho_c \; e^{-2\,\theta \tan \phi}$$

$$q_o = q \tan^2 (45 + \phi/2) \; e^{2\,\theta \tan \phi}$$

Figure 5.15

Analysis of Punching or Local Shear Failure (after Vesic).

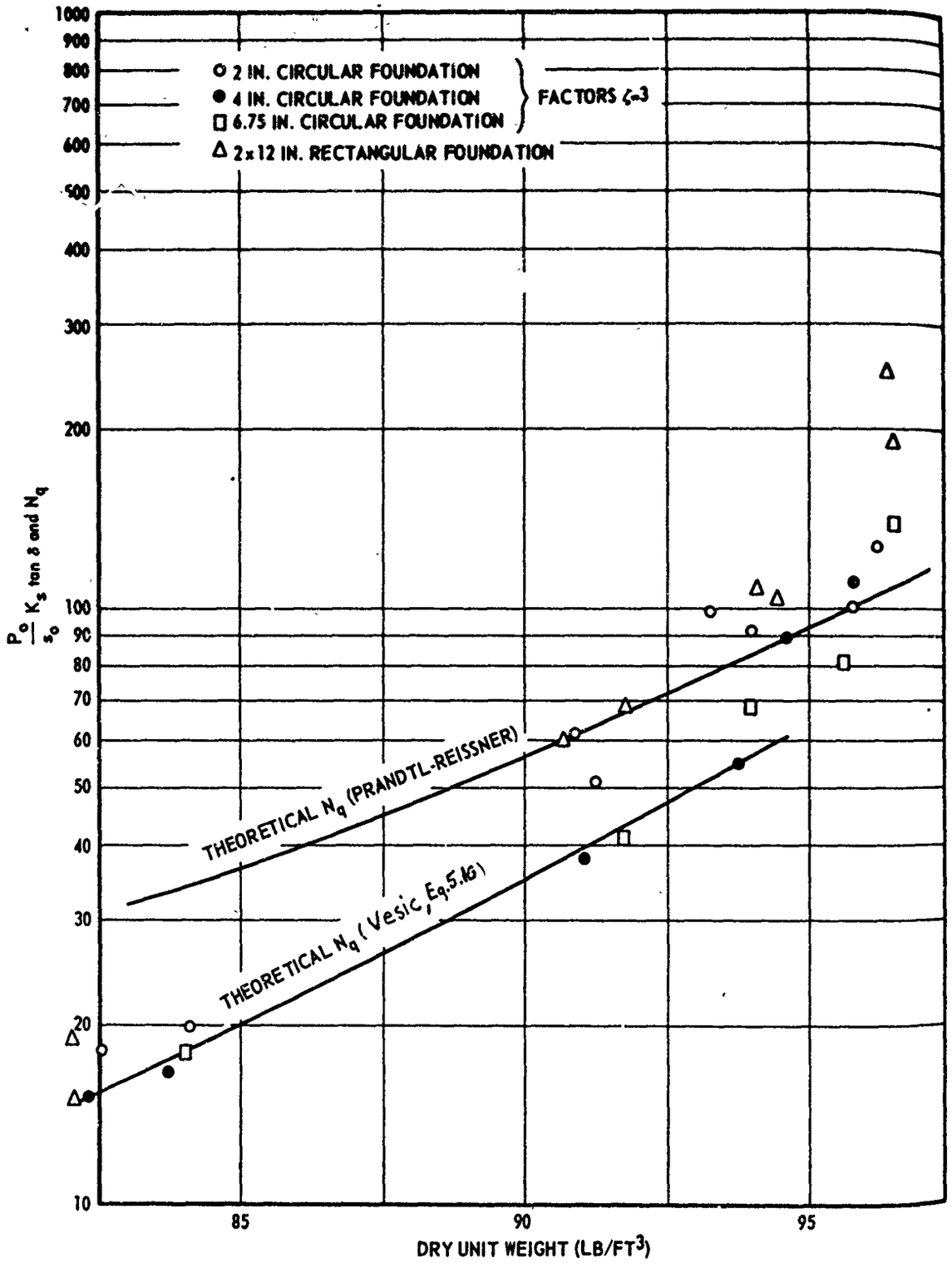

Figure 5.16

Theoretical Bearing Capacity Factors N_q at Greater Depth and Comparison of Model Test Results (after Vesic, 1967)

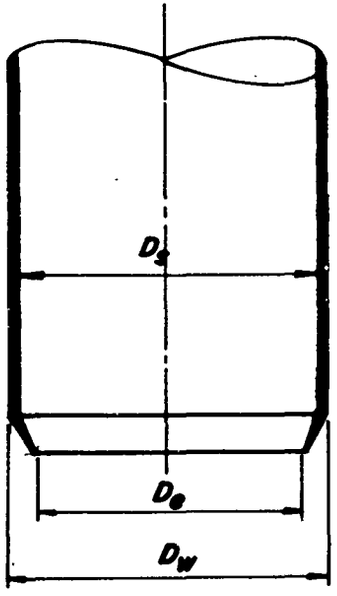

Figure 6.1a

Definition of Terms for Area and Clearance Ratio of Sediment Core Samplers

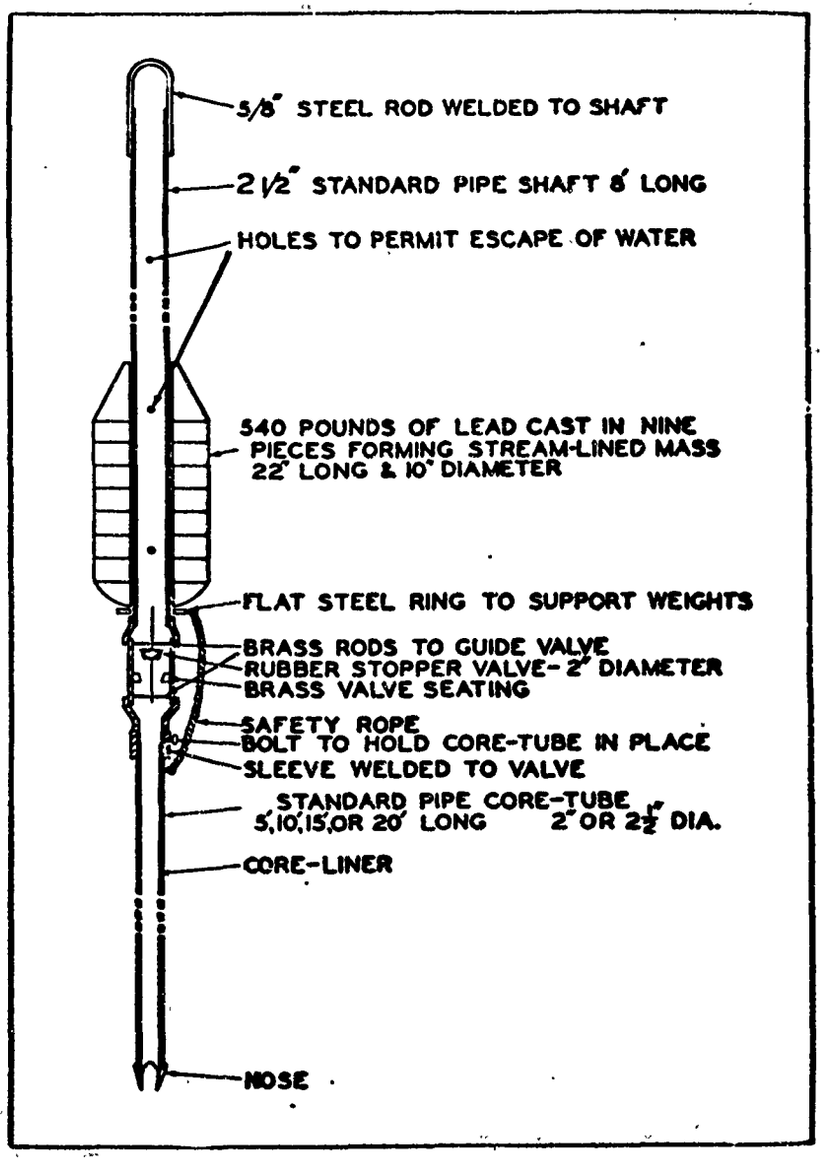

Figure 6.1

Gravity Corer of Scripps Oceanographic Institute

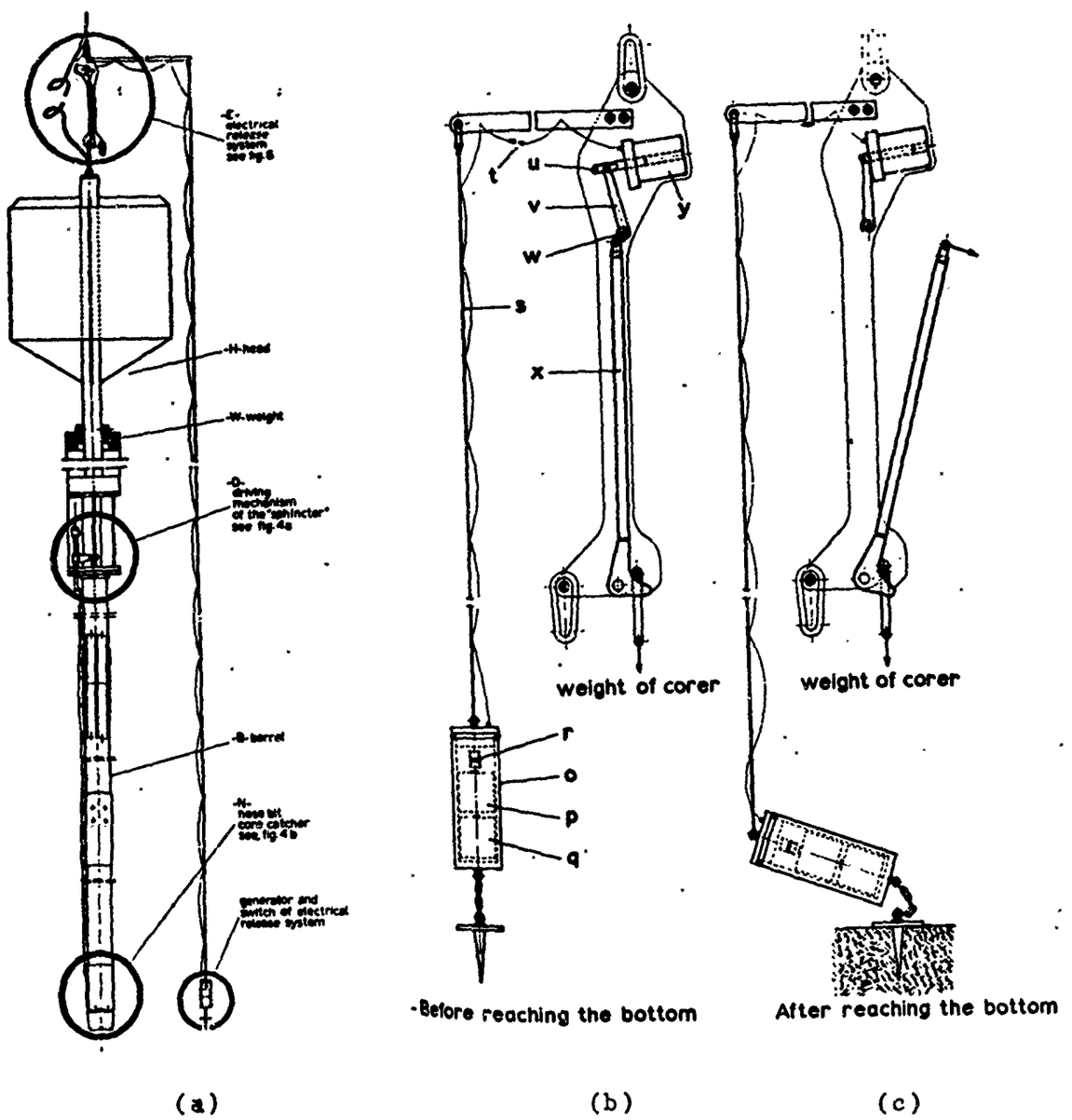

Figure 6.2

(a) The "Sphincter" 120 mm Corer

(b) and (c) Electrical Release Mechanism

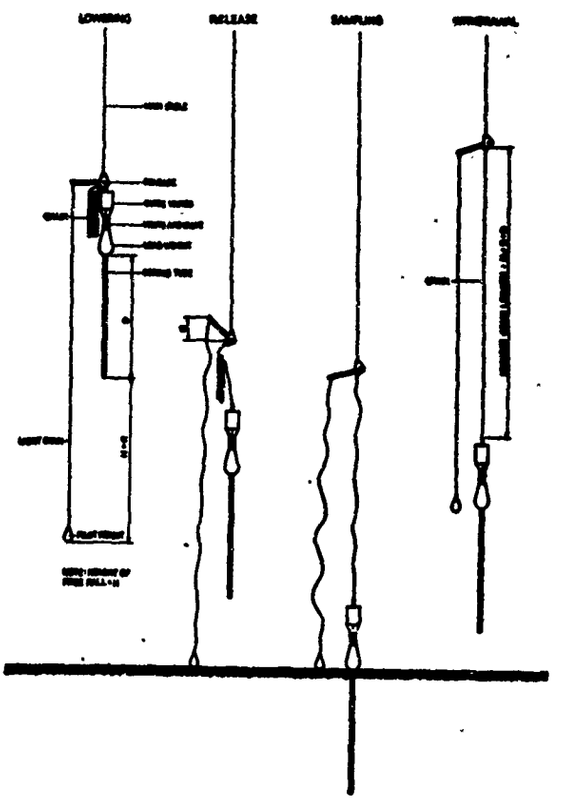

Figure 6.3

Release of Free Fall Corer by Pilot Weight (after Hvorslev & Stetson)

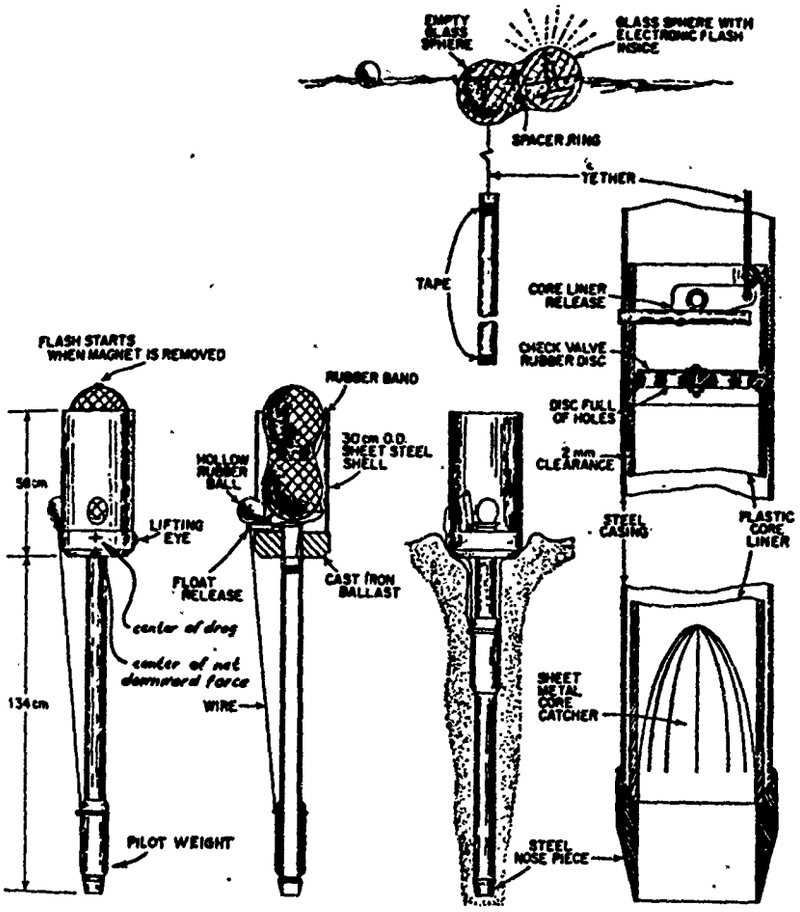

Figure 6.4

Final design of the unattached sediment sampler consisting of hollow glass-sphere float and cast-iron ballast.

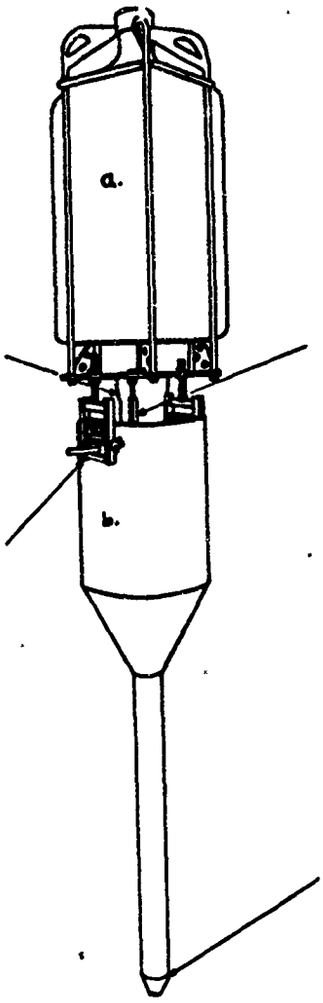

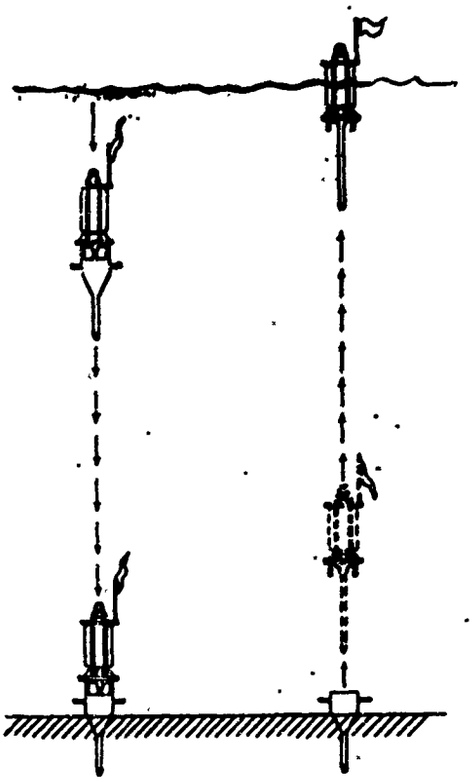

-Stages in operation of free-corer.

Figure 6.5

Diagram of free-corer with polyethylene bottle (a) which, when filled with gasoline, acts as pressure-proof buoyant chamber. Core barrel attached to buoyant chamber fits loosely inside of expendable weight-casing (b).

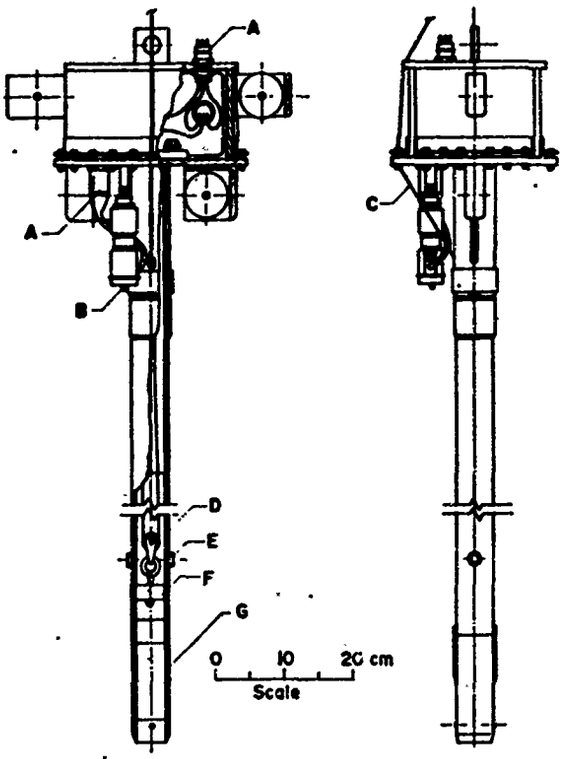

Figure 6.6(a)

Assembly drawing of vibrator housing and bore barrel. A, electrical connector; B, switch; C, piston wire; D, plastic liner; E, locking pin socket; F, piston; G, removable filler.

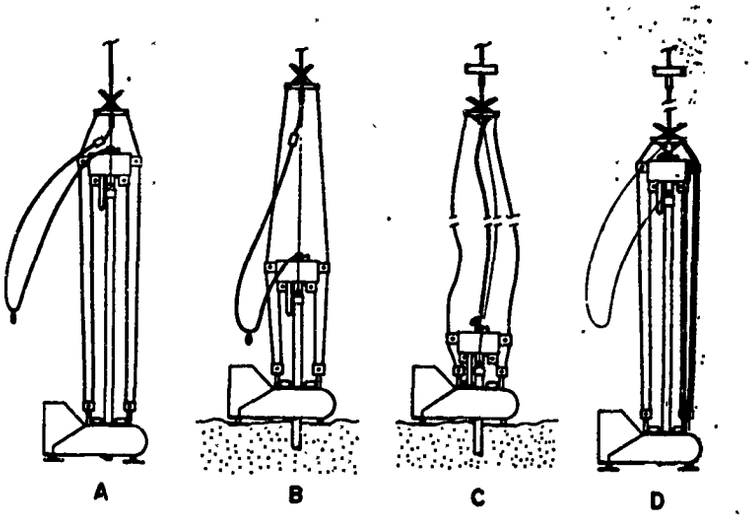

Figure 6.6(b)

Schematic diagrams of core sampler in operation. A, descending; B, coring; C, extracting; D, ascending.

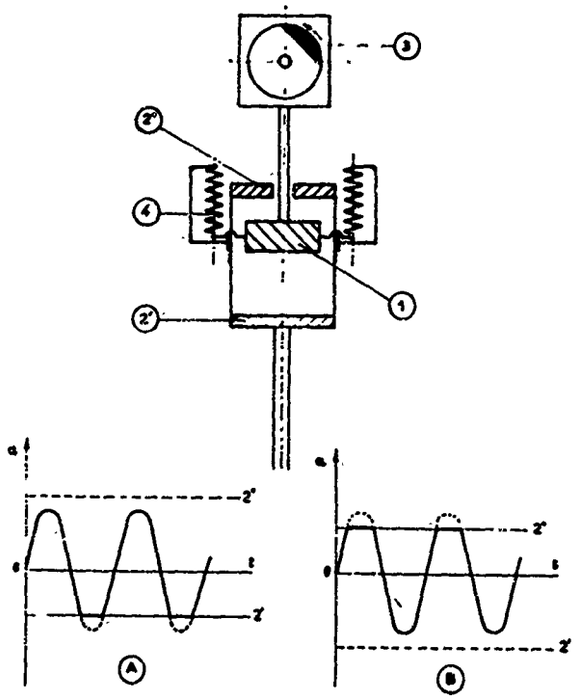

Figure 6.7(a)

Principle of Vibratory Coring. 1) hammer, 2) anvil, 3) excentric, 4) spring.

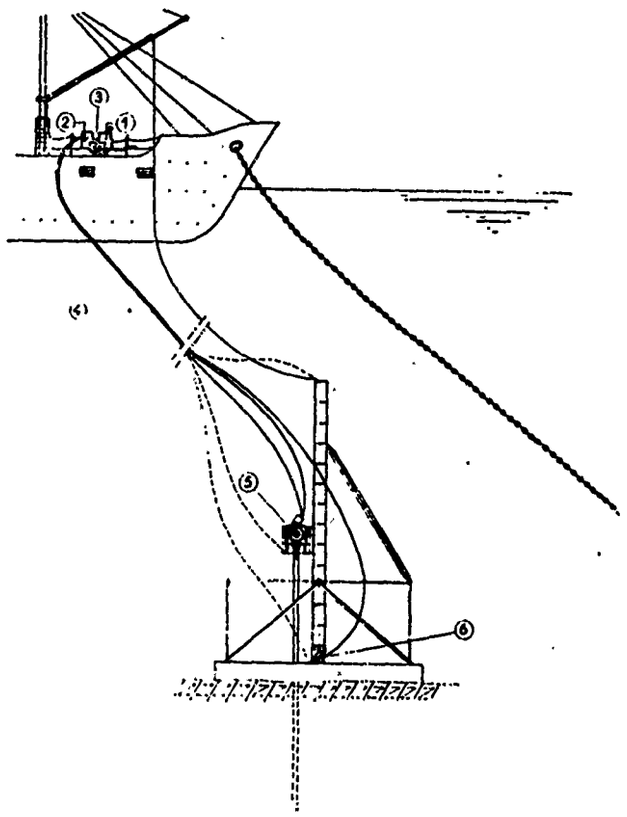

Figure 6.7(b)

Coring Assembly. 1) Diesel engine, 2) hydraulic pump, 3) mud pump, 4) hosing, 5) vibrohammer, 6) hoist motor

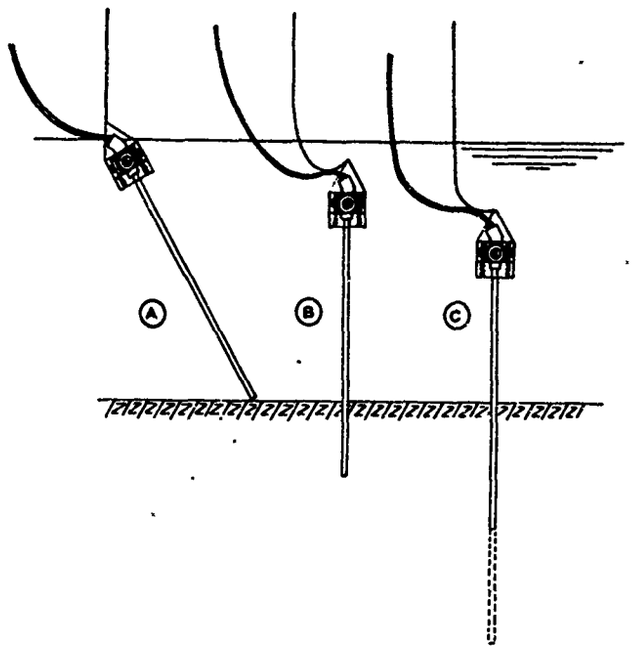

Figure 6.8(a)

Sampling Sequence.

A) lowering instrument
B) self driving by vibrations
C) self extraction by vibrations

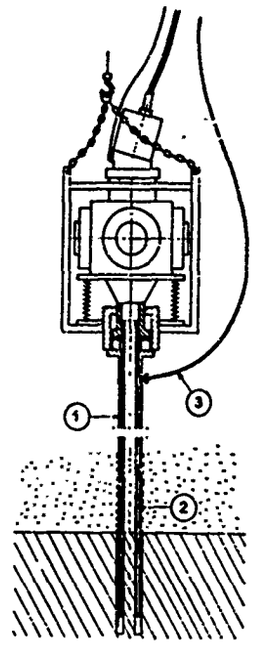

Figure 6.8(b)

Rotary vibro-hammer drilling in rock.

1) casing
2) rotary miner stem
3) mud circulation

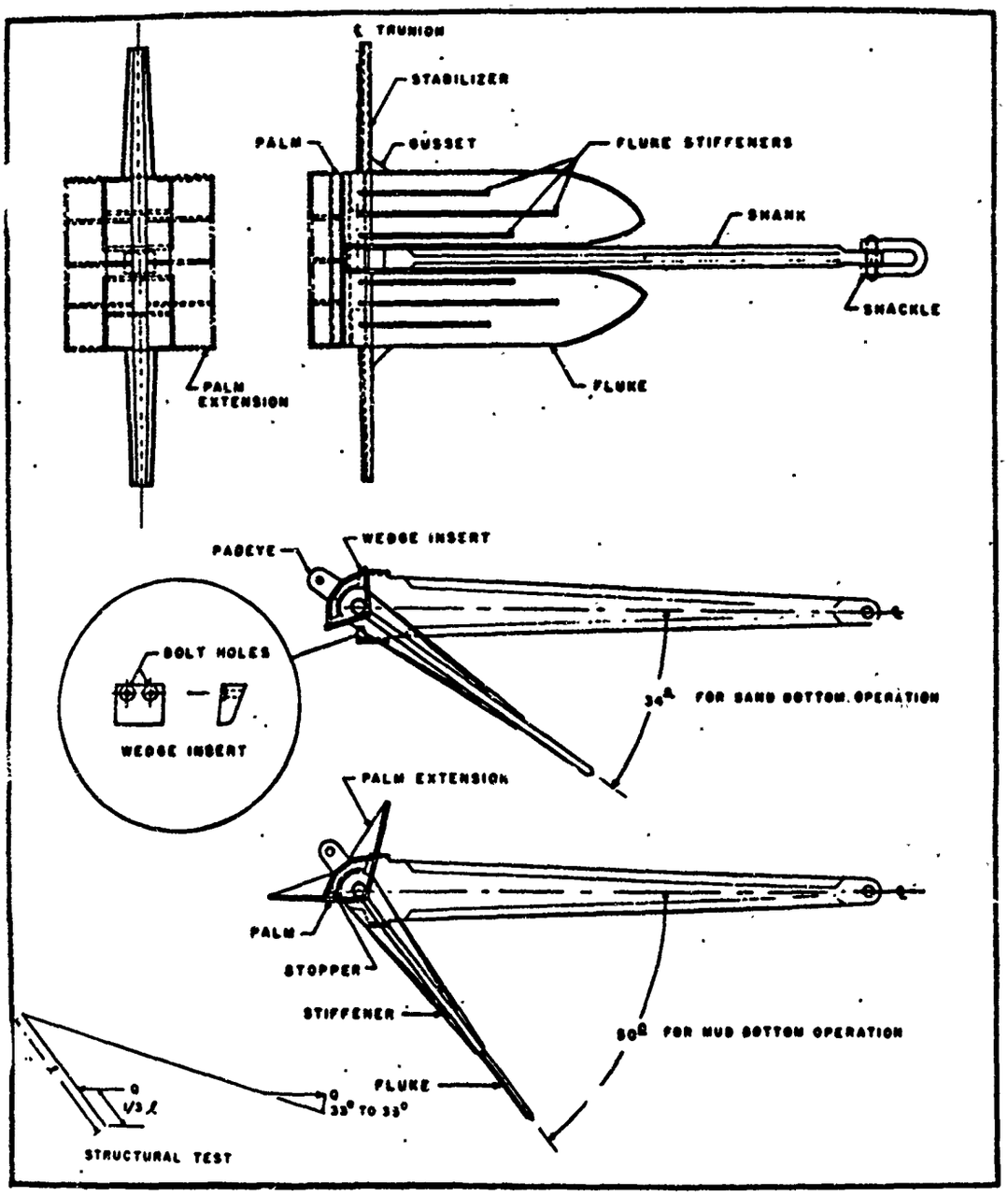

Figure 6.9

Details of BUDOCKS STATO mooring anchor.

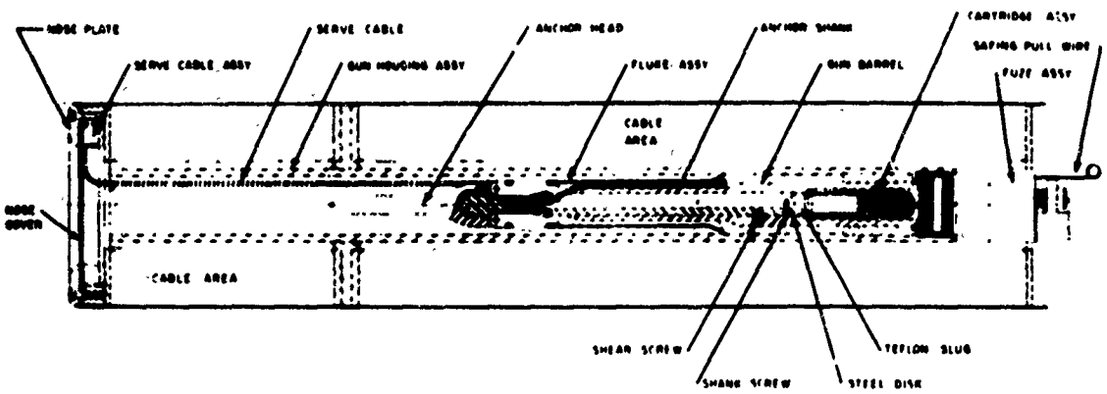

Figure 6.10a

Explosive Self-Embedment Anchor (Magnavox Co.)

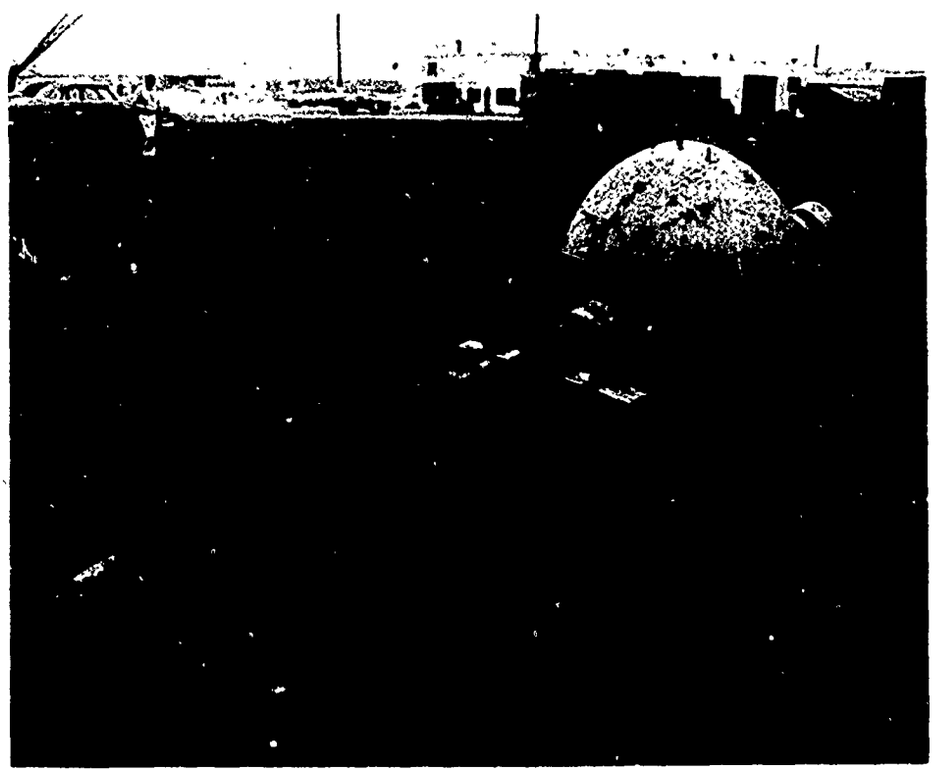

Figure 6.10b

Explosive Embedment Anchor (after Tudor)

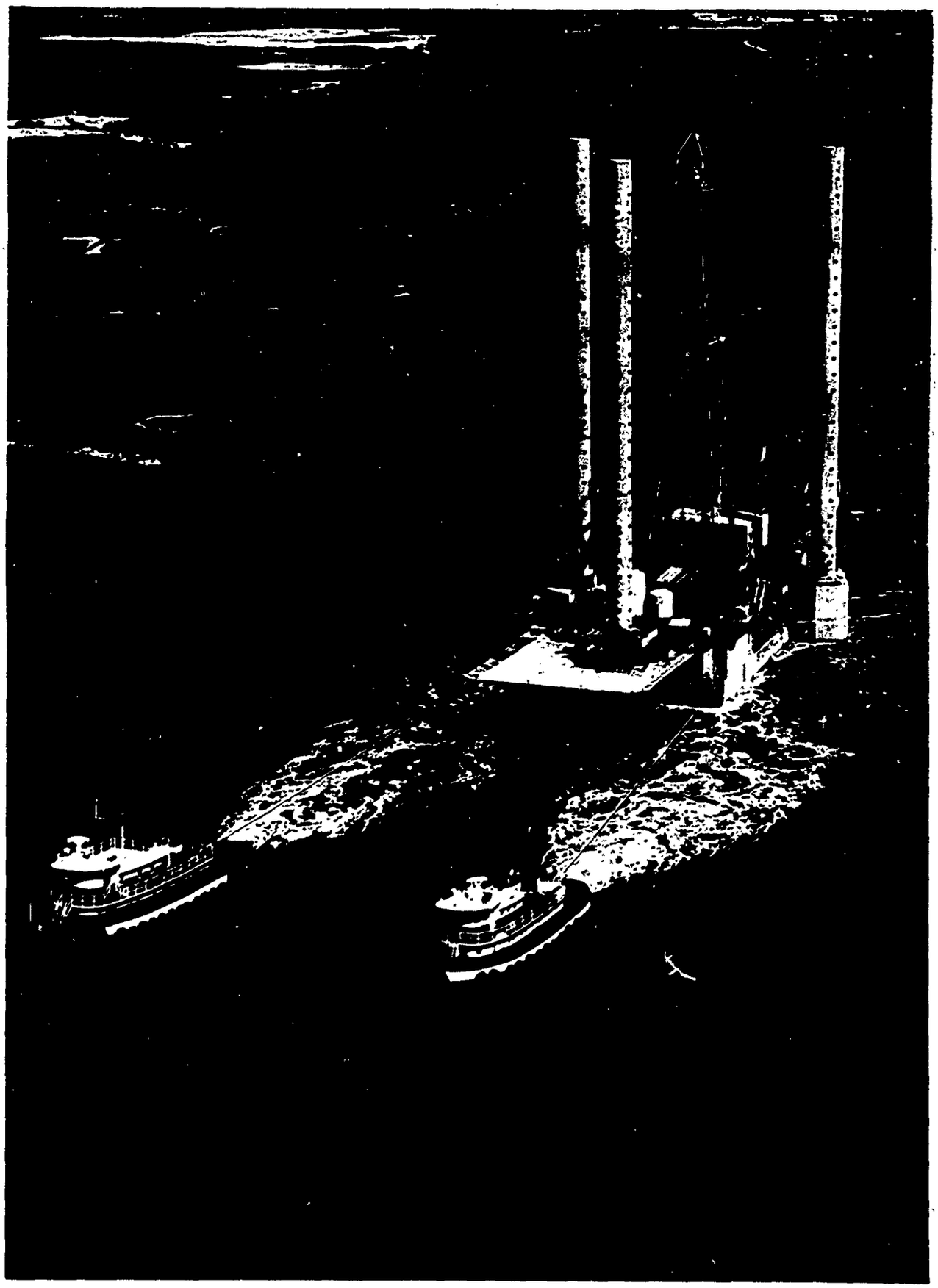

Figure 6.11

A platform being towed to sea.

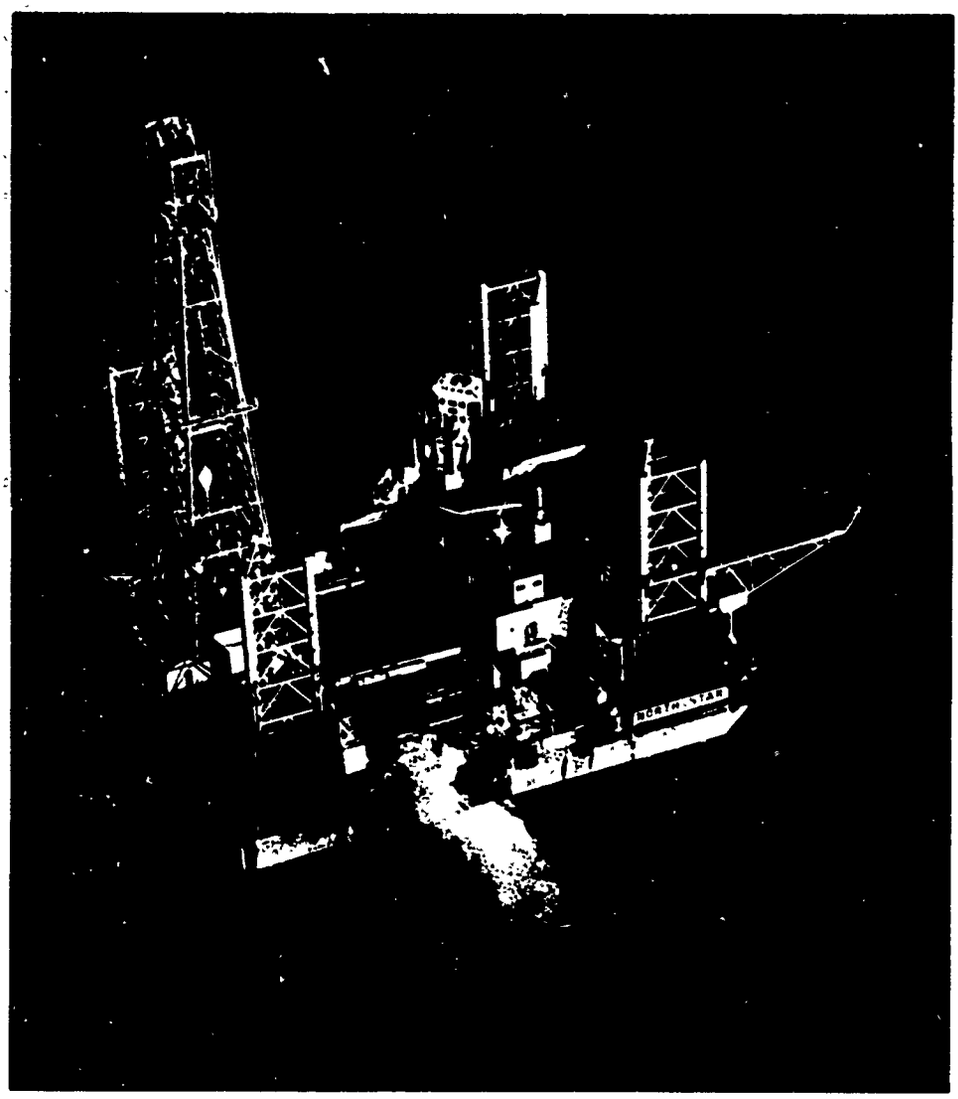

Figure 6.12
North Star - Jack-up.

Figure 6.13
Rig #57 - Offshore Company

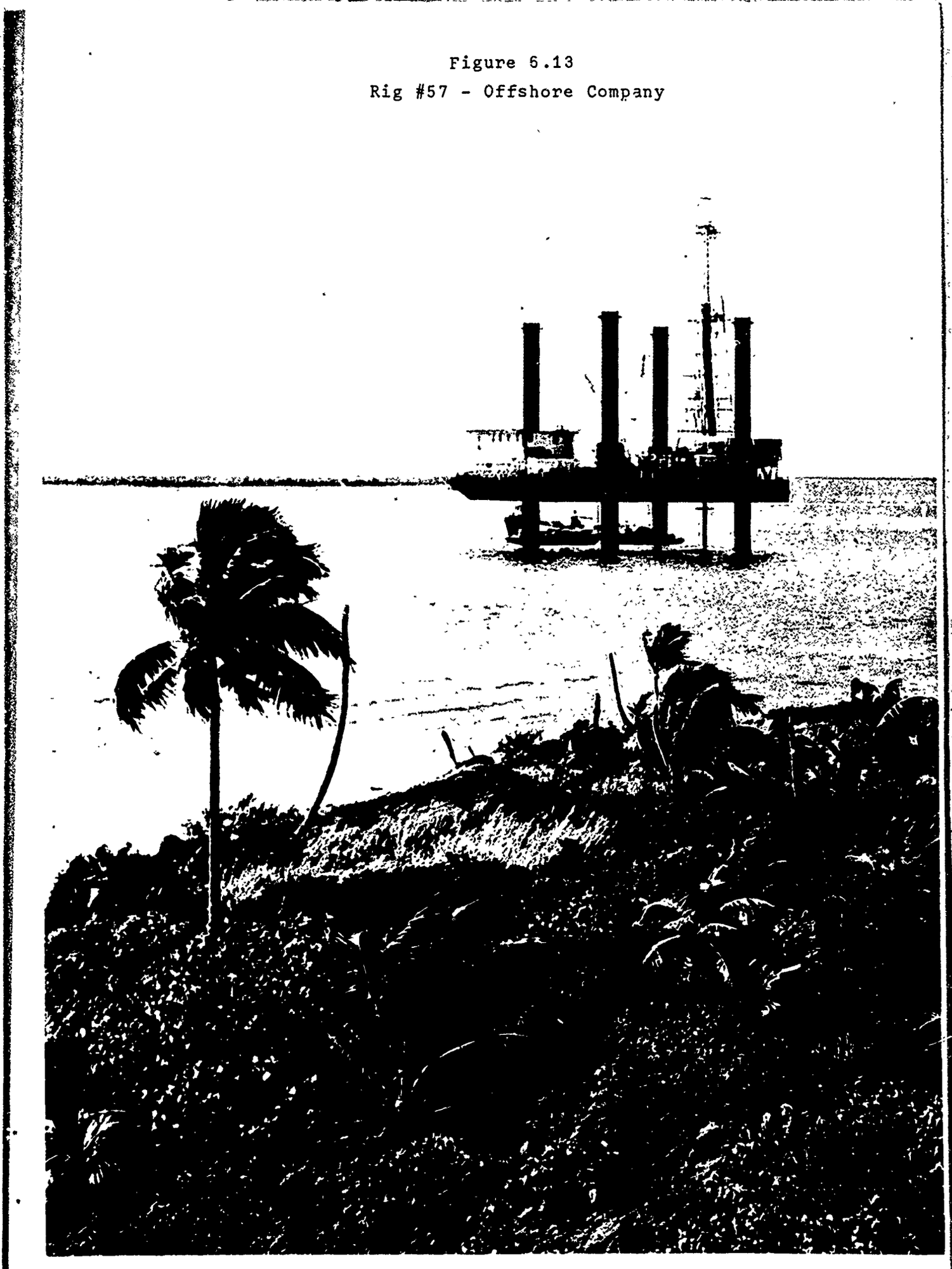

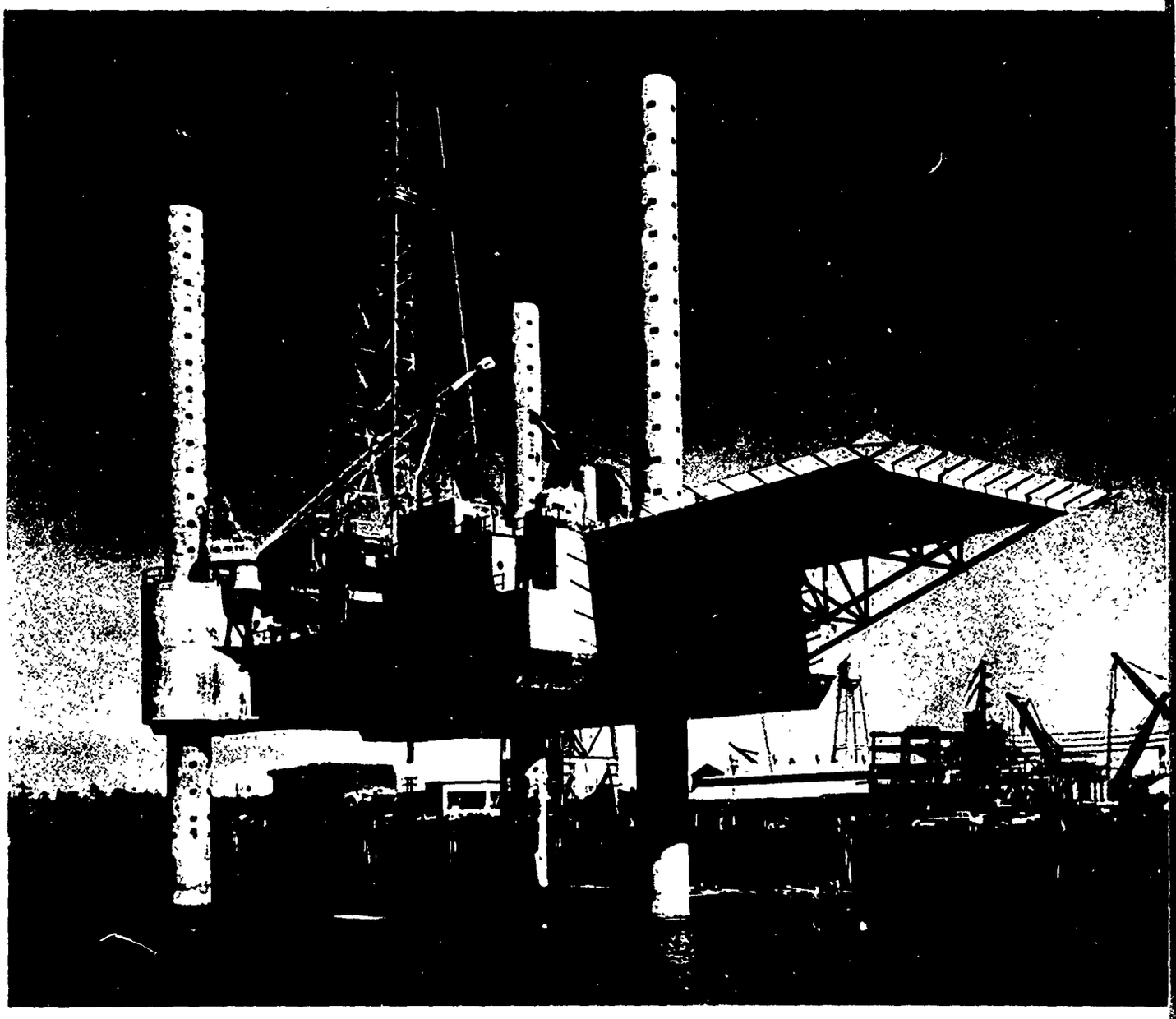

Figure 6.14

Mat-type jack-up rig.

Figure 6.15 Schematic of mat-type jack-up.

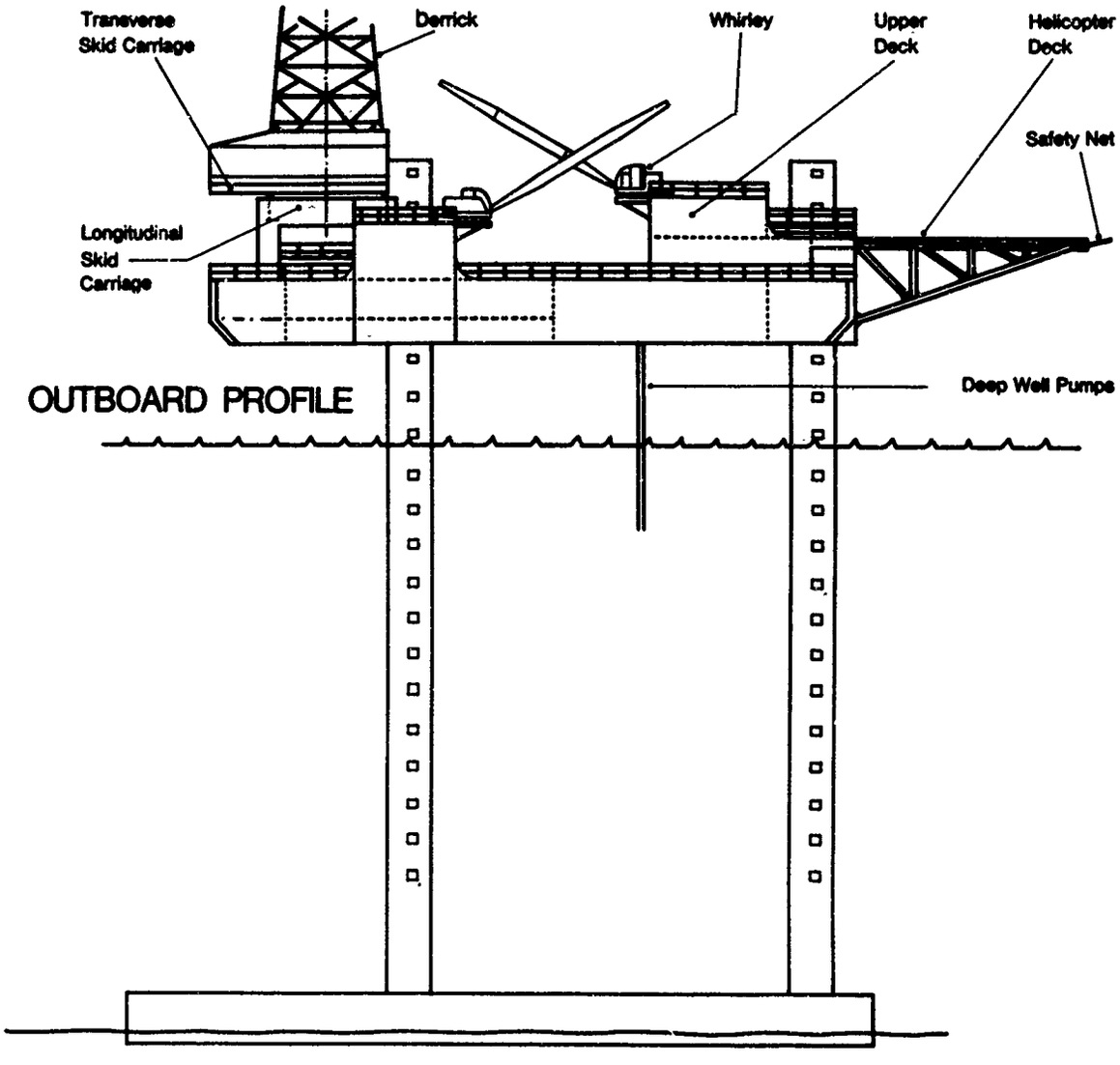

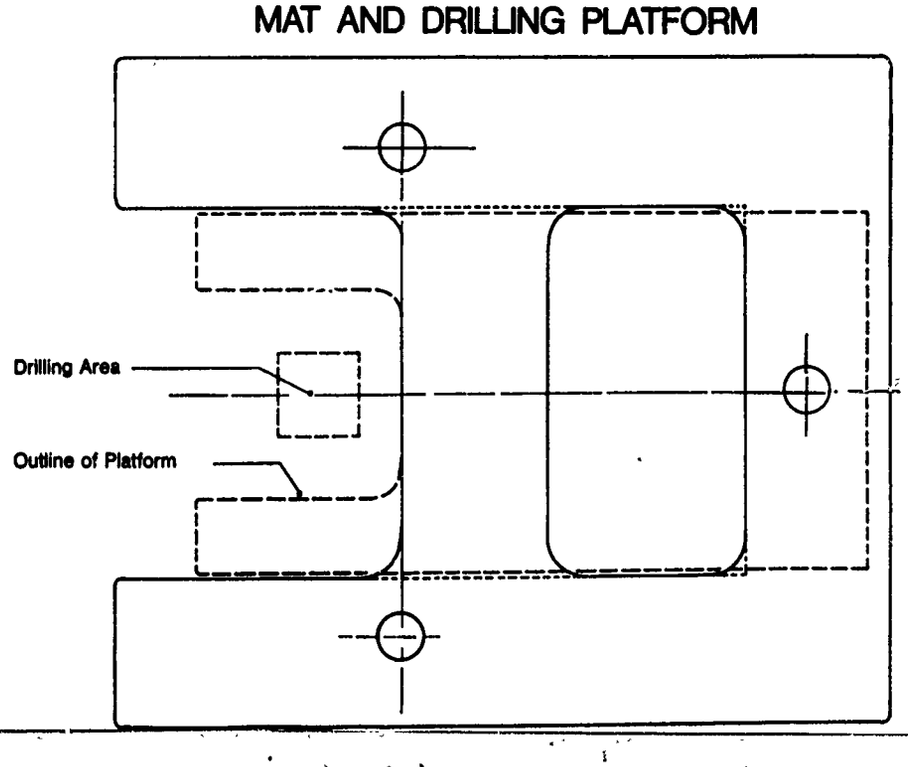

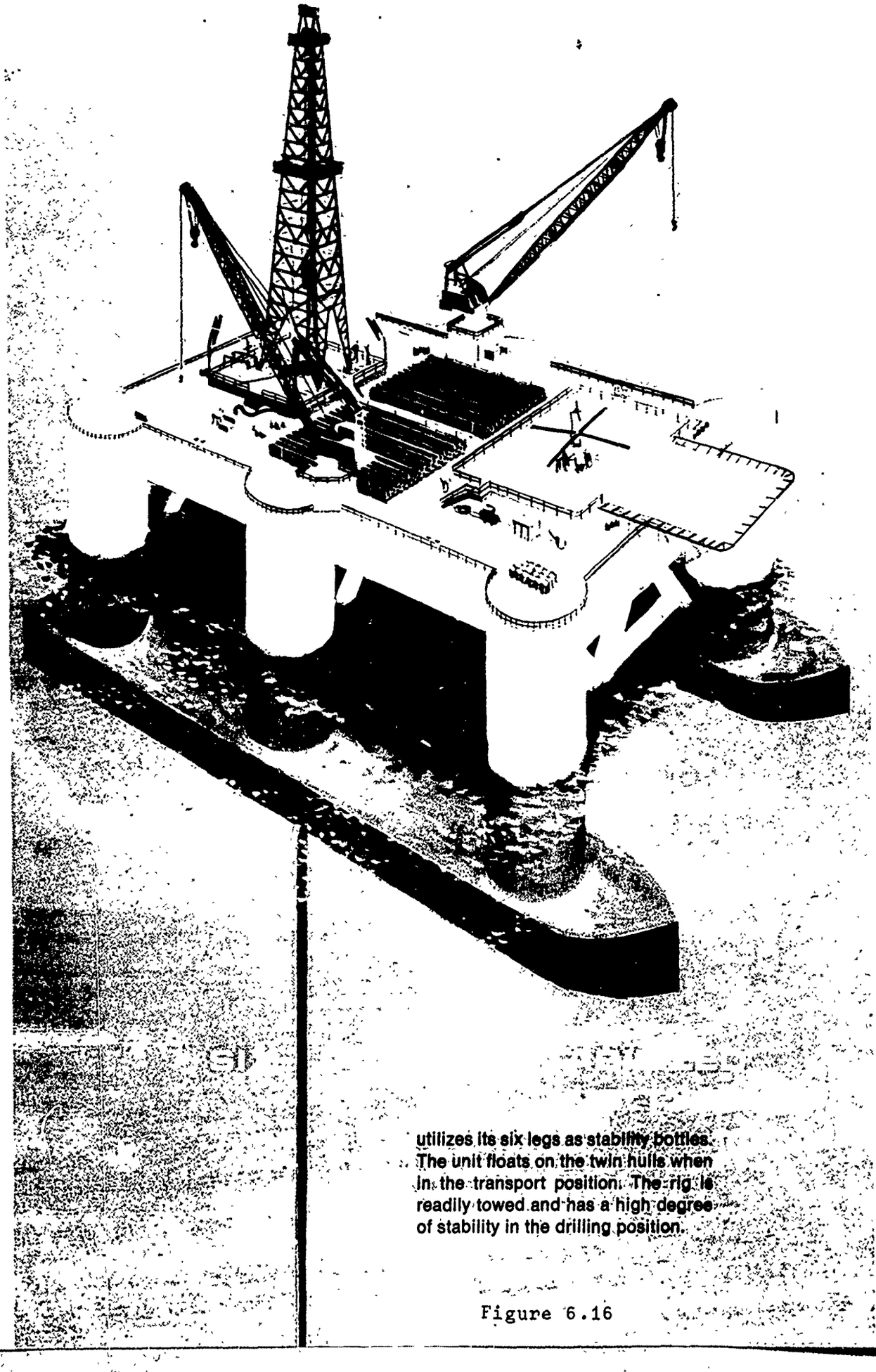

utilizes its six legs as stability bottles. The unit floats on the twin hulls when in the transport position. The rig is readily towed and has a high degree of stability in the drilling position.

Figure 6.16

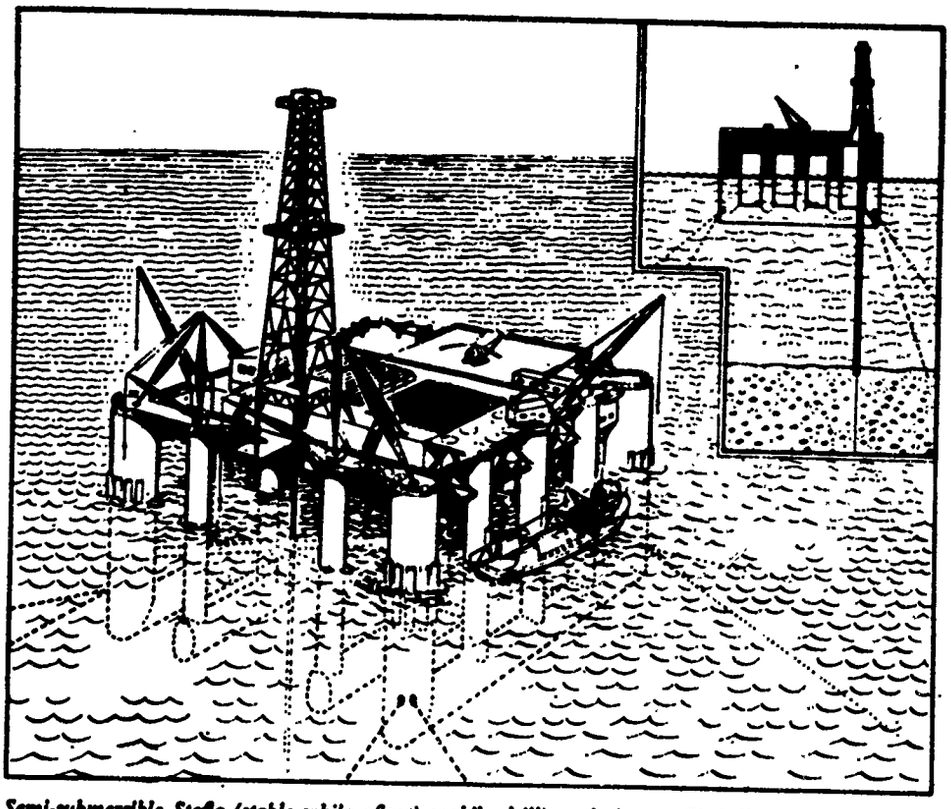

Semi-submersible Staflo (stable while afloat) mobile drilling platform will drill for Shell and Esso in North Sea when delivered by a British shipyard next year. Schematic view shows large working area and arrangement of cranes that will enable highly efficient drilling and loading of supplies. Overall height of unit, including derrick, is 275 ft.

Figure 6.17

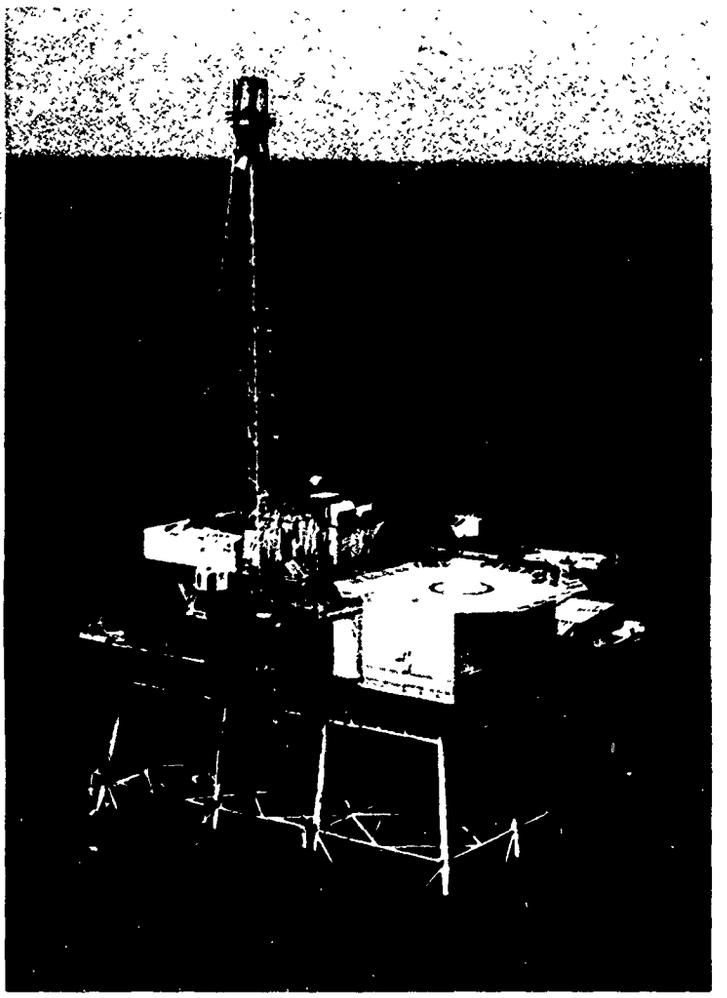

Figure 6.18

Fixed, self-contained platform.

Figure 6.19

Fixed platform llama and tender - Offshore Company.

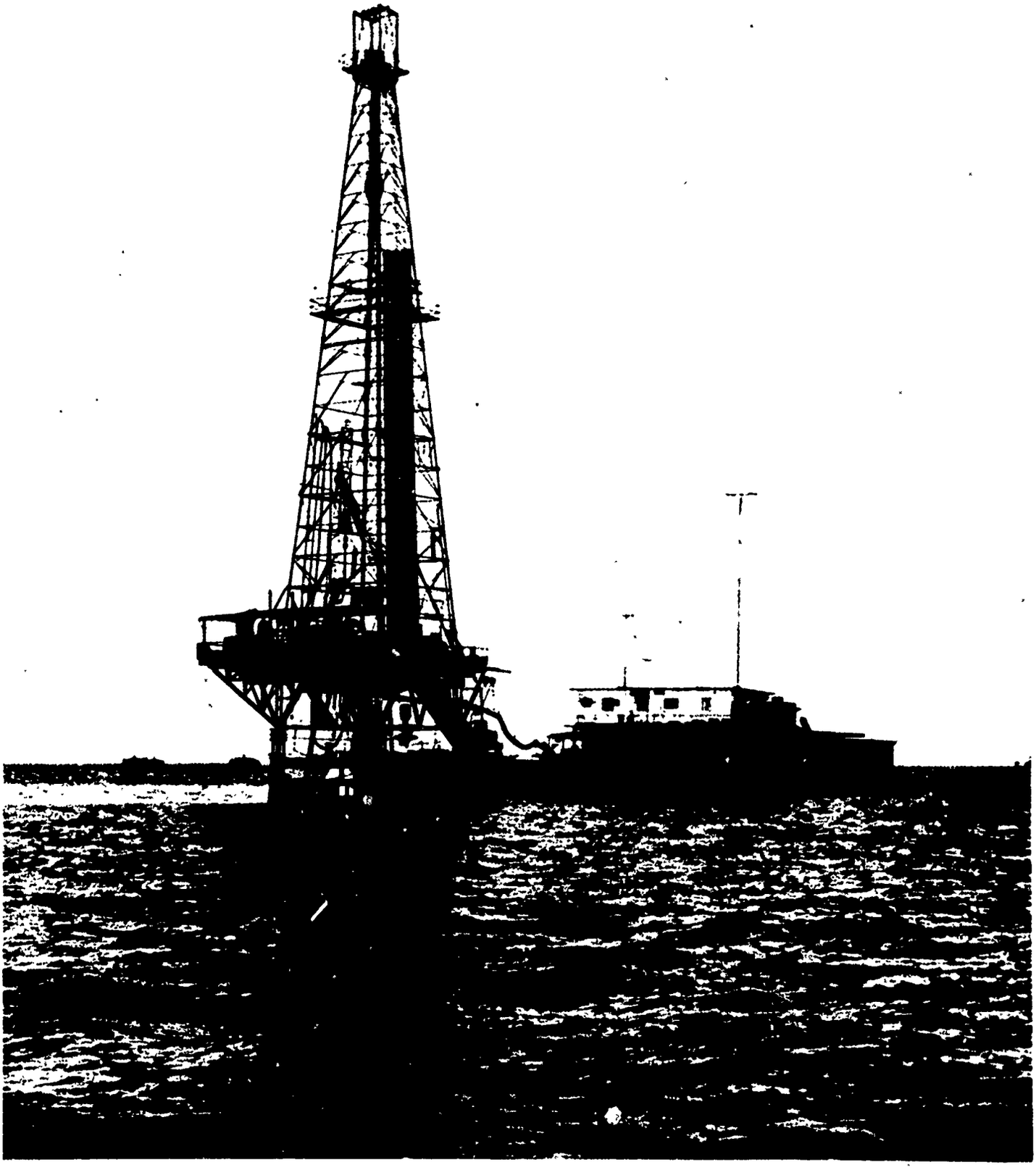

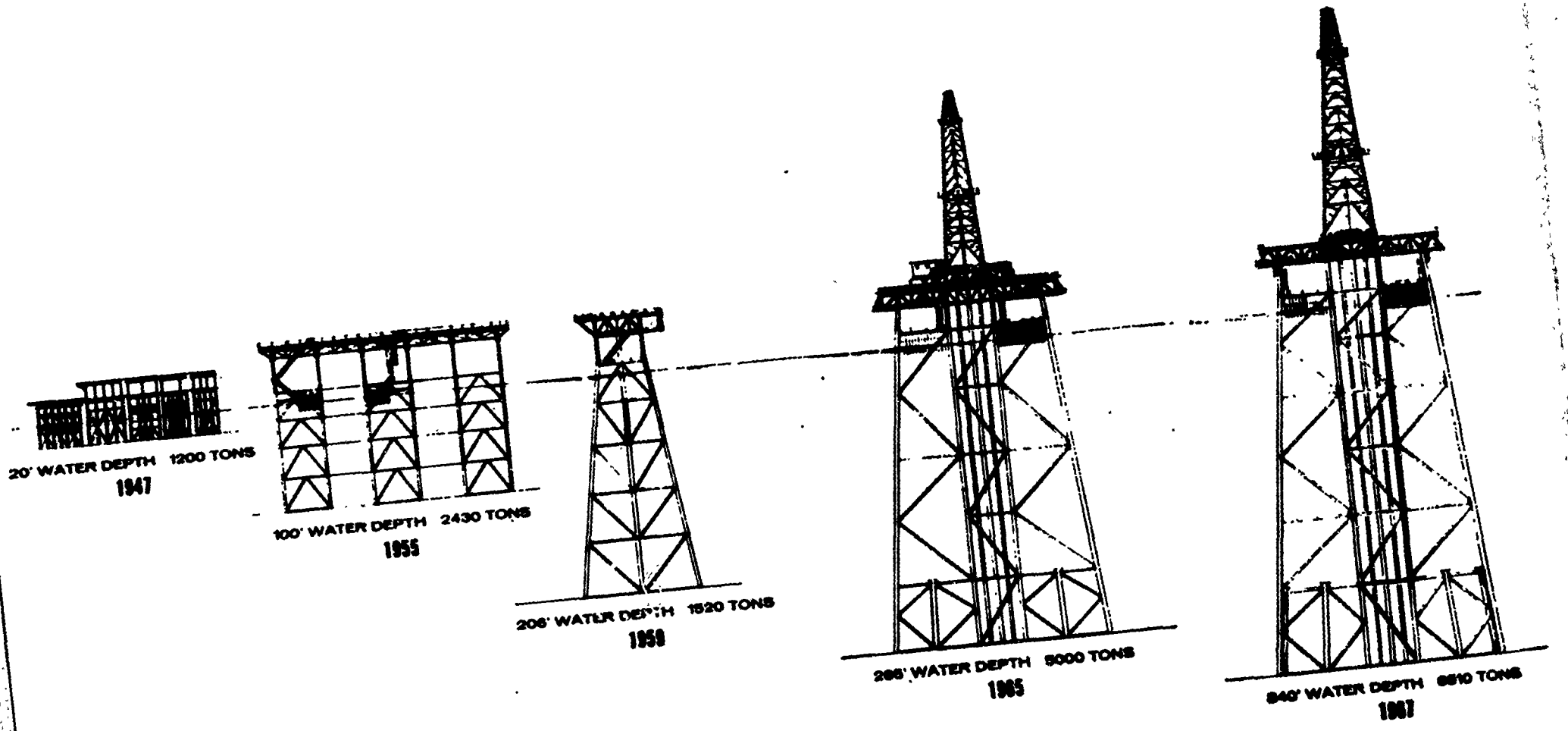

Figure 6.20

Twenty Years of Platform Development

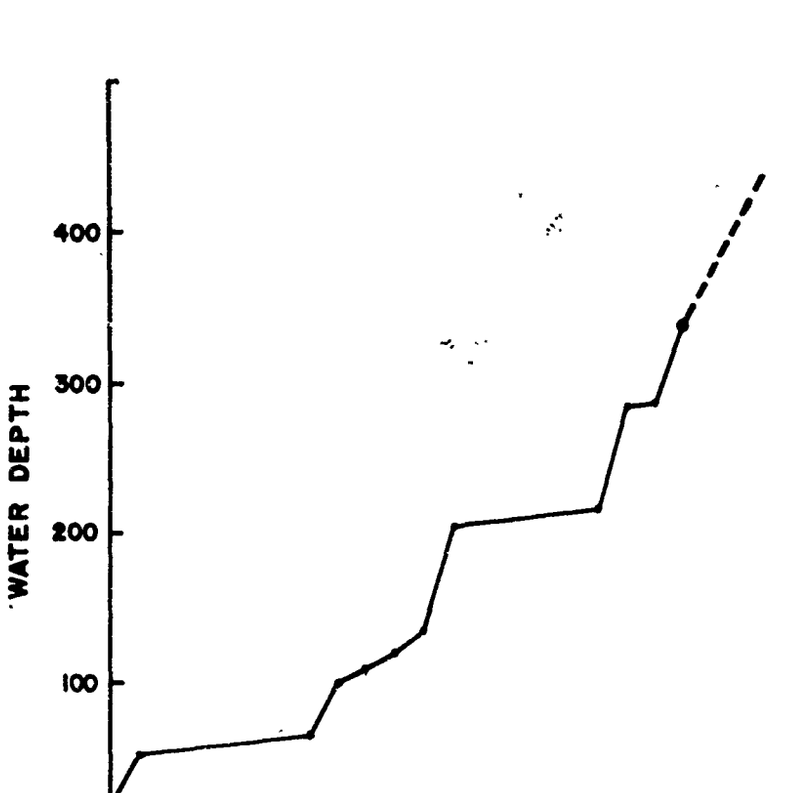

Figure 6.21

Records of Platform Construction

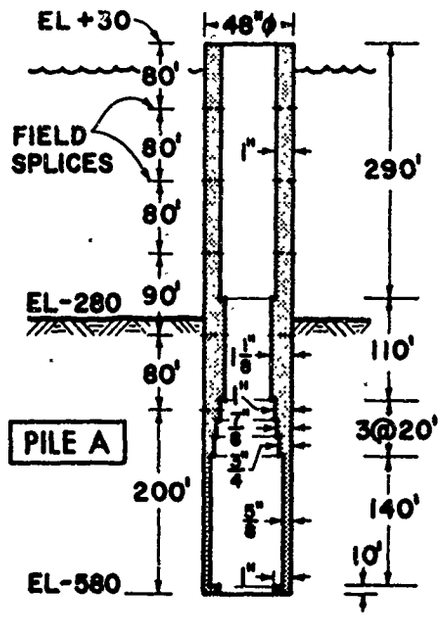

Figure 6.22

Example of design and assembly schedule for offshore pile (after McClelland et al.).

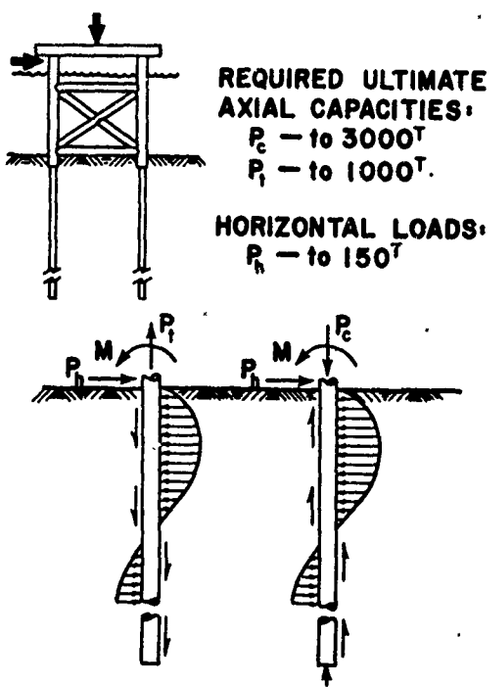

Figure 6.23

Range of pile loads used in current offshore structure design (after McClelland et al.).

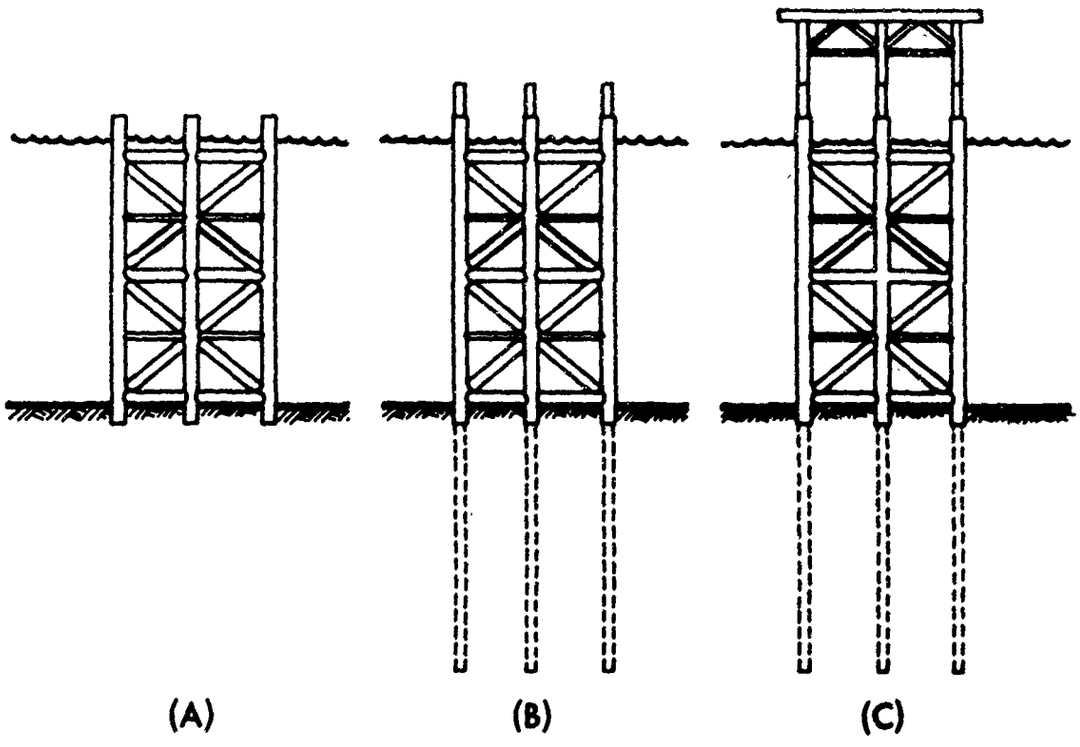

Figure 6.24

Installation procedure for template-type structures (after McClelland et al.).

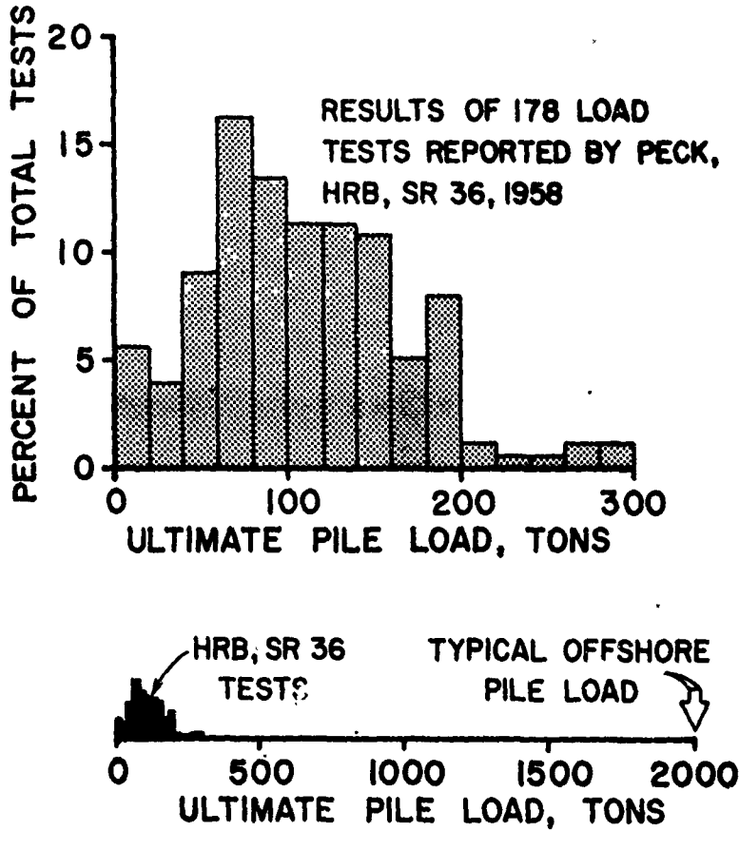

Figure 6.25

Example of the load range represented by one major source of documented pile load tests, as compared to typical offshore pile load (after McClelland et al.).

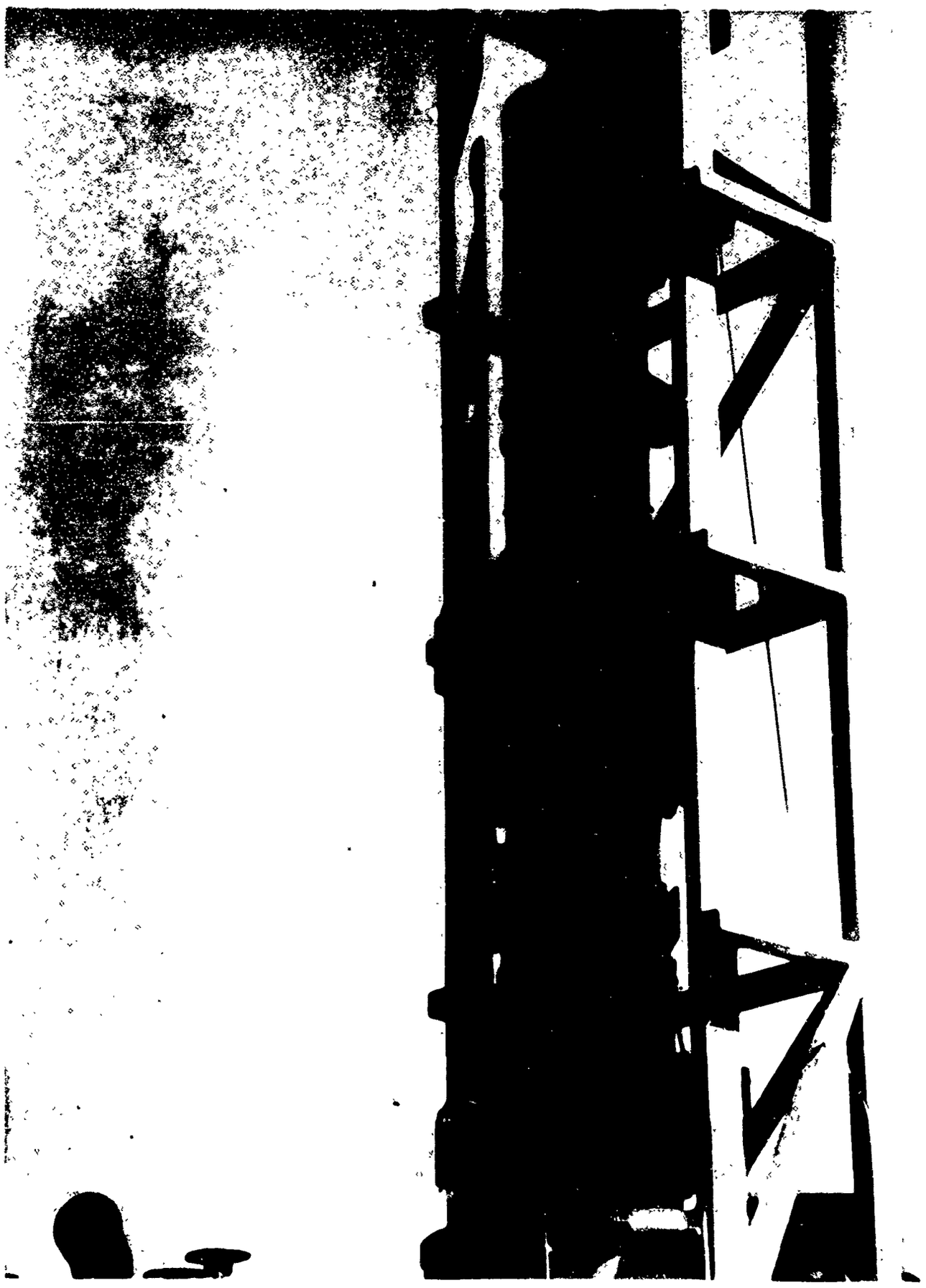

Figure 6.26

Delmag D-44 Diesel Pile Hammer with
87,000 ft.lb/blow maximum Energy

Figure 6.27

Vulcan 040 Offshore Single-Acting Steam Hammer

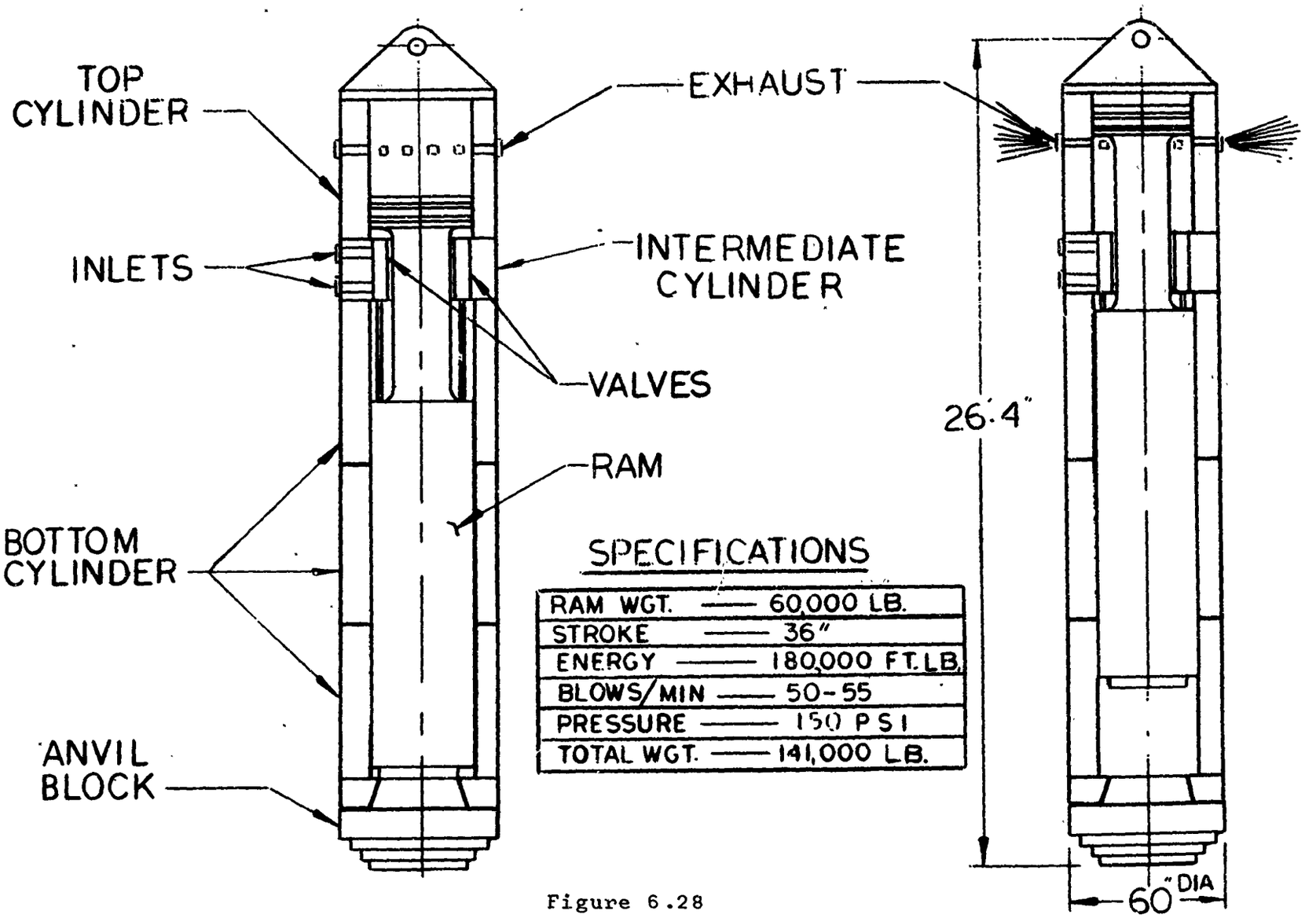

Figure 6.28

OS-60 Single Acting Offshore Pile Driver (MKT Corporation). Maximum Energy 180,000 ft.lbs./blow. Total weight 141,000 lbs.

HYDRAULICALLY POWERED

- ★ Vibration Completely Isolated From Crane
- ★ Safe Hydraulic Power
- ★ Narrow 14" Width
- ★ Not Vunerable to Damage
- ★ Quick Starting & Stopping
- ★ Quick Clamping & Unclamping
- ★ No Overload on Starting & Driving
- ★ Balanced
- ★ Internal Force Lubrication System
- ★ Sealed Against Submersion in Water
- ★ Capable of Adding Non-Vibratory Weight
- ★ Interchangeable Jaws

SPECIFICATIONS

Frequency	1650 - 1850 CPM
Available Horsepower	110
Weight	5 TON
Maximum Lifting Force	20 TON
Start or Stopping Time	5 - 7 SEC.
Clamp Open or Closing Time	2 - 3 SEC.
Max. Hydraulic Pressure	3000 PSI.
Dynamic Force (At 1850 CPM)	112,000 LBS.
Clamping Force	150,000 LBS.

Figure 6.29

V-10 Hydraulic Pile Vibrator (MKT Corporation) and its Performance Parameters.

K KOEHRING

MKT

Division of Koehring Company
Dover, New Jersey 07801

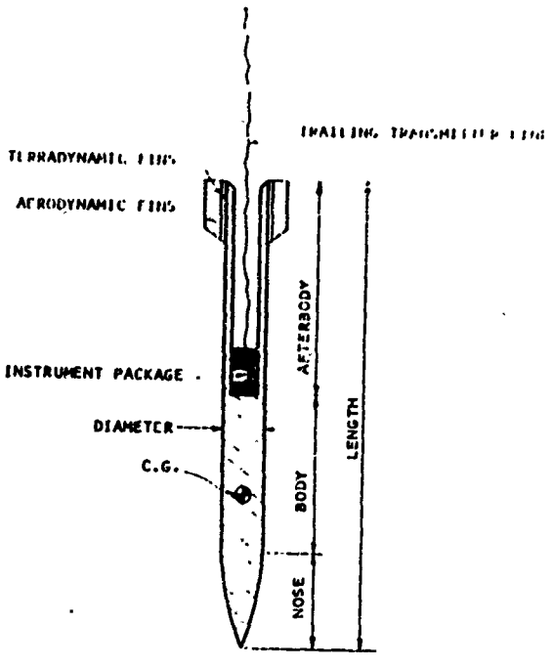

Figure 6.30

Details of Earth-Penetrating Projectile.

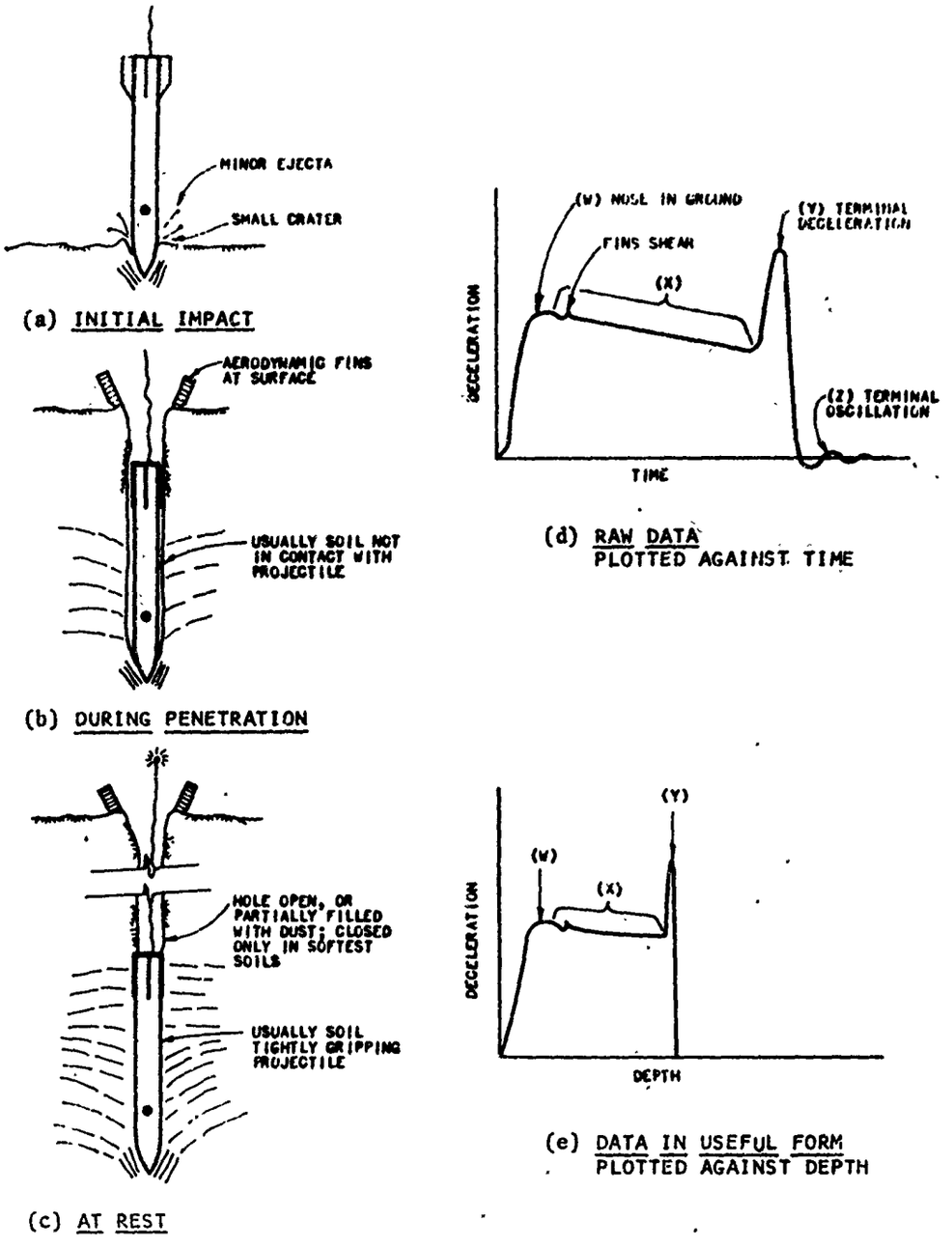

Figure 6.31

The Earth-Penetration Event
(sketches, no scale)

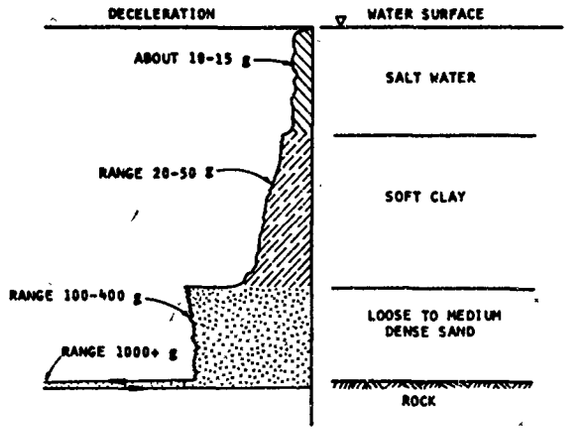

NOTE: Scale of record distorted for clarity.

Figure 6.32

Example of Offshore Probe using Projectiles.

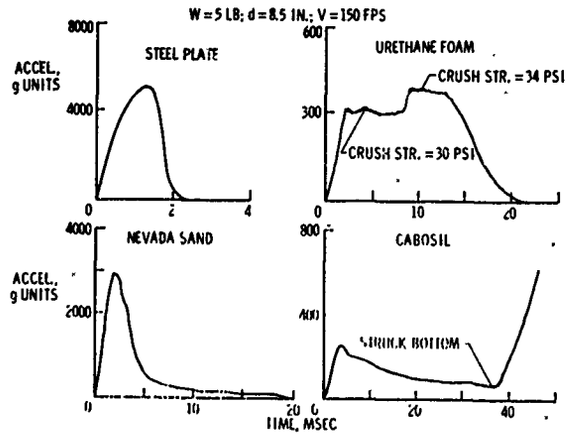

Figure 6.33

Typical Acceleration Signatures for Nominal Penetrometer.

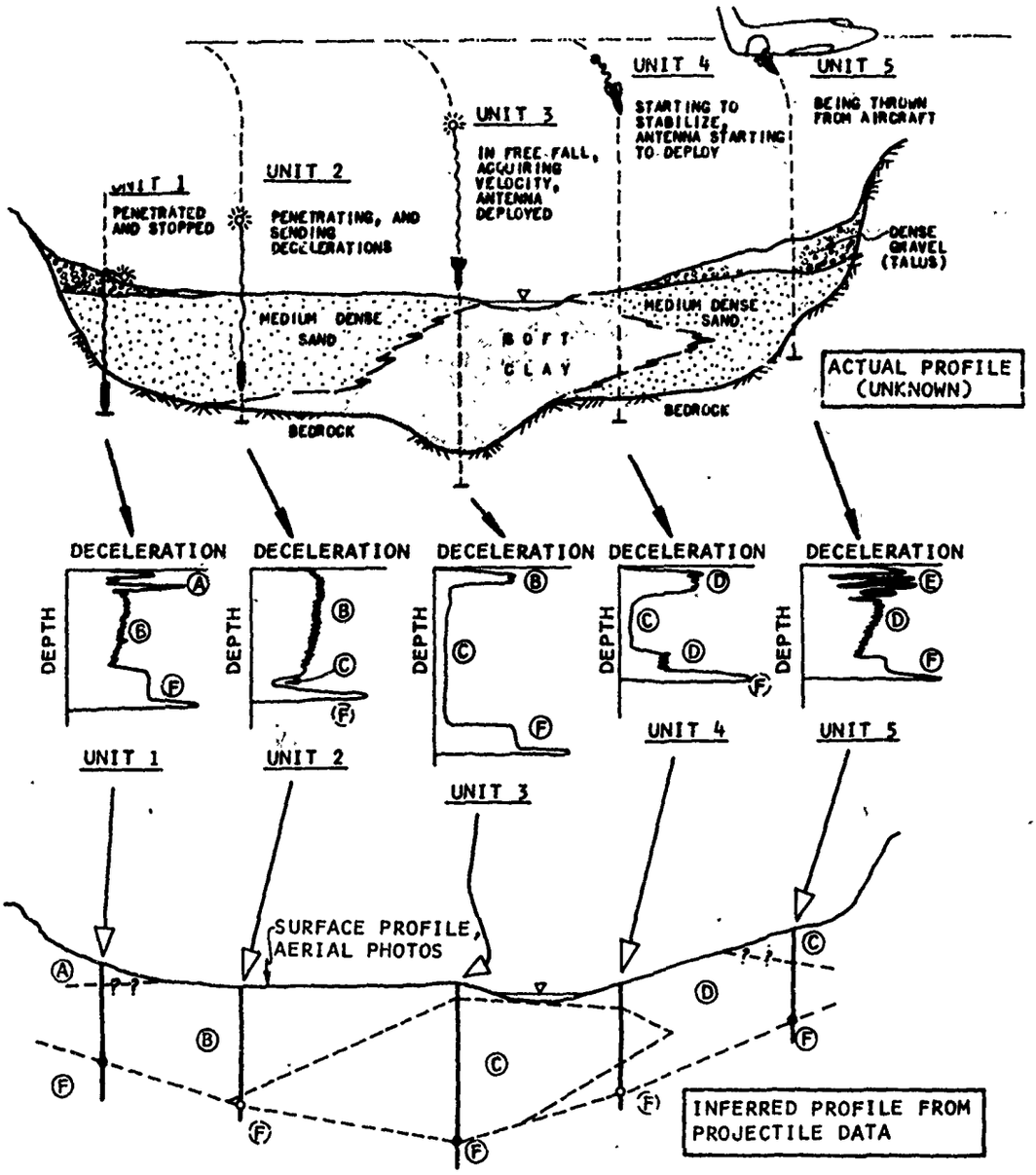

MATERIAL Ⓐ DENSE; GRANULAR; EITHER LARGE GRAINS, OR HIGHLY ERRATIC.
MATERIAL Ⓑ MEDIUM DENSE TO DENSE; GRANULAR, SAND SIZES; SEEMS UNIFORM.
MATERIAL Ⓒ SOFT; COHESIVE.
MATERIAL Ⓓ SIMILAR TO B .
MATERIAL Ⓔ SIMILAR TO A .
MATERIAL Ⓕ ROCK, MODERATE TO WEAK STRENGTH.
MATERIAL Ⓕ UNCERTAIN IF ROCK AT LEVEL SHOWN.
EXAMPLE ONLY, NOT CHECKED FOR KINEMATIC CONSISTENCY.

Figure 6.34

Example of Soil Investigation Using High-Speed Projectiles

HYDROACOUSTIC OSCILLATOR

Figure 8.1

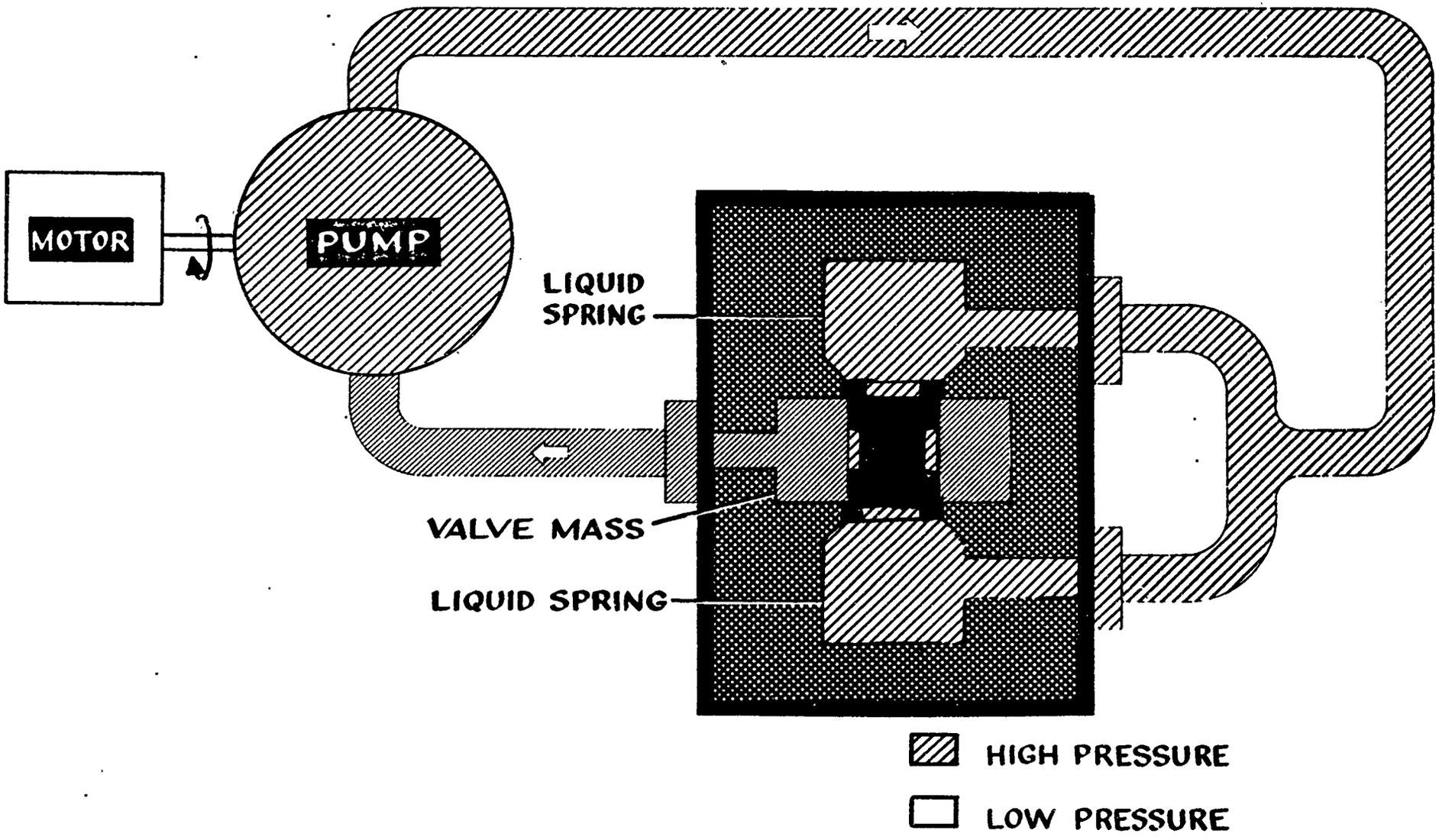

Figure 8.2

ANVIL COUPLING

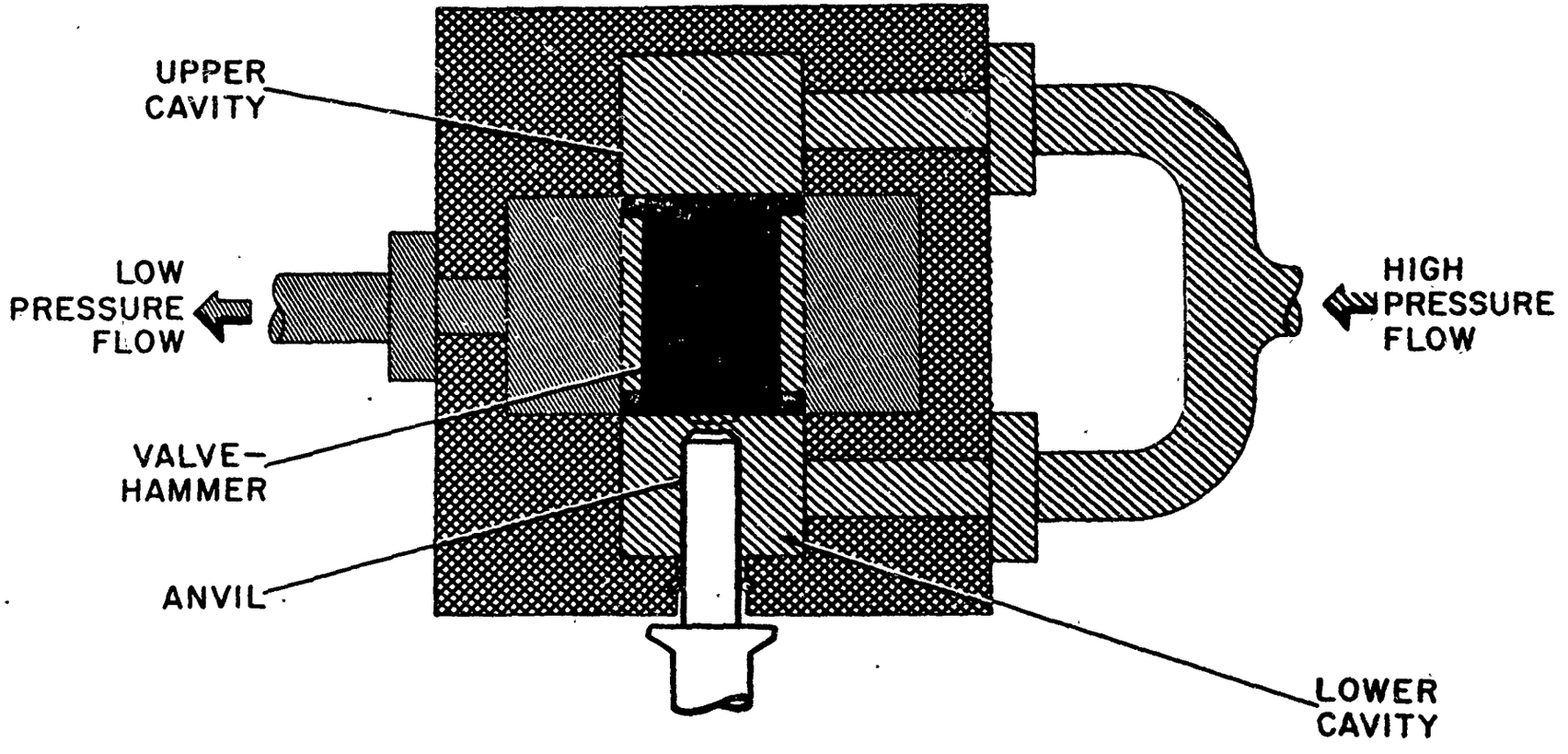

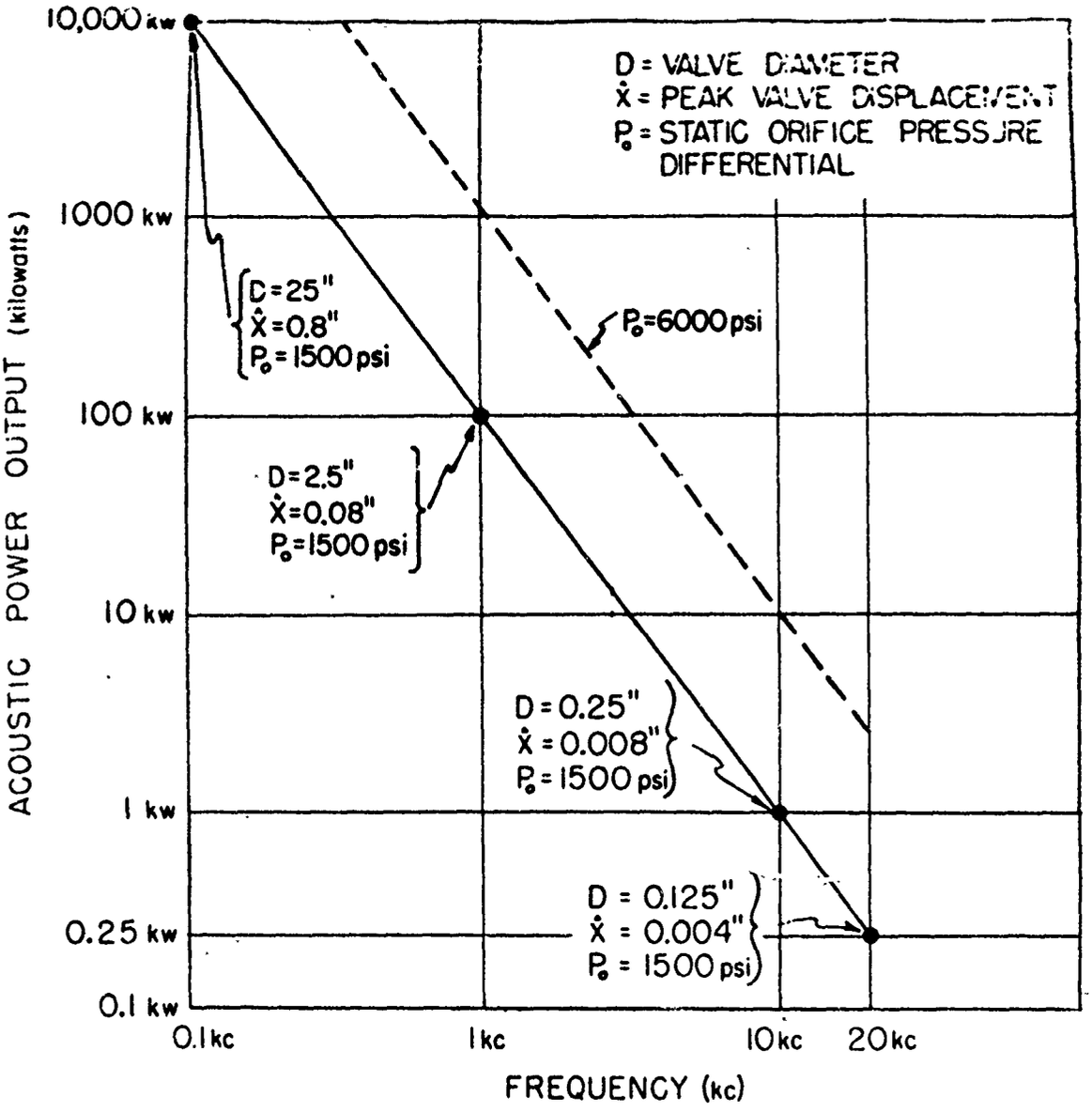

Figure 8.3 OSCILLATOR POWER OUTPUT VS. FREQUENCY

PHYSICAL DIMENSIONS HAVE BEEN SCALED
PROPORTIONAL TO THE OSCILLATION WAVELENGTH

Unclassified
Security Classification

DOCUMENT CONTROL DATA - R & D

(Security classification of title, body of abstract and indexing annotation must be entered when the overall report is classified)

1. ORIGINATING ACTIVITY *(Corporate author)*
Werner E. Schmid, P.E.
Consulting Engineer
Princeton, New Jersey 08540

2a. REPORT SECURITY CLASSIFICATION

2b. GROUP

3. REPORT TITLE

PENETRATION OF OBJECTS INTO THE OCEAN BOTTOM (The State of the Art)

4. DESCRIPTIVE NOTES *(Type of report and inclusive dates)*
Final Report 25 June 1968 - 31 March 1969

5. AUTHOR(S) *(First name, middle initial, last name)*
Werner E. Schmid

6. REPORT DATE	7a. TOTAL NO. OF PAGES	7b. NO. OF REFS
March 1969	179	204

8a. CONTRACT OR GRANT NO.
N62399-68-C-0044

b. PROJECT NO.
Y-F015-21-02-005A

c.

d.

9a. ORIGINATOR'S REPORT NUMBER(S)

9b. OTHER REPORT NO(S) *(Any other numbers that may be assigned this report)*
(18) NCEL
(19) CR 69.030

10. DISTRIBUTION STATEMENT
Distribution of this document is unlimited.
Each transmittal of this document outside the agencies of the U.S. Government must have prior approval of the Naval Civil Engineering Laboratory

11. SUPPLEMENTARY NOTES

12. SPONSORING MILITARY ACTIVITY
Naval Civil Engineering Laboratory
Port Hueneme, California 93041

13. ABSTRACT

The state of the art of predicting as well as achieving the penetration of objects into the sediments of the ocean floor is presented. Both free-fall as well as driven penetration is reviewed. The information known about ocean bottom soils is briefly summarized.

For free-fall penetration the impact velocity, attitude and direction are most important and methods for calculating these parameters are demonstrated.

Impact penetration relations are then discussed based on theoretical as well as empirical relations.

The theoretical considerations valid for driving objects into the bottom sediments are reviewed and the equipment and machinery available at present (1969) for achieving penetration or for driving piles into the ocean bottom are presented. Recommendations for immediate use and for continuing research are made.

DD FORM 1 NOV 65 1473 (PAGE 1)
S/N 0101-807-6801

Unclassified
Security Classification

14. KEY WORDS	LINK A		LINK B		LINK C	
	ROLE	WT	ROLE	WT	ROLE	WT
penetration, penetration equations	x	x				
penetrometers	x	x				
penetrators	x	x				
free fall penetration	x	x				
driven penetration	x	x				
offshore pile driving	x	x				
sediment samplers	x	x				
corers	x	x				
anchors	x	x				
explosive anchors	x	x				
ocean sediments			x	x		
sediment properties			x	x		
sediment shear strength			x	x		
bearing capacity					x	x
terminal velocity					x	x
free fall trajectory					x	x
hydrodynamic drag					x	x